EXPERIMENTAL PERFORMANCE OF REINFORCED AND PRETENSIONED PRECAST CONCRETE BENT CAPS

A Thesis

by

KEVIN JACK YOLE

Submitted to the Office of Graduate and Professional Studies of
Texas A&M University
in partial fulfillment of the requirements for the degree of

MASTER OF SCIENCE

Chair of Committee,	Anna Birely
Co-Chair of Committee,	John Mander
Committee Member,	John Nichols
Head of Department,	Robin Autenrieth

August 2017

Major Subject: Civil Engineering

ABSTRACT

The use of precast bridge substructures provides the benefits of rapid construction, reduction of traffic disruption, increased worker safety, and increased controlled conditions within the precast plants. The Texas Department of Transportation is seeking to take a step further in the advancement of precast bent caps by implementing the use of pretensioned concrete bent caps to improve strength and serviceability in their standard bent cap bridges.

The objective of this research is to provide a comparison between the performance of precast reinforced and precast pretensioned concrete bent caps. This research also focuses on construction techniques and connection details to develop serviceable recommendations for precast pretensioned bent cap specifications to be implemented by TxDOT engineers in standard bridges. An alternative connection that does not require the use of grout is investigated at the request of TxDOT engineers. Effective end region detailing to resist bursting stresses at the time of prestressing transfer is also investigated.

Testing is conducted at the Texas A&M University High Bay Structural and Materials Testing Laboratory. The experimental test setup consists of a specimen subassembly representative of a TxDOT prototype bridge with load configurations capable of recreating demands in the field and also testing the specimen to failure.

Material property tests are performed to calculate the expected strengths of the specimens and predict behaviors during testing. Multiple load patterns are applied to the specimens to study their behavior during bridge demands along with joint, maximum

achievable moments, and failure demands. Visual observations of the damage progression are presented for each load pattern.

Results from testing are analyzed to discuss the constructability and performance of the specimens in light of previous literature, to compare the results between the reinforced and pretensioned specimens, and to discuss the hierarchy of failure mechanisms.

The experimental results show a superior performance of the pretensioned bent cap in comparison to the reinforced concrete bent cap. The pretensioned bent cap exhibits delayed initial cracking, smaller average crack widths and an improved ability to reduce cracks after load removal. The pocket connection performs satisfactorily for both specimens. The end-region detailing for the pretensioned specimen is efficient in controlling bursting stress cracks during the release of strands. Recommendations for field implementation include the use of the side strand configuration, the use of shrinkage admixtures for the pocket concrete, secure hold down of the pocket during construction, and the use of plastic shims and vent holes for the construction of the bedding layer.

DEDICATION

To Maria Sileny Campos Chacón, Nicholas Valentine Yole, and John Thomas Keen.

ACKNOWLEDGEMENTS

I wish to thank my committee chair, Dr. Birely, and committee co-chair, Dr. Mander, for their guidance and support during the course of this research.

I would like to thank Dr. Nichols for serving on my advisory committee. Thank you to TxDOT personnel Darrin Jensen, Christopher Miller, Jason Tucker, Todd Speck, Buddy Williams, Manuel Padron Jr., Courtney Holle, Graham Bettis, Susan Ceballos, Frank Estrada III, Dennis Johnson, and Roger Lopez for sponsoring this research. Thank you to Bexar Concrete Works Inc. for fabricating the pretensioned specimens. I also take this opportunity to thank Dr. Keating and the laboratory technicians for their assistance during the experimental testing, and all the department faculty and staff for making my time at Texas A&M University a memorable experience.

Special thanks to my colleagues Usha Rani Barooah, Judong Lee, Codi McKee, and all the other graduate and undergraduate students involved in the project for their constant help and support.

Last but certainly not least, I am deeply thankful to my mother Maria Sileny Campos Chacón, father Nicholas Valentine Yole, step-father John Thomas Keen, sister Marla Janinne Yole, aunt Guiselle Campos Chacón, and uncle “Tio” Gelber Monge Nuñez for their devoted support, encouragement, patience, love, and prayers.

CONTRIBUTORS AND FUNDING SOURCES

This work was supervised by a thesis committee consisting of advisor Dr. Anna Birely and co-advisor Dr. John Mander of the Zachry Department of Civil Engineering, and committee member Dr. John Nichols of the Department of Construction Science.

All work for the thesis was completed by the student, under the advisement of Dr. Anna Birely and Dr. John B. Mander of the Zachry Department of Civil Engineering, and Dr. John Nichols of the Department of Construction Science.

Funding was provided by the Texas Department of Transportation, Project 0-6863 "Develop Strong and Serviceable Details for Precast, Prestressed Concrete Bent Cap Standards that Can be Implemented on Everyday Bridge Construction Projects", Darrin Jensen Project Manager.

TABLE OF CONTENTS

Page

LIST OF FIGURES

Page

LIST OF TABLES

Page

1. INTRODUCTION

The development of precast pretensioned bent caps is expected to be an important step in the advancement of precast substructures in the State of Texas. Precast bent caps will provide the benefits of rapid construction, reduced traffic disruption, increased worker safety, and increased controlled conditions within the precast plants allowing for the more efficient production of large numbers of bent caps. Additionally, precast pretensioned bent caps offer the benefits of enhanced performance with improvements in strength and serviceability.

Precast reinforced concrete bent caps have formerly been investigated and documented by others. However, studies related to pretensioned bent caps and testing to failure have not been conducted. In order to implement the use of precast pretensioned bent caps within standard bridges in the State of Texas, experimental testing is conducted to provide comprehensive performance results. An alternative connection that does not require the use of grout is also investigated at the request of TxDOT officials. The use of effective end region detailing is also investigated to control cracking during the transfer of prestress forces.

This research focuses on the experimental performance of a full-scale precast reinforced concrete and precast pretensioned bent cap. The experimental test setup incorporates a subassembly representative of a TxDOT prototype bridge with applied demands recreating realistic load patterns and behaviors in the field. Recommendations are developed from this research for field implementation and future research.

1.1. Research Motivation

Precast reinforced concrete bent caps in Texas have shown susceptibility to diagonal cracks in the regions outside the connections and a need for improvement in the constructability of the connections between bent caps and columns. TxDOT is expanding the state-of-the-practice for precast bent caps to include precast pretensioned bent caps as they seek improvements in strength and serviceability of the bridge infrastructure in the State of Texas. The use of pretensioned bent caps and its benefits have yet to be investigated by TxDOT. The experimental testing will test two full-scale subassemblies of a bent cap and validate the previously developed design procedures. An alternative connection is also investigated to improve the constructability and performance based on requests by TxDOT officials. Detailed construction techniques, analysis of the cap-to-column connection, end region detailing, bent cap performance results, and recommendations are needed to provide engineers with helpful guidelines for the proper design and efficient use of precast pretensioned bent caps in the State of Texas.

1.2. Research Objective and Scope

The primary objective of this research is to conduct an experimental investigation to study the performance of a full-scale reinforced and pretensioned bent cap. Additional objectives are to explore an alternative cap-to-column connection and modified end region detailing to control cracking during the transfer of prestressing forces. Two additional variations on a pretensioned design will be constructed. In this thesis, the results from testing are limited to the reinforced and equivalent pretensioned bent cap.

A major shortcoming from previous experimental tests is the demands were limited to negative moment demands and the shear-moment demand ratios do not accurately reflect those of bents in the field. Additionally, several experiments have tested large-scale or full-scale bents to assess the performance of connections, but did not test the bent caps to failure. The experimental testing in this study is intended to address the shortcomings of previous research while also testing full-scale components to their maximum capacity with realistic loads effects.

The results gathered from visual observations and instrumentation installed on the specimens will be studied in detail and recommendations for future research and future state-of-the practice will be provided.

1.3. Organization of Thesis

This thesis has been organized in six chapters discussing the design, construction, experimental testing, and analysis of results of the reinforced and equivalent pretensioned bent cap specimens. Chapter 2 presents a review of state-of-the-art and state-of-the-practice work on bent caps, connections, and end region detailing. Chapter 3 presents the experimental test program discussing the design considerations, test matrix, specimen construction, experimental test setup, instrumentation, material properties, and expected strengths. Chapter 4 presents the experimental testing load patterns, followed loading sequences, visual observations, damage progression, creep tests and crack widths following load removal. Chapter 5 presents an analysis discussing the results based on the chosen design considerations, previous work, expected yield and nominal strengths, a comparison between the reinforced and pretensioned bent caps, and the hierarchy of

failure mechanisms. Finally, Chapter 6 presents the summary, conclusions, and the recommendations for field implementation and future research based on the experimental results.

2. LITERATURE REVIEW

This chapter covers previous research on experimental testing on reinforced concrete bent caps, connections between bent caps and columns, prestressed end region bursting stress effects, and current construction practices for TxDOT standard I-girder bent caps. Section 2.1 discusses a brief history of precast concrete from its initial conception to its first arrival in the area of highway bridge construction in the state of Texas. Section 2.2 presents the state-of-the-art describing previous research done in the areas of bent caps, connections between columns and bent caps, and pretensioned end region detailing. Section 2.3 discusses the state-of-the-practice for precast reinforced concrete bent caps in the state of Texas. Section 2.4 presents the questions that arise from the literature review.

2.1. Brief History of Precast Concrete in Bridges

Precast concrete in bridges originated in Europe shortly after World War II because of the urgent need to reconstruct the vast amounts of bridges destroyed quickly and efficiently. This also lead to the use of prestressed concrete due to the lack of steel from war efforts (Figg and Denney, 2004).

The use of precast reinforced concrete bent caps in Texas began in the mid-1900's, mostly due to requests from contractors wishing to facilitate unique construction projects techniques. Jones and Vogel (2001) reported that one of the first projects to use precast bent caps was the replacement of the 113 span Pierce Street Project section of the I-45 in Houston. The use of the precast members proved to be beneficial as it resulted in a reduction of construction time from the estimated 548 days with a cast-in place method to

95 days with the precast bent caps. Other early applications of precast bent caps include the Redfish Bay and Morris and Cummins Cut bent caps, the US 290 Ramp E-3, the Lake Ray Hubbard Bridge and the Lake Belton Bridge (Freeby et al. 2003). Texas has continued the use of precast bent caps to improve worker safety and decrease construction time.

2.2. State-of-the-Art

This section presents previous research performed on bent caps, connections between columns and bent caps, and end region bursting stress reinforcement of pretensioned members.

2.2.1. *Bent Caps*

Ferguson (1964) performed experimental testing on the overhang region of cantilever reinforced concrete bent caps to improve the design procedures and detailing of bent caps throughout Texas. The experimental testing consisted of 36 specimens with bent caps 36-in depth and 30-in width with varying cantilever lengths at the overhands. The bent caps were supported on both square (26.5-in) and round (30-in diameter) columns. The specimens were placed on their side and supported by rollers and jacked against an anchor beam with a steel yoke placed over the second column. Variables studied were the shear span dimensions, end anchorage of longitudinal steel, web reinforcement arrangement, reinforcement bar sizes, column support geometry and material properties such as grades of steel. The loads were applied in increments with a 400 kip jack up to failure; except when the failure capacity of the specimen was greater than 400 kips (Figure 2.1.a).

Results from testing showed that cracks for both round and square columns were observed to propagate towards the column face suggesting the strain profile was higher at

the sides than the center of the supports (Figure 2.1.b). Side cracks that formed near the mid-depth were nearly as wide as the cracks in the tension face suggesting vertical stirrups did not provide any increase in strength while longitudinal steel was actually more effective in strengthening the specimen in the tension face of the cantilever ends for loads placed between 0.5 and 1.2 times the depth of the beam from the support (a/D). Failure beyond loads causing initial yield in the longitudinal reinforcement was observed in 92% of the specimens, suggesting a desirable ductile failure mechanism caused by bond or shear. The main factor affecting bond failure was found to be the anchorage distance beyond the load.

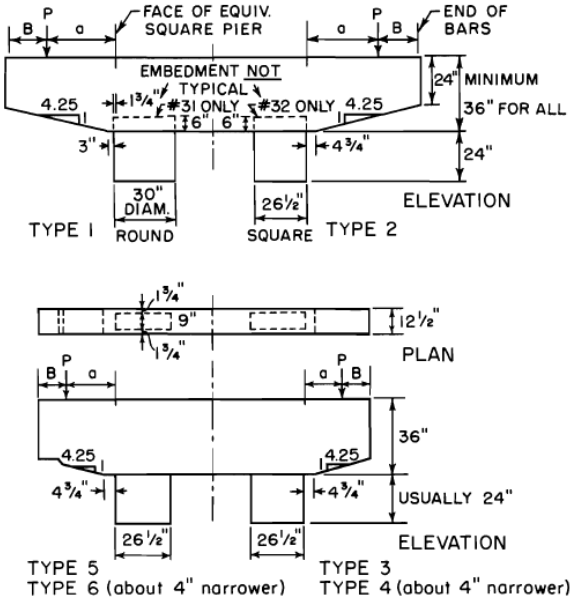

(a) Experimental Setup *(b) Column Face Crack Concentration*

Figure 2.1. 3/8-Scale Model Bent Cap Test (Ferguson, 1964).

Frantz and Breen (1978) performed experimental testing on 3/8-scale inverted-T bent cap specimens to examine the cause of excessive cracking at the mid-depth side face of large reinforced concrete beams. The specimens were designed according to ACI and AASHTO standards and test variables believed to affect the side face cracking included beam depth, cover dimensions, amount and distribution of skin reinforcement and beam cap width. The tested specimens consisted of one full-size model bridge design based on the prescribed AASHTO and ACI standards, 44 simplified models, and two re-designed models (one full size and one simplified) based on results from the earlier specimens. The model bent cap had a cross-sectional depth of 34-7/8-in with a tapered cantilever overhang decreasing to 28-7/8-in and rested on two supports (one column stub and one roller) providing a 6-ft 9-in test zone length (Figure 2.2). Symmetric loads up to ultimate demands (125 kips) were applied to the model bent cap with two exterior and two interior concentrated load points. The simplified models consisted of reduced segments constructed with the chosen test variables and 4.0-ft test zone lengths.

Testing showed initial hairline flexure cracks forming at a longitudinal steel stress of approximately 5-ksi and propagating with a general vertical trend well into the depth of the web with some cracks inclining towards the support due to shear-flexure interaction. The re-designed models showed that the most effective way to control side cracking was by placing more skin reinforcement with smaller diameter bars well distributed in the tension zone. The results also showed that increasing the amount of longitudinal reinforcement lowered the stress levels near the concrete surface, providing an effective means for crack control.

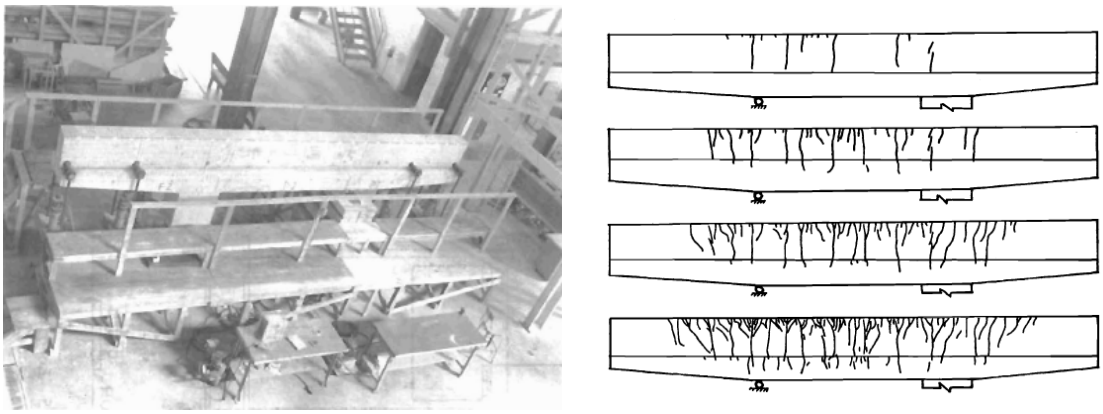

(a) Experimental Setup *(b) Crack Pattern Development*

Figure 2.2. 3/8-Scale Model Bent Cap Test (Frantz and Breen, 1978).

Mander et al. (1996) conducted an experimental investigation on a full-scale prototype bent cap-to-column sub-assemblage before and after the retrofit. The retrofit was aimed at enhancing the performance of the beam cap and joint. The un-retrofitted prototype was extracted from a three-column bent-type pier typical of bridges built in the eastern portion of the Unites States during the 1960's. The subassembly was inverted and an 1100 kN capacity actuator acting at a 27-degree angle applied the force through the points of contra-flexure in the bent cap and column to simulate different percent drifts experienced during an earthquake applied under reverse-cyclic loading (Figure 2.3.a).

Testing results for the un-retrofitted specimen showed a joint core failure from anchorage loss of the column steel and fatigue failure of the concrete in the cap beam at the joint (Figure 2.3.b). The retrofit consisted of longitudinal prestressing ducts, longitudinal temperature and shrinkage distribution steel wrapped around the column for the cap beam, and diagonal shear reinforcement at the joint forming a high strength concrete jacket (Figure 2.4.a). The retrofit failure was attributed to column shear cracking,

fracture of column hoops and some minor bond slip of the column steel. These results indicated the effects from prestressing relocated the failure zone from the joint to the column by enhancing the elasticity and strength of the cap beam and joint (Figure 2.4.b).

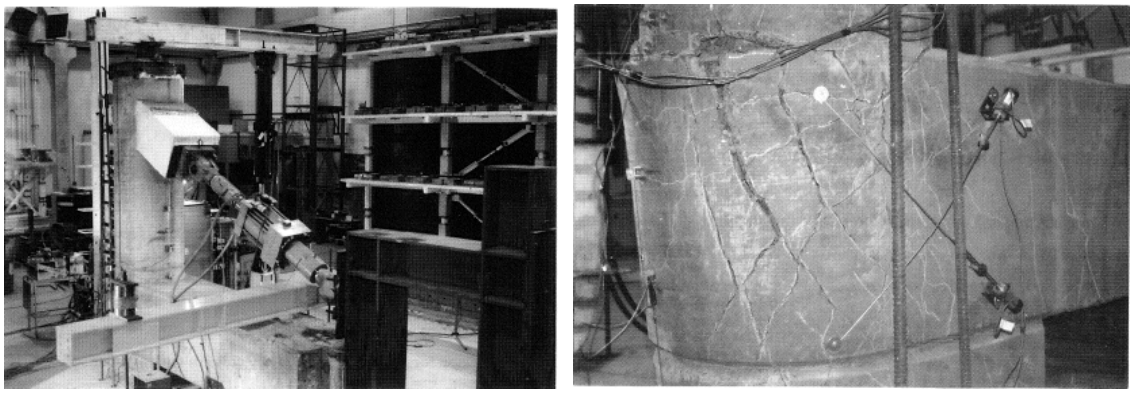

(a) Experimental Setup *(b) Damage Patterns*

Figure 2.3. Full-Scale Pre-Retrofit Testing (Mander et al., 1996).

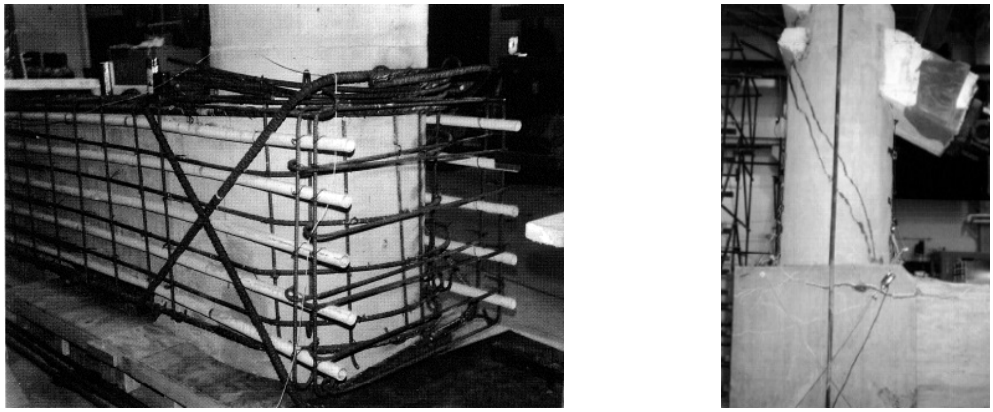

(a) Bent Cap Retrofit *(b) Retrofit Failure*

Figure 2.4. Full-Scale Post-Retrofit Testing (Mander et al., 1996).

Mander et al. (1996) also conducted experimental testing on a 1/3-scale model reinforced concrete bridge pier to evaluate the retrofit redesign philosophies developed from the companion prototype pier cap beam-column sub-assemblage investigations (Mander et al. 1996). The experimental test setup provided a 1000 kN actuator lateral load at the top of the prototype to mimic seismic loads, a lateral resistant load provided at the base by a 1100 kN hydraulic actuator to fix the base of the specimen, and a 100 kN actuator provided the vertical load to simulate the weight of the deck through a lever beam (Figure 2.5.a). All testing was conducted utilizing sinusoidal wave forms with a frequency of one cycle per minute in three different phases from low, variable and high amplitude drifts.

Testing of the un-retrofitted 1/3-scale model showed weakness in joint shear resistance and anchorage failure of column longitudinal reinforcement (Figure 2.5.b). The retrofit consisted of one layer of flexural steel installed on the underside of the cap beam, longitudinal prestressing ducts on each of side of the cap beam, and high-strength concrete to form a concrete jacket.

The retrofit prototype changed the failure mode to flexure-shear failure in the column, eliminating the undesirable failure mechanism in the joint and anchorage seen in the un-retrofitted model (Figure 2.6). These results validated the redesign philosophies of prestressing effects increasing strength in the cap beam and joint.

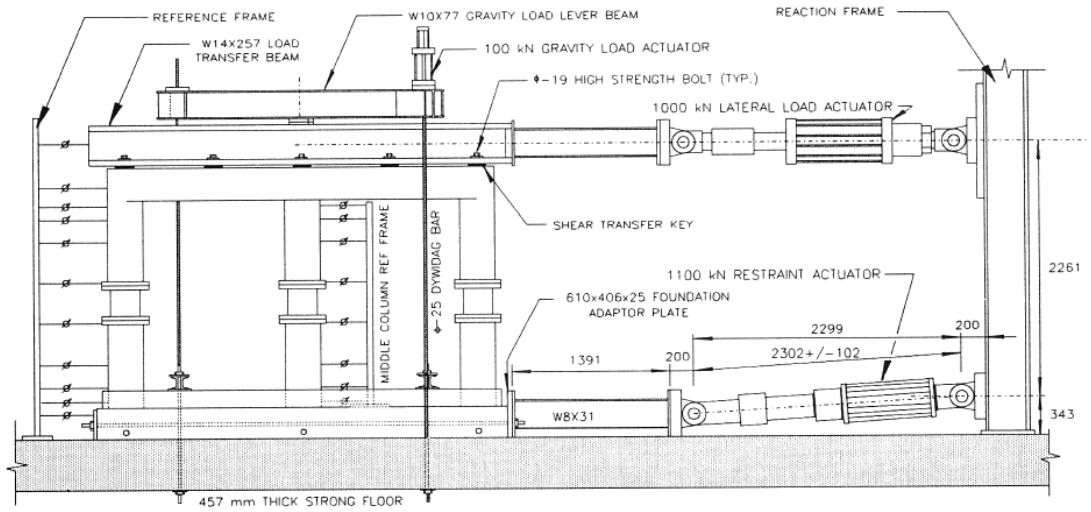

(a) Experimental Setup

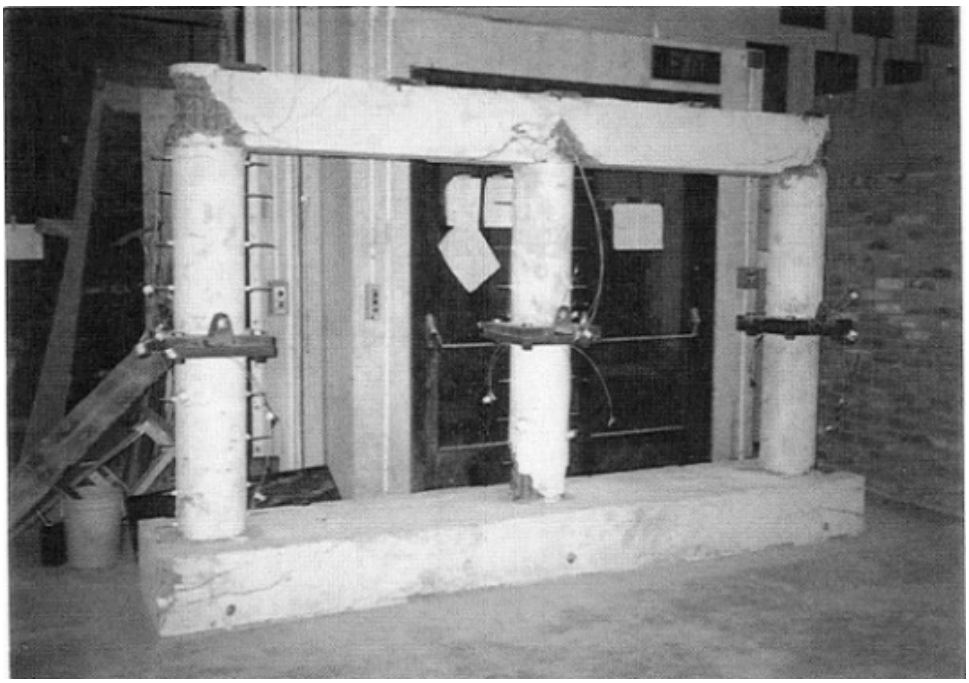

(b) Tested Specimen

Figure 2.5. 1/3-Scale Pre-Retrofit Bent Cap Testing (Mander et al., 1996).

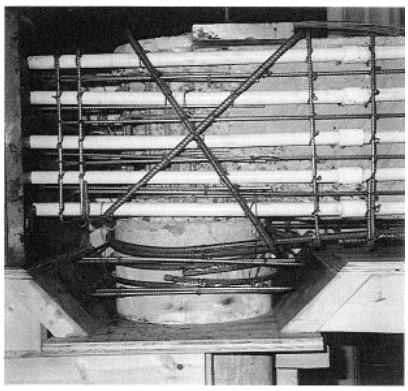

(a) Bent Cap Retrofit

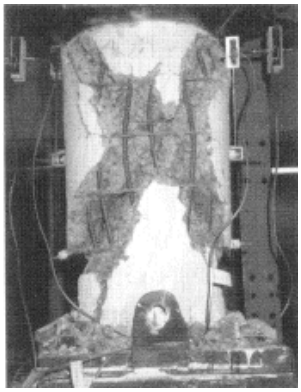

(b) Retrofit Failure

Figure 2.6. 1/3-Scale Retrofit Bent Cap Testing (Mander et al., 1996).

Bracci et al. (2001) performed experimental tests on 16 full-scale reinforced concrete bent caps to investigate cracking and to develop new design recommendations for reinforced concrete bent caps. The bent caps had a cross-section of 36-in x 36-in with tapered overhang decreasing to 36-in x 24-in. A monolithic connection was used between the bent cap and the column for all specimens. Specimen designs included standard design, modified skin reinforcement details, and increased volume of shear reinforcement. Emphasis was given to crack widths limits for moderate exposure (0.013-in) and extreme exposure (0.016-in) which corresponded to the crack width parameter 'z' in AASHTO 1998 and ACI 318-95 used to determine the distribution of flexural reinforcement in the tension region to control flexural cracking. Two 600-kip actuators imitated the location and loads from girders placed symmetrically at 4.5-ft from the center of the column support (Figure 2.7.a). Loads created demands in the column-to-bent cap negative moment joint region during service loads and up to failure.

Results from testing showed that flexure cracks occurred first for all specimens, followed by shear-flexure cracks that propagated from the load points towards the column support (Figure 2.7.b). All specimens showed cracking at service loads with cracks in several specimens reaching the extreme exposure limit of 0.016-in. The shear-flexure cracks were generally wider than flexure cracks and brittle shear failure was typically observed between the loading point and the column face along a plane of approximately 45 degrees. This report concluded that flexural cracking in bent caps initiated at longitudinal stresses of approximately 4-ksi to 7-ksi, which were below service stress limits in the current code for crack control. Additional flexural reinforcement was found to have a major role in limiting cracks while the distribution of the longitudinal reinforcement had no effect on cracking. It was also determined that increasing the shear resistance with overlapping transverse reinforcement reduced the shear transfer demands along the main compression strut from the applied load to the support by increasing contributions from the compression fan region.

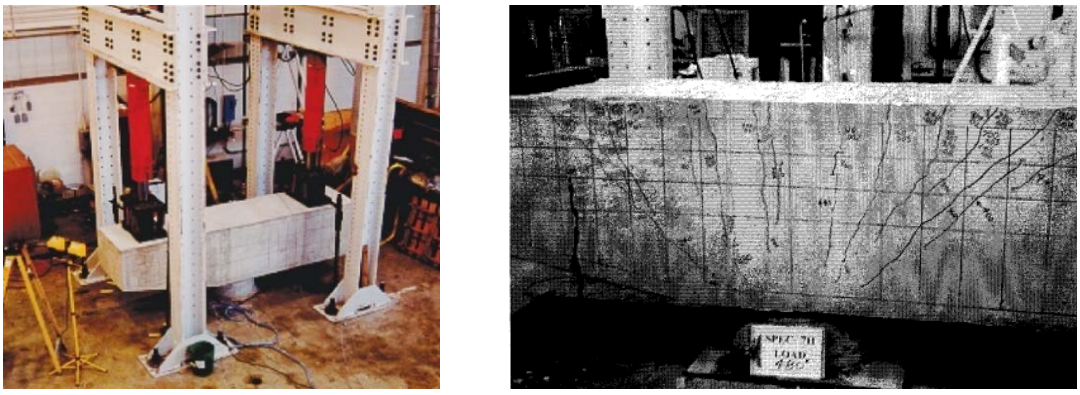

(a) Experimental Setup *(b) General Damage Pattern*

Figure 2.7. Reinforced Concrete Bent Cap Testing (Bracci et al., 2001)

Barooah (2016) studied the flexural design of pretensioned bent caps and developed design procedure recommendations to be implemented for standard TxDOT I-girder bridges as an alternative to precast reinforced concrete designs. The main objective was to provide at least equal, but preferably superior, performance to that of reinforce concrete bent caps. This was done by introducing a key limit state of no tension under dead loads, thus ensuring that cracks close under the removal of applied live loads.

A simple design procedure was introduced that first determined the minimum number of strands to provide flexural resistance greater than the cracking moment in the bent cap preventing a brittle failure. The next step was to calculate the number of strands to achieve zero tension under dead load followed by calculating the minimum required concrete compressive strength to prevent cracks under service loads. The final steps were to check the ultimate strength capacity and deflections.

The TxDOT standards for Class H (typical of prestressed members) compressive strengths were used with minimum compressive strengths of f'_{ci} = 4-ksi and f'_{c} = 5-ksi, and maximum compressive strengths of f'_{ci} = 6-ksi and f'_{c} = 8.5-ksi. Low relaxation 270-ksi 0.6-in diameter strands were used with a conservative 20% assumed prestressed losses. TxDOT software (CAP 18) was used to calculate the demands for various roadway widths (32-ft, 40-ft, and 44-ft) for non-skewed I-girders, skewed I-girders, box beams, X-beams and non-standard bridges. The movable live loads from the CAP 18 software generated demands that resulted in a more conservative design than the live loads demand computed from AASHTO LRFD provisions for frame analysis. The allowable stress limits were specified according to AASHTO LRFD provisions and were limited to 0-ksi for

tension and $-0.45\sqrt{f'_c}$ (in ksi) for compression at dead loads, and $0.19\sqrt{f'_c}$ for tension and $-0.45\sqrt{f'_c}$ for compression for service loads. The ultimate flexural moment capacity (M_n) was checked according to AASHTO LFRD provisions to be greater than the flexural demands under ultimate loads (M_u), $\Phi M_n \geq M_u$, where Φ is equal to 1 for tensioned controlled members. The members were expected to crack at $0.24\sqrt{f'_c}$ and cracked section behaviors at were expected $0.38\sqrt{f'_c}$.

Barooah (2016) predicted the design procedure of zero tension under dead and closure of cracks after removal of full live loads was achievable for TxDOT I-girder bent caps, with most bridges not expected to crack under ultimate loads. In bridges expected to crack under ultimate loads, optimization of the design procedures was introduced by providing additional strands with eccentricity to mitigate potential tensile cracking. These optimizations also introduced the possibility of elimination of an interior column in the bent, in which increased positive moment demands were provided by an eccentric prestressing layout. Experimental verification was necessary to validate the successful performance of the pretensioned bent cap design procedure.

2.2.2. *Connections*

Matsumoto et al. (2001) tested the performance of four different full-scale bent cap subassembly connections to improve the constructability and study the connection performance in precast bent caps. The types of connections included single line grouted pocket, double line grouted pocket, grouted vertical duct, and bolted connections. The grouted vertical duct connections consisted of 4-in diameter steel corrugated pipes installed during construction of the rebar cage for the precast bent caps with clearances

between ducts limited to at least 1.5-in or 4/3 times the largest coarse aggregate size. The ducts provided housing for 4#9 dowel bars that extended from the cast-in-place column.

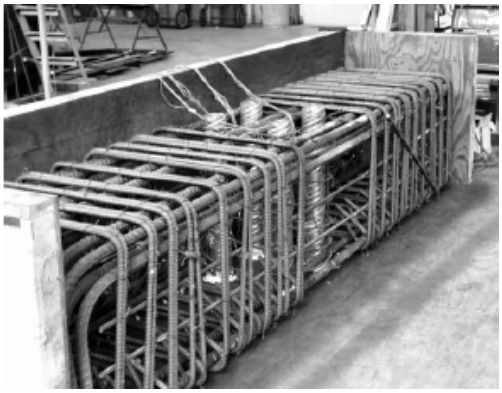

(a) Steel Cage Construction

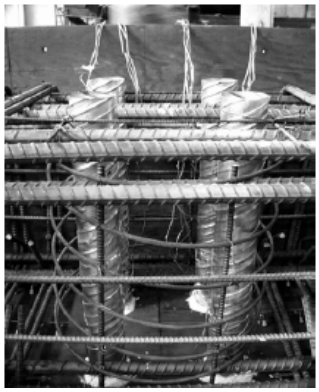

(b) Corrugated Ducts

Figure 2.8. Corrugated Vertical Duct Construction (Matsumoto et al., 2001).

The development length of the dowel bars was chosen based on results from pullout tests on epoxy-coated straight #6, #8 and #11 bars. The pull-out test showed all bars achieved yield at 13 times the diameter of the bar ($13d_b$) with an average concrete compressive strength of 5.4-ksi, which were all less than the embedment length prescribed by ACI 318-99. In addition to the grouted vertical ducts, the influence of bedding layers, shims materials and shim plan areas were studied along with proper construction and grout preparation methods to determine their influence on the performance of the connection.

Testing of the vertical corrugated duct connection was conducted on four specimens each consisting of a precast cast bent cap and a cast-in-place column stub. The bent caps were 30-in deep, 33-in wide and 12-ft long and rested on a 30-in diameter column. The test setup consisted of two 200-kip rams located on either side of the

connection approximately 41-in from the center of the column support (a/D = 0.87) and provided service, factored and failure loads. A transverse ram was also incorporated to simulate wind loads up to 40 kips (Figure 2.9). Different load combinations were applied to each specimen to investigate the effects of different longitudinal and transverse eccentricities by positioning rams at various locations on the bent cap.

The experimental results showed the use of corrugated ducts prevented cracks at the top of the bent cap from propagating inside the circumference of the ducts and no cracks formed on the surface of the grout during any load combinations (Figure 2.10.a). Vertical cracks less than 0.002-in were observed in the bedding layer at service and factored loads. Visual observations of the damage in the bent cap showed flexure vertical cracks propagating towards the center of the column and mostly symmetrical flexure-shear about the center of the column propagating towards side faces of the column support (Figure 2.10.b). The failure caused by yielding of the dowel bars at the bedding layer showed that typical bent cap sizes have adequate embedment and anchorage depths.

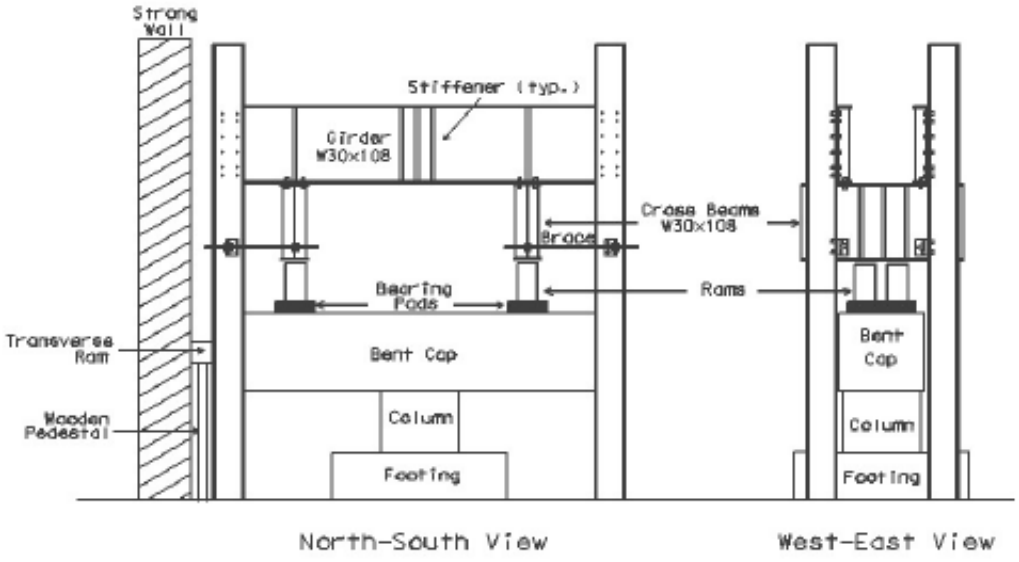

Figure 2.9. Experimental Setup Subassembly (Matsumoto et al., 2001).

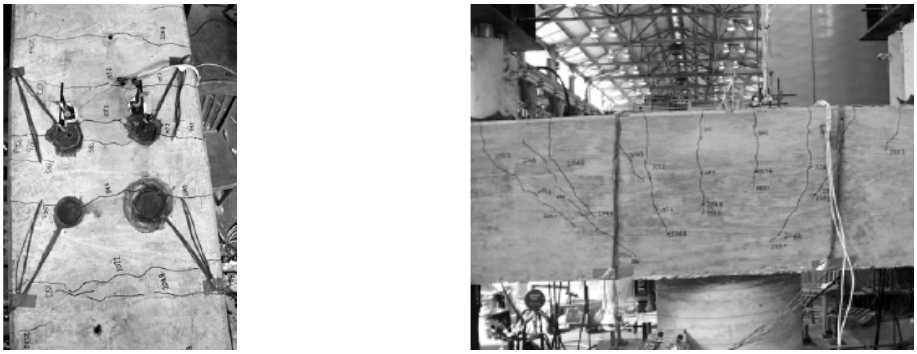

(a) Crack Pattern Above Connection *(b) Crack Pattern on Side*

Figure 2.10. Subassembly Performance at Factored Loads (Matsumoto et al., 2001).

Matsumoto et al. (2001) also tested a full-scale trestle pile bent cap and a column-bent cap to investigate the constructability issues and performance of subassembly connections. The column bent cap was 25-ft long with a square cross-section of 33-in. Three 2.5-ft diameter columns were spaced 9-ft apart center to center. Each column had a

different type of connection which included a double line grouted pocket, grouted vertical duct and bolted connections. A TxDOT Class C concrete mix with a minimum 3.6-ksi design strength was used for the bent cap and columns. Steel shims were used at the column with the grouted vertical duct connection to form the 1.5-in bedding layer and support the bent cap.

Loads were applied at four locations with rams on either side of the connections for a total of eight points loads (Figure 2.11). The first load combination created service and factored demands. The second load combination provided the maximum realistic longitudinal moment demands by applying a larger load on the rams on one edge while the third load combination consisted of removing the loads from the rams one edge; both created longitudinal eccentricities to provide a larger moment transfer to the connection. The fourth and final load combination provided a transverse moment by applying the loads at the overhang.

Under the application of service and factored loads, maximum cracks widths of 0.007-in developed in the positive and negative moment regions of the bent cap (Figure 2.12.a). The grouted vertical duct connection showed no cracks in the grout surface at the top and no opening or cracks in the bedding layer. Subsequent loads combinations produced a maximum bedding layer opening of 0.013-in and cracks at the top of the connection region of 0.007-in wide (Figure 2.12.b). Due to the limitation of the test setup and specimen configuration, it was determined that no significant damage was produced in the connection region and only minor deflections and cracks were recorded on the bent cap.

Results from testing showed no evident bond failure between the grout and the concrete at the bedding layer. Shims were limited to 2.5% of the column surface area placed at two symmetric locations in line with the longitudinal orientation of the bent cap and did not affect the performance of the connection. Constructability issues included small tolerances of duct placement (+/- 1-in), use of grout, segregation of fine aggregates in the grout, and voids in the bedding layer. The effects from the use of a corrugated vertical duct connection and grouting of the connection and bedding layer showed no significant difference in structural behavior versus that of a cast-in-place connection. The connection was considered to have a stiffness between that of a rigid (cast-in-place system) and a pinned connection (no rotational restraint). The results also closely matched the TxDOT in-house bent cap analysis program (CAP 18) pinned connection assumption at the top of the columns better than the rigid frame conditions for a monolithic connection. Based on these results, the corrugated duct connection was implemented by TxDOT as an option for a connection detail used in precast reinforced concrete bent caps for multi-column interior bent cap designs.

Figure 2.11. Experimental Setup Column Bent Cap (Matsumoto et al., 2001).

(a)Flexure Cracks on Sidewall at Factored Loads

(b) Flexure Cracks at Top of Connection at Max. Realistic Longitudinal Moment

Figure 2.12. Column Bent Cap Performance (Matsumoto et al., 2001).

Restrepo et al. (2001) (NCHRP 681) tested 7 - 42%-scale emulative and hybrid connections under reverse cyclic loading to investigate the implementation of connections between prefabricated members for use in accelerated bridge construction (ABC). The specimens consisted of subassemblies representative of the center column and bent cap of a typical three-column cast-in-place urban area highway overcrossing. The specimen consisted of a 25-in square 12-ft long bent cap placed on a 4-ft 11-in long 20-in diameter

column with a square column stump at the base. The connections tested were bar couplers, grouted ducts, pockets, member sockets, hybrid, integral, and mechanical. A cast-in-place connection was also tested to establish the performance of the connections with respect to monolithic connections.

A pocket connection was designed using the same full-ductility design basis as the cast-in-place specimen to provide a direct comparison. This pocket connection incorporated the use of a single 18-in diameter, 16-gage steel corrugated pipe installed during the construction of the precast bent cap reinforcement cage with additional hoops placed at each end of the pocket to reinforce the pipe. The corrugated pipe acted as stay-in-place formwork housing the 16-#5 longitudinal column bars that extended above the column connecting into to the bent cap during placement and also served as the equivalent joint hoop reinforcement provided in the cast-in-place connection. A 1.5-in bedding layer was constructed using a steel collar with air vents and high-strength plastic shims to support the bent cap and attain the required thickness of the bedding layer. After the bent cap was placed on the column, normal-weight concrete with maximum nominal aggregates sizes limited to 1/3 the thickness of the bedding layer was used to cast the bedding layer and the pocket to complete the connection (Figure 2.13).

Testing was conducted by inverting the specimen and connecting to a roller and pin support providing a simply-supported experimental test setup (Figure 2.14). The loads were applied with a 220-kip horizontal actuator on one side of the column stump and a 165-kip vertical actuator at the end of the column stump. The test program consisted of

applying incremental lateral drift ratios up to failure to study the column and joint response.

Inspections after testing showed the specimen with the corrugated pipe developed fewer diagonal cracks in the joint region with smaller maximum cracks widths (0.009-in) compared to the cast-in-place specimen (0.025-in). Different crack patterns were noticed between the two specimens, with the corrugated pipe connection only developing cracks through the center of the of the joint region at 3.2% drift. The cast-in-place specimen developed more widespread diagonal cracks throughout the joint region. The different crack pattern and widths in the corrugated pipe specimen were evidence of a different loads path as a result of the corrugated pipes (Figure 2.15). Smaller strains at 25% yield were recorded in the stirrups in the joint for the corrugated pipe specimen compared to the full yield strains in the cast-in-place specimen. The supplementary hoops used at the ends of the corrugated pipe reached 52% of yield showing their contribution to the joint performance, and pipe strains were limited to 37% of yield. Both specimens showed failure due to buckling and fracture of columns bars with no signs of failure in the joint.

The results from testing showed that the pocket connection performance was satisfactory and demonstrated emulative behavior to the cast-in-place specimen. Both specimens showed similar joint shear stiffness, consistent strain patterns in bent cap longitudinal reinforcement, minor signs of bar slip, and integral behavior between the bedding layer, corrugated pipe, and bent cap. Construction recommendations included the use of sufficiently flowable concrete to fill the pocket and the bedding layer using an aggregate size of 1/3 the thickness of the bedding layer to fill all voids. Recommendations

also include a locked-seam helical corrugated pipe for the connection (ASTM A670) and high-density plastic shims to ensure proper transfer of loads and avoid hard spots in the bedding layer with limited total shim plan area of less than 10% and placed away from the exposed surface of the bedding layer.

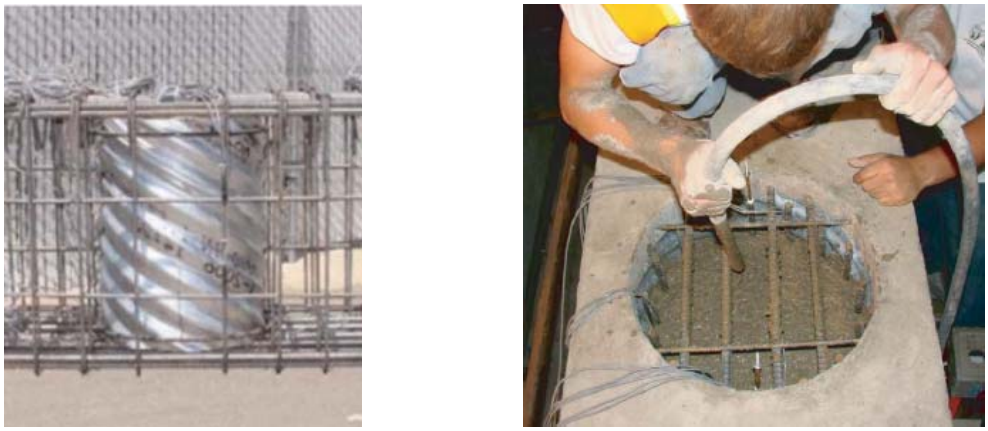

(a) Corrugated Pipe *(b) Casting*

Figure 2.13. Pocket Connection Construction (Restrepo et al., 2001).

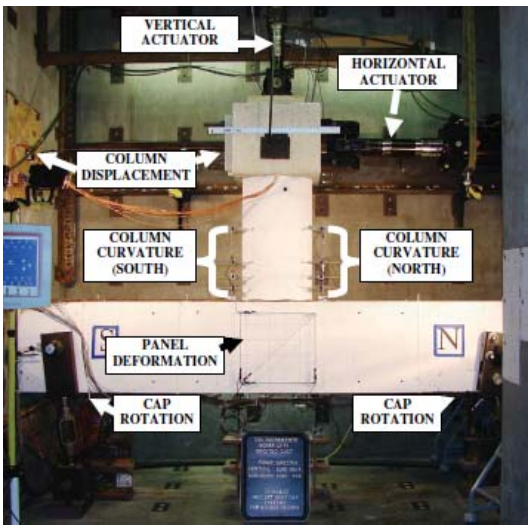

Figure 2.14. Experimental Test Setup (Restrepo et al., 2001).

(a) Cast-in-Place Specimen – East Side *(b) Corrugated Pipe Specimen– East Side*

Figure 2.15. Joint Region Post Test Damage Patterns (Restrepo et al., 2001).

Barooah (2016) studied precast prestressed bent cap connection designs to investigate an alternative to the current vertical grouted duct connection option used by TxDOT for their precast bent caps with circular columns previously developed by Matsumoto et al. (2001). The new connection design was requested by TxDOT officials to improve constructability and implement a grout-less connection. Barooah (2016) proposed incorporating a 21-in diameter 12-gage pipe pocket connection, based on the research by Restrepo et al. (2011). The pipe is installed during construction of the precast bent cap reinforcement cage and filled with regular TxDOT Class C concrete after installation of the precast bent cap. The pocket connection houses the 6-#11 dowel bars currently used by TxDOT to connect the bent cap to the columns. The size of the pocket was chosen to be as small as possible while still allowing practical column and dowel bar misalignments to enhance constructability (Figure 2.16). Discontinuities in stress flow from prestressing around the void created by the corrugated pipe were a concern when choosing the appropriate pipe thickness. The pipe thickness had to be large enough to resist the prestressing forces to allow uniform distribution of the stresses in the bent cap

without causing stress concentrations above the cracking moment at edges of the void in the bent cap. Joint shear was also analyzed in the determination of the pipe thickness to provide the equivalent transverse reinforcement at the joint. For constructability purposes, the largest pipe thickness readily available in the market without the need of special orders was recommended at 12-gage. The integration of a 21-in diameter corrugated pipe along the entire depth of the bent cap required the use of strands along the sides. The effects from a side configuration of strands were analyzed using fiber-section analysis. This indicated less than 5% decrease in nominal strength capacity when using the side configuration. Experimental verification was necessary to validate the successful implementation of the pocket connection in pretensioned bent caps.

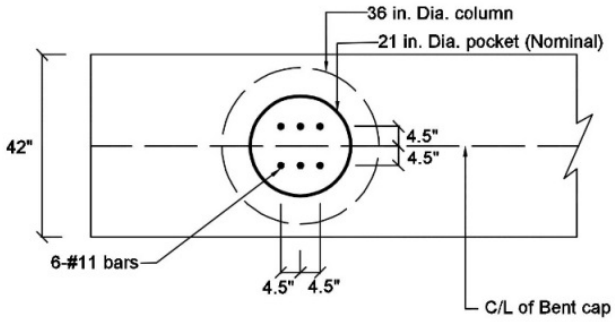

(a) Without Misalignment

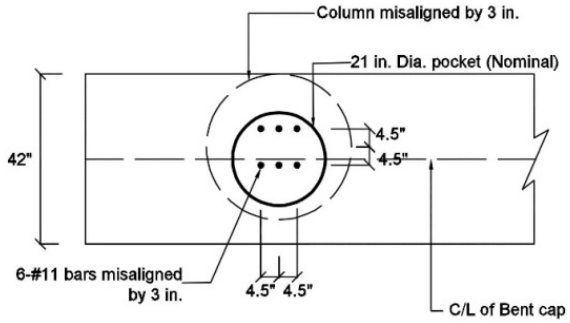

(b) With Misalignment

Figure 2.16. Proposed Pocket Connection with 6-#11 (Barooah, 2016).

2.2.3. *End Region Detailing*

Research has been conducted to investigate the amount of end region reinforcement necessary to resist splitting and bursting stresses from prestressing operations. O'Callaghan and Bayrak (2008) performed experimental tests on four full-scale Tx28 (2), Tx46 and Tx70 girder specimens to investigate cracking in the end regions of pretensioned I-girder beams and determine the necessary amount of end region reinforcement to resist bursting stresses present in the transfer length taken as 60 times the strand diameter. A pretensioning bed was built to construct the girders inside a laboratory (Figure 2.17). Strain gages were installed on the mild steel reinforcement and prestressing strands throughout the end of the beams to monitor the strain at release. Thermocouples were installed 5-ft from the end of the beam to measure the concrete curing temperatures. Prestressing strands, mild steel reinforcement and concrete materials representative of practical I-girder construction were used during the construction of the specimens (Figure 2.17.b). The provided end region reinforcement was designed by TxDOT based on AASHTO LRFD Bridge Design Specifications with limited strains 20-ksi within a distance equivalent to one-quarter of the member depth (D/4). A minimum concrete release strength of 6.5-ksi was used and slight variations of prestressing force within TxDOT code provisions were applied to investigate the effects during transfer. A total of four different regions were tested with varying sizes and patterns of the end region reinforcement based on previous field experience and practical amounts that would not hinder constructability, all within the TxDOT standards.

The maximum transfer stresses were recorded in the Tx28-II specimen at 32-ksi, which also showed the largest crack widths at 0.009-in (Figure 2.18). A higher prestressing force and lower concrete compressive strength at release for Tx28-II compared to Tx28-I resulted in the higher transverse rebar stresses. The Tx46 and Tx70 girders behaved similarly. Tx48 recorded maximum stresses of 22-ksi and cracks as wide as 0.007-in. Tx70 girder developed slightly higher stresses at 25-ksi with cracks also as wide as 0.007-in. Maximum temperatures between 102°F and 120°F were recorded, with the peak occurring close to 10-hours after the concrete was mixed.

The results showed the AASTHO provision for splitting resistance reinforcement at a distance of D/4 from the member end is only meant to handle the spalling stresses near the end of the beam, not the bursting stresses. The bursting stress showed to reach a maximum value within the transfer length and decrease quickly to nearly zero beyond the transfer length. Recommendations suggested bursting stress reinforcement be placed immediately after the splitting resistance reinforcement at D/4 to the transfer length.

(a) Prestressing Bed *(b) Casting*

Figure 2.17. Specimen Construction (O'Callaghan and Bayrak, 2008).

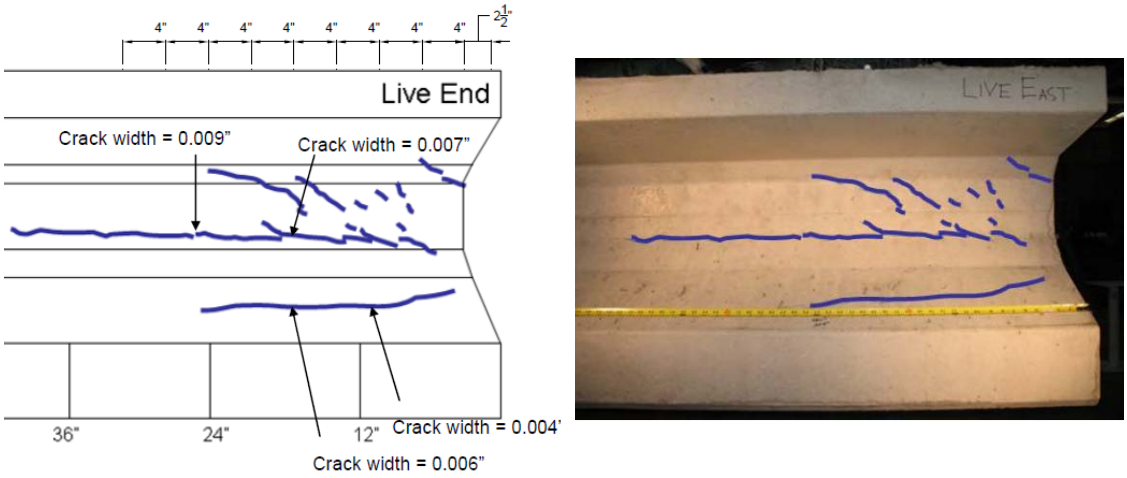

(a) Crack Width Map *(b) Crack Pattern Photo*

Figure 2.18. Tx28-II Performance (O'Callaghan and Bayrak, 2008).

In TxDOT Project 0-5831-3, Avendaño et al. (2013) conducted experiments to study bursting stresses at the time of prestress transfer and also investigated the shear capacity of box beams as an alternative to I-girder beams. Different variables were investigated such as concrete mixtures, aggregates, beam end geometries, and skewed end internal void geometry. A total of ten 30-ft long 5B40 box beams were tested. The largest possible number of prestressing strands, 76, was used to maximize the effects of bursting stresses. Target concrete strengths for strand release were between 6400-psi and 7100-psi. Emphasis was given to the box beam end block reinforcement details to improve the constructability and proportion the reinforcement to minimize cracks widths occurring at the transfer of prestressing forces. End region detailing for the first phase of box beam tests followed the TxDOT standards and also used additional #5 bars (Bars E) with 90-degree hooks installed in the 1-ft 4-in minimum thick end blocks above the strands. The additional bars were requested by TxDOT engineers to address problems observed

during previous fabrications stages in heavily prestressed beams (Figure 2.19). The second phase of testing provided improvements to the end region detailing based on the results of Phase 1 tests which included additional transverse reinforcement (Bars MT and MB) in the box beam end block (Figure 2.20). Thermocouples recorded the curing temperatures and the strain gages monitored the release stresses in the mild steel reinforcement.

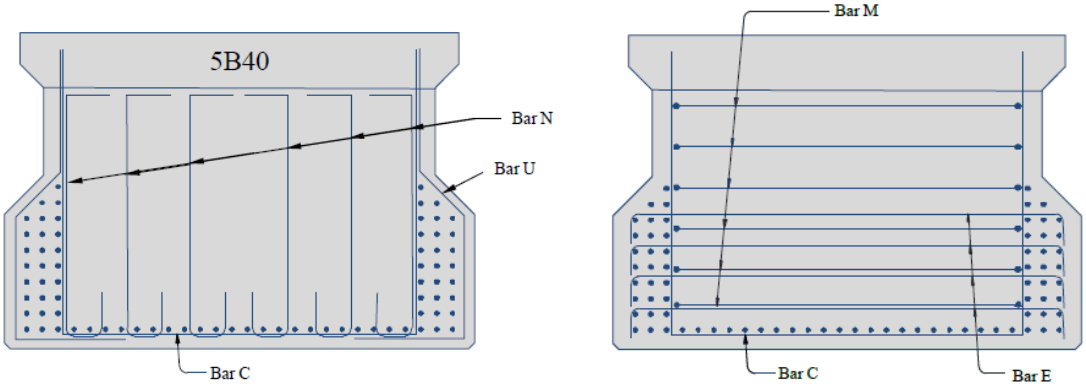

(a) Vertical Reinforcement *(b) Horizontal Reinforcement*

Figure 2.19. 5B40-2 Phase 1 First Curtain End Region Detailing (Avendaño, 2013).

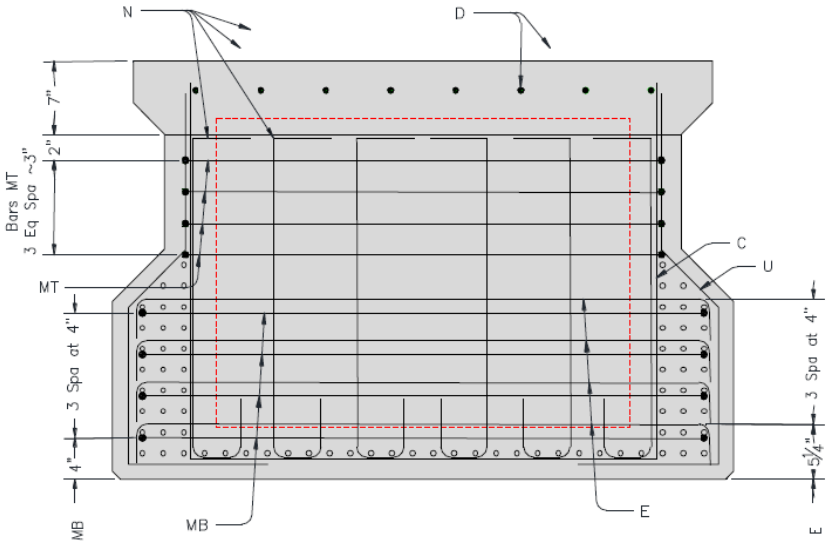

Figure 2.20. 5B40-4 Phase 2 First Curtain End Region Detailing (Avendaño, 2013).

Cracks widths of 0.007-in to 0.009-in were commonly observed with some measuring up to 0.016-in at the release of strands. Stresses were recorded up to 30-ksi in the beams without the new design recommendation and were 10-ksi above the AASHTO LRFD 2010 limits for transfer stresses in the end region reinforcement at D/4 (Figure 2.21.a). The additional box beam end block transverse reinforcement was effective in lowering the stresses in the end region reinforcement below the 20-ksi limit during the release of strands (Figure 2.21.b). The TxDOT maximum allowable temperatures (170 °F) were not reached in the specimens during curing. Although these temperatures results could have been due to mild ambient temperatures near 88 °F, benefits were seen in using fly ash to reduce the concerns with high curing temperatures (maximum recorded 155°F). Both Avendaño et al. (2013) and O'Callaghan and Bayrak (2008) recommended that bursting stress reinforcement be placed immediately after the splitting resistance reinforcement at D/4 starting from the member end.

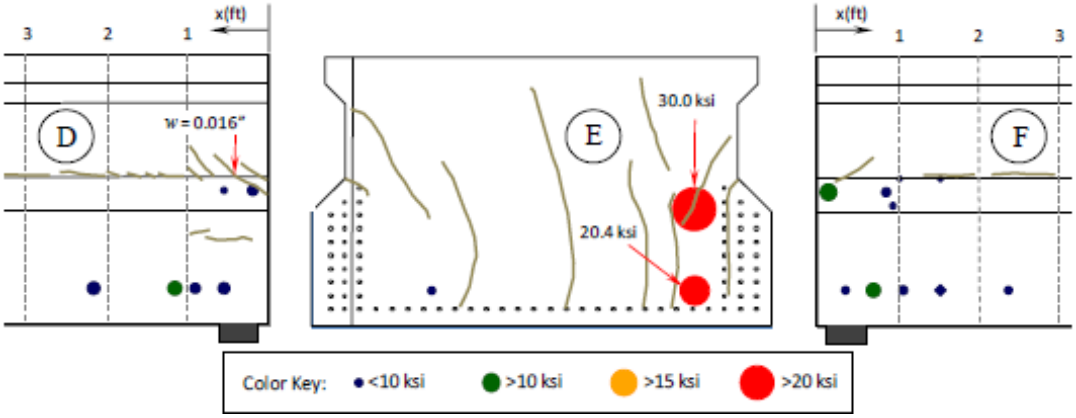

(a) Specimen 5B40-2
(No Additional End Region Reinforcement)

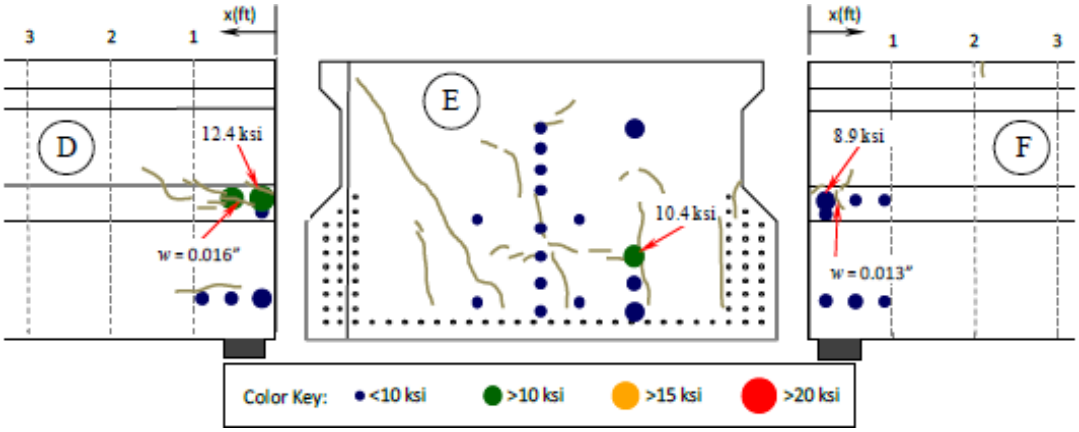

(a) Specimen 5B40-4
(With Additional End Region Reinforcement)

Figure 2.21. Cracks and Stresses at Prestress Transfer (Avendaño, 2013).

Ross et al. (2014) tested two 63-in deep Florida I-beams (FIB-63) to investigate the end region splitting cracks in the web due to vertical tensile stresses created during the distribution of prestressed forces at transfer. Load testing was also conducted after 112 days of crack inspections to study the effects of different detailing on the end region capacity. The beams were 49.5-ft long with a total of 52 strands providing a total initial

prestressing force of 2280 kips. Each girder end was detailed differently. The control specimen end (CT) purposely exceeded the area of splitting reinforcement and the opposite end specimen had the same amount of end-region reinforcement but with 23 partially shielded strands (SL). The second girder included vertical post-tensioning installed within the transfer length at both ends with total end region reinforcement areas (including post-tensioning bars) above and below the CT specimen for individual end respectively.

The specimens were constructed at a prestressing yard on a Friday and the strands were released the following Monday during the month of February. A concrete release strength of 7.32-ksi was recorded, higher than the required 6.5-ksi release strength. The higher release strength was attributed to the longer than usual time between the casting and transfer of prestressing for precast concrete plants. Flame cutting was used to release the strands at the same time between and at the ends of the girders with a release pattern typical of precast concrete girder in Florida. The girders were moved one day after prestressing transfer to the storage yard with the use of a crane and trucked to the lab for testing after approximately 3 months in storage to allow for all necessary crack observations.

The web cracks were monitored during prestress transfer and at 1, 30 and 120 days after transfer (Figure 2.22). Cracks were first observed at both the CT and SL ends. Throughout crack monitoring, the widest cracks were usually near the specimen ends. The largest cracks in all specimens were less than 0.012-in wide, which is the required treatment width specified by the Florida Department of Transportation for non-aggressive

environments. The CT was the least effective in controlling web-splitting cracks with the largest length and average crack widths measured in all specimens. The SL specimen was the most effective, showing 45% less web crack area and 22% smaller average cracks than the CT specimen. Results from load testing concluded that although that strand shielding was an effective way of controlling web-splitting cracks, it was the cause of bond shear failure because of insufficient fully bonded strands resulting in the lowest ultimate capacity of any specimen.

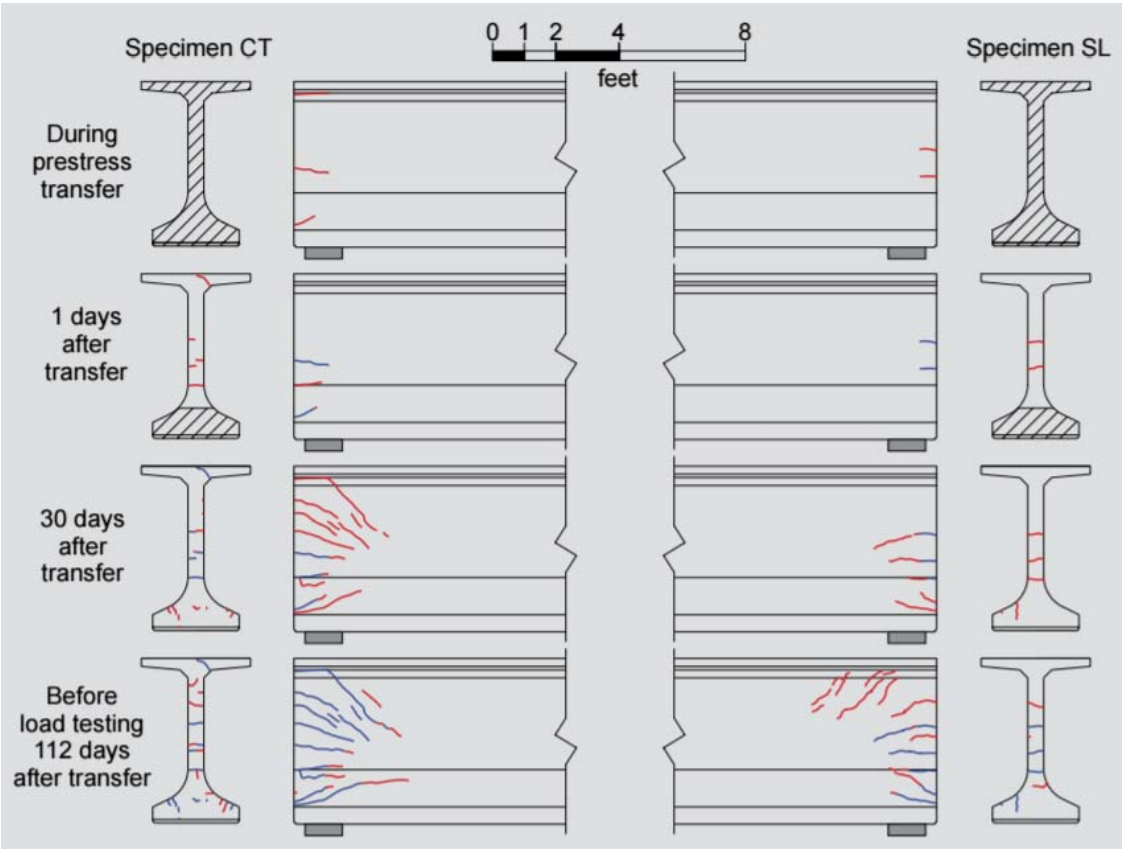

Figure 2.22. Crack Growth (Ross et al, 2014).

Okumus et al. 2012 performed nonlinear finite element analysis to create accurate modeling procedures for future methods to control cracking at the ends of girders during prestress force transfer. The nonlinear finite element modeling was first verified by recreating the stress and strains reported from previous tests. The accuracy of the finite element analysis relied heavily on verifications of input parameters such as concrete material behavior before and after cracking, concrete-steel and concrete-strand bond, prestress transfer length and bond distribution. These parameters were verified by comparing results gathered from previous tests by O'Callaghan and Bayrak (2008).

Reactions in concrete using nonlinear material properties showed less error than linear finite element analysis since elastic material models fail to recognize the stiffness loss in concrete after cracking and subsequent crack growth (Figure 2.23). The concrete-steel interaction was modeled using tension softening only in the concrete and tension stiffening was added to the concrete by the rebar once the concrete cracked. The tensioning softening was recreated by calculating the fracture energy which showed a small error of 7% in predicting the highest stresses in the rebar from tests by O'Callaghan and Bayrak (2008). The fracture energy approach showed to be directly related to tension softening and was implemented to establish the crack opening behavior instead of a stress-strain relationship. The prestress transfer was verified using bond stresses and transfer lengths also measured by O'Callaghan and Bayrak (2008) and showed lesser total average error (15%) than the assumed uniform bond stresses used by AASHTO LRFD specifications and assumed linear bond stresses over the transfer length. After the input parameters were verified, the modeling was used to resemble previous Wisconsin girder

tests that showed higher levels of cracking. Full field tensile strains were developed to evaluate the stresses in the concrete and the efficiency of end region reinforcing bars in controlling cracking at the transfer of prestressing forces.

The results from the nonlinear finite element models matched the positions and directions of the plastic strains observed in the girder tests. The comparison of the models with the girder tests provided an accurate depiction of the intricate stress and strain in the transfer length at the ends of girders (Figure 2.24) and could be used to effectively investigate future methods to eliminate or control cracking from prestressing transfer forces.

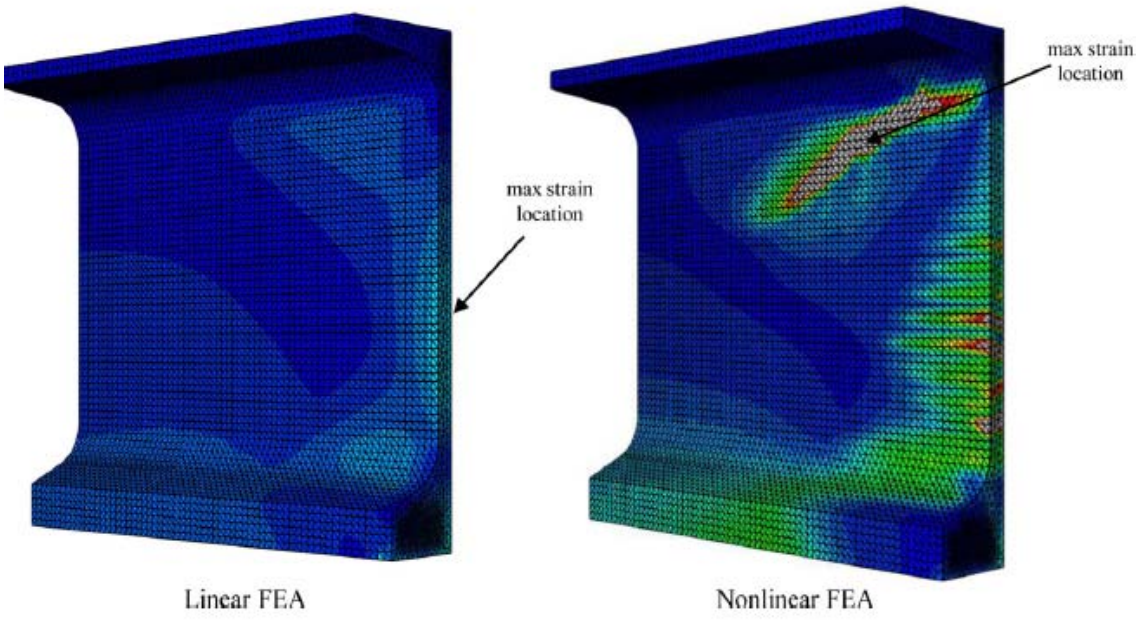

Figure 2.23. Principal Tensile Strain Comparison (Okumus et al., 2012).

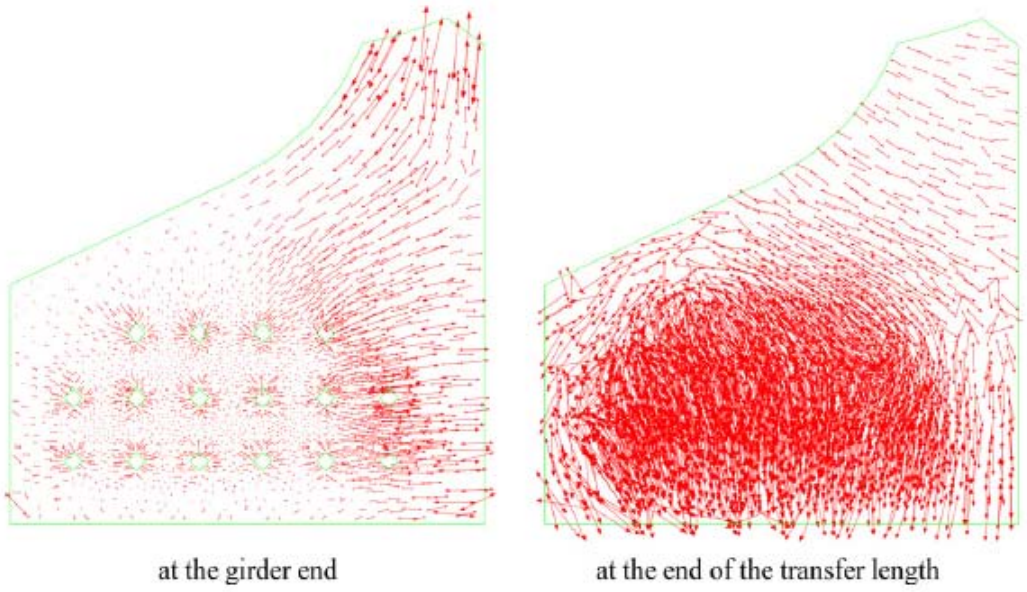

Figure 2.24. Tensile Strains at Bottom Flange Cross-Section (Okumus et al., 2012).

Barooah (2016) proposed end region detailing recommendations to control cracking from the transfer of prestressing forces during the release in precast pretensioned concrete bent caps. The recommendations were made taking into the consideration the spalling reinforcement from the AASTHO LRFD 5.10.10.1 in addition to implementing designs developed by O'Callaghan and Bayrak (2008). These recommendations were analyzed for a TxDOT 42-in square bent cap typical of 32-ft wide roadways used for non-skewed I-girder with a bent cap span length of 80-ft. A total distance of 37.5-in was available to place the end region reinforcement taking into consideration the proposed 21-in diameter corrugated pipe pocket connection at the exterior column. The end region details included bursting reinforcement immediately after spalling reinforcement based on AASHTO LRFD from D/4 to the transfer length. The reinforcement layout consisted of

individual #5 bars placed up to D/4 for the spalling reinforcement and additional #5 bars used for the bursting reinforcement up to the transfer length (Figure 2.25).

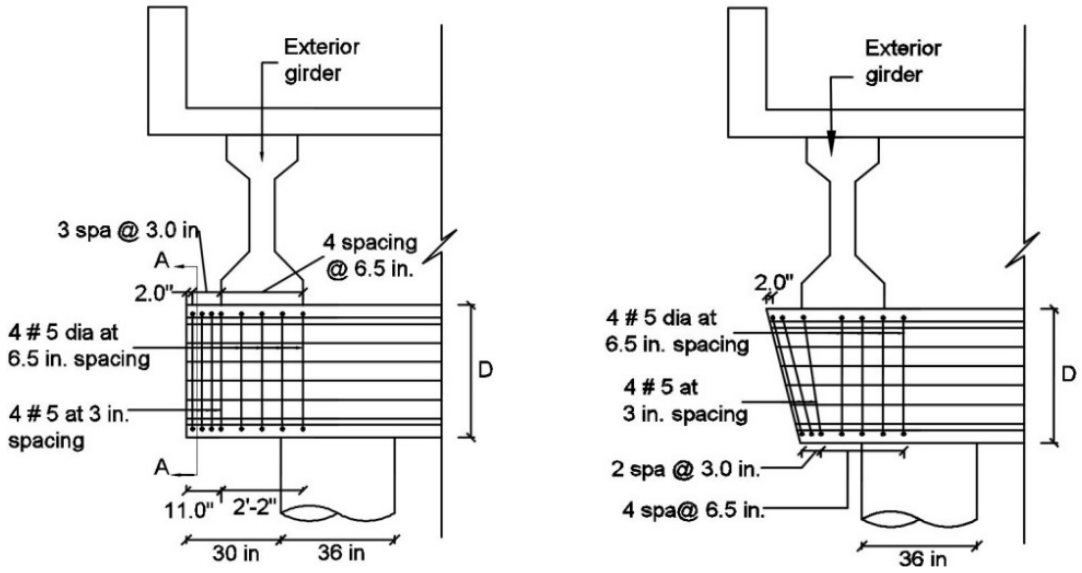

Figure 2.25. Proposed End Region Detailing Recommendations (Barooah, 2006).

2.3. State-of-the-Practice

TxDOT currently uses a Class C concrete with a minimum compressive strength of 3.6-ksi and Grade 60 reinforcing steel for the constructions of reinforced concrete bent caps (cast-in-place and precast). The widths of the cross-sections for the bent caps are required to be at least 6-in wider than the columns. For Tx62 I-girder bridges, the required column diameter is 42-in and the bent cap square cross-section is 48-in. All other I-girder bridges require a 36-in column and a 42-in bent cap.

The loads used to design the bent caps are in accordance with AASHTO LRFD Bridge Design Specifications for Strength I and Service I limits states. The load analysis

is performed using an in-house bent cap analysis program CAP 18, which calculates the demands for dead, live and factored ultimate loads. TxDOT models the bent caps as a continuous beam with simply supported connections at the columns neglecting frame action. Limits for tensile stresses at Service I load combinations are 60% of the yield stress in the tensile reinforcement. Typical reinforcement is #11 bars (A-bars) for longitudinal reinforcement and #5 bars (S-bars) for shear reinforcement. The column reinforcement is typically constructed with #9 bars (V-bars) for longitudinal reinforcement and #4 bars (Z-bars) for the spiral reinforcement having a 3-in pitch with one and a half turns at the top and bottom. Covers are 2-in for the bent cap and 3-in for the column measured from the outside edge of the shear and spiral reinforcement, respectively. Detailed construction plans for all TxDOT I-girder bridges can be found in the Bridge Division Project CAD Standards.

A monolithic connection option is available for bent caps that consists of extending the column longitudinal reinforcement a minimum distance of 2-ft 8-in into the bent cap. TxDOT also provides a grouted vertical duct connection option for precast reinforced concrete bent caps. The current standard detail in the TxDOT Bridge Standards for the grouted vertical duct connection is shown in Figure 2.26. The column longitudinal bars terminate at the top of the column and dowel bars are embedded into the core of the column and extend above the column. A bedding layer thickness of 1.5-in to 4-in is required between the column and the bent cap. The bedding layer is constructed using plastic shims limited to 6% of the column surface area or frictions collar to support the bent cap at the proper elevation before grouting. When the precast cap is installed, the dowel bars are fed

into individual corrugated ducts and filled with grout along with the bedding layer to complete the connection. Prior to grouting, all surfaces in contact with the grout must be cleaned and saturated to surface-dry conditions.

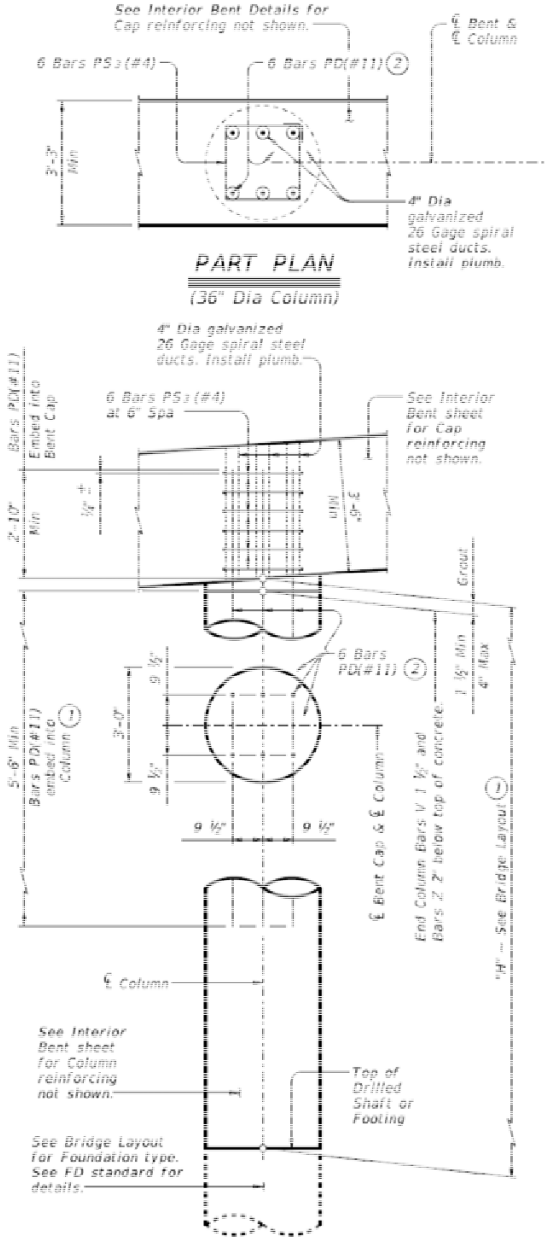

Figure 2.26. Precast Conc. Bent Cap Option for 36-in Dia. Round Columns (TxDOT Bridge Standards, 2016).

2.4. Research Questions Arising from Literature Review

The following questions arise based on the foregoing discussion of state-of-the-art and state-of-the-practice:

- ***What is the performance of current TxDOT bridge bent cap configurations in a test setup creating demands representative of multi-column bent caps in the field in order to adequately develop pretensioned I-girder bent cap standard details?***

  Most of the studies conducted on bent caps were limited to negative moment demands and the shear-moment demand ratios did not accurately reflect those in current TxDOT bent caps. Furthermore, other testing has been performed on large-scale or full-scale bents caps to evaluate the performance of connections but did not test the bent caps to failure. These previous shortcomings will be addressed in this research.

- ***Can the strength and serviceability of pretensioned bent caps prove greater than reinforced concrete bent caps?***

  Extensive research has been conducted in the field of reinforced concrete bent caps while studies in the area of pretensioned bent caps have not been performed. Thus, the benefits of pretensioned bent caps have yet to be investigated by TxDOT. This research will permit TxDOT to determine the enhancements in strength and serviceability of pretensioned bent caps.

- ***How would a pocket connection with normal-weight concrete perform compared to the current grouted vertical duct connection between precast bent caps and round columns?***

  The vertical grouted ducts connection alternative for precast bent caps for round columns has shown to have many issues with constructability with the use of grout. This research will conduct experimental testing that will eliminate the need for grout and provide sufficient joint shear reinforcement for precast bent caps.

- ***How would a pocket connection perform on pretensioned bent caps for standard TxDOT bridges?***

  This research will investigate the design and performance of a pocket connection that can resist the effects from prestressing forces in pretensioned bent caps.

- ***Can the end-region detailing recommendations by O'Callaghan and Bayrak (2008) be effective in controlling cracks during the transfer of prestress forces in pretensioned bent caps?***

  Previous studies performed on end region detailing to control cracks during the transfer of prestress forces are mostly limited to girders and U-beams. This research will investigate the effects of the recommendations by O'Callaghan and Bayrak (2008) when implemented on pretensioned bent caps.

3. EXPERIMENTAL TEST PROGRAM

The experimental test program sought to test full-scale sub-assemblages representative of TxDOT standard I-girder bent cap bridges (up to Tx-54) in order to show the benefits of pretensioned bent caps in comparison to the current TxDOT standard precast reinforced concrete bent caps. The objectives were to validate the proposed design procedure, assess performance at the service limit state (SLS) and the ultimate limit state (ULS) demands, and test the bent caps to their respective maximum capacity.

Section 3.1 presents an overview of the test program. Section 3.2 contains the design of specimens including flexure, shear, end region detailing, and pocket connection design. Section 3.3 discusses the test matrix and geometry of the specimens. Section 3.4 presents the construction of the specimens. Section 3.5 discusses the experimental setup constructed in the Texas A&M University High Bay Structural and Materials Testing Laboratory. Section 3.6 presents the instrumentation plans. Section 3.7 presents the results of the material property tests. Section 3.8 discusses the expected strengths.

3.1. Overview

The objective of the experimental test program was to investigate the performance of full-scale precast bent caps under realistic loading conditions. Bents for standard I-girder bridges in Texas have three or four columns, creating an indeterminate structure with negative moments at columns and positive moments in the spans. Although design demands are established from beams on “knife edge” supports, the column stiffness influences the demands in an actual bent and the beam-column connection must provide

sufficient strength for transfer of moment from the beam to the column. Figure 3.1 shows the shear and moment diagrams for a three-column bent with four girders. The experimental test setup must accurately simulate these demands in order to study the performance of bent caps.

Previous experimental studies of reinforced bent caps (both cast-in-place and precast) have utilized a sub-assemblage that consists of a single column with the bent cap cantilevered from both sides. A major shortcoming of these is that the demands were limited to negative moment demands and the shear-moment demand ratios did not accurately reflect those in bents. Additionally, other experiments have tested large-scale or full-scale bents to assess the performance of connections but did not test the bent caps to failure.

The test setup in this study was intended to address the shortcomings of previous research while testing full-scale components to capacity. To accomplish this, the test specimens were designed as a subassembly of a full bent cap consisting of the bent cap from the overhang to the second inflection point in the first span, and the column from the bent cap to the inflection point. This region, indicated by a blue dashed oval in Figure 3.1, allowed for experimental evaluation of the performance under positive and negative moment demands and the transfer of forces from the bent cap to the column; the red dots indicate the moment inflection points. Figure 3.2 shows a schematic of the subassembly and the shear and moment demands produced by the loads.

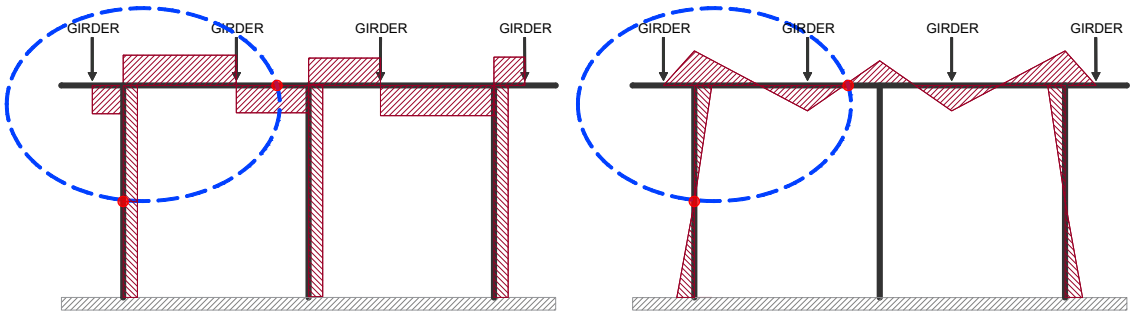

(a) Shear *(b) Moment*

Figure 3.1. Prototype Demands

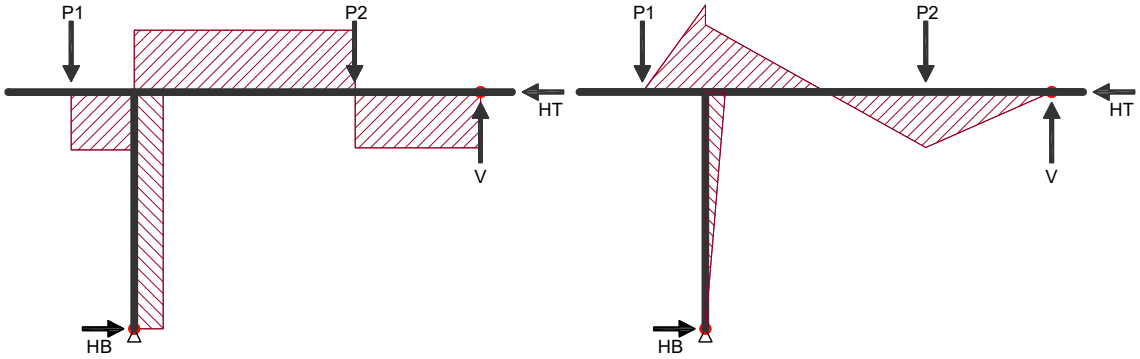

(a) Shear *(b) Moment*

Figure 3.2. Specimen Demands

Loads were introduced to the bent cap via two actuators (P1 and P2) simulating girder demands. A pin provided the necessary shear and axial reactions at the base of the column. At the right side of the specimen (referred to as the "square end"), a vertical actuator (V) and a horizontal actuator (HT) were controlled with specified forces and/or displacements to achieve the desired outcome (realistic bent demands or maximize positive or negative moment to fail the specimen). To realistically simulate the behavior of a bridge bent, the HT actuator was locked at zero horizontal displacements. The V

actuator force was specified to generate the desired shear at the inflection point. Vertical displacement was present but small at this inflection point.

The subassembly size and component strengths were controlled by limitations of the Texas A&M University High Bay Structural and Materials Testing Laboratory: 1) overhead crane capacity of 20 tons, 2) 3-ft grid for anchoring reaction towers and connection plates, 3) clearance below header beams supporting P1 and P2 actuators, 4) 600-kip capacity for the vertical actuators (P1, P2, and V), and 5) 110-kip capacity of the horizontal actuators (HT and HB). The desired prototype bridge was a standard, non-skewed I-girder bridge with girders up to Tx54. Such a bridge has 3-ft diameter columns, a 42-in square bent cap, an overhang with a battered end extending 4-ft from the center of the exterior column, and the first girder located 2-ft from the column centerline.

Given these constraints, the subassembly geometry shown in Figure 3.3 was selected. The bent cap in the subassembly was 16-ft long with a 42-in square cross-section. The P1 and P2 actuators simulating girder demands were spaced 9-ft apart. A subassembly column height of 8-ft from the base to the center of the bent cap was selected by balancing the needs of demands and clearance and can be considered a reasonable inflection point in standard bridge bent columns.

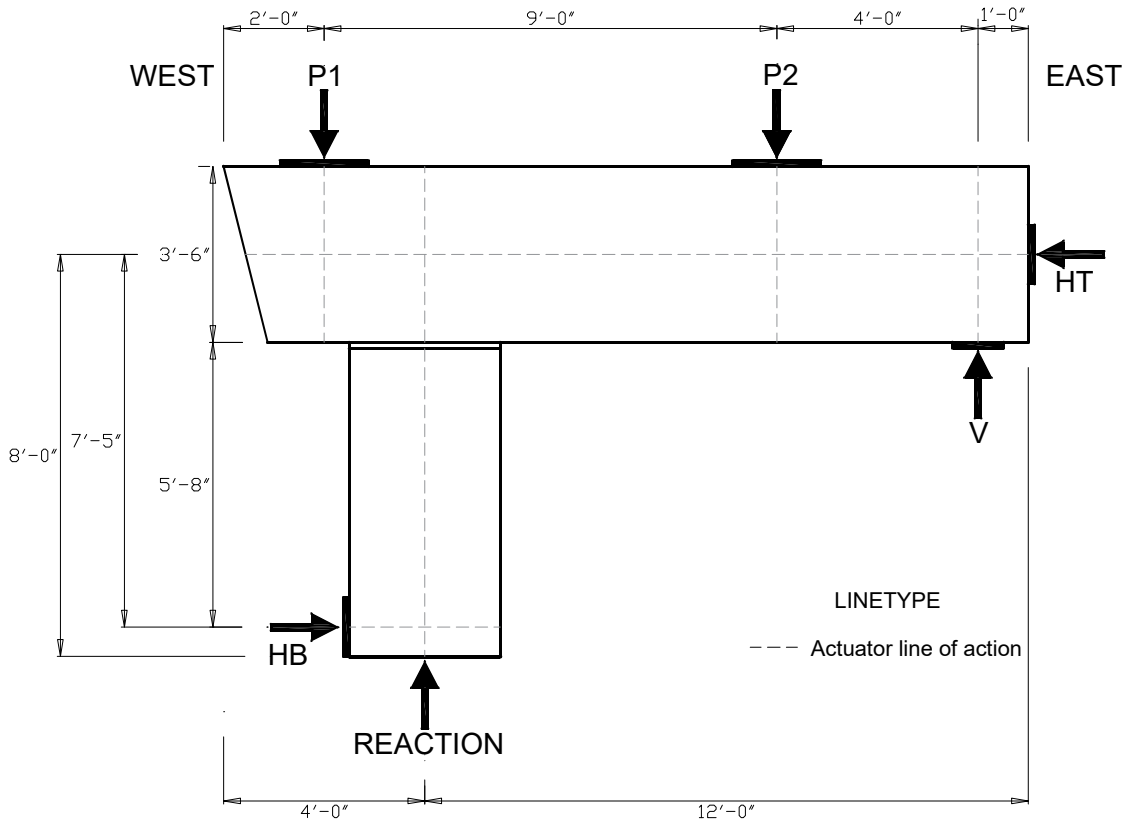

Figure 3.3. Elevation View of the Specimen

The subassembly geometry did not correlate perfectly with a standard I-girder bridge bent that could be used as a prototype, but closely resembled BIG32 (32-ft wide) and BIG40 (40-ft wide) bents. Thus, these two bridges were used as prototypes for designing the specimens and establishing dead, SLS, and ULS demands. Table 3.1 summarizes the characteristics of these prototype bents. The following section discusses the design of the test specimens, including establishing average span length of these prototypes.

Table 3.1. Prototype Bridges – BIG 32 and BIG 40

Prototype Bridges	BIG 32	BIG 40
Length (ft)	32	40
Height (in)	42	42
Width (in)	42	42
Girder Types	Tx28 - Tx54	Tx28 - Tx54
Number of Girders	4	5
Girder Spacing (ft)	9.3	9
Column Diameter (ft)	3	3
Number of Columns	3	3
Column Spacing (ft)	12	16

3.2. Design

The design of the test specimens did not follow a traditional design procedure that would be used for the design of bridge bents. Instead, it was necessary to ensure that the specimen expected capacity could be reached. To this end, selection of the flexural reinforcement was the first step in design and is described in Section 3.2.1. From the selected flexural reinforcement, the demands for a prototype bridge were identified such that the proposed design objective (zero tension stresses under dead load) could be evaluated. Section 3.2.2 summarizes the prototype bridge that was identified to result in the flexural design used. Section 3.2.3 presents the shear design for the bent cap spans. Detailing of the end regions and connections are presented in Sections 3.2.4 and 3.2.5, respectively.

3.2.1. *Flexural Design*

The flexural design of the specimens was governed by the maximum demands that could be created with the test setup (1925 k-ft). The first concern was achieving demands greater than the cracking moments (M_{cr}). The pretensioned members, by design, have a higher

concrete strength than reinforced concrete members resulting in a higher cracking moment. Preliminary calculations for a 42-in square section with 6-ksi concrete (typical of TxDOT pretensioned members) with 16 strands resulted in a cracking moment of 933 kip-ft and was considered appropriate for the capabilities of the test setup.

The next consideration was achieving demands greater than nominal strengths to test the full capacity of the specimens. A side configuration of strands was chosen in order to avoid interference between flexural reinforcement and the pocket connection. To allow comparison of the overall performance of pretensioned bent caps to reinforced concrete bent caps, a reinforced (RC) prototype was designed to have the same steel configuration and similar strength to the pretensioned prototype, leading to the use of 16-#8 bars. Figure 3.4 shows the RC cross-section. The layout of the bars was identical to the strand layout for the pretensioned section; this deviates slightly from the cover used in standard TxDOT designs. A preliminary calculation of ultimate strength of the reinforced and pretensioned concrete section showed 1162 k-ft and 1379 k-ft, respectively. Both values were considered appropriate for the capabilities of the test setup.

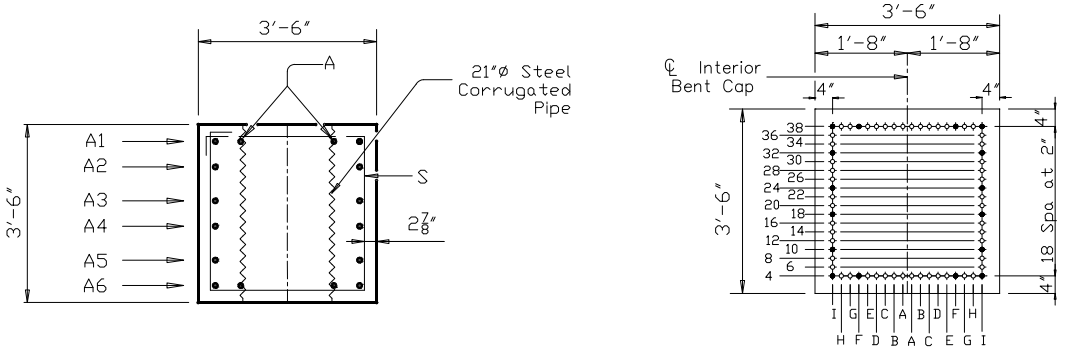

(a) Mild Steel Locations *(b) Standard Strand Layout*

Figure 3.4. Flexural Rebar Pattern.

3.2.2. *Prototype Selection*

Having established a flexural design, it was necessary to identify a prototype bridge(s) that would result in the selected design. For the section designed, the moment for zero tension is 328 kip-ft. This established the selection criterion for the prototype bridge; the pretensioned bent cap should have a maximum flexural demand under dead load of 328 kip-ft.

From a preliminary study of the bent configuration in the TxDOT bridge inventory with I-girders, the 32-ft and 40-ft roadway width bridges were observed to be a close representation of the specimen that could be built in the laboratory. An iterative analysis of the bridge with different span lengths was done in CAP18 (CAP18 Version 6.2.2) to find the span length producing these demands. The maximum dead load moment for a 66-ft span is very close to the required moment. Thus, both prototypes with 66-ft span lengths were selected as the prototype bridge to use for shear design; the configuration is shown in Figure 3.5. Maximum ultimate limit state (ULS) demands of both 32-ft and 40-ft roadway width bridges are -768 k-ft (at overhang) and 1003 k-ft (at span between columns), respectively, and do not the exceed moment capacity of the specimens or test setup capabilities.

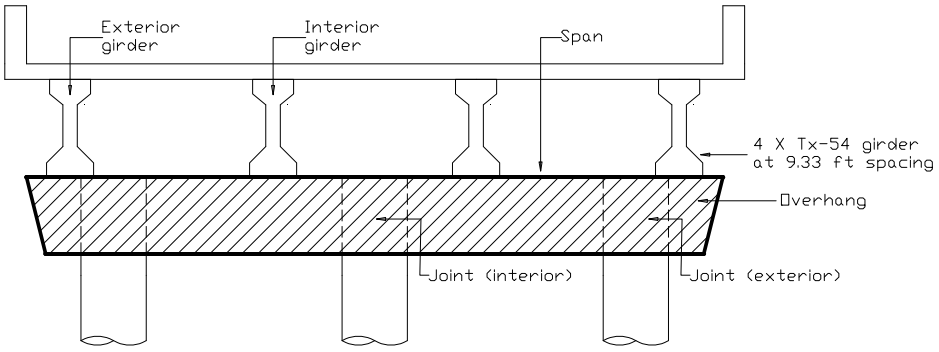

(a) BIG 32

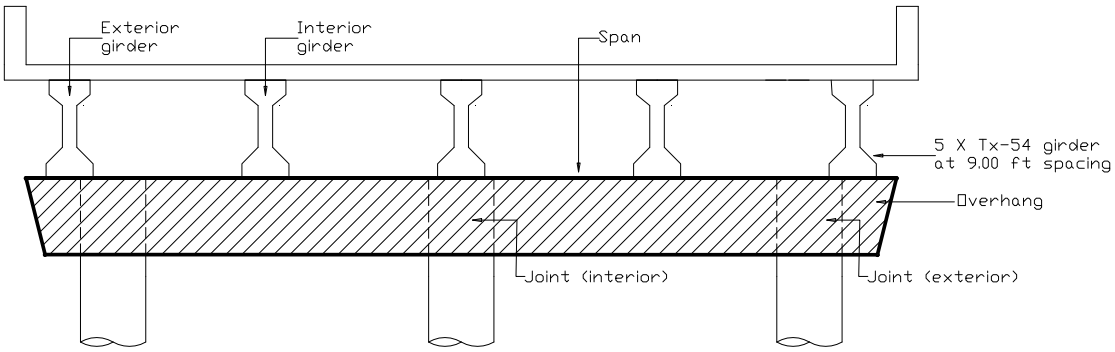

(b) BIG 40

Figure 3.5. Prototype Bridge Configurations

3.2.3. *Shear Design*

The shear design of the specimens was in accordance with Appendix B5 of the AASHTO LRFD Bridge Design Specification (2014). According to AASHTO LRFD, the sectional design method is appropriate for the design of components where the assumptions of beam theory are valid. For this reason, the shear design is conducted only in the spans between columns. Transverse reinforcement in the overhang is discussed in Section 3.2.4.

AASHTO LRFD shear design requires both moment and shear demands (M_u and V_u) to evaluate shear strength of the section. Demands from both prototype bridges were considered. Three points where shear and moment demands are significantly higher than

other locations were selected as critical locations, and those are near column faces and girder locations in both prototypes. Table 3.2 summarizes the shear and moment demands from CAP18 at three critical locations in the spans of the bent caps.

Table 3.2. ULS Demands Bridge Prototypes

	Critical 1		Critical 2		Critical 3	
Prototype	M_u (k-ft)	V_u (kips)	M_u (k-ft)	V_u (kips)	M_u (k-ft)	V_u (kips)
BIG 32	587	123	467	253	542	261
BIG 40	902	215	1004	39	673	195

Key values needed for design are summarized in Table 3.3. The first column ($V_u > \phi V_c$) indicates if the demand exceeds the capacity provided by the concrete, that is, is shear reinforcement needed to provide strength. The second value, s_{design}, is the spacing by design following the AASHTO provisions. The third value, $s_{strength}$, is the spacing that would be required to provide the necessary strength, ignoring any requirements on minimum area of steel or maximum spacing limits.

Table 3.3. Summary of Shear Design

Prototype	Critical 1		Critical 2		Critical 3	
	11.5-ft from overhang		12.0-ft from overhang		5.5-ft from overhang	
	M_u	V_u	M_u	V_u	M_u	V_u
	(k-ft)	(kips)	(k-ft)	(kips)	(k-ft)	(kips)
BIG 32	587	123	467	253	542	261
BIG 40	902	215	1,004	39	673	195

s_{design} = spacing satisfying all minimum spacing requirement in AASHTO LRFD specification including minimum area of steel (AASHTO 5.8.2.5) and maximum spacing of transverse reinforcement (AASHTO 5.8.2.7).

$s_{strength}$ = required spacing to resist demands without considering minimum area of steel and maximum spacing of transverse reinforcement.

By design, the reinforced concrete and pretensioned bent caps require 14-in and 11-in transverse reinforcement spacing, respectively, for both prototype bridges. TxDOT uses a maximum spacing of 12-in, which would lead to a revision of the reinforced concrete design. For simplicity, reinforced concrete and pretensioned prototype designs are designed to have a 12-in spacing. These designs highlight a shortcoming of the AASHTO design procedures, which is that it does not reflect the fact that prestressing improves shear resistance (Collins et al. (1986) and Runzell et al. (2007)). The design spacing for the prototype bridges is governed by the requirements for the minimum area of steel. AASHTO requirements for the minimum area of steel are dependent on the concrete compressive strength. The design concrete strength is higher in pretensioned bent caps (6-ksi) than in reinforced concrete bent caps (3.6-ksi), leading to the smaller spacing for the same area of steel.

As an alternative to the design spacing, the spacing needed to only provide adequate strength for the section was considered. When the minimum area requirements are ignored, the spacing of the transverse reinforcement for the pretensioned bent cap

increases dramatically, requiring 24-in for one prototype, while the other, theoretically, has sufficient strength from the concrete alone and does not require shear reinforcement. While a design with no transverse reinforcement or 24-in spacing would not meet design requirements in a TxDOT bridge, they were considered in establishing the experimental test matrix (see Section 3.3).

For simplicity, the transverse reinforcement was not varied along the spans. Two legs of #5 reinforcing bars were used as transverse reinforcement. In the reinforced concrete bent cap, S-bars were made of one continuous bar (Figure 3.6.a); however, S-bars in the pretensioned bent caps consisted of two separate cuts of rebar (Figure 3.6.b), similar to U-shaped rebar, tied together to form a closed hoop to accommodate the prestressing bed construction methods preferred by most precasters.

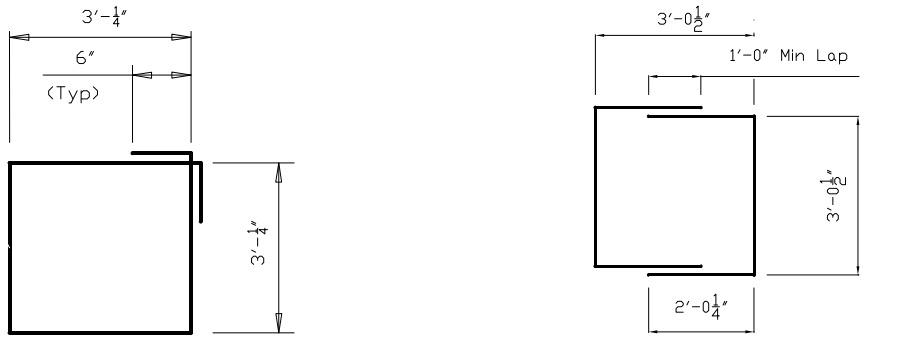

(a) Reinforced Concrete *(b) Pretensioned Concrete*

Figure 3.6. S-bar Transverse Reinforcement Configurations

3.2.4. *End Region Detailing*

The end region detailing for the pretensioned bent caps took into the consideration the spalling reinforcement design considerations from AASTHO LRFD 5.10.10.1 and the

recommendations by O'Callaghan and Bayrak (2008) to include bursting reinforcement immediately after spalling reinforcement from D/4 to the transfer length of 60 strand diameters as defined by AASHTO LRFD 5.11.4.1. Individual C-bars (#5 bars) were used at D/4 for the spalling reinforcement. C-bar and S-bar pairs were used for the bursting reinforcement up to the transfer length (Figure 3.7).

The end region detailing for the battered end of the pretensioned beams consisted of one U-bar placed parallel to the battered end face, two C-bars for the spalling and shear reinforcement up to D/4 with four pairs of S-bars and C-bars for bursting forces and shear reinforcement up to the transfer length of the prestressing steel. The end region detailing for the square end consisted of pairs S-bars and C-bars for the spalling reinforcement up to D/4 and equal reinforcement as the battered end for the bursting and shear reinforcement up to transfer length.

For the reinforced concrete bent cap, similar layouts for the end region detailing were designed to have a viable comparison between the reinforced concrete and pretensioned concrete models and did not follow current TxDOT standards. The end region detailing for the reinforced concrete specimen used S-bars consisting of single pieces of rebar forming the closed hoop and did not incorporate any C-bars (Figure 3.8).

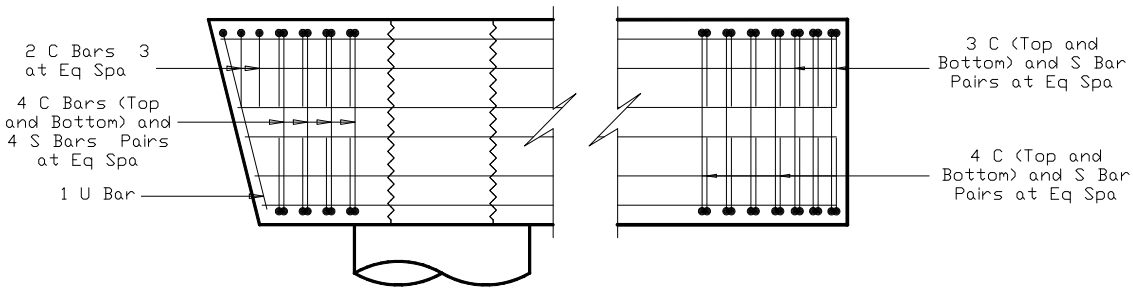

(a) Battered End *(b) Square End*

Figure 3.7. Pretensioned Specimens End Region Detailing.

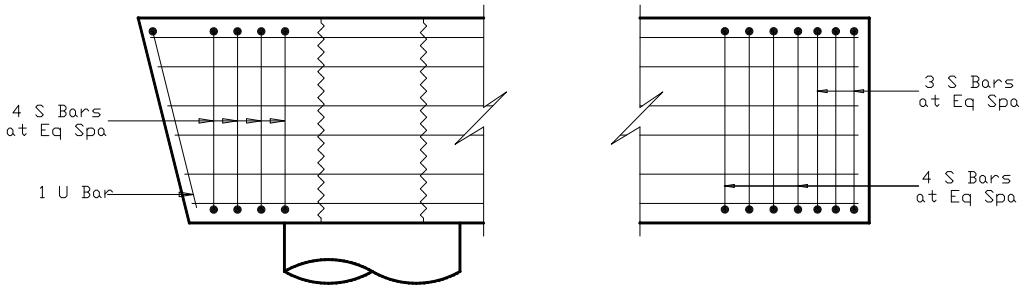

(a) Battered End *(b) Square End*

Figure 3.8. Reinforced Specimen End Region Detailing.

Damage from prestressing operations during construction of pretensioned members has been present in previous TxDOT and was brought to the attention of the research team by the precaster. Based on recommendations from the precaster at Bexar Concrete Works, additional end region and transverse reinforcement near the pocket were added to enhance the performance of the pretensioned bent caps (Figure 3.9). In order to demonstrate the results from the additional end region and transverse reinforcement, changes were only made to three of the six end regions and two of the three pocket connections.

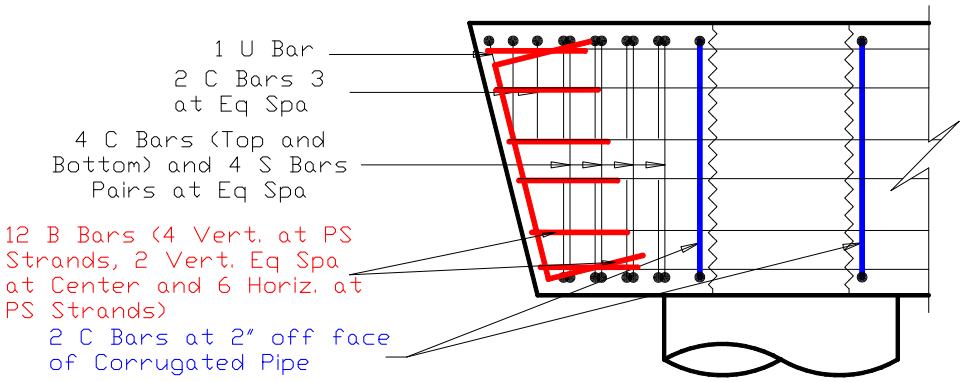

(a) Battered End Elevation

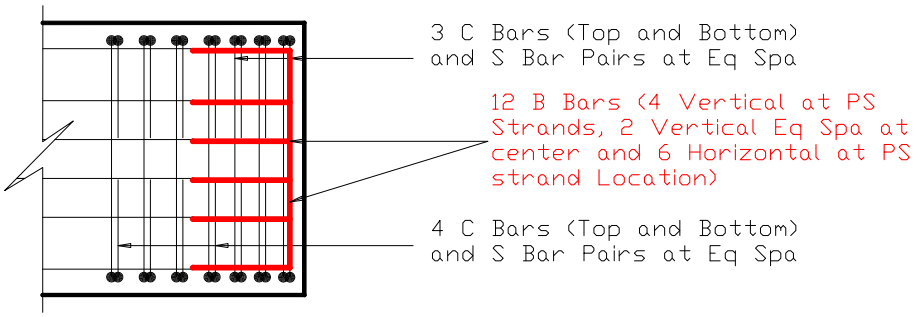

(b) Square End Elevation

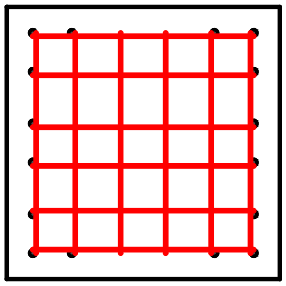

(c) Battered and Square End Elevations

Figure 3.9. Precaster Detailing Recommendations.

3.2.5. *Columns and Connection Design*

The design of the column longitudinal and spiral reinforcement was the same as current TxDOT design standards for pretensioned concrete girder bridges. The column diameter was 3-ft with 10-#9 the longitudinal reinforcement and #4 deformed bar spiral reinforcement.

To connect the precast bent caps to the columns, a pocket connection was designed to provide a connection that emulates monolithic connections and allows for the use of normal-weight concrete instead of grout. The connection replaces the 4-in diameter vertical ducts in current TxDOT standards with a single large pocket connection that will enclose the dowel bars extending from the column. Current TxDOT connection details call for 6-#11 bars. The spacing of the bars was modified to improve the ease of construction and allow a maximum misalignment of 3-in in the longitudinal direction of the bent cap. The size of the pocket was chosen to allow for a 3-in misalignment and to also cause the least amount of disturbance to the cross-section, therefore minimizing the stress concentrations from pretensioning.

The layout of pocket and dowel bars is shown in Figure 3.10. A single 21-in nominal diameter corrugated pipe (Figure 3.11) serves as a stay-in-place form along the full depth of the bent cap. The chosen pipe thickness was based on the ensuring uniform distributions of prestressing forces during the release of strands using the following equation:

$$t_{pocket} = \frac{\sigma_{ps} d_{pocket}}{2 f_{st}} \tag{3-1}$$

where f_{st} = allowable stress of the corrugated pipe taken as 60% of yield stress of the pipe (33-ksi); t_{pocket} = thickness of the corrugated pipe; σ_{ps} = F_i/A = compressive stress due to initial prestressing, F_i = initial prestressing force with assumed $0.75f_{pu}$ immediately prior to release; A = cross-sectional area of bent cap; and d_{pocket} = diameter of the pocket. The total compressive stress from the initial prestressing of 16 270-ksi 0.6-in diameter low relaxation strands generated an approximate stress 0.399-ksi onto the corrugated pipe. Calculations determined a minimum pipe thickness of 0.2-in. Taking into consideration the largest pipe thickness readily available from manufacturers without the need of a special order and the conservative working stress principles of 60% yield stress used to calculate the necessary thickness of the pipe, a 12-gage corrugated pipe with a thickness of 0.109-in was implemented. The steel pipe also provides resistance to compensate for the circumferential forces from the prestressing operations and acts as confining and shear reinforcement on the joint.

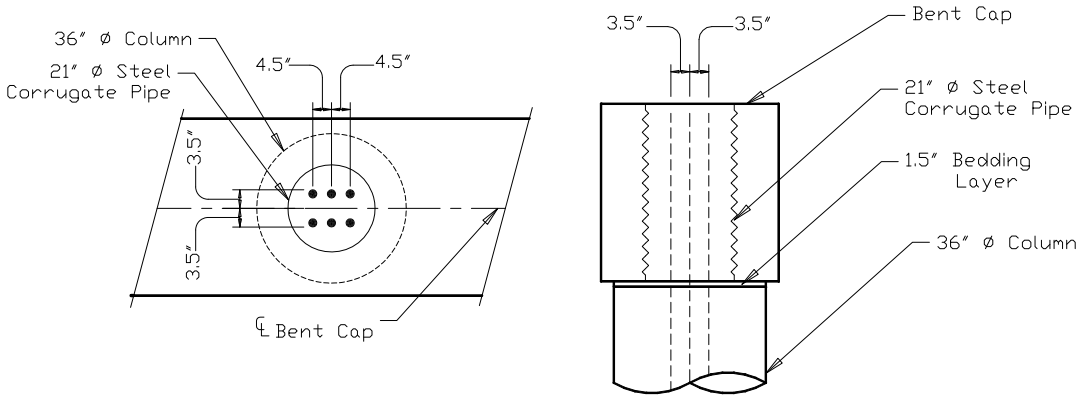

(a) Plan View *(b) Cross-Section View*

Figure 3.10. Steel Corrugated Pipe Connection.

Figure 3.11. 21-in Nominal Diameter, 12-gage Steel Corrugated Pipe.

3.3. Test Matrix

The design of a prototype pretensioned bent cap and an equivalent reinforced concrete bent cap were presented in Section 3.2. These designs were used to establish the experimental test matrix. Four specimens were designed and constructed. The objective of the test matrix is to investigate a pretensioned design, an equivalent reinforced concrete design, and two variations on a pretensioned design. The variations considered are less shear reinforcement and the use of an interior void to reduce weight. Table 3.4 shows the names and characteristics of each test specimen. The naming of the specimens has the first set of characters showing the type of specimen (RCS = Reinforced Concrete Solid, PSS = Pretensioned Solid, PSV = Pretensioned Void). The second set of characters shows the number of reinforcement bars or strands. The third set of characters indicates the spacing of the span shear reinforcement in inches.

Table 3.5 provides a summary of the specimens and locations of the precaster recommendations implemented during the construction of the pretensioned bent caps discussed in Section 3.2.4.

Table 3.4. Test Matrix Overview

Specimen	Flexural Reinf.	Shear Reinf. Spacing (in)	Description
RCS-16-12	16-#8 bars	12	Reinforced concrete design
PSS-16-12	16-0.6-in ϕ	12	Pretensioned design
PSS-16-24	16-0.6-in ϕ	24	Reduced shear reinforcement
PSV-16-12	16-0.6-in ϕ	12	Void for reduced weight

Table 3.5. Test Matrix Detailing

Specimen	Battered End	Near Pocket	Square end
RCS-16-12	Regular	Regular	Regular
PSS-16-12	Regular	**Additional**††	**Modified**†
PSS-16-24	Regular	Regular	Regular
PSV-16-12	**Modified**†	**Additional**††	**Modified**†

† End Region Detailing as seen in Figure 3.9
†† Transverse Reinforcement as seen in Figure 3.9

RCS-16-12 was designed based on the reinforced concrete prototype design. PSS-16-12 was based on the pretensioned prototype design. PSS-16-24 consisted of an equal strands configuration as PSS-16-12 but with shear reinforcement spacing of 24-in in the span. PSV-16-12 incorporated a 26-in x 26-in cross-section void. The void began 2-in from the inside edge of the column and extended for 7-ft. The void size was selected based on the minimum thickness (8 in.) expected to be used by TxDOT. The voided specimen does not reflect a prototype design but was instead selected to provide a comparison of solid and voided caps with the same strand configuration and the same

shear reinforcement. Figure 3.12, Figure 3.13 and Figure 3.14 show the elevation views of RCS-16-12, PSS-16-12 and PSS-16-24, respectively. Figure 3.15 shows the plan, elevation and side view of PSV-16-12. A full set of design drawings is provided in Appendix A.

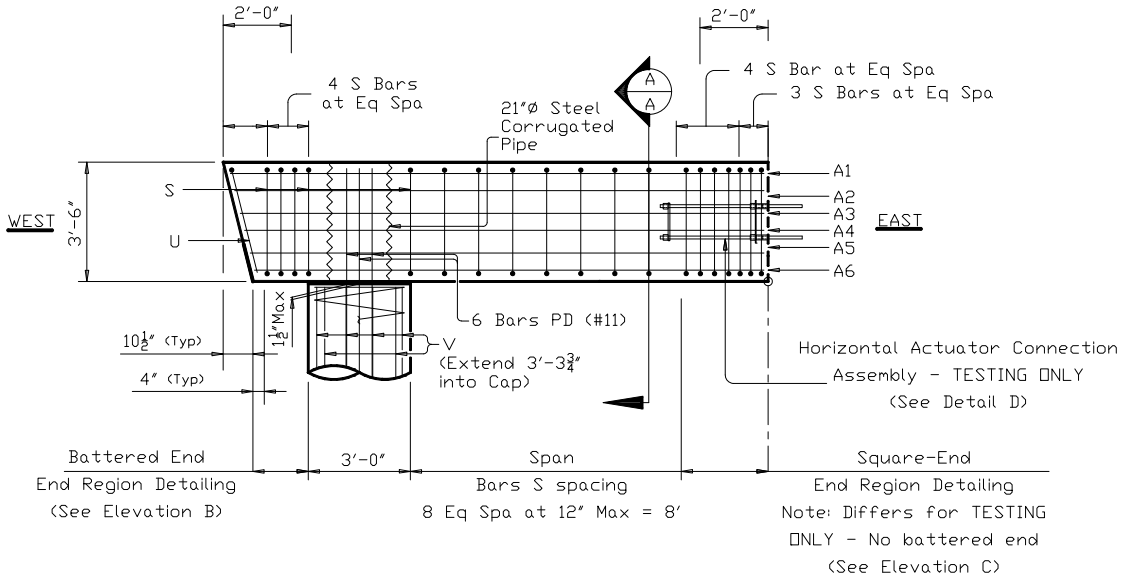

Figure 3.12. RCS-16-12

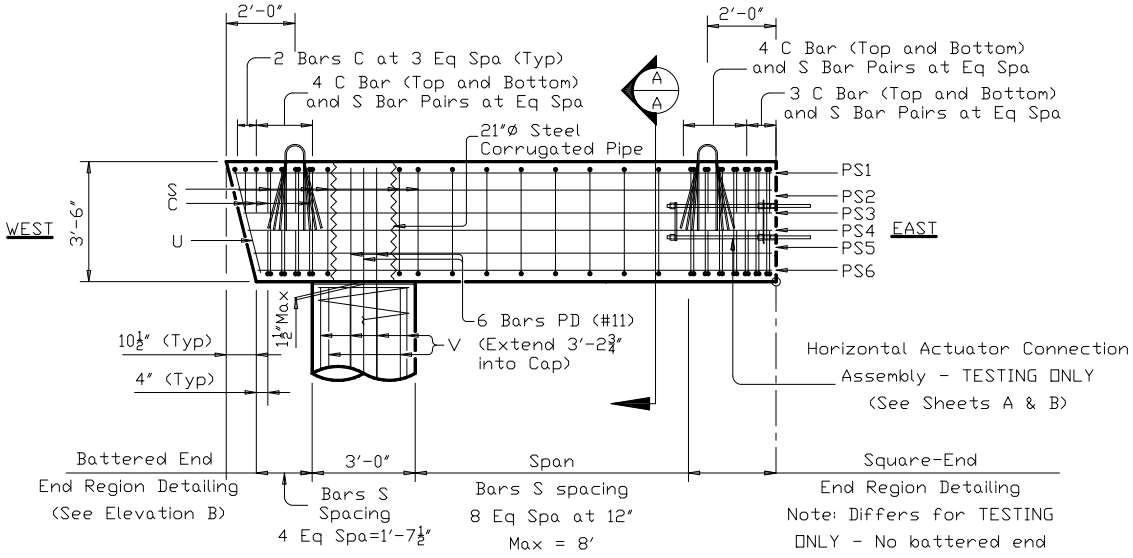

Figure 3.13. PSS-16-12

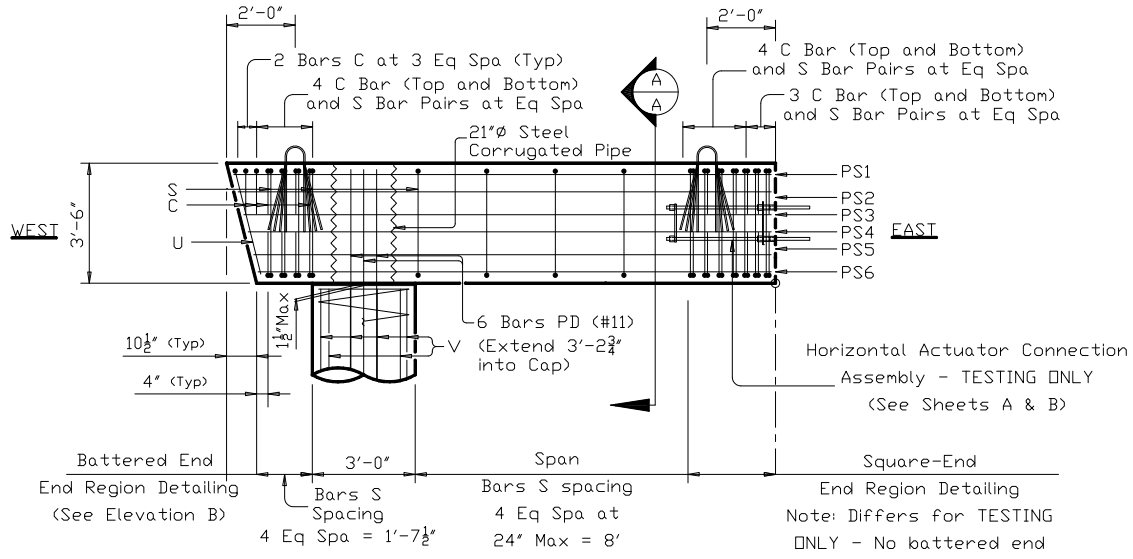

Figure 3.14. PSS-16-24

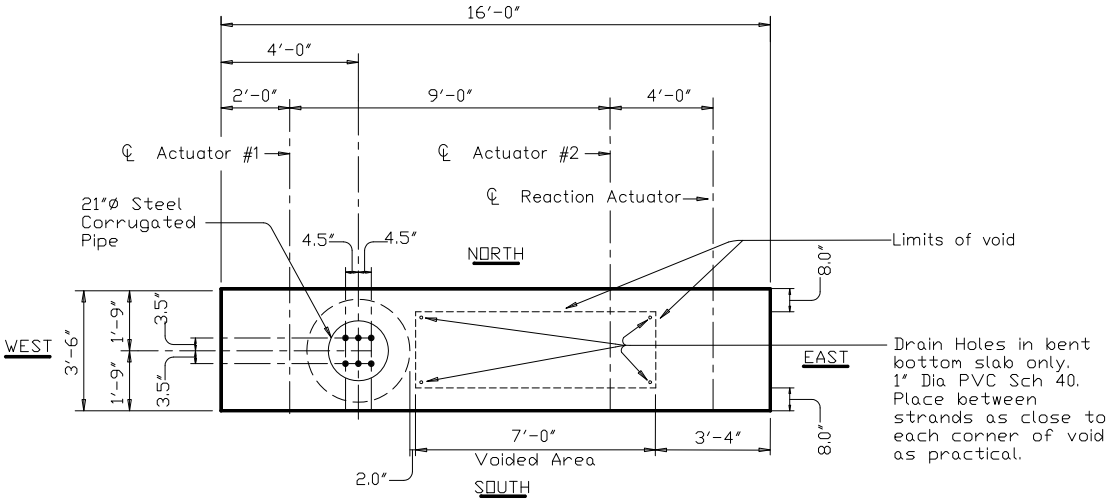

(a) Plan View

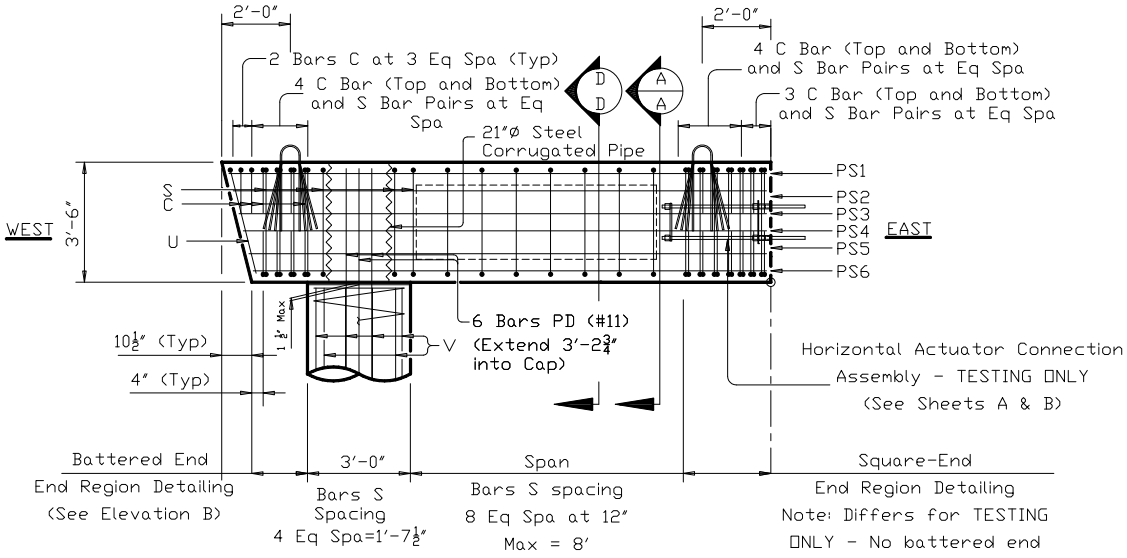

(b) Elevation View

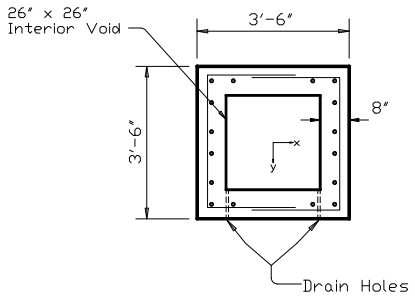

(c) Cross-Section View

Figure 3.15. PSV-16-12

3.4. Specimen Construction

The construction of the RCS-16-12 bent cap and all support columns took place in the Texas A&M University High Bay Structural and Materials Testing Laboratory. All pretensioned bent caps were fabricated by Bexar Concrete Works in San Antonio, Texas under the inspection of TxDOT and Texas A&M Transportation Institute personnel. Subassemblies were constructed in place in the structural lab.

3.4.1. *Precast Reinforced Concrete Bent Cap (RCS-16-12)*

Wood formwork was constructed for RCS-16-12. Figure 3.16 shows completed formwork. Appendix B shows the front, plan and sides views of the formwork drawings. Star flat head screws were used to ease formwork demolition. To secure the formwork walls, additional braces were incorporated with scrap cuts of lumber. Details of lumber materials are provided in Appendix B.

(a) Square End *(b) Battered End*

Figure 3.16. Bent Cap Formwork.

The construction of the bent cap steel reinforcement cage followed strict guidelines to ensure the proper locations of all parts. The first step was to mark all flexural reinforcement (A-bars) with the location of the shear reinforcement (S-bars) and vice versa. The overhead crane was used to hoist the top corner A-bars while the S-bars and corrugated pipe (pocket) were placed in their corresponding locations. The bottom A-bars were then installed to provide the initial stability of the steel cage. The S-bars were tied to the top and bottom A-bars with 16-gage tie wire double ties. Two 4-ft #6 bars were temporarily installed on the outside vertical faces of the steel cage at opposite angles to brace the steel cage against sway during construction and installation; bars were removed prior to casting concrete. The remaining A-bars were tied to the S-bars in their corresponding locations. A second pair of #6 bars was fed through perpendicular to the longitudinal orientation of the steel cage in order for the crane to lift the steel and installed the bottom cover chairs. Once all the steel reinforcement was tied in place, the locations of all S-bars and A-bars were verified to match the RCS-16-12 plans (Figure 3.17). The overhead crane was used to place the steel cage in the formwork. The corrugated steel pipe for the pocket connection was also installed using the overhead crane and fastened into its proper location with compressed wood stumps. Once the steel cage and corrugated pipe were installed, the square end wall of the formwork was constructed to completely enclose and seal the cap formwork. Finally, two lifting hooks at equal distances from the center of gravity of the bent cap were installed for lifting the bent cap (Figure 3.18).

(a) Marking Location of S-bars

(b) Installed Bottom A-bars

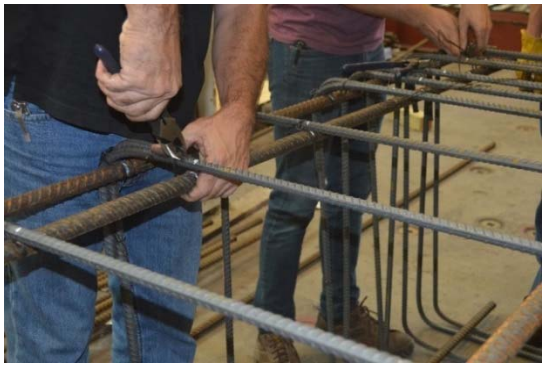

(c) S-bars Ties

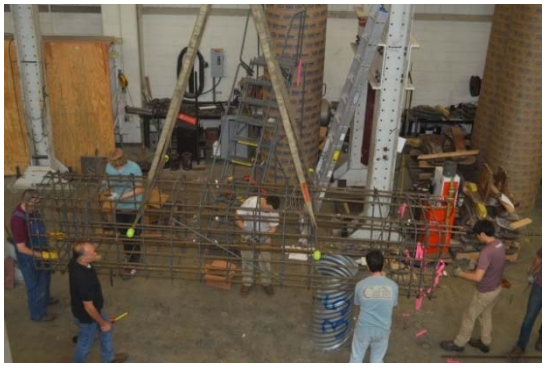

(d) Hoist Steel Cage to Install Chairs

(e) Chair Ties

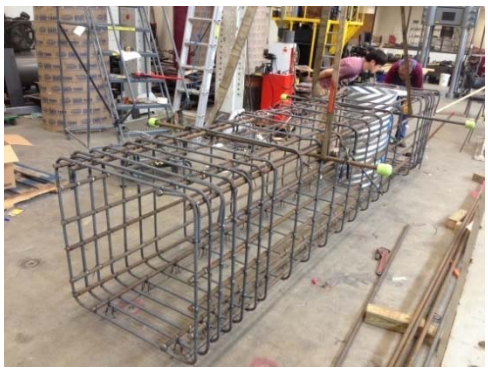

(f) Final Inspection of Steel Cage

Figure 3.17. Bent Cap Steel Reinforcement.

(a) Placing Steel Cage in Formwork

(b) Placing Corrugated Pipe

(c) Final Inspection

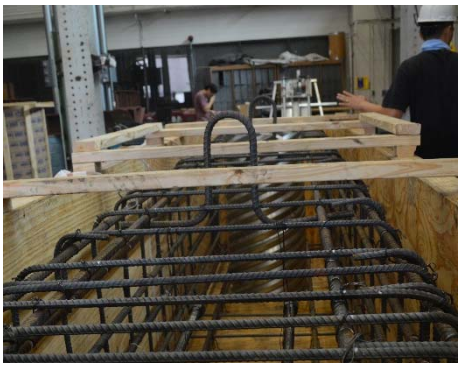

(d) Lifting Hooks

Figure 3.18. Placing Bent Cap Reinforcement into Formwork.

Concrete was provided by Martin Marietta Materials and poured inside the temperature-controlled Texas A&M University High Bay Structural and Materials Testing Laboratory. A slump of 5.5-in was recorded. A hopper supported by the laboratory overhead crane were used to transport the concrete from the concrete truck to the bent cap formwork and the lever handle on the side of the shoot regulated the flow rate of concrete into the formwork. The 42-in height of the bent cap was cast in three lifts of approximately 14-in, with vibrations (15000 rpm) provided to each lift. The pocket was held in position

by compression with lumber and thin plywood. During the first lift of concrete, a shift in the position of the pocket occurred from placing the concrete at a high rate into the battered end of the bent cap. The pocket was reset to its original location by spreading the concrete around and away from the corrugated pipe and pushing it back into position. After all concrete lifts were complete, the bent cap top surface was finished with smooth trowels and floated. Filleted trowels were used approximately an hour after the last concrete lift to provide smooth round edges at the top surface of the bent cap. Once the concrete had set (5 hours), the top surface of the bent cap was watered, covered with soaked towels and covered again with a black tarp for 4 days of moist curing (Figure 3.19).

In an effort to protect the strain gages during the casting of the bent cap, improper vibrating resulted in honeycombing in certain areas of the bent cap after releasing the formwork as seen in Figure 3.20. According to the Chapter 2 - Damage Assessment and Repair Types of the TxDOT Concrete Repair Manual (Freeby, 2015), the honeycombing was determined to be minor with no effects to the structural integrity of the specimen. The average depths of the honeycombs were less than 7/8-in. The only two areas of largest honeycombs were 1-1/8-in and 1-1/2-in deep (depth of cover concrete 2-7/8-in). No rebar was exposed. Repair guidelines were followed and the areas were cleaned and filled with cement grout. The surface of the specimen was finished with a diamond concrete surface grinder. After all the honeycombing was repaired, the specimen was placed on support blocks (Figure 3.21).

(a) Concrete Lifts

(b) Consolidation

(c) Pocket Anchorage Side View

(d) Pocket Anchorage Top View

(e) Surface Finishing

(f) Finished Surface

(g) Wet Curing Towels

(h) Impermeable Curing Tarp

Figure 3.19. Casting the Reinforced Concrete Bent Cap.

(a) Honeycombing– Front Face of Bent Cap

(b) Span

(c) Battered End

Figure 3.20. Honeycombing (RCS-16-12).

(a) Honeycombing Repairs – Front Face of Bent Cap

(b) Span

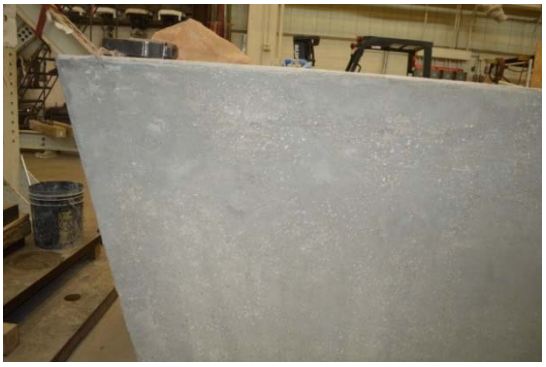

(c) Battered End

Figure 3.21. Honeycomb Repairs (RCS-16-12).

3.4.2. *Precast Pretensioned Bent Caps*

The construction of pretensioned bent caps PSS-16-12, PSS-16-24 and PSV-16-12 took place at Bexar Concrete Works in San Antonio, Texas under the close supervision of both TxDOT and Texas A&M Transportation Institute (TTI) personnel. All three pretensioned bent caps were constructed along the same prestressing bed (Figure 3.22 and Figure 3.23). The first steps consisted of placing the formwork for each end of the specimen. Metal

formwork was used for the battered end and wood formwork was used for the square end (Figure 3.24). The strands were placed in the specified locations according to plans and anchored at one end of the prestressing bed and stressed at the opposite end (Figure 3.25). Four metal stumps were welded to the prestressing bed to secure the steel corrugated pipes (Figure 3.26). The styrofoam void and drains were installed and secured at the bottom with No. 3 rebar and to prevent floating, three 3/4-in plywood sheet cuts were installed at the top of the styrofoam and held in place with threaded bars that fed through the side wall formwork braces (Figure 3.27). Six additional C-bars were placed vertically and horizontally (twelve total) at the battered and square end of PSV-16-12 and at the square end of PSS-16-12 to prevent cracking from the releasing of the strands based on recommendations from the precaster. To validate the effectiveness of additional C-bars at the end region of bent caps, no additional bars were provided in PSS-16-24 (Figure 3.28). Two additional transverse reinforcement bars were provided 2-in from each of the corrugated pipe faces in both the east and west directions for PSS-16-12 and PSV-16-12. To allow comparison, no additional transverse reinforcement was placed in PSS-16-24. The additional end region and transverse reinforcement followed the details previously presented in Figure 3.9 and Table 3.5.

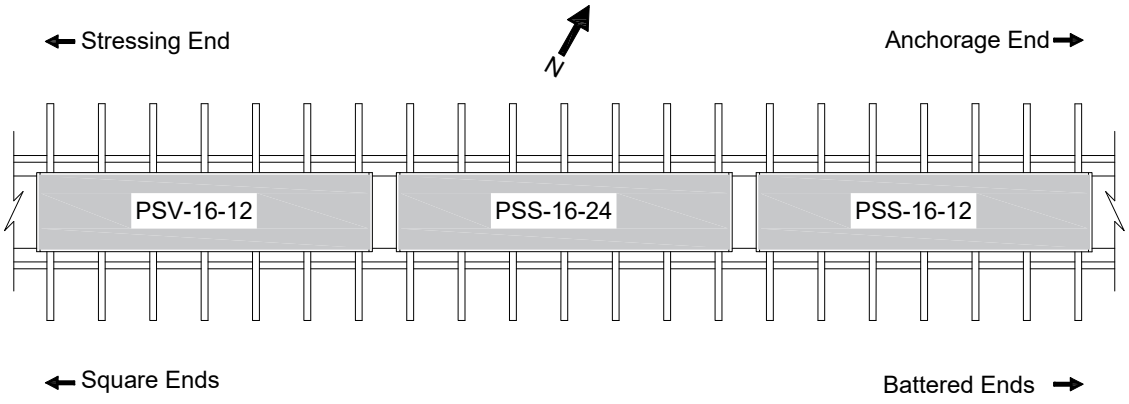

Figure 3.22. Specimens Prestressing Bed Layout.

Figure 3.23. Prestressing Bed.

(a) Metal Formwork – Battered End

(b) Wood Formwork – Square End

Figure 3.24. End Formwork.

(a) Stressing End

(b) Anchorage End

Figure 3.25. Stressing of Strands.

(a) Corrugated Pipe Stumps

(b) Steel Corrugated Pipe

Figure 3.26. Installation of Steel Corrugated Pipe.

(a) Bottom Cover and Drain Pipes

(b) Top Cover Plywood Cuts

Figure 3.27. Void Installation.

(a) Battered End

(b) Square End

Figure 3.28. Additional End Region Reinforcement.

The initial target compression strength was 4-ksi for strand release and a target value for 28-day strength was between 6-ksi and 7-ksi. Figure 3.29 shows the distribution of batches in the three specimens. An initial slump of 7-in was recorded, and molded cylinders and beam specimens were made for each concrete batch (Figure 3.30). The first concrete batch (A) filled approximately two-thirds of PSS-16-12, and the second concrete batch (B) filled the remaining portion of PSS-16-12 and the bottom third of PSS-16-24. The third (C) and fourth (D) concrete batches filled the remaining of PSS-16-24. The

remainder of the fourth batch (D) was discarded after topping off PSS-16-24 because of an interruption in the pour due to a displacement in the pocket, which was partially corrected and less than 1/4-in of rotation at the base remained. The fifth batch (E) filled over two-thirds of PSV-16-12. The sixth and final batch (F) of concrete filled the remainder of PSV-16-12 (Figure 3.29). Extra material testing samples were made with the remaining concrete from the final batch. After the concrete pours were completed and vibrated for proper consolidation, the tops of the specimens were finished with wood trowels. A water irrigation system was installed above the specimens to provide the proper curing of the top concrete surface and maintain humid conditions (Figure 3.31 and Figure 3.32).

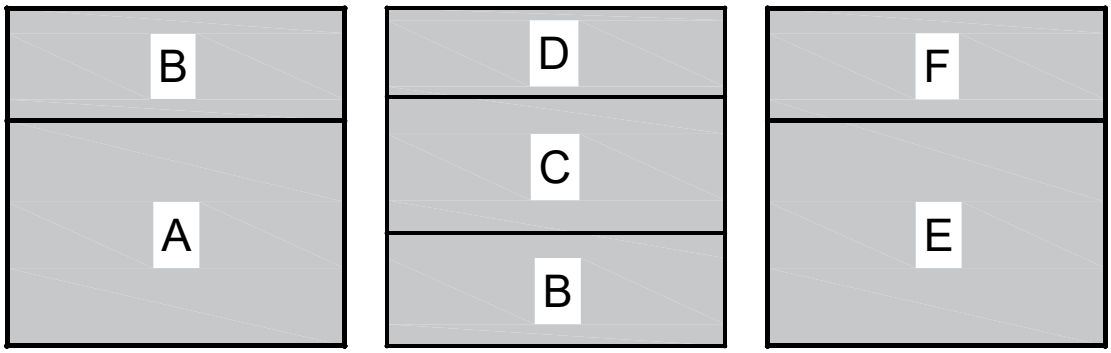

(a) PSS-16-12 *(b) PSS-16-24* *(c) PSV-16-12*

Figure 3.29. Concrete Batch Layers.

(a) Slump Test

(b) Cylinder and Beam Molds

Figure 3.30. Concrete Material Samples.

(a) Concrete Pour

(b) Consolidation

Figure 3.31. Casting Pretensioned Specimens

(a) Wood Trowel Finish

(b) Curing

Figure 3.32. Finishing and Curing of Concrete.

Thermocouples were placed in the cover and center concrete areas for all specimens to record the variations of temperatures during the curing of the concrete. For PSS-16-12 and PSS-16-24, the thermocouples were installed at approximately 8-ft from the battered end. Because of the location of the void, the thermocouples were placed at 3-ft from the battered end for PSV-16-12. Detailed locations of the thermometers are given in Figure 3.33. Data gathered from the thermocouples starting on August 26, 2017, at 9:26 a.m. is shown in Figure 3.34 and the numerical data is provided in Appendix C.

In addition to the thermocouples installed in the specimens, external temperatures of the specimens were measured using a portable infrared thermometer. Temperatures were measured on both the front and back sides at the center of the specimen for PSS-16-12 and PSS-16-24, and right next to the corrugated pipe for PSV-16-12; matching similar locations to the embedded thermocouples. The measured temperatures are summarized in Table 3.6. The maximum ambient temperature during the day of casting was 102°F.

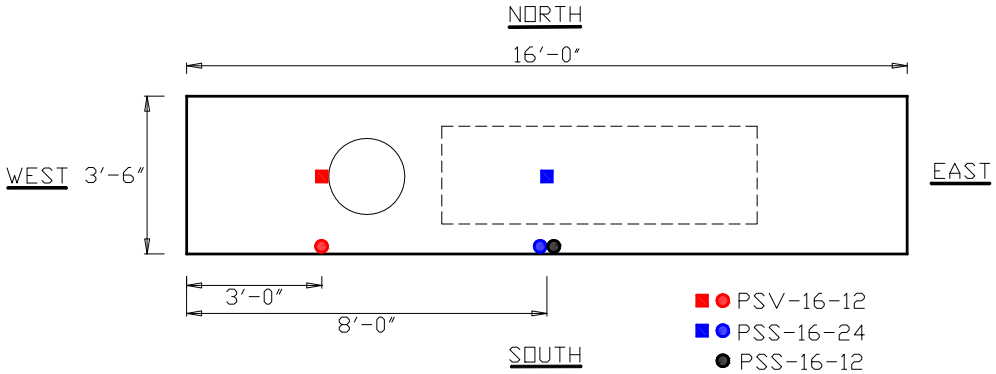

(a) Plan View

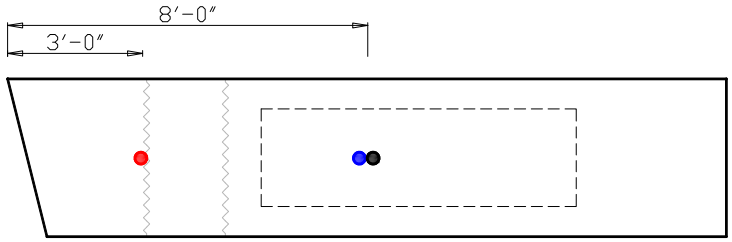

(b) Elevation

Figure 3.33. Thermocouple Plan

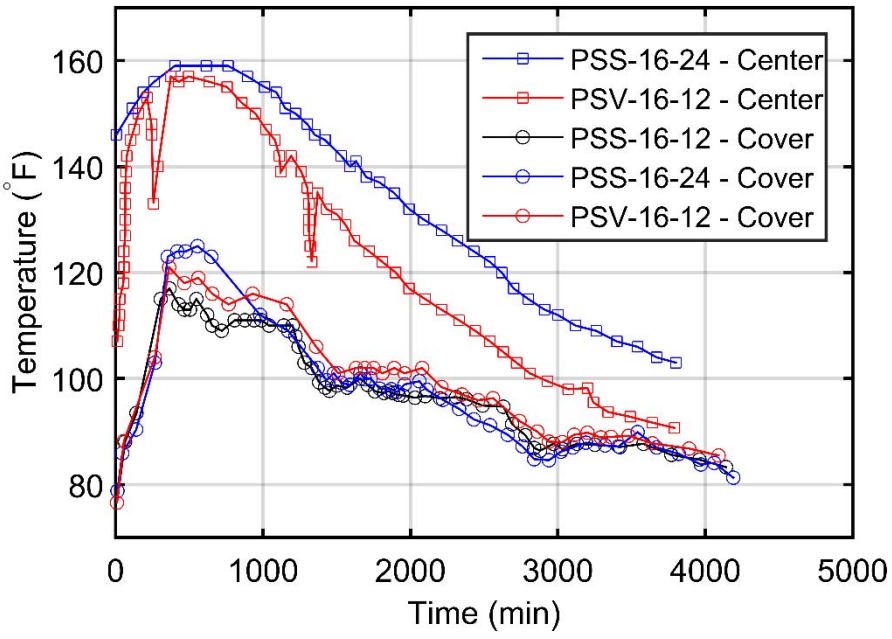

Figure 3.34. Temperature vs. Time Thermocouples Recorded Data. (PSS-16-12 – Center thermocouple failed to recorded data)

Table 3.6. Measured Surface Temperature

Specimen	Time		Front		Back	
			Concrete (°F)	Steel (°F)	Concrete (°F)	Steel (°F)
PSS-16-12	8/26/2016 09:15	Concrete pour	82.6	80.8	80.9	83.5
	8/26/2016 11:00	+ 2 hours	87.2	83.2	87.3	94.6
	8/26/2016 17:00	+ 8 hours	87.6	96.4	84.3	98.1
	8/27/2016 10:30	+ 25 hours	83.5	82.4	84.9	88.4
	8/29/2016 09:00	+ 72 hours	74.8	71.8	75.0	74.4
PSS-16-12	8/26/2016 09:15	Concrete pour	80.8	80.6	80.4	79.3
	8/26/2016 11:00	+ 2 hours	91.3	86.4	90.6	96.8
	8/26/2016 17:00	+ 8 hours	92.6	98.7	87.6	100.4
	8/27/2016 10:30	+ 25 hours	86.6	82.1	88.3	104.2
	8/29/2016 11:00	+ 72 hours	74.4	72.5	76.6	75.1
PSS-16-12	8/26/2016 09:15	Concrete pour	78.1	78.7	80.9	84.1
	8/26/2016 11:00	+ 2 hours	92.4	85.1	89.8	94.8
	8/26/2016 17:00	+ 8 hours	89.7	98.0	86.6	97.8
	8/27/2016 10:30	+ 25 hours	85.3	83.4	86.8	101.9
	8/29/2016 09:00	+ 72 hours	74.2	73.1	75.1	78.9

The formwork for all specimens was removed and the strands were released on the third day after the concrete was poured. During the release of the strands, a jack was used to lower the tension of the strands at the stressing end and flame torching techniques were used to release the strands at the anchorage end and in between each specimen (Figure 3.35). Strands were released individually in a symmetrical pattern. Compressive strengths of the collected cylinder samples averaged close to 4.5-ksi. No cracks were present in the specimens before or after the release of the strands (Figure 3.36). The ends of the strands were prepared by melting approximately 2-in into the cover concrete and patching with grout to prevent corrosion of the strands (Figure 3.37).

(a) Formwork Removal *(b) Flame Torch Strand Release*

Figure 3.35. Formwork Removal and Strand Release.

(a) Battered End *(b) Square End*

Figure 3.36. Post Strand Release Crack Inspections.

(a) Melting Strand Ends

(b) Grout Strand Patches

Figure 3.37. Strand End Preparation.

3.4.3. *Pretest (Construction) Damage Post-Delivery*

The results from the end region detailing recommendations discussed in Section 3.2.4 are presented for PSS-16-12, PSS-16-24, and PSV-16-12 in Figure 3.38, Figure 3.39, and Figure 3.40, respectively. These figures show pretesting cracks on the side faces and ends of the specimens; with the square end showing the strand layout and the four actuator connection rods. No pretesting cracks were recorded on the top and bottom faces of the specimens. As mentioned in Section 3.4.2, no cracks were seen at the time of prestressing transfer, and all the pretesting cracks were first observed days after delivery to the laboratory. The benefits of the additional end region detailing were observed in the battered end of PSV-16-12, which was the only specimen with the additional end region detailing in the end shape representative of current TxDOT bent caps. The square end developed construction cracks in all specimens. Consistency in benefits from the additional end region detailing was not observed. It should also be noted that the square

end is not representative of current TxDOT bent cap end region shapes and was constructed for experimental testing purposes only.

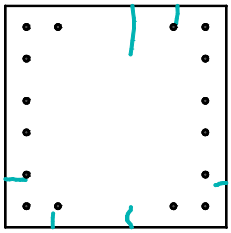

(a) Battered End

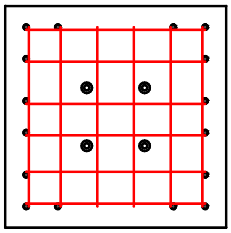

(b) Square End

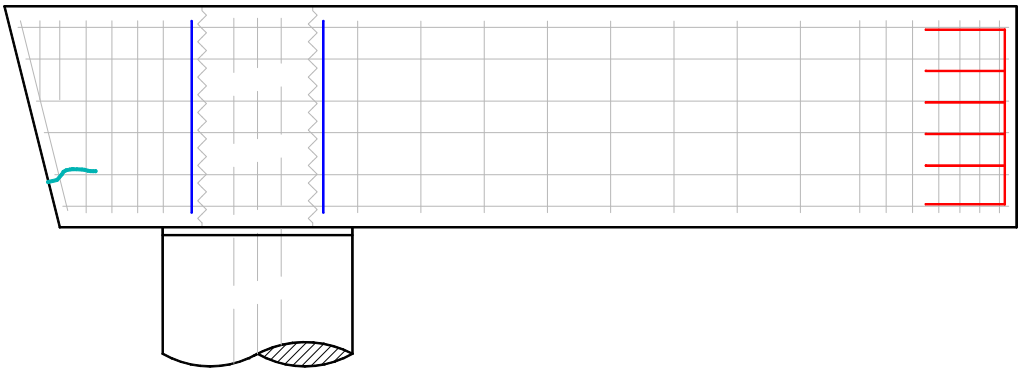

(c) Front Face

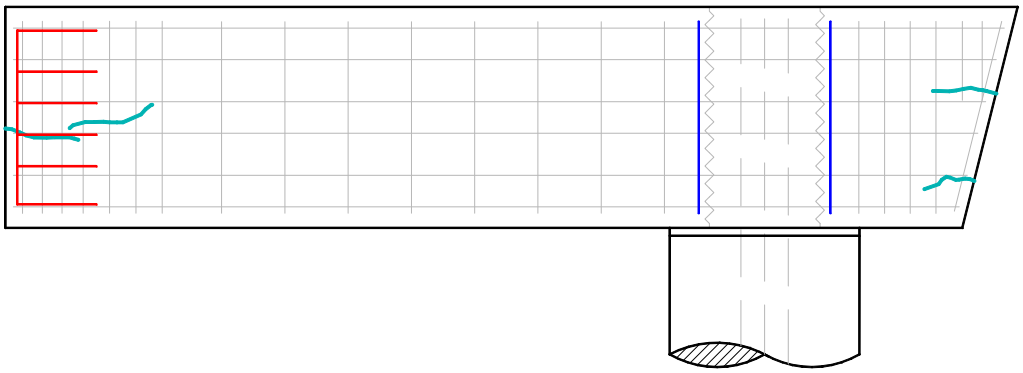

(d) Back Face

Figure 3.38. Construction Damage – PSS-16-12.

(a) Battered End *(b) Square End*

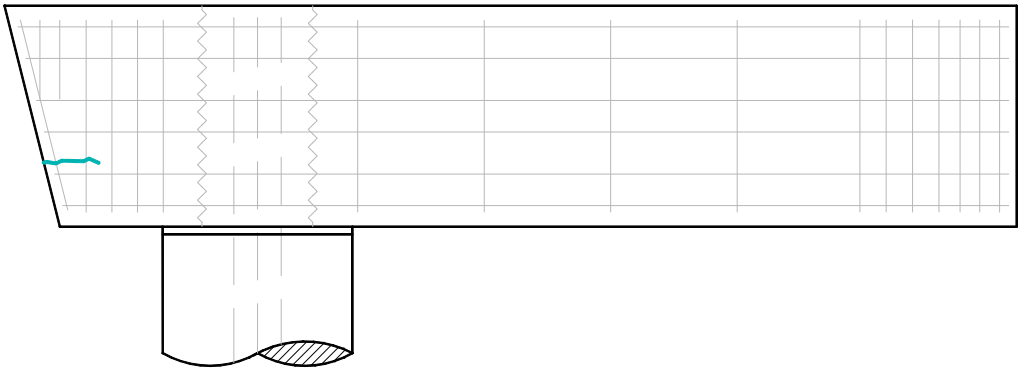

(c) Front Face

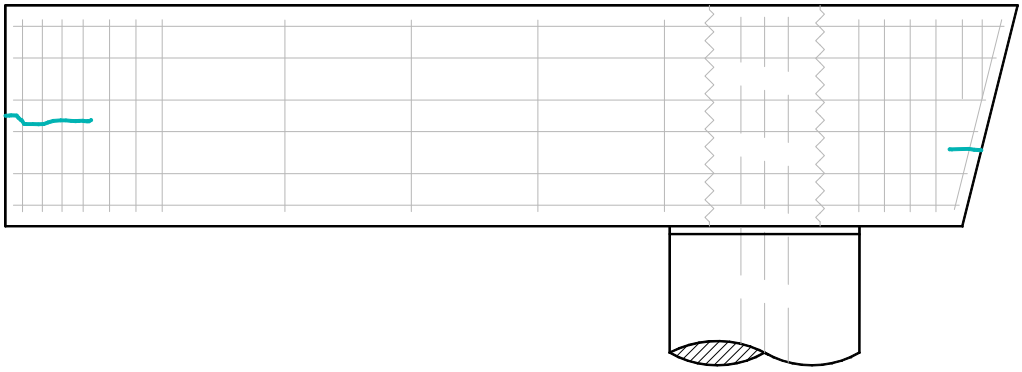

(d) Back Face

Figure 3.39. Construction Damage – PSS-16-24.

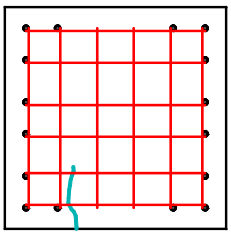

(a) Battered End

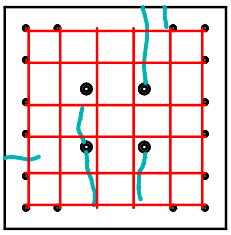

(b) Square End

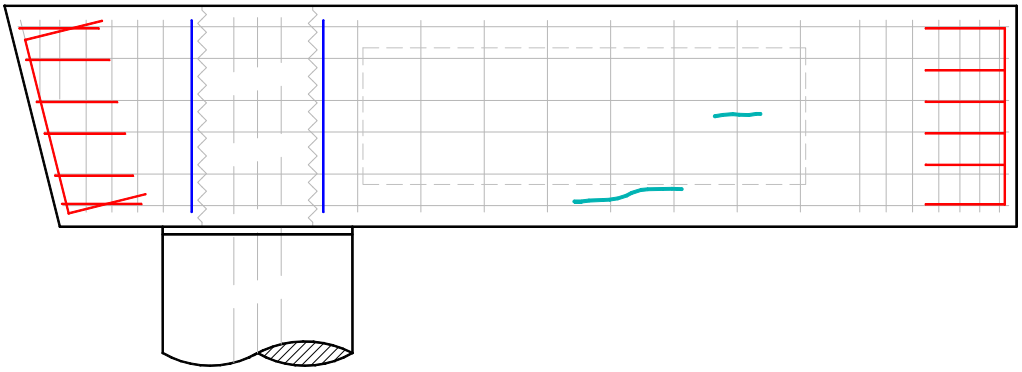

(c) Front Face

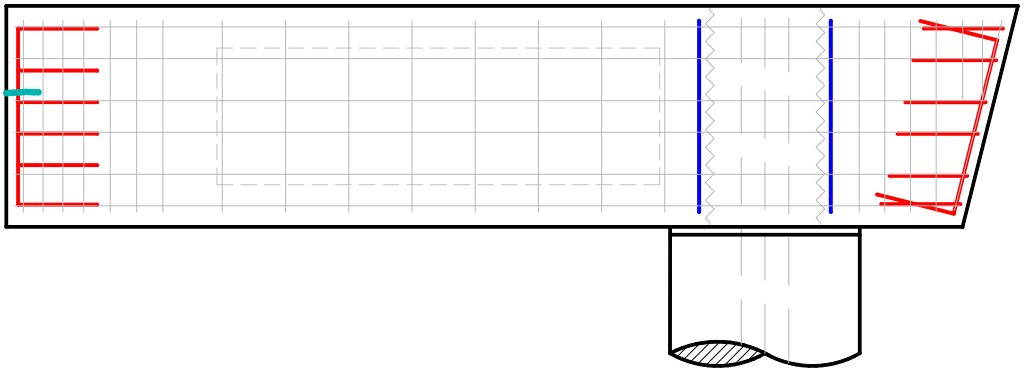

(d) Back Face

Figure 3.40. Construction Damage – PSV-16-12.

3.4.4. *Columns*

The construction of the reinforcement cage for the column began by threading the bottom of the column longitudinal bars into a 1-in steel plate (Figure 3.41(a)).

The construction of the column steel cage followed a similar procedure as the bent cap, by marking the 6-in pitch of the spiral reinforcement on the column longitudinal bars. The overhead crane lifted the spiral reinforcement to the marked locations on the longitudinal reinforcement. One complete loop of spiral reinforcement was tied to the bottom of the longitudinal reinforcement and the 6-in pitch was continued thereafter. An extra full loop of spiral reinforcement was tied at the top of the longitudinal reinforcement (Figure 3.41(b)). The spiral reinforcement was tied at every column longitudinal reinforcement bar.

The dowel bars for the connection between the bent cap and the column extended 5-ft 6-in into the column and 3-ft 2-3/4-in into the bent cap. To install the dowel bars in the correct position, formwork made of 2 x 4 cuts of lumber with holes matching the spacing of the dowel bars were placed at the top of the column steel reinforcement cage. Clamps were used to secure the dowels bars at the correct alignment and elevation. A second point of alignment was created by installing temporary spare rebar inserted through the spiral reinforcement perpendicular to the length of the column longitudinal bars near the base of the column. This additional point of alignment secured the dowel bars into a level position and fixed the dowel bars against any rotation of misalignment during the casting of the column base. The dowel formwork was temporarily removed to place the

sonotube over the column steel reinforcement cage after the casting of the column base concrete (Figure 3.42).

(a) Threaded Longitudinal Bars

(b) Deformed Spiral

Figure 3.41. Column Reinforcement.

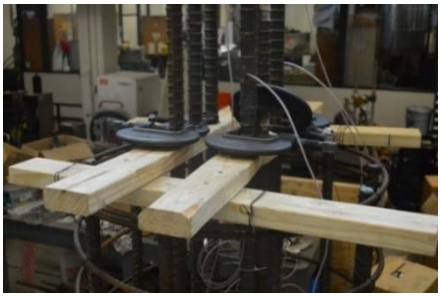

(a) Top of Column

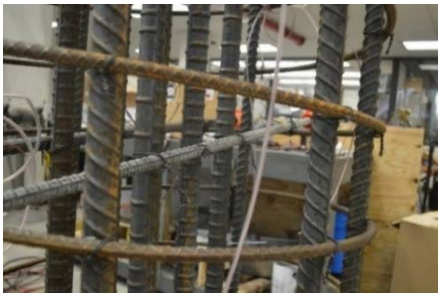

(b) Column Midheight

Figure 3.42. Temporary Dowel Formwork.

Three components were used for the construction of the column formwork. The first component was the steel plate mentioned with the column reinforcement cage. The second consisted of an octagonal base necessary for a flat contact surface for the connection of the bottom horizontal actuator. The third and final component was the remaining circular column on which the bent cap would be installed. Figure 3.43 shows plans for the 14.5-in high octagonal base that was constructed using 2 x 8 cuts of lumber. The formwork for the octagonal base was secured to the plate with all-thread rods fastened by custom cut steel plates as seen in Figure 3.44. Concrete for the column base was poured prior to casting the main portion column to provide a solid foundation for the column formwork.

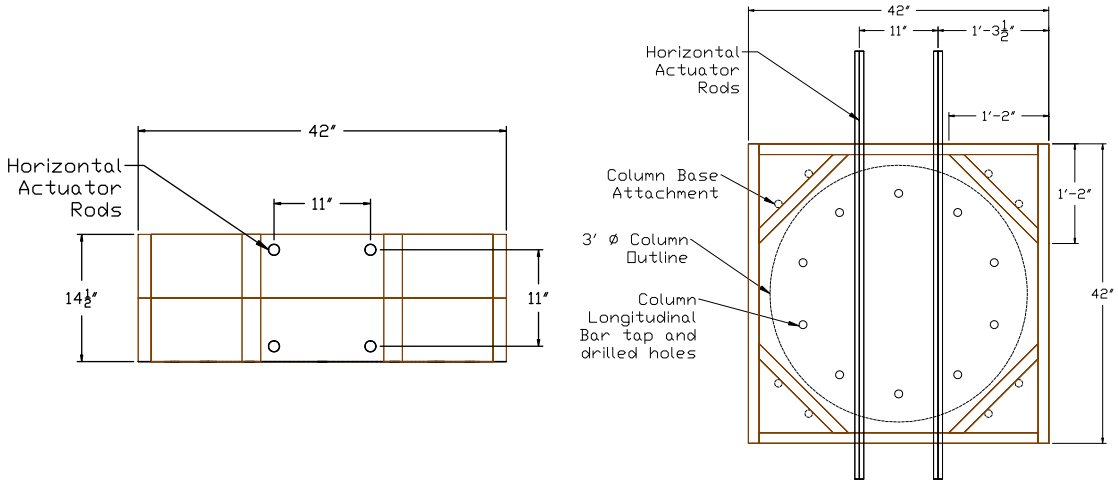

(a) Elevation *(b) Plan*

Figure 3.43. Octagonal Base Formwork Plan.

(a) Column Base Formwork Installation

(b) Column Base Cage

Figure 3.44. Octagonal Base Formwork.

The column formwork consisted of a 36-in diameter cardboard sonotube. Shipping and storage prior to delivery caused the sonotubes to deform into an oval shape. Bracing was added to the top and bottom (Figure 3.45) to provide support for the sonotube and to maintain the 36-in diameter. The correct alignment and floating prevention of the sonotube during casting were ensured by screwing the bottom braces of the sonotube to the column base formwork.

The formwork from the octagonal base was left in place during the casting of the column allowing the bottom lumber formwork of the sonotube to attach to the column base formwork (Figure 3.46). The formwork at the top of the dowel bars was reinstalled onto the top of the sonotube to secure the dowel bars during concrete casting (Figure 3.47). The column base concrete was transported from the concrete mixer truck to the formwork by wheel barrels filled with concrete, then vibrated for consolidation. The top surface of the octagonal column base was left with a rough finish to increase the bond between the two separate pours. The outer edges were finished with trowels to provide a smooth

contact surface for the sonotube. The octagonal column base was cast at a minimum of 24 hours prior to the column.

A hopper with a side shoot was used to place the concrete in the column. The column was cast in three lifts, with each vibrated for consolidation. The top surface was left with a rough finish to provide a stronger bond with the bedding layer (Figure 3.48).

Figure 3.45. Column Sonotube Formwork.

(a) Placement of Concrete with Wheel Barrels

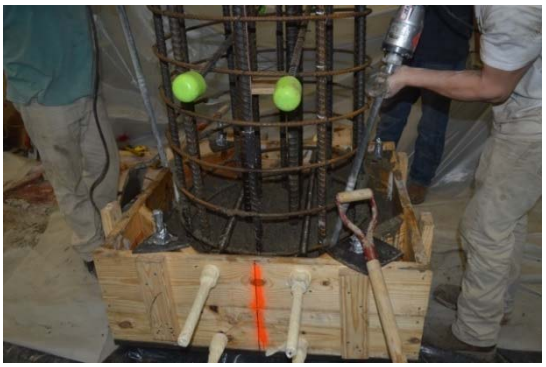

(b) Consolidating of Concrete

(c) Rough Finish

Figure 3.46. Casting Column Base.

(a) Sonotube Installation

(b) Dowel Bars Supports

Figure 3.47. Column Concrete Pour Preparation.

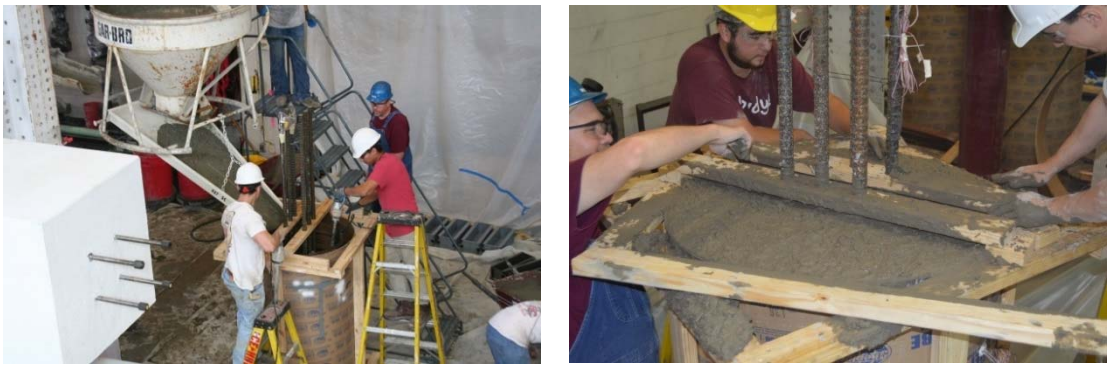

(a) Hopper and Side Shoot *(b) Rough Finish*

Figure 3.48. Casting Column.

3.4.5. *Component Assembly*

The next step in the construction of the experimental test specimen consisted of assembling the components. The column was placed onto a roller foundation simulating a pin connection at the moment inflection of the prototype bridge column (described in Section 3.1) by attaching lifting straps with a double-choke to the overhead laboratory crane. Screw jacks on each corner of the 2-in plate were used to fix the roller foundation in position and ensure the specimen maintained a level position prior to testing (Figure 3.49).

(a) Cured Concrete

(b) Installing onto Test Setup

Figure 3.49. Column Installation.

After the column was secured onto the roller, the bent cap was placed on top of the column which took place by attaching the overhead crane to the lifting hooks. The ease of installment of the bent cap onto the column with the use of the larger single pocket connection allowed for a quick assembly of the specimen in the laboratory (Figure 3.50). Temporary shoring for the east end of the bent cap was provided by two angle iron headers attached to the reaction towers. Wood shims were used to obtain the correct height and level installation of the bent cap resting on the angle iron headers.

(a) Placing Bent Cap

(b) Bedding Layer and Shims

(c) Placed Bent Cap Top View

(d) Dowel in Pocket Connection

Figure 3.50. Installation of Bent Cap onto Column.

Previous research conducted by Matsumoto et al. (2001) and Restrepo et al. (2011) recommended the use of plastic shims to support the bent cap on the column and provide the space for the bedding layer. According to this research, the use of plastic shims instead of steel shims prevented corrosion and reduced concerns of "hard spots" that could develop at the column-bent cap interface as the plastic is expected to creep and better transfer connection loads to the bedding layer. The plastic shim dimensions were 4-in x 4-in x 1 ½-in, occupied less than 2% of the column area and consisted of rigid high-density polyethylene (HDPE). The shims were placed 3.5-in from the edge of the column along the centerline of the bent cap allowing the shims to sit at the outside edge

of the pocket connection (Figure 3.51). The 1-1/2-in thickness of the shims provided the necessary minimum thickness of the bedding layer according to TxDOT standards for grouted vertical duct connections. The areas where the shims were installed on the column were prepared by grinding to provide a level surface on the rough finish left at the top of the column to ensure the shims could be placed level.

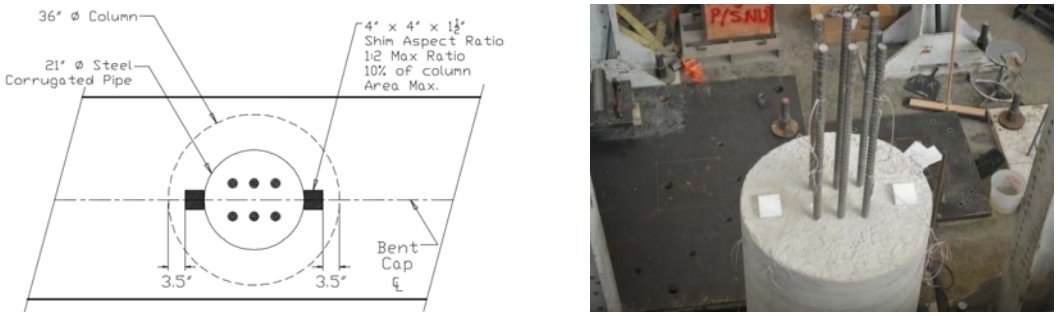

(a) Plans *(b) Placement*

Figure 3.51. Shim Installation.

The pocket connection consisted of a 21-in diameter corrugated pipe. A sleeve made of sheet metal with a spring-loaded chain and latch was constructed to provide the formwork for the bedding layer. The latch and the spring provided the necessary stiffness in the sleeve to remain in place during casting and consolidation of the pocket concrete. For the construction of RCS-16-12, two 1/2-in inner diameter clear tube vents were installed behind each of the two shims placed along the centerline of the bent cap to allow any entrapped air to exit the interface between the edge of the column and pocket during the casting of the bedding layer (Figure 3.52). Although a 3/4-in aggregate was used for the pocket, the concrete flow through the clear tubes was minimal. Making use of just the

cavities created for the tubes in the sheet metal proved adequate to release the entrapped air during the construction of the bedding layer for PSS-16-12.

Prior to casting the bedding layer, the concrete at the top of the column inside the pocket connection was hydrated to ensure the bond of the bedding layer to the top of the column. Soaking with water immediately prior to the concrete pour was implemented for RCS-16-12, while PSS-16-12 used overnight soaked towels to hydrate the concrete at the top of the column; no significant impact between either technique was observed. Concrete slumps of 4.5-in and 5.5-in were recorded for RCS-16-12 and PSS-16-12, respectively. The overhead crane and a side shoot on the concrete bucket were used to cast the concrete into the corrugated pipe connection (Figure 3.53). The pockets were cast in three equal layers and consolidated at each level. Additional vibration was applied to the first layer around the bottom circumference of the corrugated pipe to ensure the concrete filled the bedding layer and spread around the plastic shims.

The difficult access to the bedding layer from the top of the pocket connection made spreading and consolidating of concrete challenging. During the construction of RCS-16-12, two small areas of honeycombing were present in the bedding layer as a result of the constructability problems encountered while casting the pocket connection and the lower slump (Figure 3.54). The level of honeycombing in the bedding layer was determined to be minor and showed to have no negative effects on performance during testing. The honeycombing areas were cleaned and repaired using cement grout.

Table 3.7 provides a complete list of dates for all concrete pours and assembly of components for all specimens.

(a) Formwork

(b) Air Vents

Figure 3.52. Bedding Layer Formwork and Air Vents.

(a) Bottom View

(b) Top View

Figure 3.53. Casting of the Bedding Layer.

Figure 3.54. Honeycombing in Bedding Layer – Front Face.

Table 3.7. Construction Timetable.

Specimen	Activity	Date
RCS-16-12	Cap Pour	6/2/2016
	Base Pour	6/3/2016
	Column Pour	6/6/2016
	Assembly	7/14/2016
	Pocket Pour	7/18/2016
PSS-16-12	Cap Pour	8/26/2016
	Strand Release	8/29/2016
	Base Pour	8/11/2016
	Column Pour	8/12/2016
	Delivery	11/3/2016
	Assembly	11/3/2016
	Pocket Pour	11/7/2016
PSS-16-24	Cap Pour	8/26/2016
	Strand Release	8/29/2016
	Base Pour	11/18/2016
	Column Pour	11/22/2016
	Delivery	1/18/2017
	Assembly	1/18/2017
	Pocket Pour	1/26/2017
PSV-16-12	Cap Pour	8/26/2016
	Strand Release	8/29/2016
	Base Pour	11/18/2016
	Column Pour	11/22/2016
	Delivery	12/15/2016
	Assembly	12/15/2016
	Pocket Pour	12/19/2016

3.5. Experimental Test Setup

Figure 3.55 shows a 3D rendition of the experimental setup in the Texas A&M University High Bay Structural and Materials Testing Laboratory. The specimen has a bent cap length of 16-ft and a column height of 6.3-ft (8-feet to the center of bent cap). The column rested on a roller foundation bolted to a 10-ft x 7-ft steel plate. Horizontal actuators (HT, HB) attached to the horizontal load reaction steel frames provide stability. Two top vertical actuators (P1, P2) supported on 9-ft headers between the vertical reaction towers simulate the girder loads. The bottom vertical actuator acted as the shear at the bent cap inflection point and connected to the strong floor by a 4-ft x 4-ft steel plate. The following sections describe in detail the connection of the specimen, actuators, and support towers.

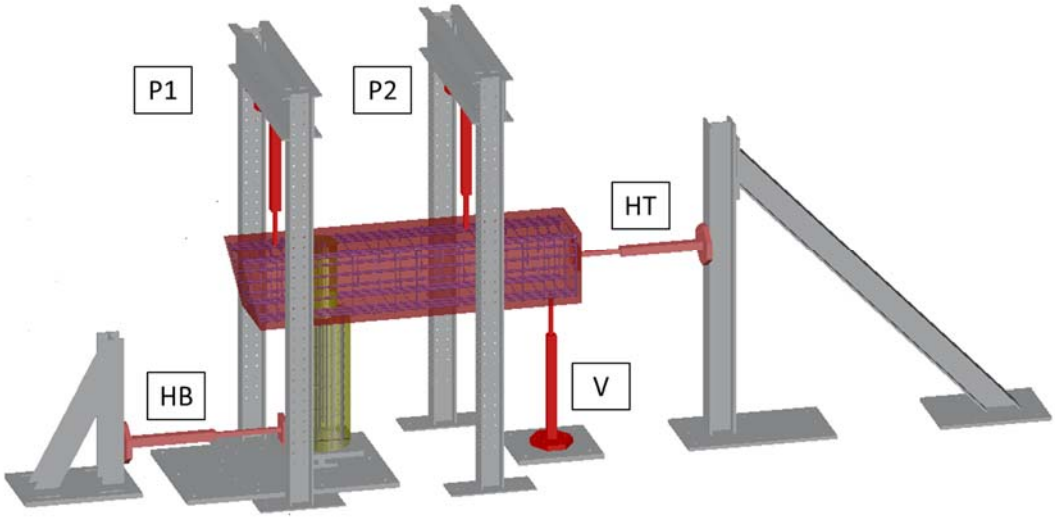

Figure 3.55. Laboratory Experimental Setup – 3D Rendition.

3.5.1. *Connection Details – Reaction Frames*

The strong floor consists of 3-in diameter holes spaced at 3-ft. The vertical reaction towers, reaction plate and horizontal reaction frames for the specimens were attached to the laboratory strong floor by 2.5-in Dywidag threaded bars and each tensioned to 3,000 psi (Figure 3.56). The specimen was aligned above a strong floor foundation wall to accommodate the large forces acting on the specimen (See Figure 3.57 and Figure 3.58).

Figure 3.56. Post-tensioned Dywidag Connection to Strong Floor.

(a) Bottom Horizontal Reaction Frame

(b) Top Horizontal Reaction Frame

Figure 3.57. Horizontal Reaction Frames.

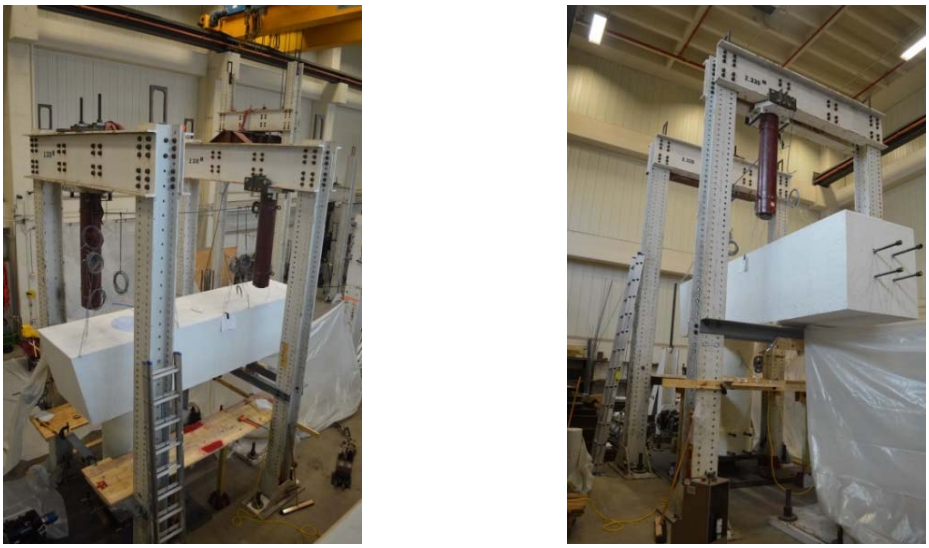

(a) Top View *(b) Bottom View*

Figure 3.58. Vertical Reaction Towers.

3.5.2. *Connection Details – Specimen Foundation Base Plate*

The Texas A&M University High Bay Structural and Materials Testing Laboratory had in its inventory a 10-ft x 7-ft x 3-in plate that served as the base plate for the column to attach securely to the laboratory floor. The roller foundation was attached to the 10-ft x 7-ft base plate using 1-in diameter tap and drilled bolts connections. Additional 3-in diameter holes for the Dywidag were necessary for the base plate as seen in Figure 3.59. The additional Dywidag holes required the use of a magnetic drill press kit with a 3-in diameter and 3-in cutting depth titanium coated high-speed Weldon 1-1/4-in shank annular cutter (Figure 3.60). The roller foundation plate was attached to the 10-ft x 7-ft plate in a similar fashion. The magnetic drill was used to drill 7/8-in holes and tapped for a 1-in 8 UNC (Figure 3.61 and Figure 3.62).

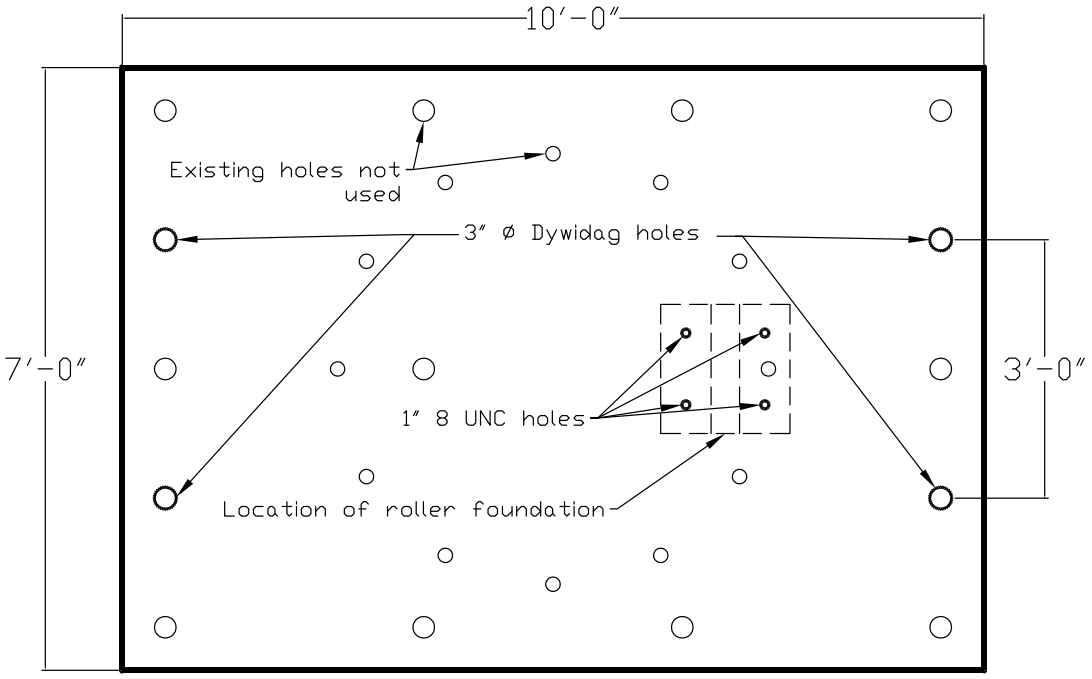

Figure 3.59. 10-ft x 7-ft Base Plate.

(a) Magnetic Drill *(b) Drilling 3-in Holes*

Figure 3.60. Drilling 3-in Holes for Dywidag Bars.

(a) Drilling 7/8-in holes

(b) Tapping 1-in 8 UNC

Figure 3.61. Drilling and Tapping 1-in Roller Foundation Threads.

Figure 3.62. Installation of Roller onto 10-ft x 7-ft Base Plate.

3.5.3. *Connection Details – Column Roller Foundation Assembly*

The roller foundation assembly acted as a pin connection at the inflection point of the exterior column of the prototype bridge. Brazos Industries Inc., a local machinery shop, was contracted to construct the roller foundation consisting of a 4-in diameter by 18-in long roller (Part D) welded to a 2-in steel plate and three other separate steel plates (Parts A-C) manufactured with ASTM 572 Grade 50 steel (Figure 3.63).

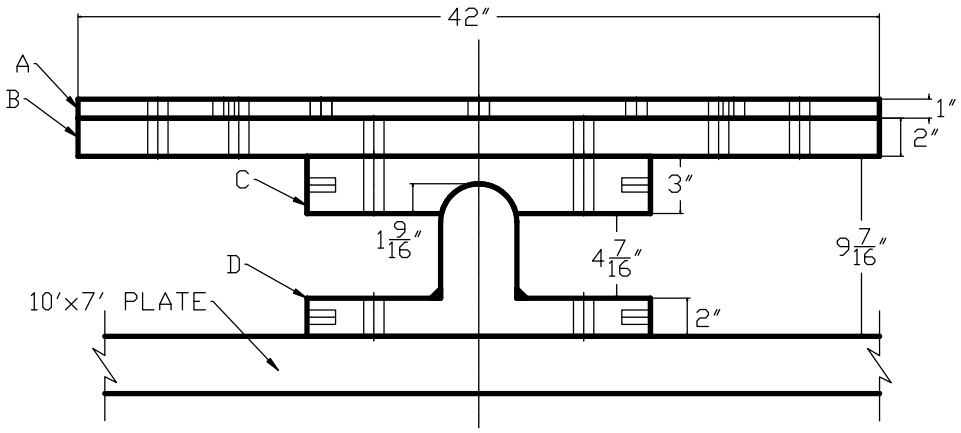

Figure 3.63. Roller Foundation Plans.

Part A consisted of a 42-in x 42-in x 1-in steel plate that incorporated the drilled and taped 1-in 8-UNC holes for the column longitudinal bars which were threaded into the 2-in plate connecting the column base to the roller foundation (Part B). Two 1-1/16-in through-holes at each corner were also included in Part A for 1-in bolts that would attach to Part B. Part A was designed to be disposed of after each test. Part B had dimensions of 42-in x 42-in x 2-in with the 1-1/16-in through-holes at each corner to connect to the Part A. Four additional holes were tapped and drilled near the center of Part B for 1 in – 8 UNC to attach to Part C. Part C consisted of an 18-in x 18-in x 3-in steel plate that was machined to have a 4-in diameter "half circle" void matching the top of the roller of Part D. Part C also had four holes tapped and drilled for 1-in -8 UNC to attach to Part B. Part D acted as the main component of the roller foundation representing the pin at the moment inflection point at the exterior column of the prototype bridge and consisted of two pieces of steel. The top vertical piece was a 6-in x 4-in block of steel machined to

have a 4-in diameter half circular surface at the top and was then welded with 1/2-in E70XX electrodes on both sides to the 18-in x 18-in x 2-in horizontal plate. The horizontal plate also had 1-1/8-in through-holes to attach 1-in threaded bolts to the 10-ft x 7-ft base plate (Figure 3.64 and Figure 3.65).

(a) Plate A - 1-in

(b) Plate B - 2-in

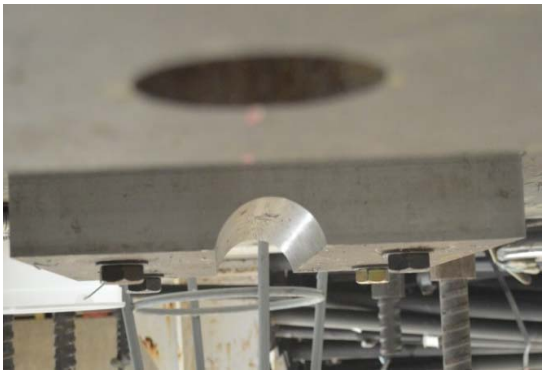

(c) Part C – Top Half Circle

(d) Part D - Roller

Figure 3.64. Roller Foundation Assembly.

Figure 3.65. Installed Roller Foundation Assembly onto Test Setup.

3.5.4. *Connection Details – Actuators*

The 110 kip actuators providing the horizontal stability (HT and HB) for the specimens required the installation of rods cast into the specimens as seen in Figure 3.66. The cleats of the 110 kips actuators had four 1-1/4-in holes located 11-in apart. Williams Form Engineering 150-ksi 1-in all-thread rods were cast into the column base and the square end of the bent cap to provide the attachment of the 110 kip actuators to the specimen. The horizontal actuators were mounted to the horizontal reaction frames.

The two top vertical actuators acting as the girder loads (P1 and P2) were attached to 9-ft headers at the top of the steel towers (Figure 3.67.a). The bottom vertical actuator (V) rested on a 3-in thick base plate attached to the laboratory floor (Figure 3.67.b).

(a) HT Actuator Connection

(b) HB Actuator Connection

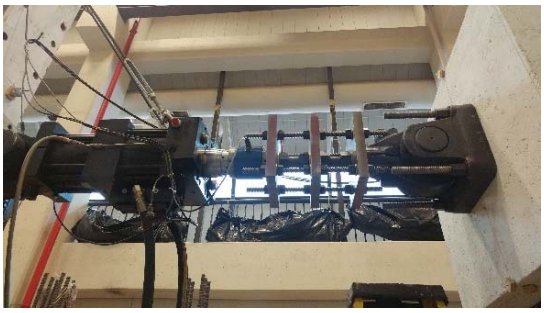

(c) Installed HT Actuator

(d) Installed HB Actuator

Figure 3.66. Horizontal Actuator Connections.

(a) P1 and P2 Actuators

(b) V Actuator

Figure 3.67. Vertical Actuator Connections.

The bearing pads were purchased from TxDOT approved producer Dynamic Rubber Inc. The two bearing pads simulated the ends of two girders as they rest on the bent cap. The dimensions and locations of the bearing pads followed the guidelines from elastomeric bearing and girder end details (Figure 3.68 and Figure 3.69).

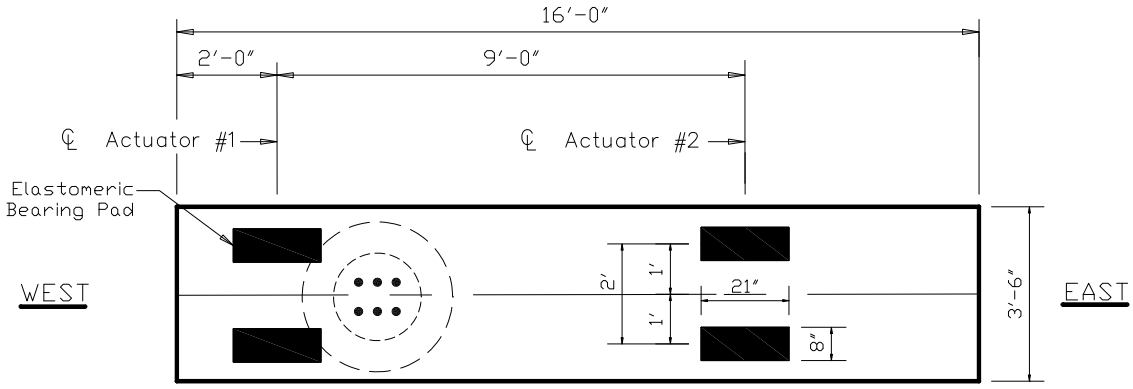

Figure 3.68. Bearing Pad Layout Plans.

(a) P1 Actuator Bearing Pad

(b) P2 Actuator Bearing Pad

Figure 3.69. Elastomeric Bearing Pads.

Two actuator load assemblies were designed to evenly distribute the loads from the single actuator ram to the two bearing pads. Each actuator contact assembly consisted of two A-992 steel 10X30 C-channels welded to a 2-in plate and with an additional 2-in plate resting between the actuator load assembly and the actuator ram (Figure 3.70).

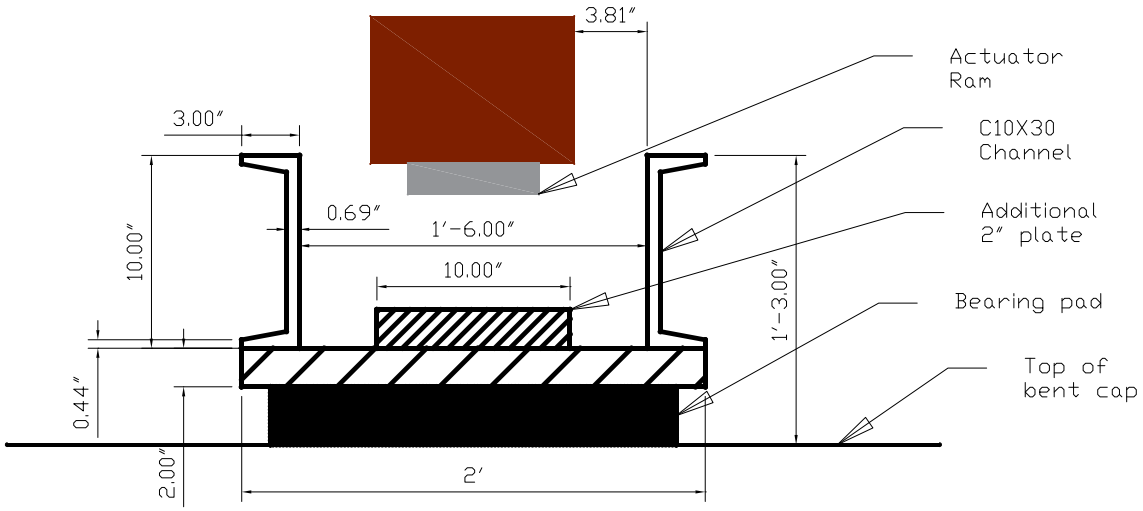

(a) Actuator Load Assembly Plan

(b) Installation

(c) Additional 2-in Plate

Figure 3.70. Actuator Load Assembly.

3.6. Instrumentation

A major objective of this experimental study was to obtain reliable data for the evaluation of the bent cap specimens. To obtain the desired data, different types of instruments and their locations were carefully chosen. The instruments were categorized into internal and external instrumentation. The internal instrumentation was strain gauges. The external instrumentation was linear string potentiometers, linear variable differential transformers (LVDT), and stationary cameras. The following sections explain the installation plan and description of each instrument. Detailed instrumentation plans are provided in Appendix D.

3.6.1. *Strain Gauges*

Strain gauges were used to measure the strain at critical locations. In RCS-16-12, a total of 38 strain gauges were attached to bent cap flexural reinforcement, shear reinforcement, column longitudinal bars, steel corrugated pipe and dowel bars. Pretensioned specimens had the same strain gauge layout, but without strain gauge on flexural reinforcement. Locations are shown in Figure 3.71 and the number of strain gauges is summarized in Table 3.8.

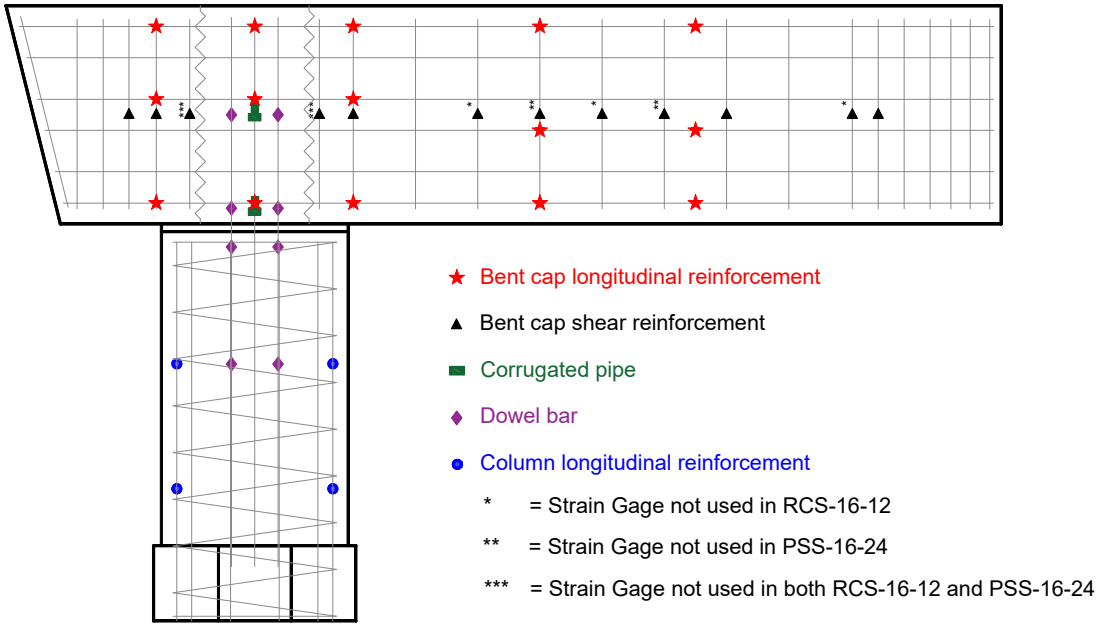

Figure 3.71. Strain Gage Layout

Table 3.8. Summary of Strain Gauge

Specimen	Bent cap		Column Longitudinal	Dowel bar	Pipe	Total
	Flexural	Transverse				
RCS-16-12	15	7	4	8	4	38
PSS-16-12	0	12	4	8	4	28
PSS-16-24	0	10	4	8	4	26
PSV-16-12	0	12	4	8	4	28

For the bent cap flexural reinforcement, strain gauges were attached at column faces, the center of the column, and at the P2 and V actuator locations. At these locations, gages were placed on top, middle, and bottom bars to allow generation of strain profiles. For shear reinforcement, strain gauges are placed at the points where significant shear force and change are expected. Strain gages on transverse reinforcement were located at

the vertical center of the hoop. Two strain gauges were evenly distributed for each of two column longitudinal bars. Eight strain gauges were installed on two dowel bars at the mid-depth of the bent cap, bottom of the bent cap near the joint, top of the column near the joint, and middle of the column, respectively. Two horizontal and two vertical strain gauges are placed on the corrugated pipe at the bottom and mid-depth of the bent cap.

Strict guidelines were followed during the installation of strain gages. The first step was to prepare the rebar surfaces with flap sanding discs for nonmetals with a 320 grit to ensure the diameter of the bars was not reduced, followed by a cleaning with acetone and installation tape (Figure 3.72). A straight edge was then used to draw a lightly pressed marked line parallel to the length of the bar and another line perpendicular to the length of the bars to ensure the proper location of the strain gage. A second strip of installation tape was used to assist in the placement of the Vishay CEA-06-250UN-350 strain gages and CPF-75C port. The tape was partially rolled back with the attached strain gage and port, and the M-Bond 200 was applied to the bottom of the strain gage and port then lightly pressed back onto the rebar for at least 30 seconds to allow the M-Bond 200 to cure; the tape was removed afterward (Figure 3.73). The strain gages and terminals were connected using lead based solder and copper wires, and the terminals were soldered to the 326-DFV wires with sufficient length to exit the bent cap formwork (Figure 3.74). The 326-DFV wires were then fed through 1/8-in clear heat shrink tube to for protection during the casting of concrete and coated with M-Coat B to increase the bond with the M-Coat JA. The final M-Coat JA and protective tape where applied to seal the strain gages against any moisture and chemicals from the concrete (Figure 3.75). The strain gage wires were then

fed to the chosen exit locations on the bent cap away from all loading points. Plastic bags were used to cover the name tags placed on each strain gage to protect from damage during concrete placement (Figure 3.76). The final step was to splice the ends of the 326-DFV wires exiting the specimen to the Belden shield twisted wire that connected to the laboratory data acquisition system.

(a) Flap Sanding Disk *(b) Sanded Surface*

(c) Acetone Cleaning Agent *(d) Installation Tape*

Figure 3.72. Surface Preparation.

(a) Parallel Marking

(b) Perpendicular Mark

(c) Tape Strain Gage Installation

(d) Secure Placement of Strain Gage

(e) M-Bond 200 Adhesive

(f) Application of M-Bond 200 Adhesive

Figure 3.73. Strain Gage Installation.

(a) Soldering Kit

(b) Soldered Ports

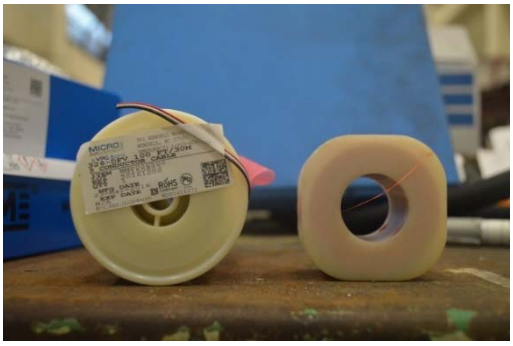

(c) 326-DFV and Copper Wire

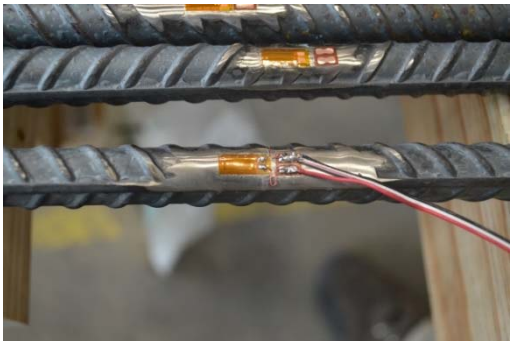

(d) Soldered 326-DFV Wires

Figure 3.74. Soldering and Wiring of Strain Gages.

(a) M-Coat A

(b) Application of M-Coat A

(c) M-Coat B

(d) Application of M-Coat B

(e) M-Coat JA

(f) Application of M-Coat JA

Figure 3.75. Application of Protective Coats.

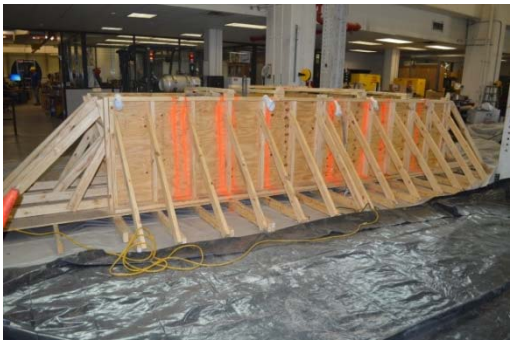

(a) Before Casting Concrete

(b) After Casting Concrete

Figure 3.76. Strain Gage Wire Exit Locations.

3.6.2. *LVDT (Linear Variable Differential Transformers)*

Six LVDTs were installed on at the bent cap-column connection, and two LVDTs two installed under bent cap adjacent to the column (Figure 3.77). LVDTs within the bent cap-to-column connection measured relative vertical, horizontal and diagonal displacement to monitor joint shear deformations. The vertical LVDTs under the bent cap adjacent to the column measured opening at the bedding layer.

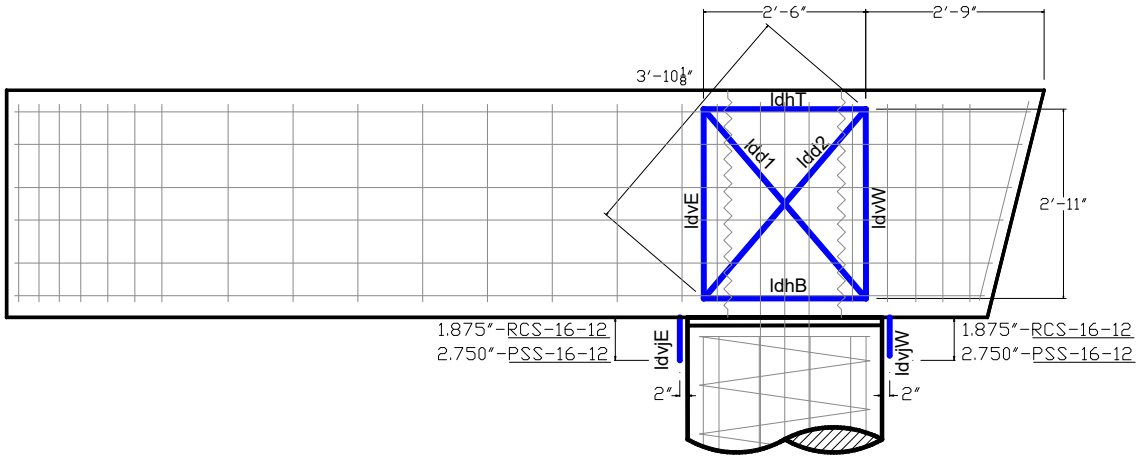

Figure 3.77. LVDT Layout.

3.6.3. *Linear String Potentiometers*

Twenty-six linear string potentiometers were used to measure the horizontal and vertical displacement of the specimens (Figure 3.78). Thirteen vertical string potentiometers were placed along the bottom center of the bent caps to measure vertical displacements. Four additional string potentiometers placed at corners were to monitor torsion. Nine string potentiometers were placed horizontally on the west side of bent cap and column to measure displacement. Two on the east side monitored displacement at the top horizontal actuator. Two string potentiometers at the octagon column based were installed to check whether slip occurs.

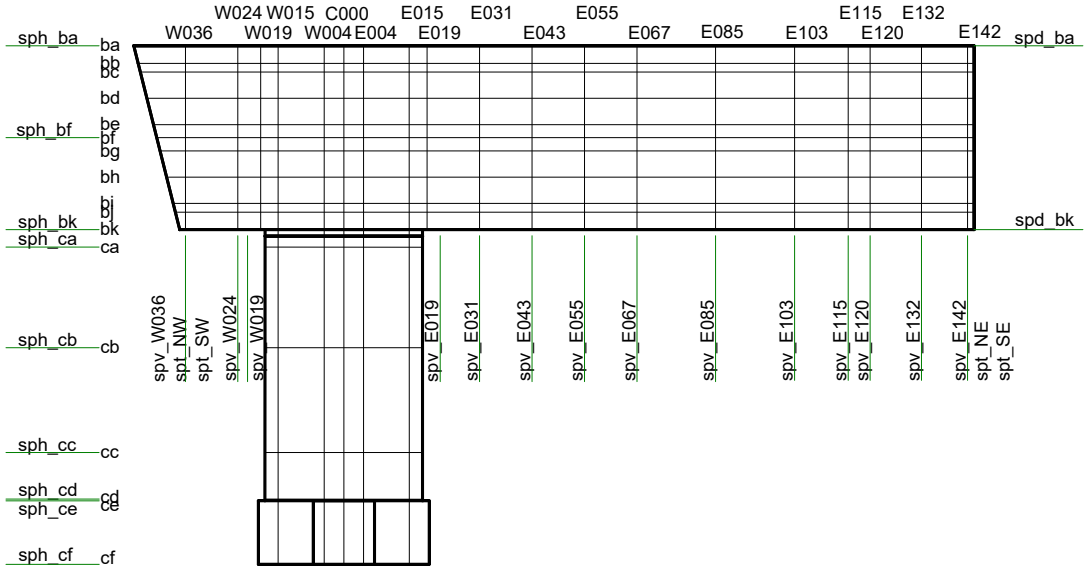

Figure 3.78. Linear String Potentiometer Layout.

3.6.4. *Stationary Cameras*

Eight stationary GoPro cameras were installed throughout the experimental test set setup to capture the formation of cracks in the specimens. Cameras 1 and 2 were installed to capture damage in the bedding layer at the east and west faces of the column. Cameras 3, 4, and 5 were installed on the reaction towers to record the formation of damage along the front face at the joint, mid-span and span. Camera 6 was installed on actuator P1 to record damage at the top of the pocket connection. Figure 3.79 shows the location of the cameras capturing damage on the specimen taken by camera 7. Camera 7 was installed on the back wall of the laboratory to provide a complete picture of the entire specimen. Camera 8 was installed in front of a data acquisition system computer screen to relate all the images relate each image to its relative time step and actuator loads. Figure 3.80 shows the close location and supports used to install each individual camera.

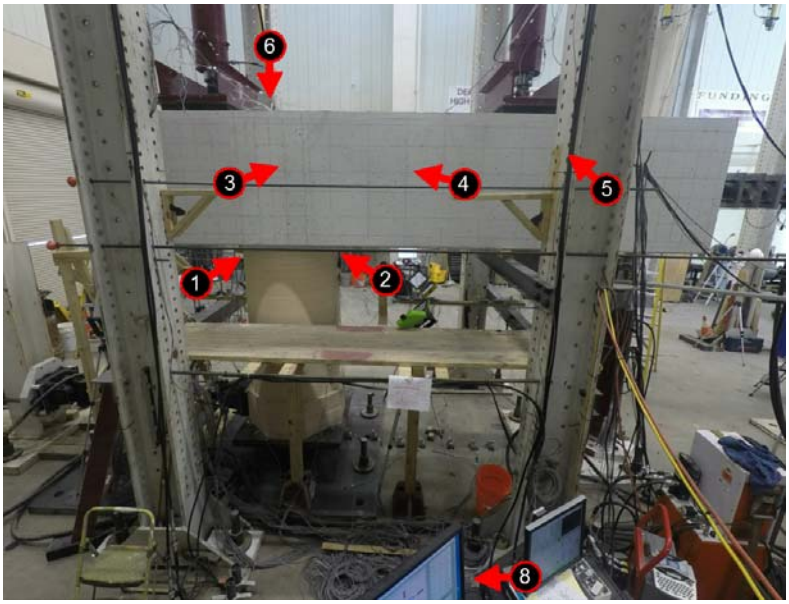

Figure 3.79. GoPro Camera Locations (Image taken by Camera #7).

(a) Camera 1

(b) Camera 2

(c) Camera 3

(d) Camera 4

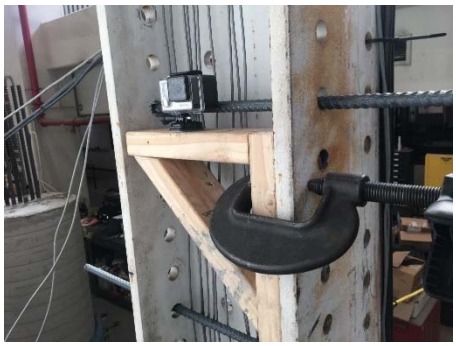

(e) Camera 5

(f) Camera 6

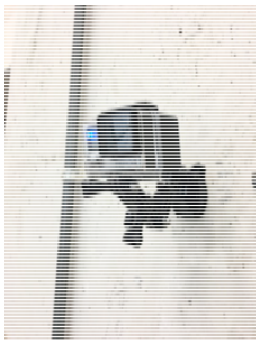

(g) Camera 7

(h) Camera 8

Figure 3.80. GoPro Cameras Mounting Positions.

3.7. Material Properties

The following sections present the material properties results gathered for testing of samples collected for both concrete and steel.

3.7.1. *Concrete Mix Designations*

Multiple concrete mix designs were used to meet the needs of the experimental program. Separate mixes were used for bent caps (B), columns and bases (C), and pockets (P). All mixes were TxDOT Class C, Class H, or modifications of these. Table 3.9 summarizes each mix designation, the base concrete class, and any modifications.

Mix B-1 was TxDOT Class C modified to have a higher water-cement ratio (w/c) in order to achieve a 28-day compressive strength of less than or equal to 3.6-ksi. Concrete mix B-2 was a Class H concrete used for the pretensioned beams with a 28-day compressive strength less than or equal to 7.0-ksi. Table 3.10 shows the specifications of the standard Class C concrete mix design provided by Martin Marietta.

Mix design C-1 was the standard Class C concrete provided by Martin Marietta. Mix design C-2 used for PSS-16-12 had a 3/4-in aggregate for the column base due to a miscommunication with the supplier.

Several mix designs were tested for the pocket connection concrete to eliminate the use of grout since concrete is significantly less expensive and more compatible with the surrounding concrete used for other bridge components on a job site. Mix design P-1 was specifically designed for the pocket connection using a lower aggregate size of 3/4-in nominal diameter, lower paste content to reduce shrinkage, shrinkage compensating admixtures, and additional superplasticizer to increase the workability from the lower

paste. Mix design P-2 was a modification of mix design P-1. This mix included the 3/4-in nominal diameter aggregate, shrinkage admixture, used the standard paste content as a result of the poor workability from the low paste content while casting the first pocket connection and had no additional superplasticizer. Mix design P-3 was a modification of P-2 that did not use any shrinkage admixture without changing any other parameters. This mix design was chosen to evaluate the effects of the shrinkage admixtures on the performance of the pocket connection. Table 3.11 provides the specifications for the P-1 mix design created to meet the research project needs.

Table 3.9. Concrete Mix Designation

Mix ID	Specimen	Component	Concrete Class	Modifications
B1	RCS-1612	Bent Cap, Column, Base	C*	0.62 w/c ratio to delay 28-day strength
B2	All Pretensioned	Bent Cap	H	Modified water/cement ratio to meet 4-ksi release strength
C1	PSS-16-12, PSS-16-24, PSV-16-12	Column, Base	C	-
C2	PSS-16-12	Base	C*	3/4-in aggregate
P1	RCS-16-12	Pocket	C*	3/4-in nominal size aggregate, lower paste, shrinkage admixture, additional superplasticizer
P2	PSS-16-12	Pocket	C*	3/4-in nominal size aggregate, shrinkage admixture
P3	PSV-16-12	Pocket	C*	3/4-in nominal size aggregate
P3	PSS-16-24	Pocket	C*	3/4-in nominal size aggregate

** Modified Class C Concrete*

Table 3.10. Standard Class C Concrete

Material	Description	Specific Gravity	Weight (unit/yd)
Cement	ASTM C150 - Type I/II Cement	3.15	358 lb
Alt. Binder	ASTM C618 - Class C Fly Ash	2.63	193 lb
Fine Agg.	ASTM C33 - Concrete Sand	2.63	1133 lb
Coarse Agg.	ASTM C33 - #57 Limestone	2.79	2070 lb
Water	ASTM C94 - 30 Gallons		250 lb
Air	ASTM C260 - MB-AE-90		3 oz
WR	ASTM C494 - PolyHeed 997		21 oz
		Totals:	4006 lbs

Specified Slump: 5.00" +/- 1.50"
Designed Units Weight: 148.5 lbs/cu.ft.
Specified Air: 4.50% +/- 1.50%
Designed w/cm ratio: 0.45

Table 3.11. Modified Class C Concrete for P-1

Material	Description	Specific Gravity	Weight (unit/yd)
Cement	ASTM C150 - Type I/II Cement	3.15	374 lb
Alt. Binder	ASTM C618 - Class C Fly Ash	2.63	161 lb
Fine Agg.	ASTM C33 - Concrete Sand	2.63	1333 lb
Coarse Agg.	ASTM C33 - #67 Limestone	2.79	1900 lb
Water	ASTM C94 - 29 Gallons		242 lb
Air	ASTM C260 - MB-AE-90		5 oz
WR	ASTM C494 - PolyHeed 997		22 oz
		Totals:	4010 lbs

Specified Slump: 5.00" +/- 1.50
Designed Units Weight: 148.5 lbs/cu.ft.
Specified Air: 4.50% +/- 1.50%
Designed w/cm ratio: 0.45

3.7.2. *Concrete Material Properties*

Concrete material properties tests were conducted for the slump, compression strength, modulus of elasticity, tensile strength, and modulus of rupture. Representative samples of fresh concrete were collected according to ASTM C172/C172M standards. All molded cylinders and beam specimens were collected according to the requirements of ASTM C31/C31M (Figure 3.81).

For each concrete delivery, a standard test for a slump of hydraulic-cement concrete was conducted following ASTM C143/C143M to determine the consistency of the concrete, relative fluidity, mobility of the concrete mixture, and to ensure compliance with TxDOT specifications for hydraulic cement concrete.

Cylinder compressive strength tests were carried out according to ASTM C39/39M. Three 6-in x 12-in cylindrical specimens were tested for each test and the final results were provided as averages of the compression strengths. Target testing dates were 1, 3, 7, 14 and 28 day and the experimental testing date compressive strengths. Several testing dates did not meet the target date and have been noted accordingly. Table 3.12 provides a summary of the slump and compression strength test results for all concrete deliveries. Figure 3.82 shows the strength of concrete (f'_c) versus time plots for all specimens.

(a) Sample Collection

(b) Curing Room

Figure 3.81. Collecting and Curing Concrete Samples.

Table 3.12. Cylinder and Slump Test Results

Name	Comp.	Mix ID	Slump (in)	f'_c (ksi)					
				1 day	3 day	7 day	14 day	28 day	Test day
RCS-16-12	Cap	B1	5.50	0.64	*2.37	2.73	3.90	4.61	5.59
	Column	C1	6.25	0.55	1.54	2.07	2.75	**3.33	4.49
	Base	B1	2.50	-	1.90	2.77	3.48	†4.43	4.83
	Pocket	P1	4.50	1.98	3.23	4.83	5.42	5.96	5.93
PSS-16-12	Batch A	B2	7.00	-	4.06	-	-	6.84	7.46
	Batch B	B2	7.00	-	4.13	-	-	7.19	8.01
	Column	C1	7.00	-	2.56	3.73	4.84	5.61	6.66
	Base	C2	6.50	1.62	-	3.83	5.16	†5.88	7.00
	Pocket	P2	5.50	1.55	3.52	4.48	5.02	-	5.41
PSS-16-24	Batch B	B2	7.00	-	4.13	-	-	7.19	8.01
	Batch C	B2	7.00	-	4.82	5.85	6.51	7.65	7.81
	Batch D	B2	7.00	-	4.60	-	-	7.55	8.34
	Column	C1	8.00	-	2.56	3.73	4.84	5.61	6.32
	Base	C1	6.00	1.62	-	3.83	5.16	†5.88	6.21
	Pocket	P3	6.50	1.82	-	5.96	5.68	6.61	6.61
PSV-16-12	Batch E	B2	7.00	-	3.85	-	-	7.90	8.82
	Batch F	B2	7.00	-	4.04	-	-	7.65	8.83
	Column	C1	8.00	1.04	-	3.33	4.48	5.37	5.92
	Base	C1	6.00	-	2.12	4.22	4.23	5.71	6.15
	Pocket	P3	5.50	0.91	2.48	-	3.78	**4.79	4.72

**4 day, **29 day, †32 day*

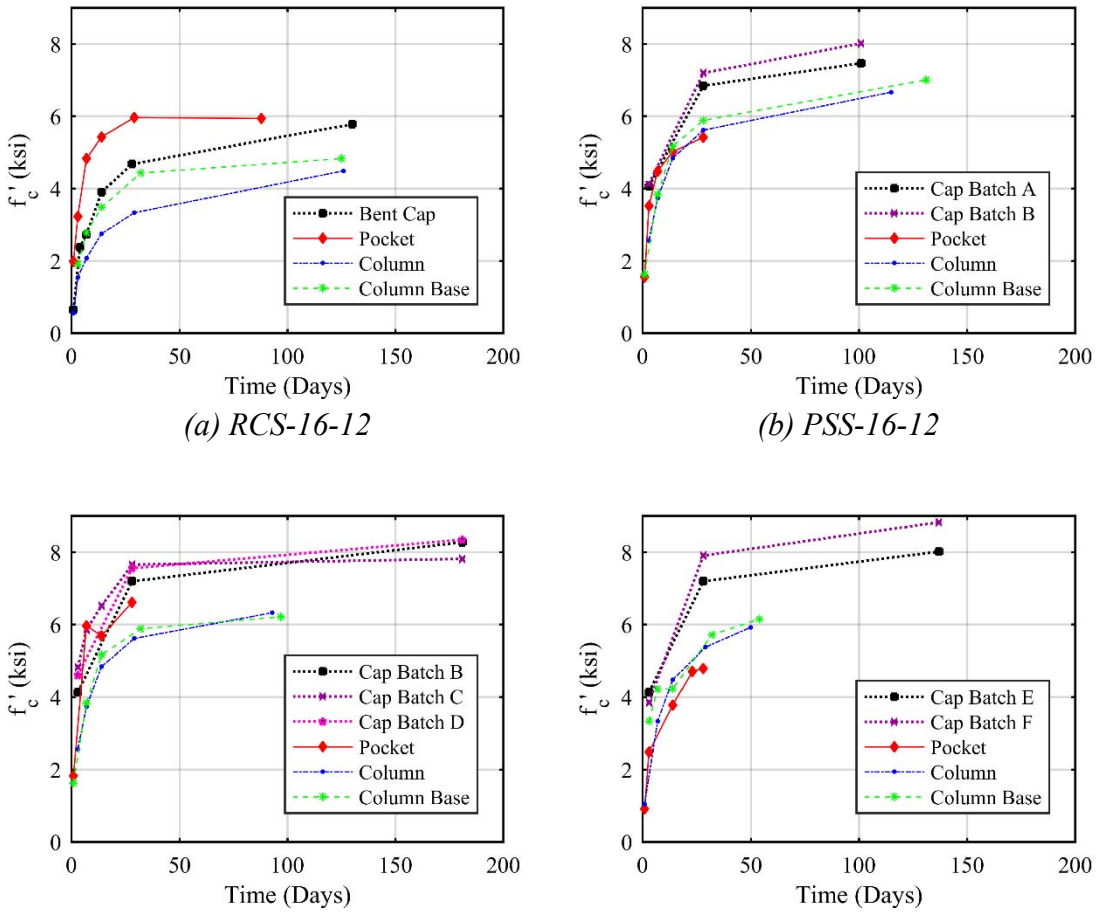

(a) RCS-16-12 *(b) PSS-16-12*

(c) PSS-16-24 *(d) PSV-16-12*

Figure 3.82. Components' Compressive Strengths vs Time.

Modulus of elasticity (E_c), tensile strength (f_{ct}), and modulus of rigidity (f_r) tests were conducted the same day as the 28-day compression strength tests and on test day. The modulus of elasticity tests followed the procedures of ASTM C469/C469M in order to provide stress-strain curves to calculate the modulus of elasticity. The splitting tensile strength tests were carried out according to ASTM C496/C496M. Modulus of elasticity and tensile strength tests used 4-in x 8-in cylinders. The modulus of rupture was

determined according to ASTM C78/C78M and used 6-in x 6-in x 21-in beams. Table 3.13 gives a summary of the E_c, f_{ct} and f_r tests results for all concrete deliveries. Figure 3.83 show material properties testing setups for the cylinder compression, modulus of elasticity, tensile strength, and modulus of rigidity material testing setups following their respective ASTM standard.

Table 3.13. MOE, Split Tensile, and MOR Test Results

Specimen	Component	Mix ID	E_c (ksi)		f_{ct} (ksi)		f_r (ksi)	
			28 day	Test day	28 day	Test day	28 day	Test day
RCS-16-12	Cap	B1	5402	6195	0.67	0.73	0.67	0.79
	Column	C1	4927	5574	0.68	0.64	0.59	0.74
	Pocket	P1	-	6024	-	0.83	-	0.89
PSS-16-12	Cap-Batch A	B2	-	4920	-	0.95	-	-
	Cap-Batch B	B2	-	3914	-	0.87	-	-
	Column	C2	5447	6340	0.77	0.77	0.93	0.92
	Pocket	P2	-	5840	-	0.79	-	0.85
PSS-16-24	Cap-Batch B	B2	-	-	-	-	-	-
	Cap-Batch C	B2	3976	-	0.83	-	0.85	-
	Cap-Batch D	B2	-	-	-	-	-	-
	Column	C1	5447	-	0.93	-	0.77	-
	Pocket	P3	-	-	-	-	-	-
PSV-16-12	Cap-Batch E	B2	-	-	-	0.91	-	-
	Cap-Batch F	B2	-	-	-	0.90	-	-
	Column	C1	-	5333	0.72	0.72	0.84	0.92
	Pocket	P3	-	5027	0.71	0.63	0.74	0.77

(a) Compressive Strength

(b) Modulus of Elasticity

(c) Modulus of Elasticity

(d) Modulus of Rupture

Figure 3.83. Material Properties Test Setups

3.7.3. *Steel Material Properties*

Steel material properties test were conducted through a tensile test. The tensile tests provided the yield strength, ultimate strength, modulus and elasticity and yield strain of the mild steel incorporated in the construction of the specimens. Applied Technical Services was contracted to test the rebar sizes #5, #8 and #11 that were used during the construction of RCS-16-12 and PSS-16-12. A total of three tensile test were performed for each rebar size. Table 3.14 provides the average value reported for each of the parameters according to the size of rebar tested.

Table 3.14. Steel Tensile Test Results

Size	f_y (ksi)	f_u (ksi)	E (ksi)	ε (in/in)
#5	64	103	28480	0.00225
#8	66	107	29497	0.00225
#11	68	106	28147	0.00240

3.8. Expected Strengths

Expected strengths of the specimens were calculated prior to conducting the experimental test to assist in the development of the load patterns. Measured material properties were obtained from the materials testing covered in Section 3.7. Flexure and shear strengths were both considered and the expected strengths calculations in this section are limited to RCS-16-12 and PSS-16-12. Details are explained in the following sections.

3.8.1. *Flexural Strength*

Flexural moment strength includes zero tension, cracking, yield and nominal moment capacities. Within the elastic range, the stress at the extreme tension fiber (f_t) of a pretensioned cross-section is calculated by:

$$f_t = -\frac{F}{A} + \frac{M}{S_x} \tag{3-2}$$

in which A = area of cross-section; and S_x = section modulus, M = external flexural demand; and F = prestressing force is given by:

$$F = nT_{strand} \tag{3-3}$$

where n = number of strands; T_{strand} = prestressing force per strand and is calculated by:

$$T_{strand} = f_{pbt} A_{ps} (1 - \Delta f_{pT}) \tag{3-4}$$

in which f_{pbt} = stress limit in low relaxation strand immediately prior to transfer (= $0.75 f_{pu}$); f_{pu} = specified tensile strength of prestressing strand (= 270-ksi, AASHTO LRFD Table 5.4.4.1-1); A_{ps} = area of each strand (= 0.217 in^2 for 0.6-in diameter strand); Δf_{pT} = prestress loss in pretensioned members (assumed= 20%).

Since the objective of the experimental testing program is to validate the zero tension under dead load philosophy, Equation 3-2 is used to calculate the moment producing stress of zero at the extreme tension fiber. The 42-in square section with 16 0.6-in diameter strands has a zero-tension moment equal to 328 k-ft. The cracking moment, M_{cr}, for reinforced concrete and pretensioned concrete was calculated by: -

$$M_{cr} = \frac{I_g}{y_t}\left(f_r + \frac{F}{A}\right) \tag{3-5}$$

in which; I_g = gross moment of inertia; y_t = distance from the neutral axis to the extreme tension fiber (inch); and A = area of gross section, f_r = modulus of rupture of concrete. Two different methods value were used for the modulus of rupture of concrete, i) the theoretical value of $0.24\sqrt{f'_c}$ obtained from AASHTO LRFD 5.4.2.6 and ii) the results from the modulus of rupture material tests. Values for the cracking moment were calculated for each batch of concrete used in the construction of each specimen. Table 3.15 gives a summary of the expected cracking moments. Two separate batches were used during the construction of PSS-16-12 and separate positive and negative cracking moments were calculated respectively. Material properties for the modulus of rupture were for only conducted for Batch C. A ratio of $\beta_r = f_r / f'_c$ from the measured modulus of rupture properties from Batch C was used to calculate the f_r values for Batch A and B using their corresponding f'_c measured properties.

Table 3.15. Summary of Expected Cracking Moment Strengths

Specimen	Moment Region	AASHTO		Measured Properties	
		f_r (ksi)	M_{cr} (k-ft)	f_r (ksi)	M_{cr} (k-ft)
RCS-16-12	-	0.576	593	0.787	810
PSS-16-12	Negative	0.679	1027	0.872	1225
	Positive	0.656	1003	0.812	1164

Yield strength (M_y) and nominal strength (M_n) are computed by the Menegotto-Pinto strain compatibility method for both reinforced and pretensioned specimens. Yield strength is defined as the point where the strain at the level of the tension steel is equal to the yield strain. RCS-16-12 steel yield strain (ε_y) was defined from the measured steel properties in Section 3.7.3 and PSS-16-12 strand yield strain (ε_{py}) used the theoretical yield strain for low relaxation strands. Nominal strength is defined as the point where the extreme compression fiber reaches a strain of 0.003 in/in. All values of f'_c used in yield and nominal strength calculations were gathered from measured material properties in Section 3.7.2. Table 3.16 gives a summary of the expected yield and nominal moment strengths.

Table 3.16. Summary of Expected Yield and Nominal Moment Strengths

Specimen	Moment Region	f'_c (ksi)	ε_y, ε_{py} (in/in)	M_y (k-ft)	ε_{cu} (in/in)	M_n (k-ft)
RCS-16-12	-	5.59	0.00225	1010	0.003	1201
PSS-16-12	Negative	8.01	0.01200	1332	0.003	1435
	Positive	7.46	0.01200	1323	0.003	1425

3.8.2. *Shear Strength*

Expected shear strengths are considered to investigate the effects of flexure-shear interaction since the specimens will be subjected to both shear and flexure rather than pure flexure. The cracking shear was calculated by analyzing the principle planes and stresses using Mohr's Circle. The nominal shear strengths were calculated using the LRFD sectional design method in Appendix B5 of AASHTO LRFD 2014 derived from the modified compression field theory.

The initial shear crack angle (θ_{cr}) may be obtained from:

$$\cot \theta_{cr} = \sqrt{1 + (\frac{P}{A_g f_t})} \tag{3-6}$$

in which P = total prestress force after losses; A_g = gross cross-sectional area; and f_t = tensile strength of concrete = 4 $\sqrt{f'_c}$ *(ksi)*.

Thus, the average cracking shear capacity was calculated using the following equation:

$$V_{cr} = f_t A_g \cot\theta_{cr} \tag{3-7}$$

The following equations were used to calculate the nominal shear strength:

$$V_n = V_c + V_s + V_p \tag{3-8}$$

$$V_c = \beta\sqrt{f'_c}\, b_v d_v \tag{3-9}$$

$$V_s = A_v f_y d_v \cos\theta \tag{3-10}$$

in which V_c = nominal shear resistance provided by tensile stresses in concrete; V_s = shear resistance provided by shear reinforcement; V_p = component in the direction of the applied shear of effective prestressing force; s = spacing of transverse reinforcement, β = factor indicating ability of diagonally cracked concrete to transmit tension and shear; f'_c = specified compressive strength of concrete; b_v = effective web width; d_v = effective shear depth; A_v = area of shear reinforcement within s; f_y = yield strength of reinforcing bars; and θ = angle of inclination of diagonal compressive stresses.

The net longitudinal tensile strain (ε_s) is required to compute β and θ in both methods. In LRFD sectional design method, ε_s is given by:

$$\varepsilon_s = \frac{\left(\frac{|M_u|}{d_v} + 0.5N_u + 0.5|V_u - V_p|\cot\theta - A_{ps}f_{po}\right)}{2(E_s A_s + E_{ps}A_{ps})} \tag{3-11}$$

in which $|M_u|$ = absolute value of the factored moment; N_u = factored axial force; V_u = factored shear force; A_{ps} = area of prestressing steel on the flexural tension side of the member; f_{po} = a parameter taken as modulus of elasticity of prestressing tendons (= $0.7f_{pu}$); E_s = modulus of elasticity of reinforcing bars; A_s = area of non-pretensioned steel on the flexural tension side of the member; and E_{ps} = modulus of elasticity of prestressing tendons.

The parameters for β and θ are obtained from Table B5.2-1 and Table B5.2-2 in LRFD AASHTO specification for the section with more than minimum transverse reinforcement and the section with less than minimum transverse reinforcement, respectively, using computed ε_s. An iterative process is required to validate computed ε_s. β and θ are given by:

For more than minimum transverse reinforcement:

$$\beta = \left(\frac{4.8}{1+750\varepsilon_s}\right) \tag{3-12}$$

For less than minimum transverse reinforcement:

$$\beta = \left(\frac{4.8}{1+750\varepsilon_s}\right)\left(\frac{51}{39+s_{xe}}\right) \tag{3-13}$$

$$\theta = 29+3500\varepsilon_s \tag{3-14}$$

in which s_{xe} = equivalent value of s_x which allows for influence aggregate size; and s_x = crack spacing parameter. Material properties for split tensile strength were for only conducted for Batch C. A ratio of $\beta_t = f_t / f'_c$ from the measured split tensile properties of Batch C was used to calculate the f_r values for Batch A and B using their corresponding f'_c measured properties. Table 3.17 gives a summary of the expected cracking and nominal shear strengths using the ACI and measured properties values for f_t. It should be noted that for the initial cracking shear, the cracks initiate from mid-height.

Table 3.17. Summary of Cracking and Nominal Shear Strengths

Specimen	f'_c (ksi)	f'_t (ksi)	θ_{cr} *(deg)*	V_{cr} *(kips)*	θ *(deg)*	β	ε_s *(in/in)*	V_n *(kips)*
RCS-16-12	5.77	0.456	45.0	406	34.5	2.33	0.0008	384
PSS-16-12	7.46	0.345	34.2	563	26.8	2.92	0.0003	505

4. EXPERIMENTAL TESTING

This chapter provides the load patterns and summarizes the experimental results for RCS-16-12 and PSS-16-12. Section 4.1 discusses the chosen load patterns. Section 4.2 provides a detailed explanation of the followed loading sequences. Section 4.3 discusses the visual observations. Section 4.4 presents the damage progression observed at each load pattern. Section 4.5 presents the crack widths following load removal. Section 4.6 summarizes the damage during bridge demands. Section 4.7 summarizes the damage during maximum moment, joint and failure demands.

4.1. Load Patterns

Figure 4.1 shows the forces applied to the specimen. Two vertical actuators, P1 and P2, simulate girder loads. A third vertical actuator, V, simulates shear at the inflection point. The upper horizontal actuator, HT, at the square end provided an axial load in the bent cap. The lower horizontal actuator, HB, was slaved to HT to provide equilibrium of horizontal forces on the specimen. All specimens were tested under multiple load patterns. The main pattern (Pattern A) generated shear and moment demands characteristic of multi-column bridge bent caps. All other patterns were selected to generate the largest demands permitted by the experimental test setup.

Figure 4.2 shows the moment diagrams for each load pattern. To achieve each load pattern, P1, P2, V, and HT actuators were controlled through a mix of force and displacement control settings. Table 4.1 summarizes the actuator controls for each load pattern. The following paragraphs provide additional details.

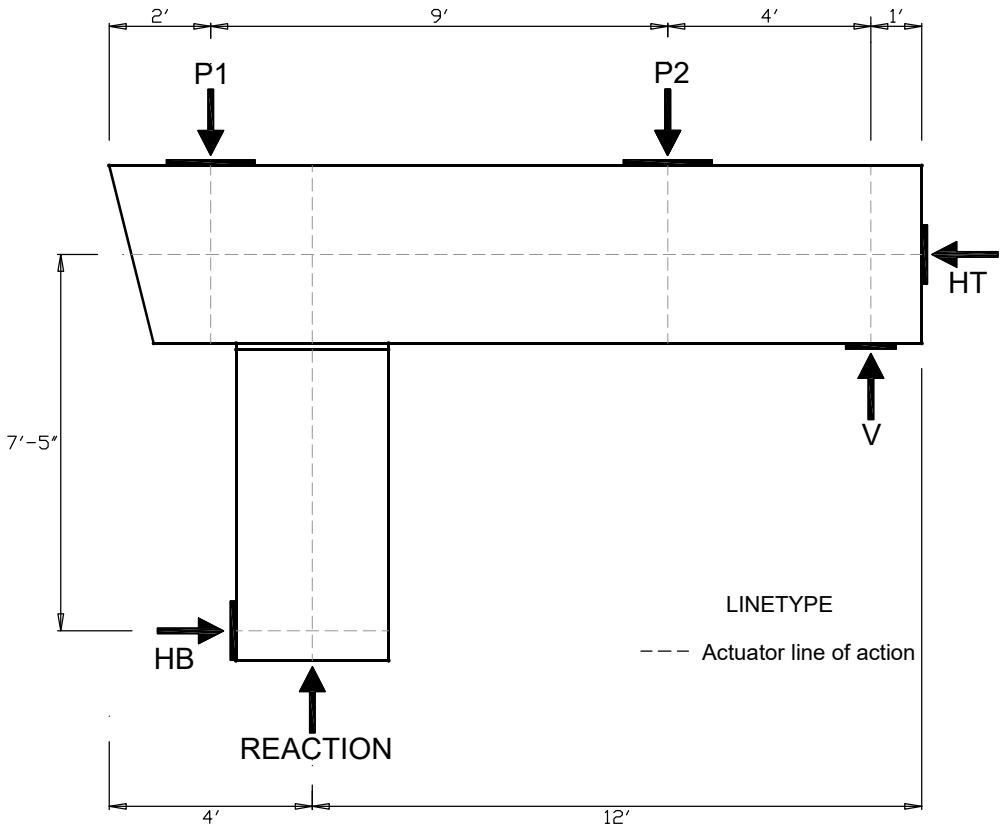

Figure 4.1. Schematic Drawing of Specimen with Actuator Forces.

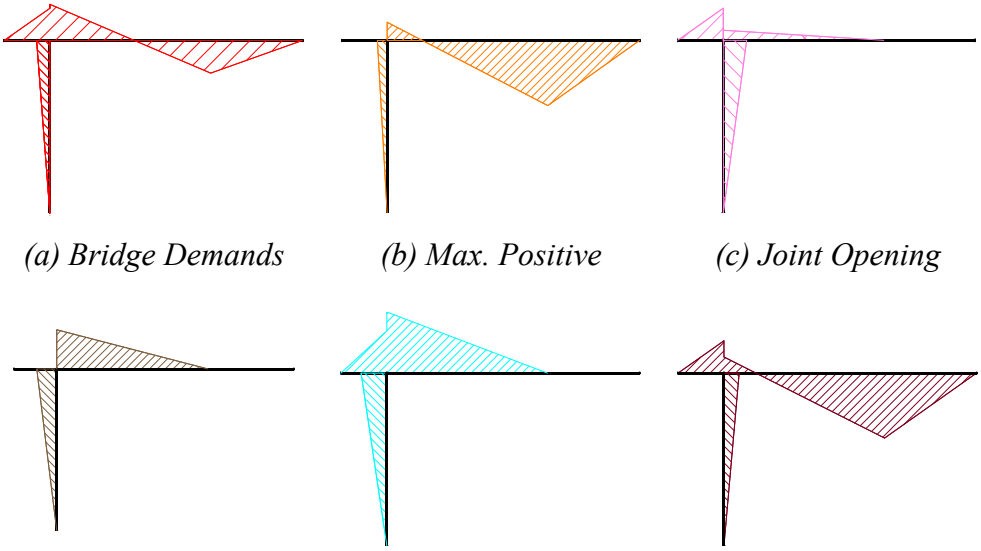

(a) Bridge Demands *(b) Max. Positive* *(c) Joint Opening*

(d) Joint Closing *(e) Max. Negative* *(f) Failure*

Figure 4.2. Load Pattern Moment Diagrams.

Table 4.1. Actuator Pattern Control

Load Pattern	Description	P1 (kips)	P2 (kips)	V (kips)	HT (kips)
A	Bridge Demands	160	160	0.48P2	Δ = 0
		270	270	0.48P2	Δ = 0
		400	400	0.48P2	Δ = 0
		Max. Capacity	Max. Capacity	0.48P2	Δ = 0
B	Max. Positive Moment	0	Max. Capacity	0.64P2	Δ = 0
C	Joint Opening	Δ = 0	0	0	100 (T*)
D	Joint Closing	0	Δ = 0	0	100 (C*)
E	Max. Negative Moment	Max. Capacity	Δ = 0	0	100 (C*)
F	Failure	Max. Capacity	Max. Capacity	Max. Capacity	105 (T*)

T (Tension), C (Compression) for HT.
Δ=Displacement Control governed by zero change in displacement
P1, P2, and V compression only.

Pattern A generated shear and moment demands characteristic of multi-column bent caps. To generate the demands seen in Figure 4.2.a, P1 and P2 increased simultaneously to simulate girder demands. To generate the desired shear demands at the span, V was set to be a factor α of P2. The HT actuator was set to zero displacement; for the prototype discussed in Section 3.2.2, α was set to 0.48. In Pattern A, P1 and P2 forces of 160 kips generated dead load P_D. Live load was assumed to be approximately 67% of dead load. Thus, $0.67P_D$ (= 110 kips) was considered as live load P_L. Service limit state (SLS) demands were the sum of dead and live loads. The ultimate limit state (ULS) demands were based on $1.25P_D + 1.75P_L$ in accordance with AASHTO LRFD 3.4.1; for simplicity during testing 400 kips was used as the ULS demand. 140% ULS was the maximum capacity that could be achieved with both actuators having the same load. Although the simultaneous loads in P1 and P2 differs from AASHTO LRFD specifications, which has different live load factors for exterior and interior girders, it is in accordance with TxDOT design practice.

Pattern B generated the maximum positive demands in the span of the bent cap that were achievable with the current test setup. Creating the demands represented in Figure 4.2.e required locking HT in displacement control, completely removing P1 and increasing P2 to its maximum capacity while V was set to force control at 0.64P2.

Pattern C provided demands testing the connection between the bent cap and column by opening the joint at the interior face of the column. To achieve the demands seen in Figure 4.2.f, P1 was locked in displacement control to simulate a reaction at the overhang while HT was increased to its maximum tensile capacity. The P2 and V loads

were removed from the specimen. The loads created positive moments at the interior face of the joint to study the performance of the bedding layer, dowel bars, and pocket connection design.

Pattern D also provided demands to test the connection by closing the joint at the interior face of the column. The loads that generated the demands seen in Figure 4.2.g were the reverse of Pattern C. The loads were applied by lowering P2 to make contact with the specimen and locked in displacement control acting as a break and HT was increased support the self-weight of the specimen. After P1 and V loads were removed, HT was increased to its maximum capacity. These loads created negative moments at the interior face of the joint to study the performance of the bedding layer and the pocket connection design.

Pattern E generated the maximum negative moment demands achievable with the current test setup. Creating the demands represented in Figure 4.2.h required lowering P2 to make contact with the specimen acting as a break and increasing P1 to its maximum capacity while setting HT to its maximum compression capacity with V completely removed from the specimen. This configuration allowed the study of the negative moment capacity of the specimen at the top of the connection region between the bent cap and column and also the performance of the pocket connection under large moment demands.

Pattern F was the final load pattern and created the necessary demands to study the different failure mechanisms between the reinforced and pretensioned concrete bent cap specimens. In order to cause failure in each specimen, actuators P1, P2, HT (tension) were set to force control at their respective maximum load capacities while V was set to

displacement control acting as a reaction. Control of V was changed to force control near the final stages of Pattern F to increase the force provided by P2.

4.2. Explanation of Loading Sequences

This section explains the specific steps taken to reach each of the previously discussed load patterns. The loads were applied incrementally from dead to 140% ULS demands. The order at which the subsequent load patterns were reached was chosen in a manner that allowed the least amount of reconfiguration of actuators. As each load pattern was reached, the loads were momentarily held constant in order to inspect and document all damage in the specimens. A summary of the main loading stages and inspection points for RCS-16-12 and PSS-16-12 are detailed in Table 4.2 and Table 4.3, respectively.

Day 1 of testing RCS-16-12 verified the proper function of all actuators, instrumentation, and data acquisition systems; no significant loads were applied to the specimen. Bridge demands up to ULS were applied on Day 2. The loads were first increased in small increments to safely monitor the response of the test setup. After reaching dead load demands, the loads were held for a one-hour period. On the way to SLS demands, the first crack appeared in the negative moment region of the specimen when P1 and P2 reached 74% of SLS (P=200k). Next, SLS and ULS demands were applied. On Day 3, the specimen was again loaded to ULS and crack growth was monitored over a six-hour period. Day 4 of testing loaded the specimen to 140% ULS (the maximum achievable loads for Pattern A) and maximum positive moment demands (Pattern B). Day 5 consisted of applying loads to open the joint (Pattern C). On Day 6, the loads were applied to close the joint (Pattern D) and generate the maximum negative

moment demands (Pattern E). The final day of testing, Day 7, consisted of creating the necessary demands to study the failure mechanism of the specimen (Pattern F).

Day 1 of testing PSS-16-12, all bridge demands up to 140% ULS were applied (Pattern A), along with a one-hour creep at design loads. Day 1 also included the application maximum positive (Pattern B), joint opening (Pattern C), joint closing (Pattern D), and maximum negative moment demands (Pattern E). Day 2 consisted of reloading the specimen to 140% ULS to study crack growth and residual crack behavior before applying the necessary demands to investigate the failure mechanism of the pretensioned concrete specimen.

Table 4.2. Loading Sequence – RCS-16-12

Date	Loads	Cracks Measured	Creep (hrs)	Unload (kips)
Day 1 10/10/2016	No loads			
Day 2 10/12/2016	Dead		1	
	74% SLS	✓*		
	SLS	✓*		
	ULS	✓*		0†
Day 3 10/13/2016	SLS	✓		
	ULS	✓	6	270/160/0
Day 4 10/14/2016	Dead	✓		
	SLS	✓		
	ULS	✓		
	125% ULS			
	138% ULS	✓		
	140% ULS	✓		
	88% Max Positive	✓		
	97% Max Positive	✓		
	Max Positive	✓		0
Day 5 10/17/2016	Joint Opening	✓		0†
Day 6 10/28/2016	Joint Closing	✓		
	58% Max Negative	✓		
	Max Negative	✓		0
	Joint Opening			
	Max Positive			
Day 7 10/31/2016	Failure			0†

* *Cracks measured on front face only*
† *Cracks not measured*

Table 4.3. Loading Sequence – PSS-16-12

Dates	Loads	Cracks Measured	Creep (hrs)	Unload (kips)
Day 1 11/30/2016	Dead			
	SLS	✓		160
	ULS	✓	1	
	140% ULS	✓		
	Max Positive	✓		160/0
	Joint Opening	✓		
	Joint Closing	✓		
	Max Negative	✓		0
Day 2 12/2/2016	Dead	✓		
	SLS	✓		
	ULS	✓		
	140% ULS	✓		270/160
	Failure			0†

† *Cracks not measured*

4.3. Visual Observations

During the experimental testing, it was possible to closely observe the specimens for the appearance of cracks. All longitudinal and transverse reinforcement and the corrugated pipe were drawn in pencil on the front face of each specimen. Cracks at each load pattern were marked in different colors to create a better perspective of their formation. Figure 4.3 shows the extent of cracking and damage seen at the failure load patterns on the front face and top of the pocket connection for the reinforced concrete specimen, RCS-16-12, and the pretensioned specimen, PSS-16-12. A description of the damage progression for each load pattern is presented in the following sections.

(a) Negative Moment Region

(b) Midspan

(c) Positive Moment Region

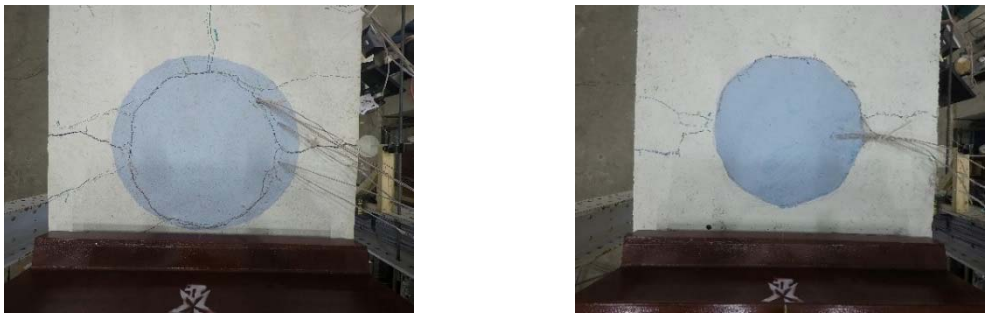

(d) Pocket Connection

Figure 4.3. Visual Observations at Failure; Blue paint extends beyond edge of pocket in RCS-16-12. (Left: RCS-16-12, Right: PSS-16-12)

4.4. Damage Progression

This section presents a summary of damage progression in the reinforced concrete, RCS-16-12, and pretensioned concrete, PSS-16-12, specimens during the experimental testing conducted in the Texas A&M University High Bay Structural and Materials Testing Laboratory.

PSS-16-12 exhibited fewer and finer cracks during the bridge demand load patterns and a higher ability for these cracks to close at residual loads. Figure 4.4 presents an overall summary of the front face crack progression; back face crack progression figures are included in Appendix F. Crack data gathered during all load patterns are included in Appendix E.

The pocket connection performed satisfactorily for both specimens. No cracks developed in the confined concrete and cracks were limited to outside the inner circumference of the 21-in nominal diameter corrugated pipe, with less damage observed in PSS-16-12. Figure 4.5 shows the overall summary of the pocket connection performance for both specimens.

The damage from each load pattern is presented and discussed in the following sections. Figures in these sections present the moment diagrams with moments on the tension side. The shear is marked as the slope of the moment diagram along the span. Line types distinguish the largest cracks seen in each positive and negative moment region with a thick line, and cracks developed from previous load patterns are shown in light gray and closed cracks with dashed lines, where applicable. Colors are also provided to distinguish the widths of cracks. Cracks are categorized with reference to the AASHTO Standard

Specifications Section C.5.7.3.4 crack width limit of 0.017-in (Class 1 exposure). The Class 1 exposure crack width limit is based on a physical crack model rather than a statistically-based model used in previous editions. It is considered to be an upper bound limiting bar spacing instead of crack width in regards to appearance and corrosion (AASHTO, 2012). The smallest crack widths are hairline cracks and widths up to 0.001-in. Cracks ranges are then categorized by widths between 0.002-in up to 0.010-in followed by cracks between 0.011-in and 0.017-in. Cracks greater than 0.017-in are also categorized in ranges by different colors according to their respective widths. No damage was observed at dead load demands either of the specimens.

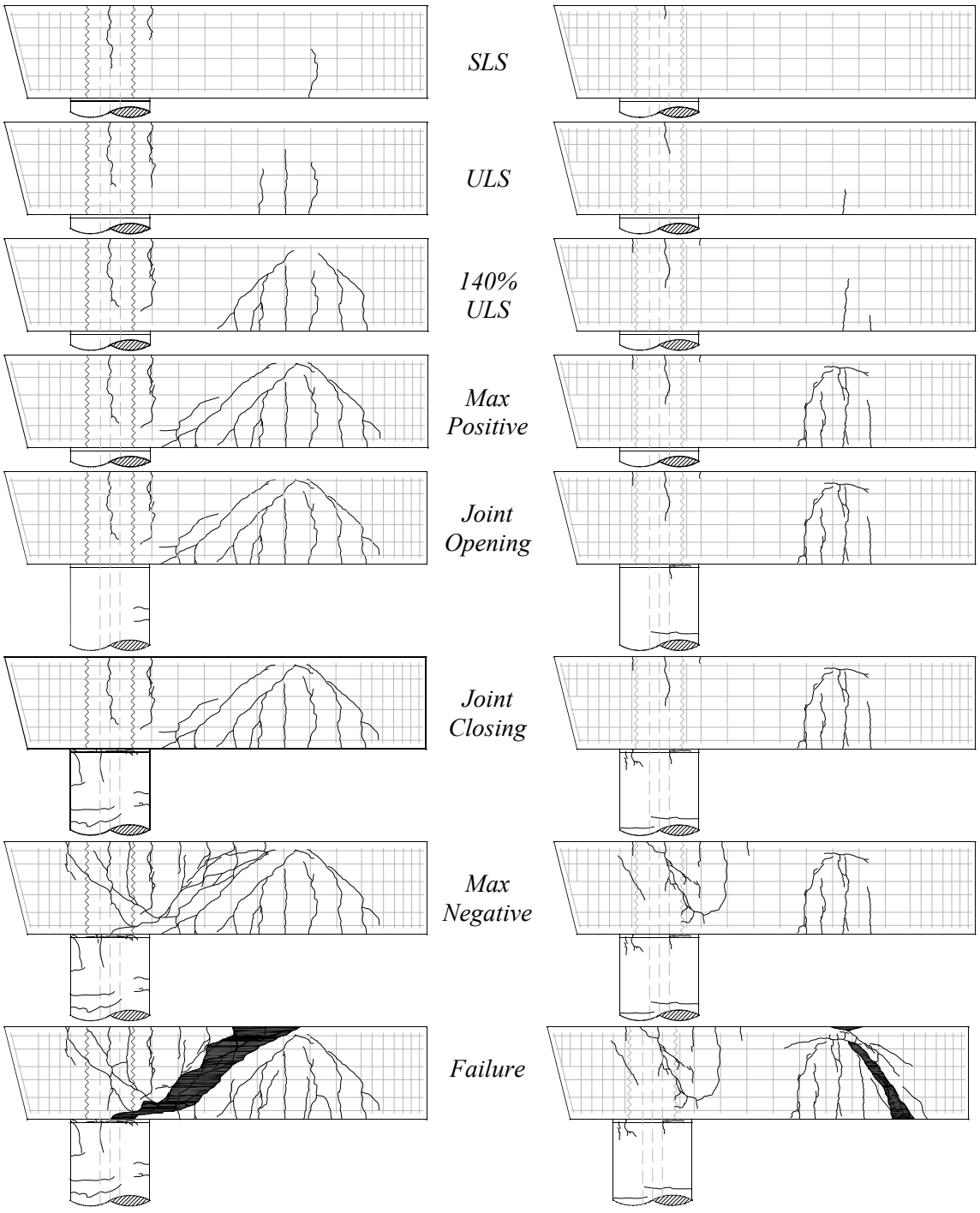

Figure 4.4. Crack Progression; Shaded area represents a loss of concrete. (Left: RCS-16-12, Right: PSS-16-12)

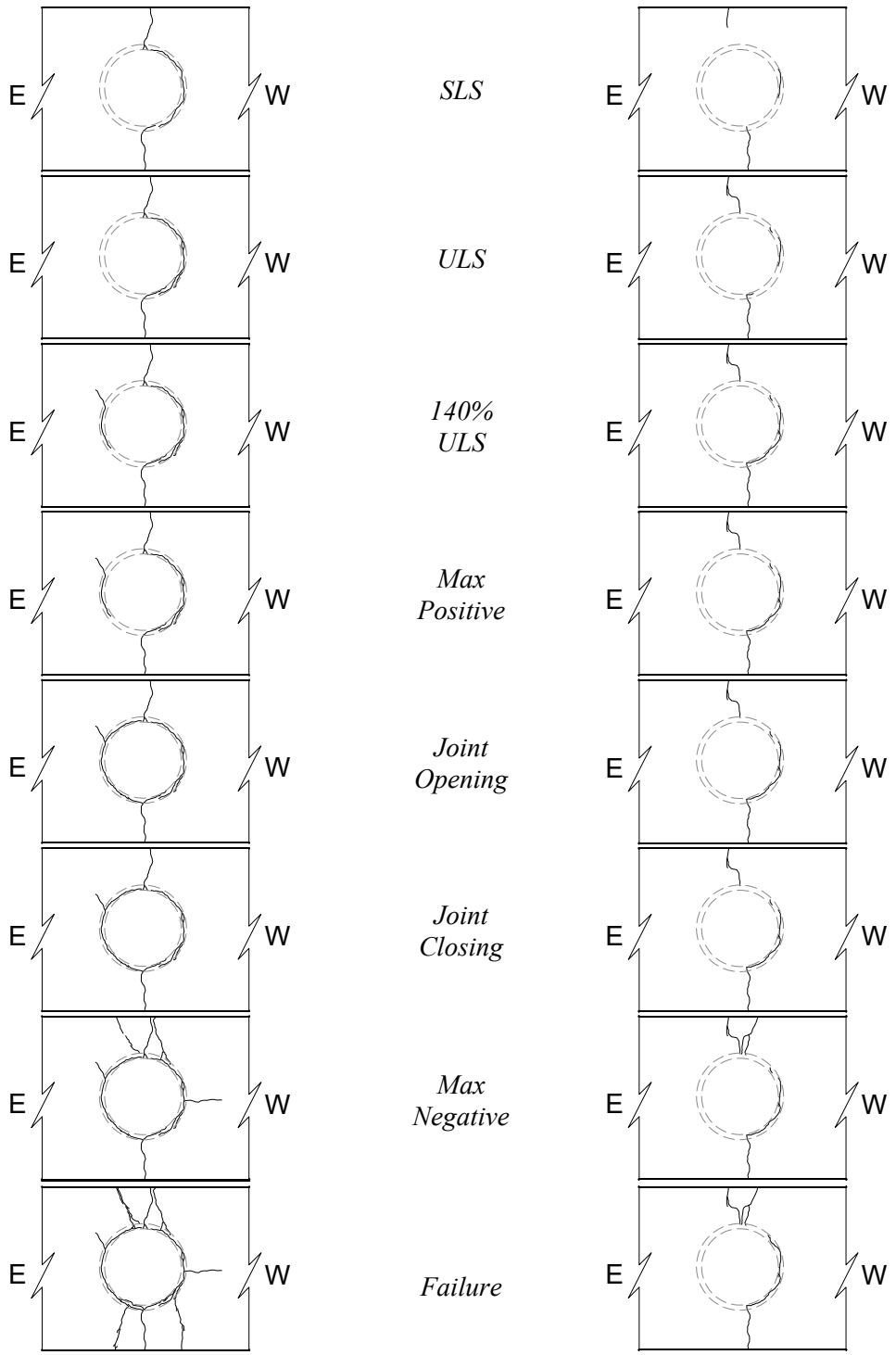

Figure 4.5. Crack Progression at the Top Face of Bent Cap and Pocket; Dashed gray lines indicate inner and outer circumference of the pocket pipe. (Left: RCS-16-12, Right: PSS-16-12)

4.4.1. *Bridge Demands*

The first part of testing applied Pattern A demands (AASHTO design loads). Table 4.4 provides a summary of the initial flexure cracking observed in comparison to the expected cracking moments for both positive and negative moment regions in each specimen.

The actual cracking moments in both specimens were lower than expected. RCS-16-12 first cracked in the negative moment region at 523 k-ft which corresponded to 74% of SLS demands (P=200 kips). Cracks in the positive moment region of RCS-16-12 appeared at SLS demands at an applied moment of 520 k-ft. The first signs of cracking in PSS-16-12 developed in the negative moment region at SLS demands corresponding to a moment of 605 k-ft. The positive moment region of PSS-16-12 first cracked at ULS demands with an applied moment of 784 k-ft.

Table 4.4. Flexure Cracking Summary – Actual vs. Expected.

Specimen	Region	Load Pattern	M_{cr}^{actual} (k-ft)	$M_{cr}^{expected}$ (k-ft)	$M_{cr}^{actual}/M_{cr}^{expected}$
RCS-16-12	-	A - 74% SLS	523	810	0.65
	+	A - SLS	520	810	0.64
PSS-16-12	-	A - SLS	605	1125	0.54
	+	A - ULS	784	1164	0.67

4.4.1.1 Serviceability Limit State (SLS)

Figure 4.6 shows the demands and cracks at the SLS demands. SLS demands were all significantly below the expected yielding and nominal strengths for both specimens and all cracks were below the 0.017-in AASHTO crack width limit for Class 1 exposure. In RCS-16-12, the initial crack that appeared during 74% SLS demands in the negative moment region increased to approximately 0.008-in, and additional cracks appeared in both the positive and negative moment regions; all within the range of 0.002-in to 0.010-in. PSS-16-12 developed a single hairline crack above the center of the column.

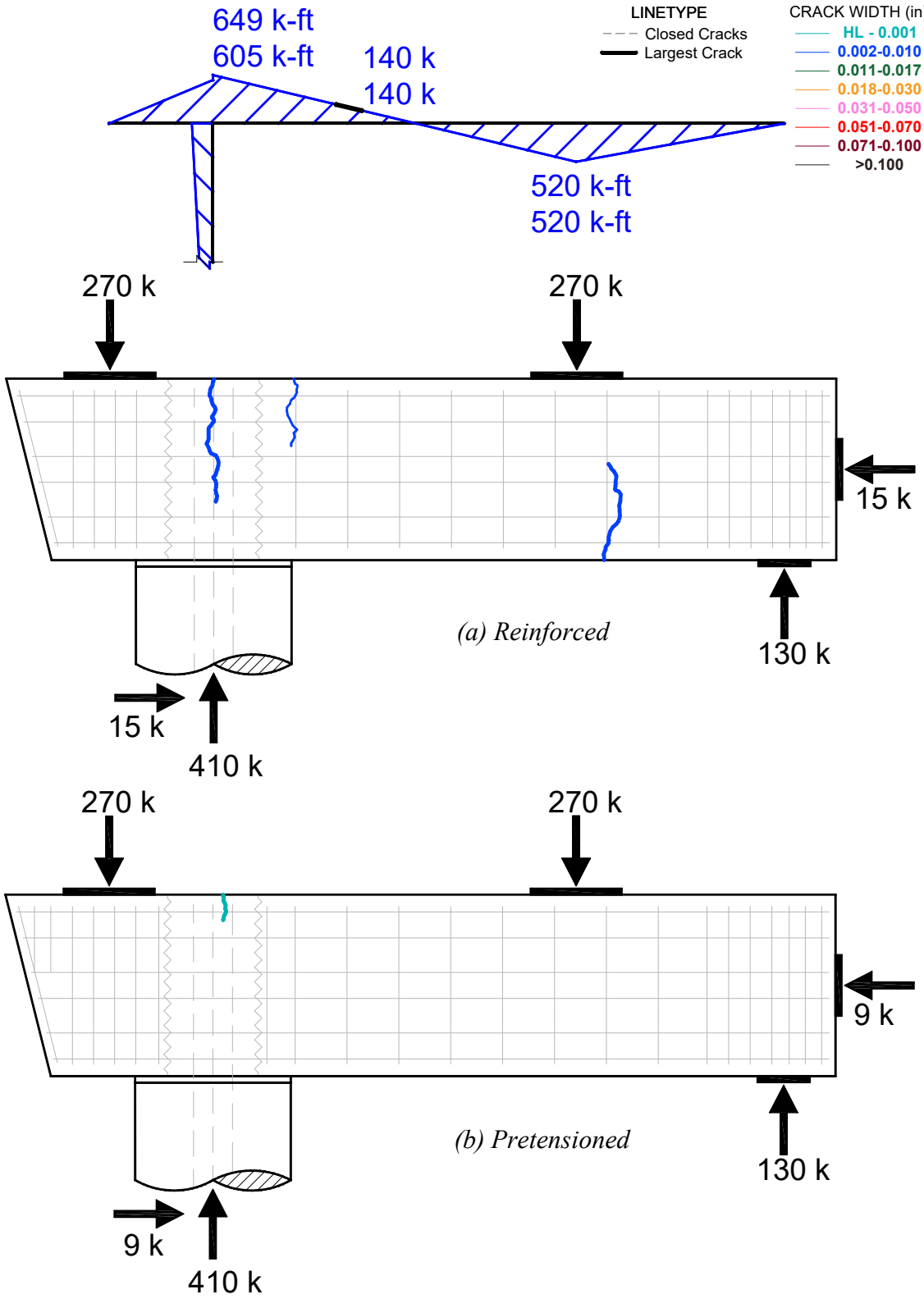

Figure 4.6. Crack Patterns – SLS Demands.

4.4.1.2 Ultimate Limit State (ULS)

Figure 4.7 shows the cracks and the moments created at the ULS demands. These demands were below the expected yield and nominal strengths. Crack propagation and formation of new cracks were observed for both specimens.

In RCS-16-12, the largest crack width measured 0.020-in above the interior face of the column, exceeding the 0.017-in AASHTO Class 1 exposure limit. No other cracks exceeded this limit. Three cracks in the positive moment region were no larger than 0.010-in.

In PSS-16-12, the crack in the negative moment region migrated further down the face of the specimen without increasing in width. As shown in Table 4.4, an initial hairline crack in the positive moment region first appeared at 520 k-ft.

All cracks maintained the behavior of flexural cracks as they continued to appear and progress in vertical directions in the areas of highest moments.

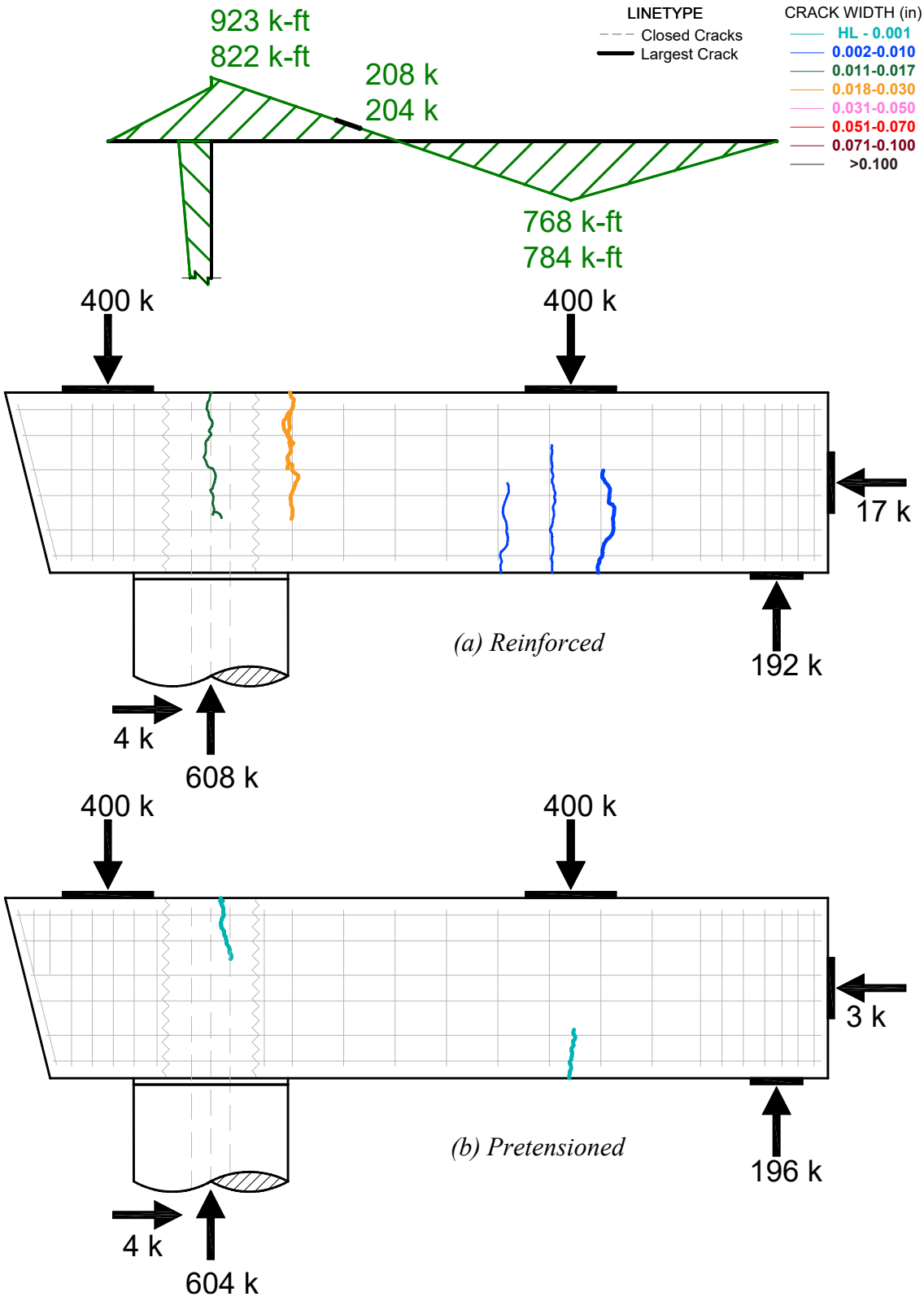

Figure 4.7. Crack Patterns – ULS Demands.

4.4.1.3 Creep

After the ULS load patterns were reached, loads were held constant to study the effects of creep. Figure 4.8 and Figure 4.9 show the cracks from the ULS load demands and the creep observed for RCS-16-12 and PSS-16-12, respectively.

ULS load pattern demands were held constant on RCS-16-12 for 6-hrs and signs of creep were observed in both the negative and positive moment regions. In the negative moment region of RCS-16-12, the crack near the center of the joint did not propagate but expanded from 0.016-in to 0.022-in; becoming larger than the AASHTO Class 1 exposure crack limit, and the second crack near the interior face of the column expanded from 0.020-in to 0.024-in and extended approximately 6-in further. All cracks in the positive moment region experienced growth. The two cracks closest to the column showed a small increase in width from 0.004-in to 0.008-in and 0.004-in to 0.008-in respectively, with no propagation. The crack closest to the V actuator had the largest increase in width, (from 0.004-in to 0.012-in) and also propagated further up the specimen by approximately 3.75-in.

The creep test for PSS-16-12 only sustained the ULS loads for 1-hr and very minor signs of creep were observed in both the negative and positive moment regions. PSS-16-12 only showed a small amount of propagation (less than 1.5-in) in both the positive and negative moment cracks with no increase in width.

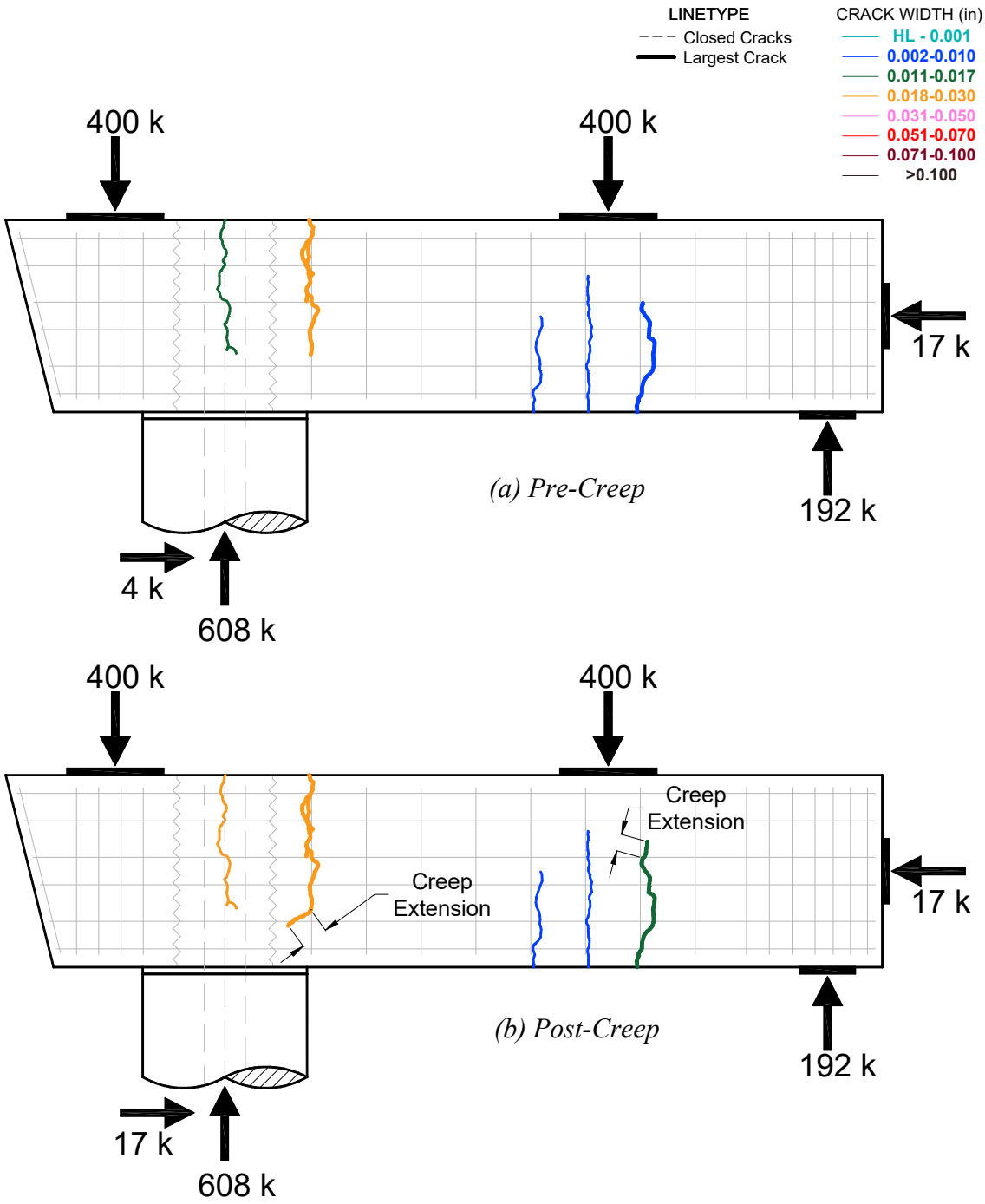

Figure 4.8. ULS Creep – RCS-16-12.

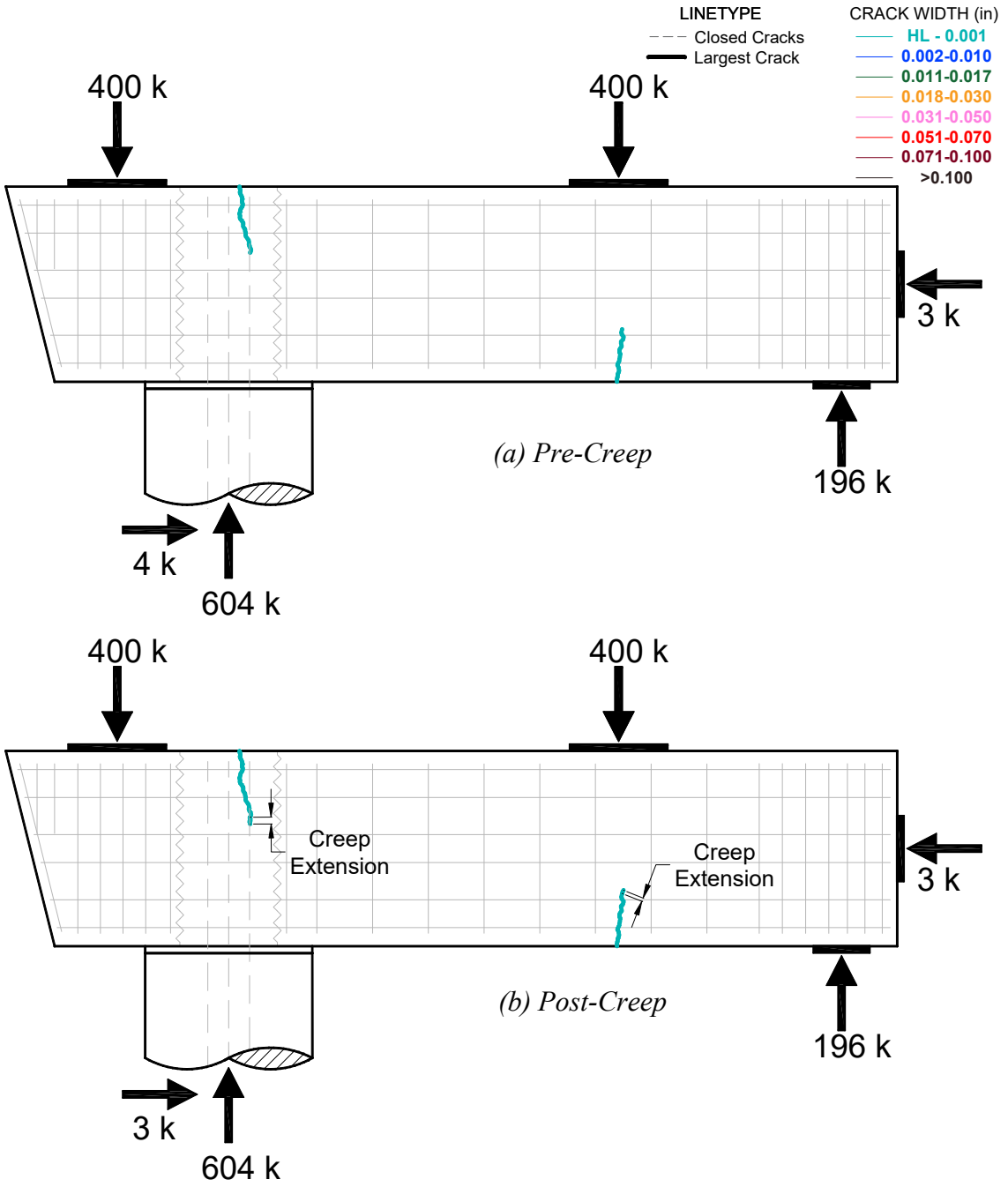

Figure 4.9. ULS Creep – PSS-16-12.

4.4.1.4 140% ULS

The last step in Pattern A was to apply the maximum simultaneous loads in the P1 and P2 actuators. Figure 4.10 shows the cracks formed on both specimens and the moments created at the 140% ULS demands.

In RCS-16-12, the moments created at 140% ULS demands exceeded the expected yield strength capacity for the positive and negative moment regions. The large increase in crack widths served as evidence that yielding of the reinforcing bars had initiated. Because of the exceeded yield strength demands, many of the cracks were considered permanent damage. New cracks in the positive moment region of RCS-16-12 initiated as vertical flexure cracks and propagated to inclined cracks. The first signs of shear cracks appeared on the left side of actuator P2. The two cracks in the negative moment region of RCS-16-12 measured 0.039-in and 0.037-in, and the three cracks in the negative moment region measured 0.018-in, 0.020-in, and 0.018-in. All the cracks that developed during the previous ULS demands exceeded the AASHTO Class 1 exposure limit.

The moments created in PSS-16-12 at 140% ULS demands were below the expected yield strength for positive and negative moment regions. The low number and widths of cracks validated the expected yield and nominal moment strengths of the specimen had not been reached. PSS-16-12 exhibited an increase in crack widths in the negative and positive regions. The two cracks from the previous load case measured 006-in at the negative moment region and 0.008-in at the positive moment regions. Fine and short new hairline cracks were also observed in the positive and negative moment regions. All cracks in PSS-16-12 remained below the AASHTO Class 1 exposure limit.

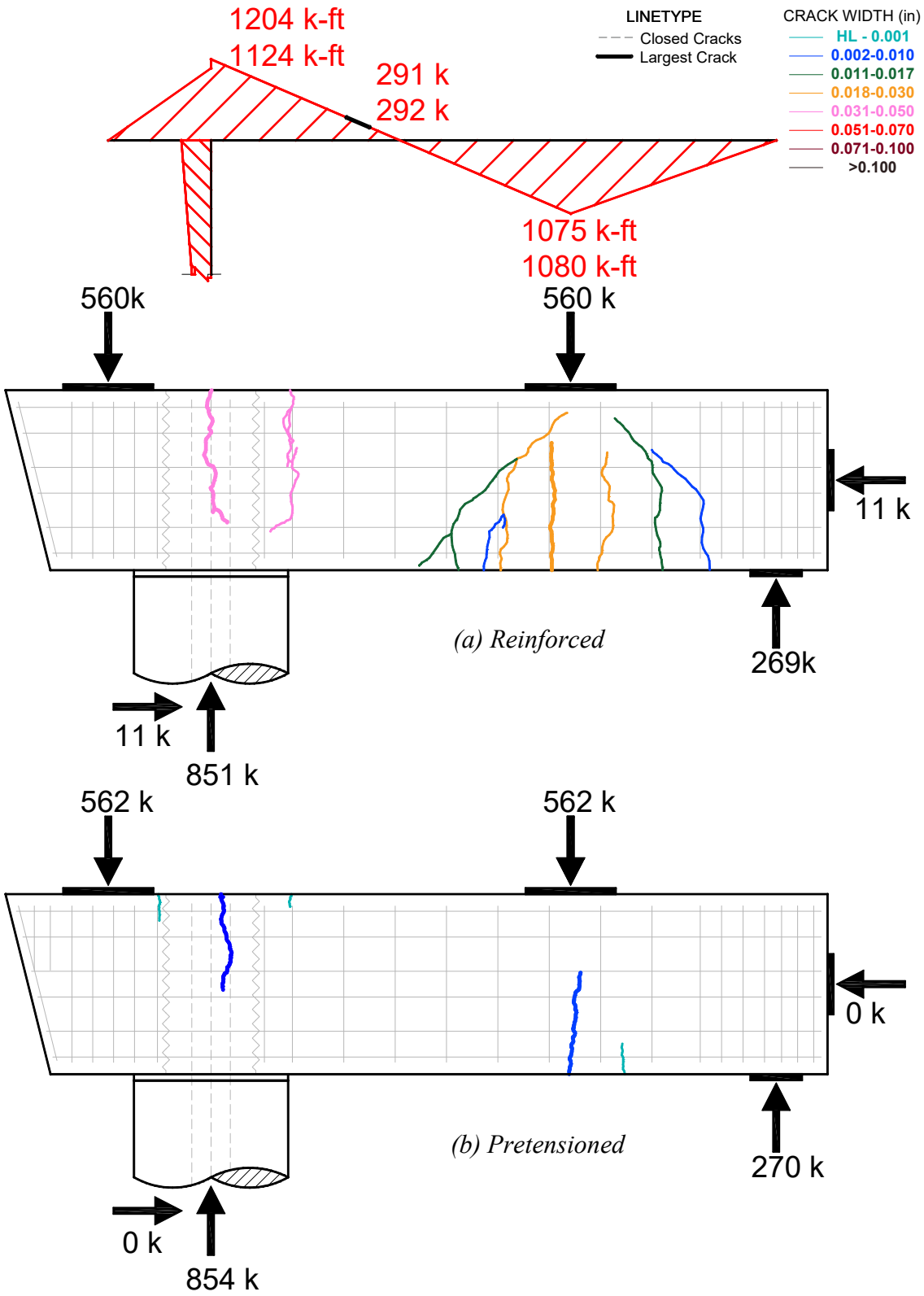

Figure 4.10. Crack Patterns – 140% ULS Demands.

4.4.2. *Maximum Bent Cap, Joint, and Failure Demands*

After all bridge demands from Pattern A were completed, the maximum achievable demands with the current test setup were applied to the RCS-16-12 and PSS-16-12. These demands corresponded to Patterns B through F.

4.4.2.1 Maximum Positive Moment

Figure 4.11 shows crack patterns and moments created during the maximum positive moment demands (Pattern B). The gray lines in this figure indicate previous cracks that were not measured during this load pattern. The positive moments created during Pattern B exceeded the expected yield and nominal moment strength capacity for both specimens.

In RCS-16-12, these demands created further crack formation along the entire positive moment region and crack propagation upwards towards the bearing pads for actuator P2. Most of the cracks extended the entire depth of the web of the bent cap stopping approximately 3.5-in from the load point of actuator P2. Two new cracks were inclined shear cracks appeared in the span of RCS-16-12 beginning at the bottom of the bent cap near the interior face of the column support and extended to actuator P2. The new shear crack propagated at a general angle of 35° and their widths measured at 0.018-in and 0.030-in. The flexure cracks of RCS-16-12 increased to widths between 0.051-in and 0.098-in. The cracks in the negative moment region of RCS-16-12 decreased in width to 0.004-in and 0.006-in as the negative moment demands were removed with the retraction of actuator P1. Although many of the cracks in the positive moment region of RCS-16-12 were close to reaching the top of the bent cap, no crushing was observed.

PSS-16-12 experienced an increase from two to four cracks in the positive moment region. The cracks in PSS-16-12 remained underneath the bearing pad of P2. The largest crack from the 140% ULS demands located directly below P2 extended vertically and increased in width to 0.059-in. The largest new crack measured at 0.035-in and began to turn into an inclined crack near the top of the specimen. The two other vertical flexure cracks had measured widths of 0.004-in each. The 0.059-in and 0.035-in were both well past the AASHTO Class 1 exposure limit and served as evidence that Pattern B demands initiated yielding of the strands.

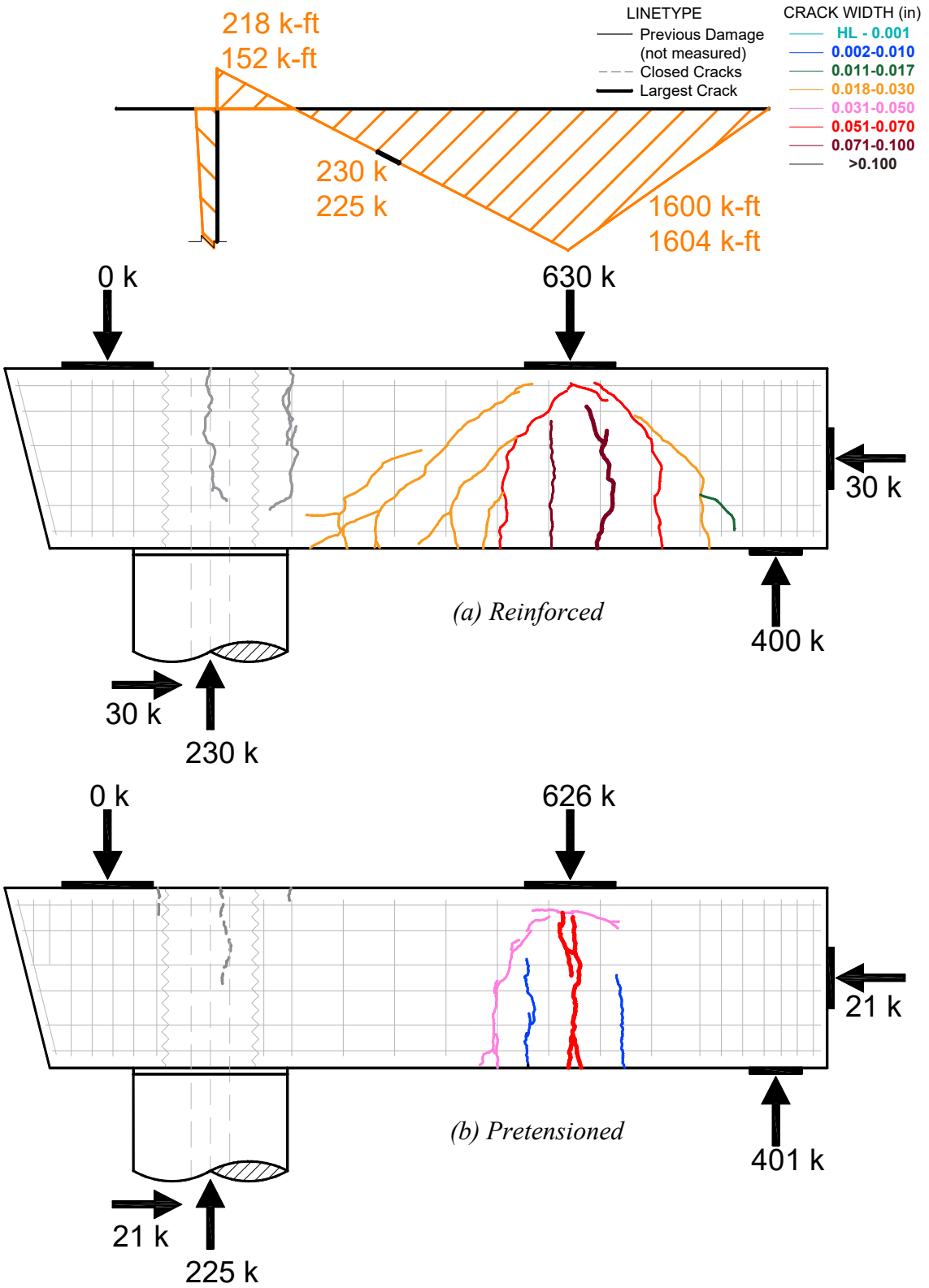

Figure 4.11. Crack Patterns – Maximum Positive Demands.

4.4.2.2 Joint Opening and Closing

Pattern C and Pattern D applied joint opening and closing demands, respectively, to test the performance of the bedding layer and dowel bars in the connection of the column and the bent cap. Figure 4.12 shows the crack formation during joint closing and joint opening for both RCS-16-12 and PSS-16-12.

Joint opening demands created cracks at the interior face of the column of RCS-16-12 with a maximum width of 0.012-in. No cracks were observed in the bedding layer. Joint closing demands created hairline cracks in the exterior face of the column and 0.026-in cracks in the bedding layer that propagated both horizontally and vertically.

Joint opening demands in PSS-16-12 formed cracks in the column and the bedding layer with a maximum measured width of 0.004-in. Joint closing demands created hairline cracks on the exterior face of the column and the bedding layer which also propagated horizontally and vertically. No signs of pull out from the dowel bars were observed during either joint opening or joint closing demands.

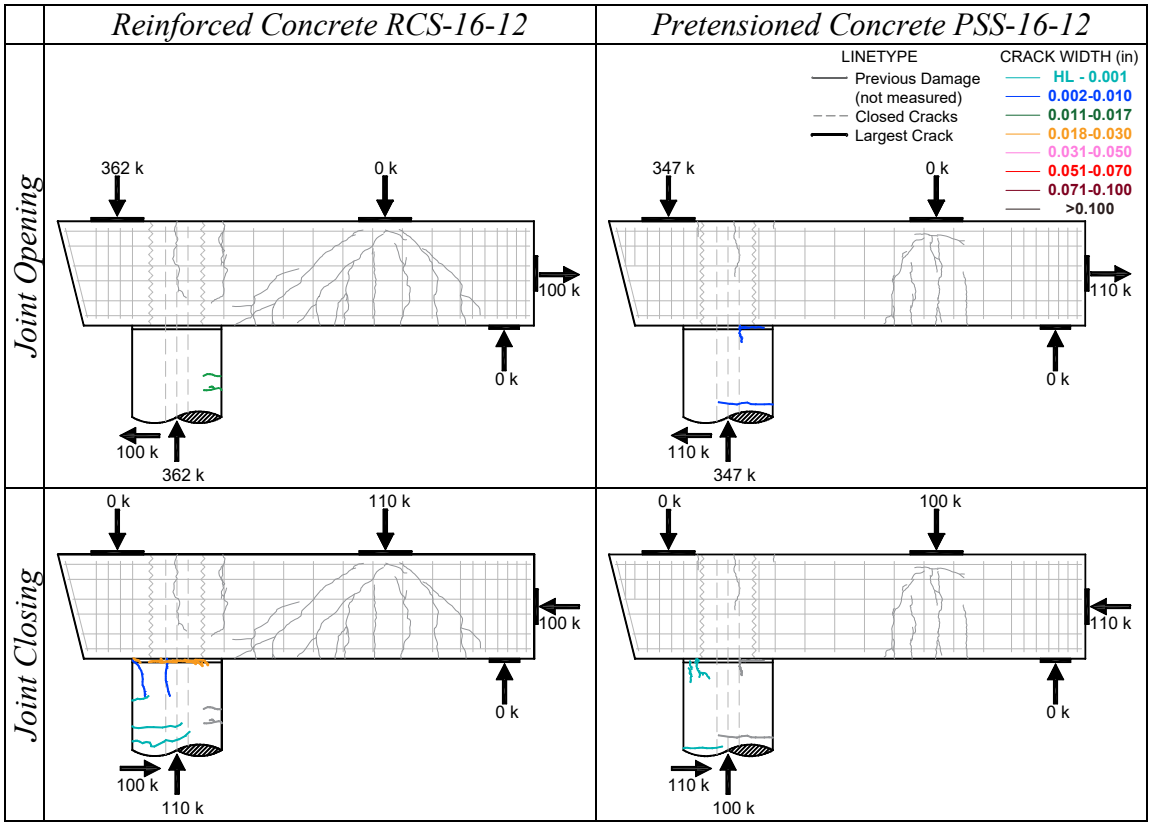

Figure 4.12. Crack Patterns – Joint Opening and Joint Closing Demands.

4.4.2.3 Maximum Negative Moment

Pattern E created the largest negative moment demands achievable with the test setup. These demands allowed further study of the capacity of the specimens and the performance of the pocket connection. Figure 4.13 shows the cracks formed on both specimens and the moments created at the maximum negative moment demands.

The maximum negative moments exceeded the expected nominal strengths for both specimens. These large cracks showed evidence that significant yielding of both mild steel and strand longitudinal reinforcement had occurred.

RCS-16-12 experienced an increase from two to seven main cracks in the negative moment region. Cracks were very dispersed and extended along the entire front face of the bent cap. Crack widths also increased with two cracks measuring 0.198-in and four others measuring 0.157-in, 0.118-in, 0.177-in and 0.098-in. Shear cracks were present in both the overhang and span extending from both P1 and P2 to the interior face of the column. Crushing initiated at the bottom of the bent cap above the interior face of the column (Figure 4.14). Cracks in the positive moment region were not measured for RCS-16-12.

The number of cracks in PSS-16-12 increased from three to seven. Cracks extended to approximately 5-in from the bottom of the bent cap. Damage concentrated at a single large crack (0.198-in). Two other flexure cracks measured 0.059-in and 0.020-in width while the remaining four cracks were only 0.001-in hairlines cracks. One of the hairline cracks was a shear crack that developed in the overhang propagating from P1 to the center of the column stopping near the mid-depth of the bent cap. The cracks were less dispersed in comparison to RCS-16-12. No crushing was observed near the bottom of the bent cap for PSS-16-12.

Both RCS-16-12 and PSS-16-12 showed crack patterns extending to the interior face of the column. The largest crack in RCS-16-12 propagated vertically above the interior face of the column while the largest crack in PSS-16-12 propagated from the center of the joint region to the inside face of the column. Although both specimens had equal maximum crack widths (0.198-in) at maximum negative moment demands,

RCS-16-12 clearly showed more damage and higher quantity of larger cracks than PSS-16-12.

Damage at the top of the pocket was also the greatest during maximum negative moment demands for both specimens (Figure 4.15).There was no evidence of yielding of the corrugated pipe and no cracks appeared inside the circumference of the pocket connection for either specimen. RCS-16-12 developed cracks on both the east and west side of the pocket with portions of the corrugated pipe clearly exposed, while PSS-16-12 showed less damage to the pocket connection as cracks developed only on the east side.

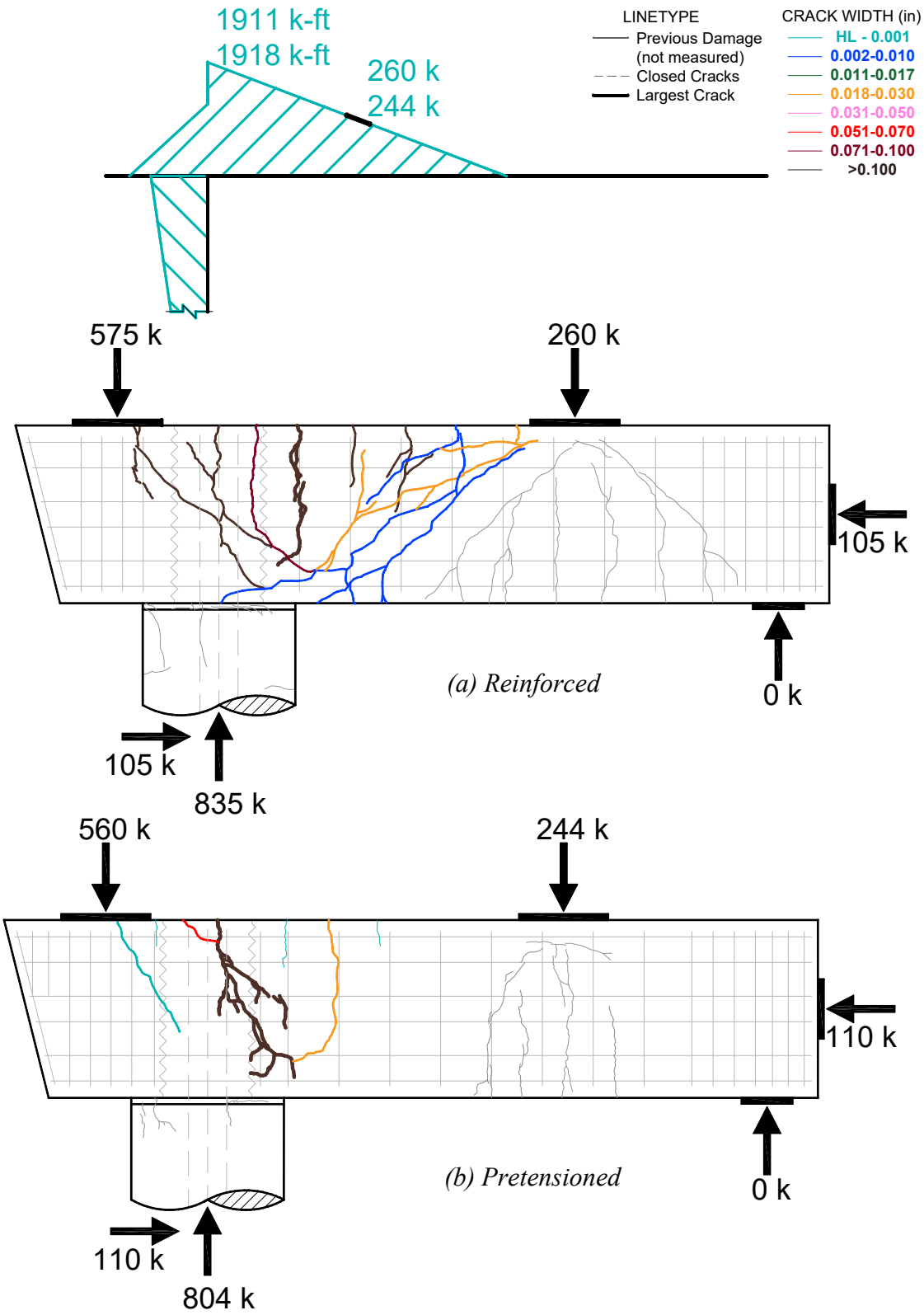

Figure 4.13. Crack Patterns – Maximum Negative Demands.

Figure 4.14. Crushing at Interior Face of Column – RCS-16-12.

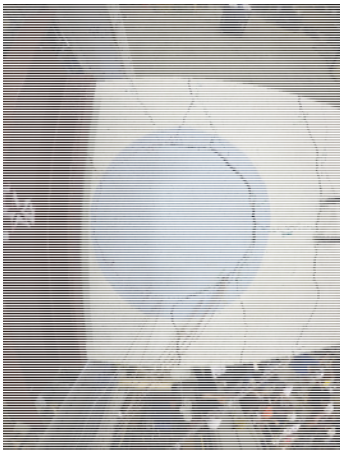

(a) RCS-16-12

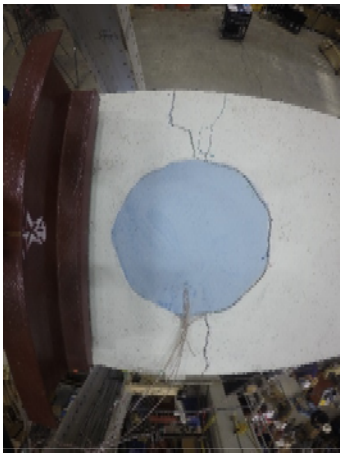

(b) PSS-16-12

Figure 4.15. Pocket Connection Damage.

4.4.2.4 Failure

Pattern F was the final load pattern applied and was implemented to study the failure mechanisms of each specimen. Demands created during Pattern F produced failure in the positive moment region for both specimens. Figure 4.16 shows the failure planes on the front and back faces of both specimens. No cracks were measured during Pattern F for either specimen.

RCS-16-12 developed significant damage along the span during Pattern B and Pattern E, and the failure of this specimen developed as a continuation from this previously seen damage. The actuators were set to the configuration of Pattern F discussed in Section 4.1. A compression strut formed along the span when the actuators were near their maximum capacity. The compression strut failure developed between the interior face of the column and actuator P2 at an angle of approximately 40°. Crushing of concrete under actuator P2 and above the inside face of the column was observed, and exposure of longitudinal and shear reinforcement was seen along the failure plane (Figure 4.17.a).

PSS-16-12 developed failure between actuators P2 and V. The location of failure for PSS-16-12 was damage not seen during any previous load patterns. A compression strut developed between actuators P2 and V with cracks first appearing during the initial stages of Pattern F. The failure of PSS-16-12 took place when all actuator loads were to their maximum capacity. Exposure of prestressing strands and shear reinforcement was observed along the failure plane and crushing developed at the top of the specimen near the load area of P2 (Figure 4.17.b).

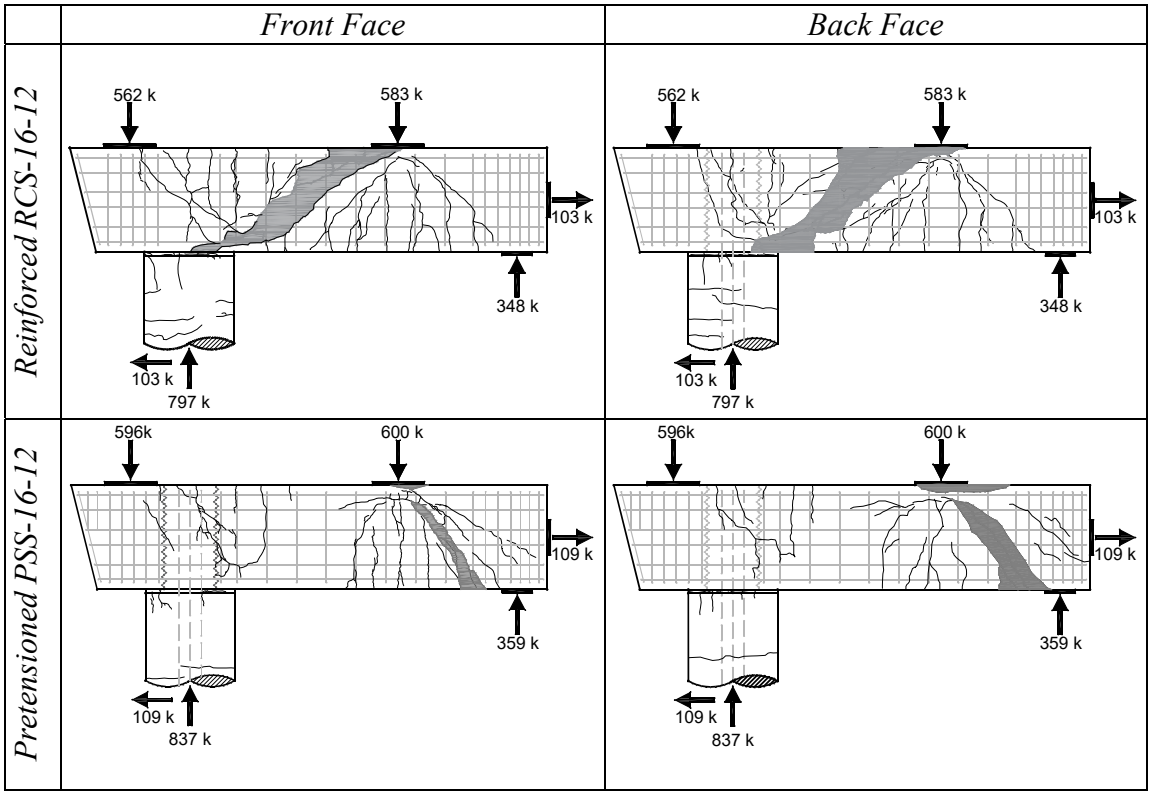

Figure 4.16. Crack Patterns – Failure Demands.

(a) RCS-16-12 *(b) PSS-16-12*

Figure 4.17. Failure Planes (Back Face).

4.5. Crack Widths Following Load Removal

Both specimens were monitored to study the closure of cracks following the removal of loads. Figure 4.18 and Figure 4.19 show the main load patterns at which the crack widths were measured before and after the removal of loads for RCS-16-12 and PSS-16-12, respectively.

Figure 4.18.a shows the crack widths at ULS demands and Figure 4.18.b shows the cracks widths after the loads were lowered back to dead load demands for RCS-16-12. Although no cracks closed at dead load demands, all crack widths reduced to below the AASHTO Class 1 exposure limit. The two cracks in the negative moment region reduced to 0.010-in and all three cracks in the negative moment region reduced to 0.004-in.

Figure 4.19.a shows the crack widths at Pattern B and Figure 4.19.b shows the cracks widths after the loads were lowered back to dead load demands in the span for PSS-16-12. With only two hairlines cracks at ULS demands, PSS-16-12 was loaded up to maximum positive moment demands (Pattern B) before it was unloaded back to dead load demands. At dead load demands in the positive moment region, only one crack remained with a measured width of 0.004-in; a significant reduction from 0.059-in at Pattern B demands. PSS-16-12 was also unloaded to zero loads in P1 and P2 after Pattern B, and the cracks widths remained the same width from dead load demands in the positive moment region.

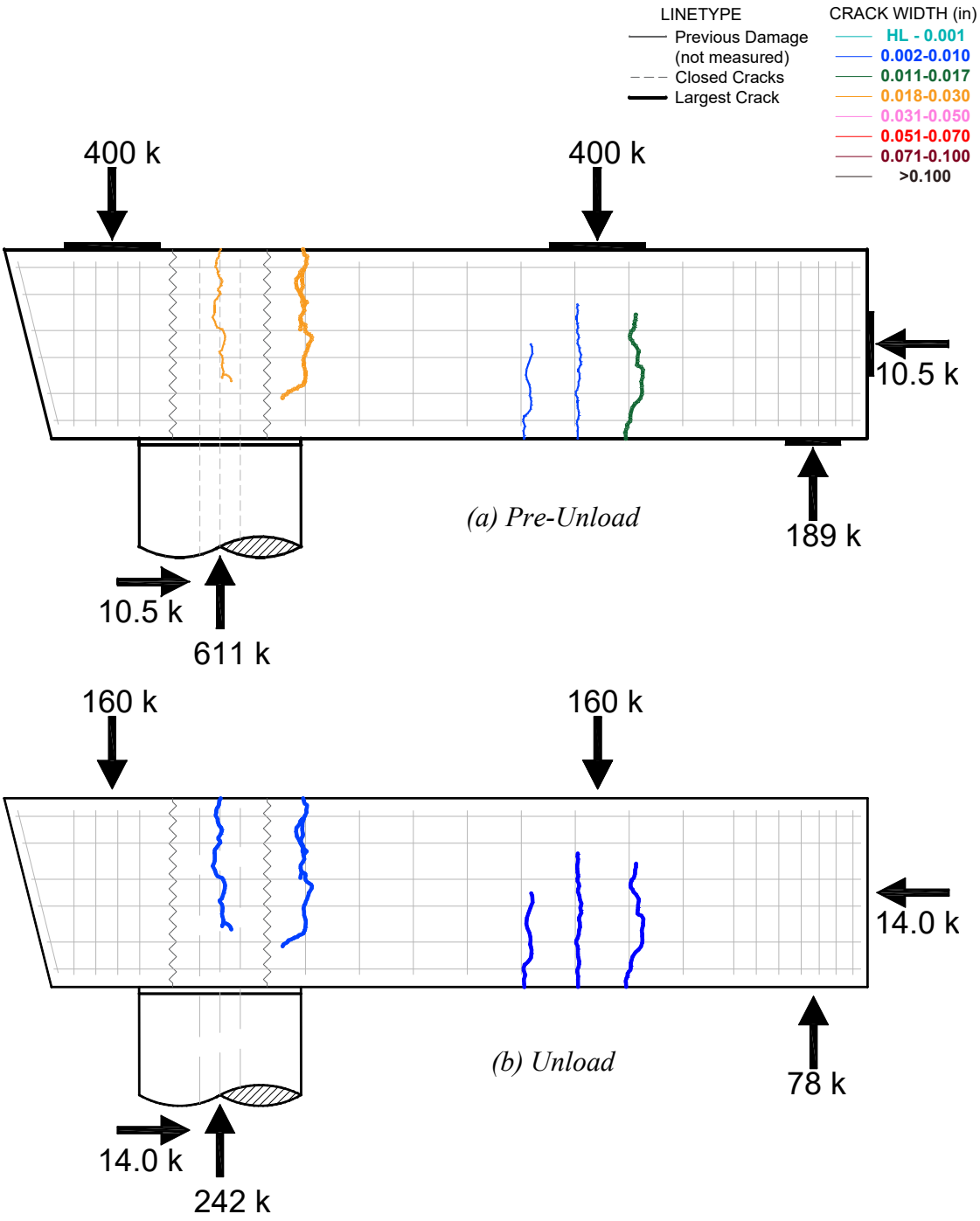

Figure 4.18. Crack Widths Following Removal of Loads– ULS to Dead – RCS-16-12.

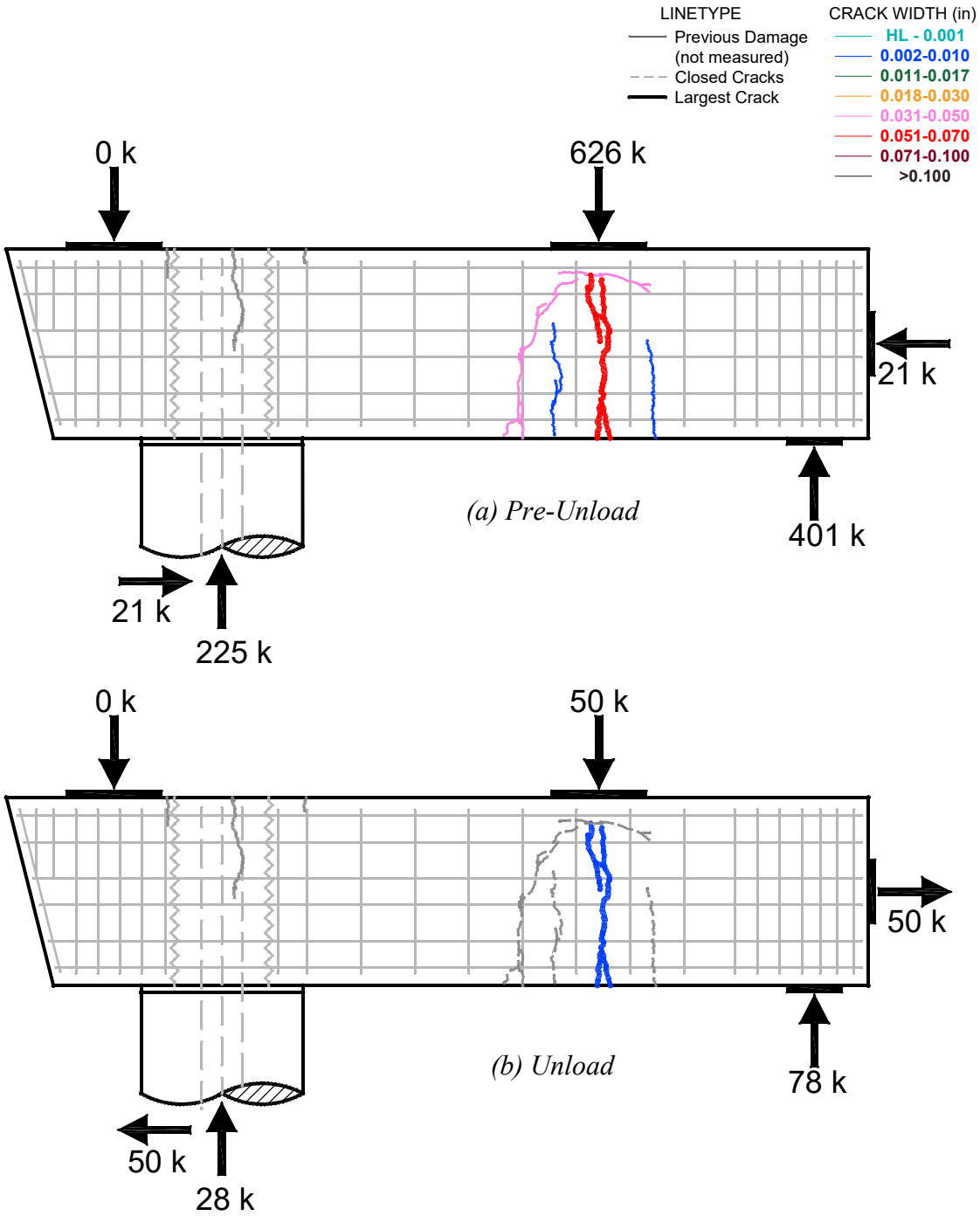

Figure 4.19. Crack Widths Following Removal of Loads – Pattern B to Dead – PSS-16-12.

Figure 4.20 provides a graphical representation of the numerical values of measured crack widths following the removal of loads. The data includes that presented in Figure 4.18, Figure 4.19, as well as other removal of load cases monitored during testing for RCS-16-12 and PSS-16-12 (see Table E.1 for details of all load removals).

RCS-16-12 was also unloaded to zero kips in P1 and P2 after the application of maximum positive demands (Pattern B) and maximum negative demands (Pattern E). Cracks widths after the removal of Pattern B and Pattern E remained as large as 0.060-in and 0.098-in, respectively. These drastically larger remaining crack widths showed evidence that yielding occurred in the longitudinal bars (Figure 4.20.a).

PSS-16-12 was first unloaded to dead load demands after the application of SLS demands to show the closure of the small hairline crack that developed in the negative moment region. Crack widths after the application of Pattern E were also measured in PSS-16-12 with zero load in P1 and P2 and only two crack widths of 0.026-in and 0.004-in remained in the negative moment region. The larger crack width after the removal of loads from Pattern E also showed that the yielding had occurred in the longitudinal strands. The last observation for crack widths following the removal of loads was after the second application of 140% ULS demands to study the performance of PSS-16-12 in closing cracks after yielding of the strands at SLS and dead load demands. The largest crack width was 0.037-in at SLS demands and 0.026-in at dead load demands (Figure 4.20.b).

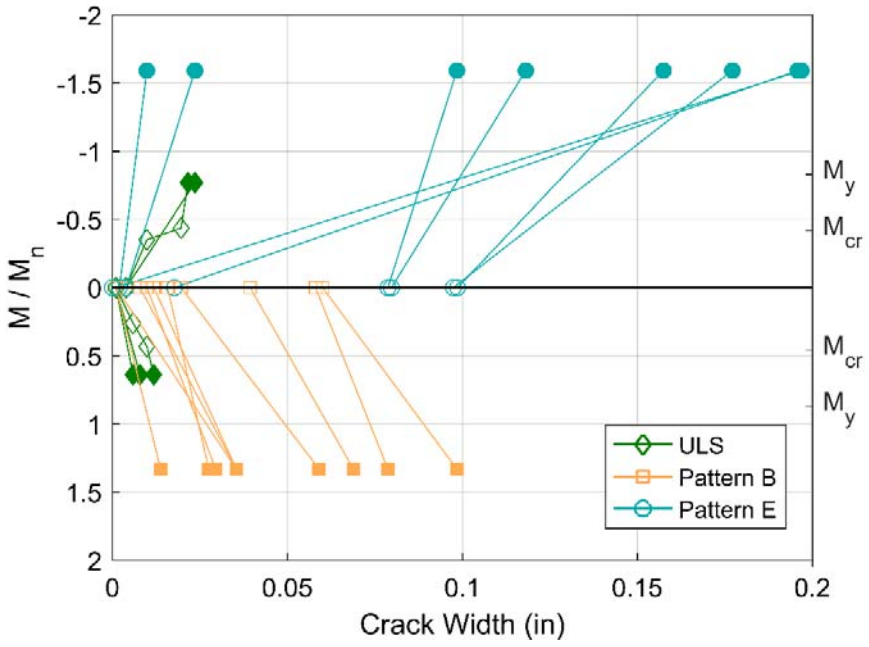

(a) RCS-16-12

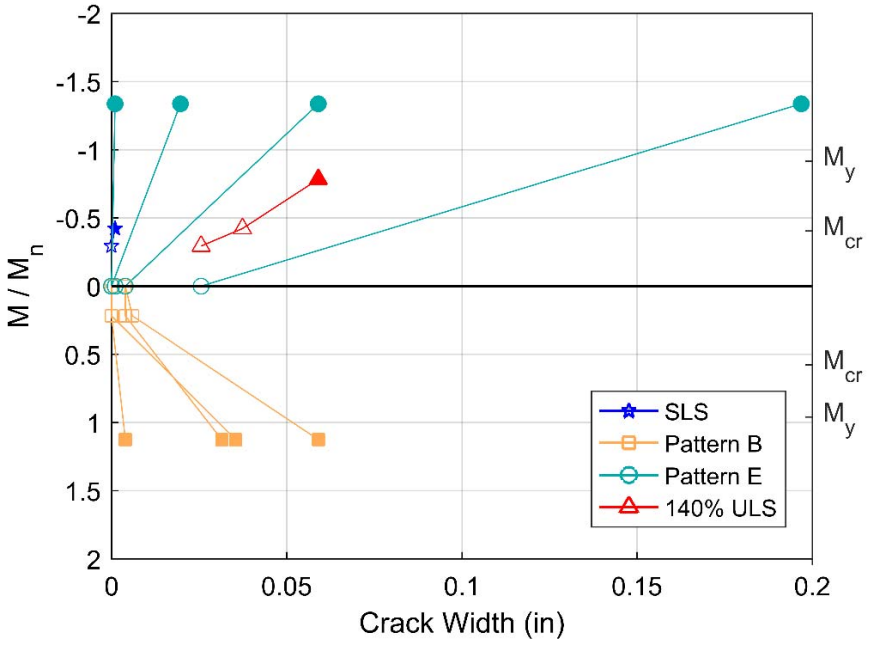

(b) PSS-16-12

Figure 4.20. Crack Widths Following Load Removal – All Unloads (Markers are unique to each highest load pattern reached before unloading; Filled markers represent crack measurements prior to unloading)

4.6. Summary of Bridge Demands

Figure 4.21 and Figure 4.22 show graphical representations of the numerical values for the progression of crack widths in both specimens. The moments from Pattern A are shown with dashed horizontal lines; filled circular markers show the crack width measurements at each demand; the right axis shows the expected cracking moment, expected yield and expected nominal strengths for the negative and positive moment regions; and the AASHTO Class 1 (0.017-in) and Class 2 (0.013-in) exposure limit are shown with black vertical dashed lines.

RCS-16-12 consistently developed larger quantity and larger widths of cracks during all demands in Pattern A in comparison to PSS-16-12. Crack widths in RCS-16-12 exceeded the AASHTO Class 1 and Class 2 exposure limits in the negative moment region during ULS demands and in the positive moment region during 140% ULS demands. No cracks in PSS-16-12 exceeded the Class 1 and Class 2 exposure limits during Pattern A demands.

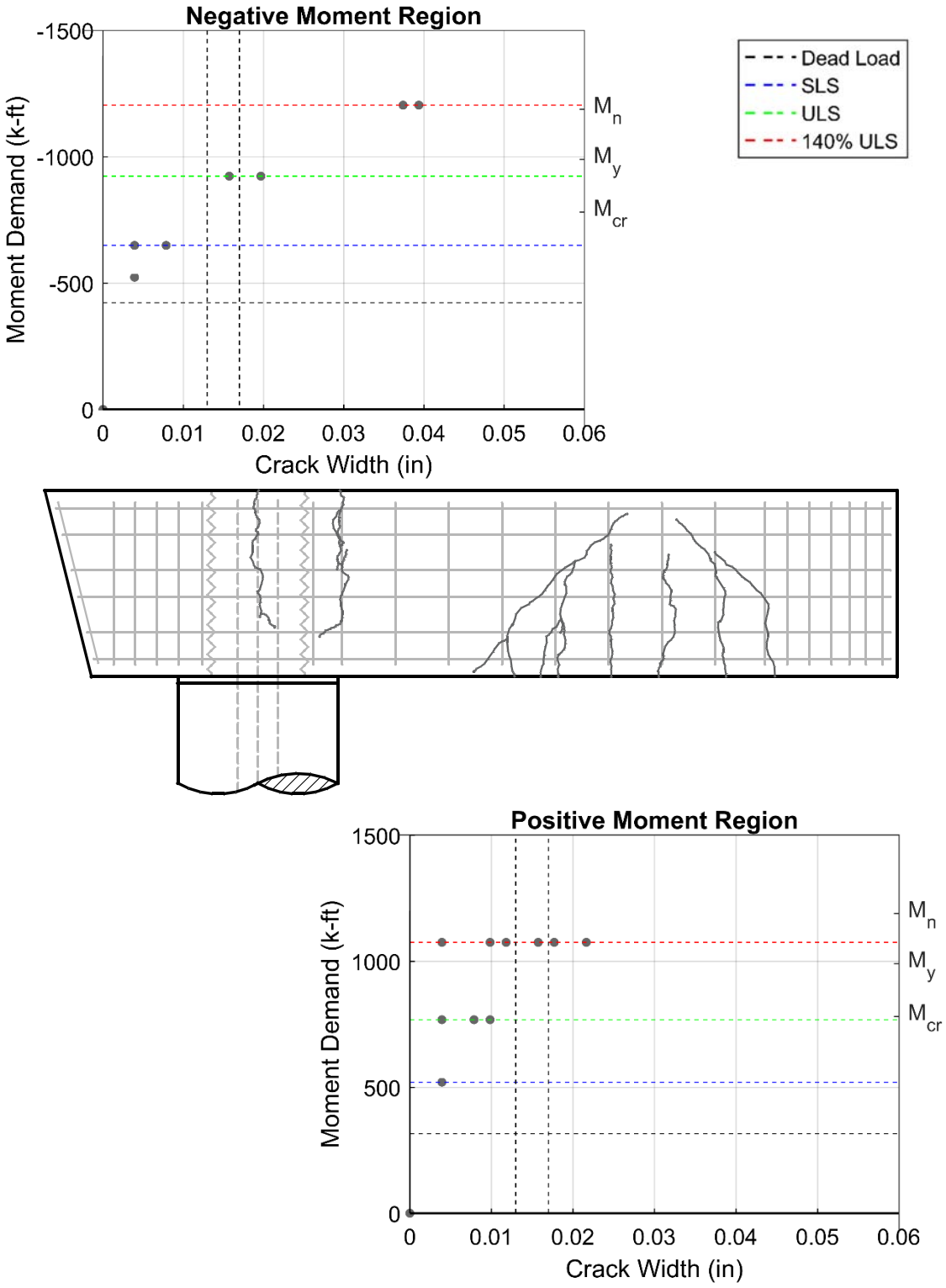

Figure 4.21. Pattern A Crack Progression – RCS-16-12.

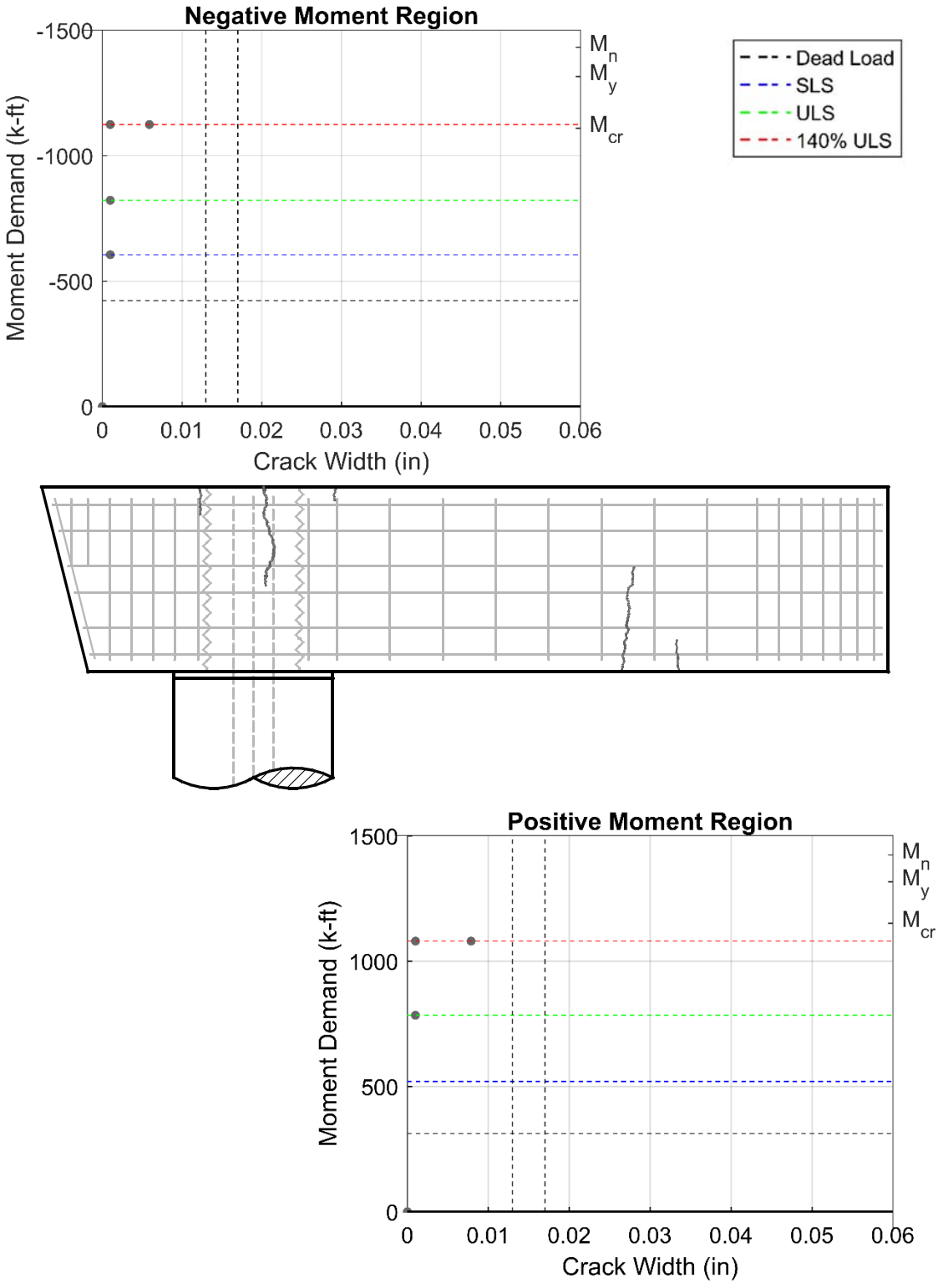

Figure 4.22. Pattern A Crack Progression – PSS-16-12.

4.7. Summary of Maximum Bent Cap, Joint, and Failure Demands

Figure 4.23 and Figure 4.24 provide a graphical representation of the crack progression through all the stages up to maximum achievable moments (Patterns C and D not included and Pattern F cracks were not measured).

The moment demands for Pattern A, Pattern B, and Pattern E are shown with colored dashed horizontal lines; filled circular markers show the crack width measurements at each demand; the right axis shows the expected cracking moment, expected yield and expected nominal strengths for the negative and positive moment regions; and the AASHTO Class 1 (0.017-in) and Class 2 (0.013-in) exposure limit are shown with black vertical dashed lines.

Cracks widths in PSS-16-12 did not exceed the Class 1 exposure limit during until Pattern B demands while RCS-16-12 exceeded the Class 1 and Class 2 exposure limit as early as ULS demands in the negative moment region. PSS-16-12 displayed localized and less number of cracks near the locations of higher moment demands compared to RCS-16-12 which developed more widespread cracks throughout the positive and negative moment regions.

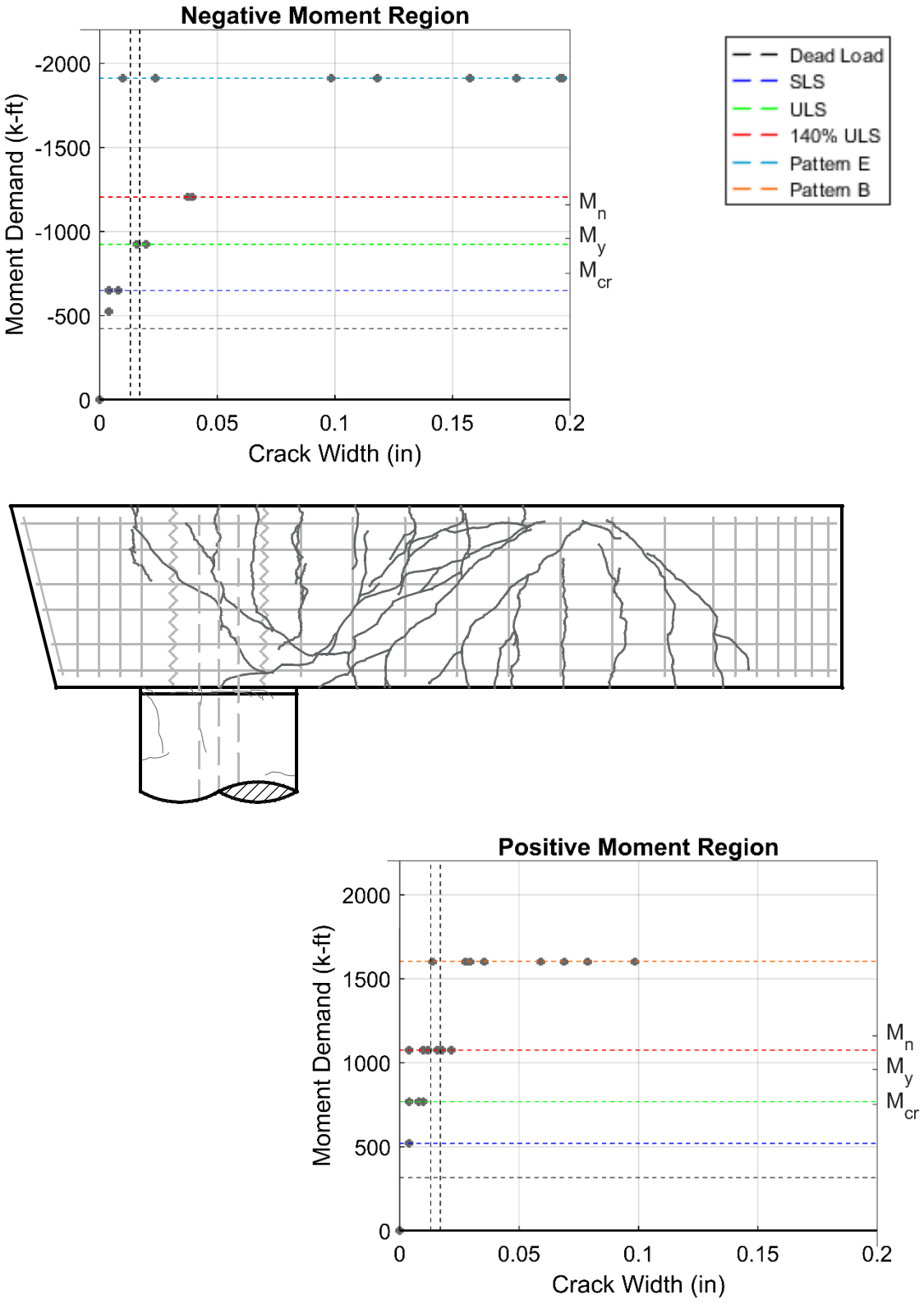

Figure 4.23. Pattern A, Pattern B and Pattern E Crack Progression – RCS-16-12.

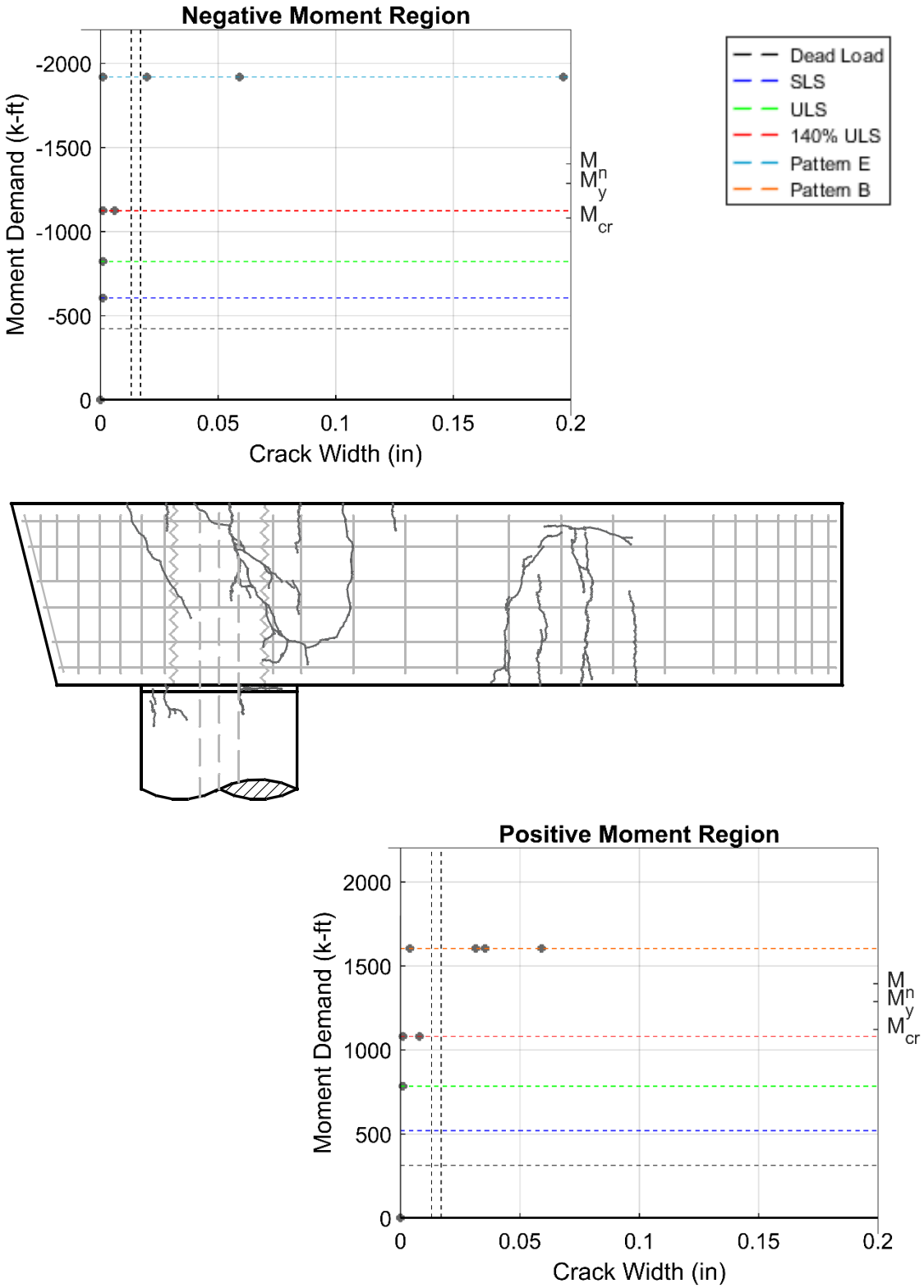

Figure 4.24. Pattern A, Pattern B and Pattern E Crack Progression – PSS-16-12.

4.8. Summary of Strain Gage and Joint LVDT Data

Data acquired from the strain gages installed on the mild steel longitudinal reinforcement was very limited as most malfunctioned prior to testing. The largest moment demands occurred in the negative moment region and only one strain gage in RCS-16-12 showed yielding of a longitudinal reinforcing bar (refer to Instrumentation Plans in Appendix C). This strain gage was located near the top of the joint region and indicated that yielding occurred during the application of Pattern E. The strain gages installed on the dowel bars of RCS-16-12 showed the highest strains of both specimens during Pattern D (Figure 4.25). These values did not indicate yielding.

Two LVDT's were placed on both faces of the column to record displacements between the bottom of the bent cap and the bedding layer (refer to Instrumentation Plans in Appendix C). The readings from the LVDTs were converted to strains by dividing the total change in length over the distance between the bottom of the bent cap and the center of the bracket mount on the column where the LVDTs were installed. These LVDTs showed the largest displacements during Pattern C and Pattern D for both RCS-16-12 and PSS-16-12, shown in Figure 4.26. In this figure, the calculated strains across the bedding layers are shown on the two y-axis and the distance from the centerline of the column is shown on the x-axis. Red lines represent the values recorded for Pattern C and blue lines represent the values recorded for Pattern D. RCS-16-12 values are shown with the solid lines and PSS-16-12 values are shown with dashed lines. The vertical gray lines represent the column faces, the black dashed lines represent the location of the dowel bars, and the solid lines represent the centerline of the column (also the location of the center dowel

bars). The calculated strains are believed to be significantly larger than the strain gage values as a result of the combination of strain penetration, the opening of the bedding layer, and the deformation within the bent cap joint region and are not exclusively representative of strains in the dowel bars at the bedding layer. The differences in these values between RCS-16-12 and PSS-16-12 can also be a result of the minor variations in the position of the LVDTs during installation between each specimen test.

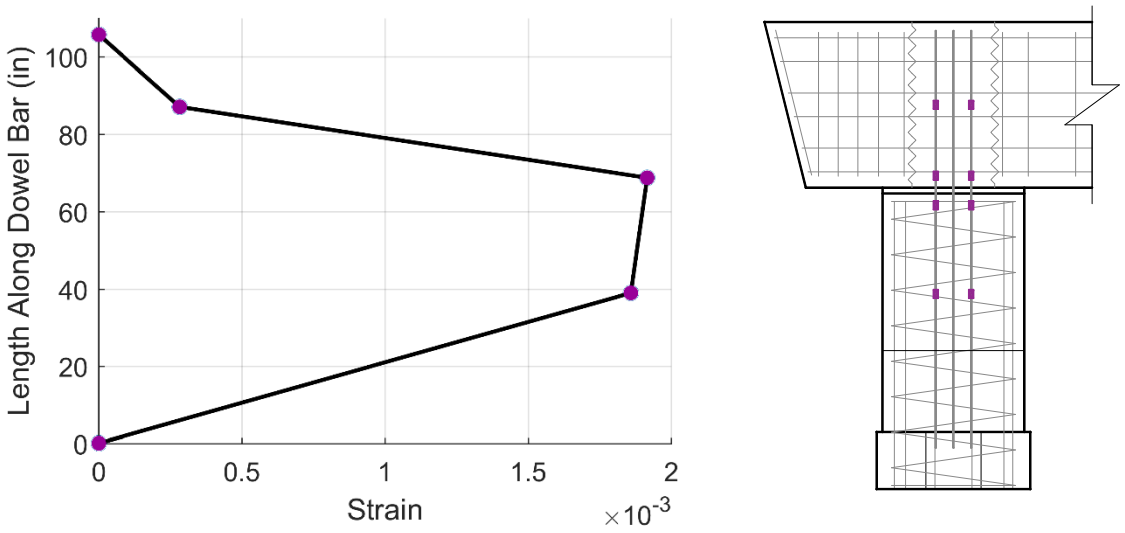

(a) Strains *(b) Locations*

Figure 4.25. Largest Dowel Bar Strains – Pattern D – RCS-16-12.

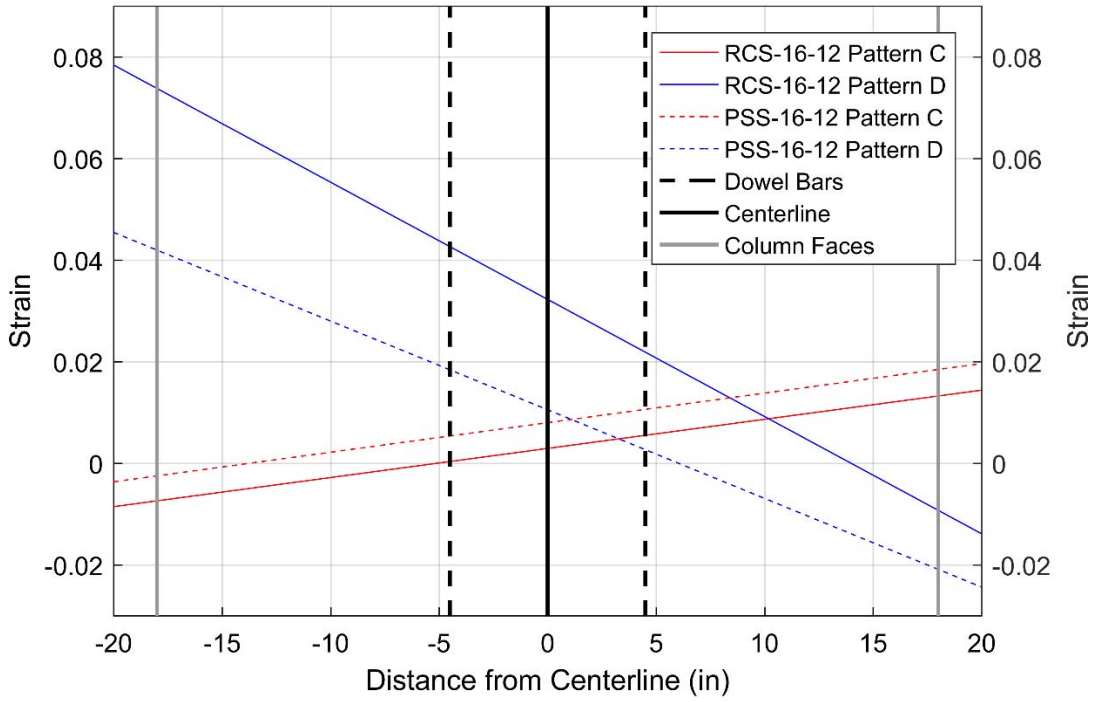

Figure 4.26. Bedding Layer LVDT Strains.

4.9. Conclusions

The experimental testing examined the performance of the reinforced concrete and pretensioned bent cap specimens at bridge demands and maximum bent cap, joint and failure demands. The performance of the 21-in corrugated pipe connection was also investigated for both specimens. The following conclusions can be made:

- Initial Cracking – *The effects of prestressing delay the onset of cracking in bent caps.* Although the actual initial cracking moment for both specimens was lower than expected, the pretensioned bent cap cracked at a higher moment demand compared to the reinforced concrete specimen.

- AASHTO Class 1 and Class 2 Exposure Limits – *Pretensioned bent caps are expected to contain crack widths below 0.017-in under bridge load demands.* The pretensioned bent cap specimen did not exceed the exposure limits during the application of the bridge demands up to 140% factored loads. The first signs of cracks exceeding the Class 1 exposure limit for the pretensioned bent cap took place during the application of loads greater than the expected nominal capacity. The reinforced concrete specimen exceeded the Class 1 and Class 2 exposure limits at factored loads demands.
- Creep – *Pretensioned bent caps improve the resistance against the creep of cracks under sustained loads.* The pretensioned specimen displayed a high resistance against the growth and widening of cracks when subjected to sustained factored load demands with minor extension of cracks and no increase in cracks widths. The reinforced concrete specimen displayed significant extension and widening of cracks compared to the pretensioned specimen.
- Crack Patterns – *The effects of prestressing localize the areas of damage in bent caps and reduce the growth of cracks.* The effects of prestressing provided the pretensioned specimen with localized damage and smaller average crack widths compared to the reinforced concrete specimen. The damaged areas in the pretensioned specimen were limited to the regions near the maximum moment demands while the reinforced concrete specimen develop extensive damage through the entire length of the beam.

- Pocket Connection – *A 21-in diameter pocket connection is an acceptable alternative for a precast bent cap system. Typical bent cap sizes provide sufficient embedment depth.* The pocket connection performed satisfactorily during testing for both specimens. No signs of yielding and no major exposure of the pipe was recorded throughout the experimental testing. No signs of yielding or pull out were recorded in the dowel bars of the connection during the maximum joint demands.
- Closure of Cracks Following Load Removal – *The effects of prestressing provide the ability for the closure of cracks. These prestressing effects also increase the ability to reduce cracks after removal of loads greater than expected yield and nominal moment demands.* The pretensioned bent cap was effective at closing most cracks after removal of loads greater than the expected yield and nominal moment strengths. The effects from pretensioning also allowed higher reduction of cracks following the removal of loads in comparison to the reinforced concrete specimen. The reinforced concrete bent cap was unable to provide any closure of the cracks following the removal of loads.
- Ductile Behavior – *Both specimens reinforced concrete and pretensioned bent caps display sufficient ductile behavior prior to failure.* The reinforced and pretensioned bent cap specimens both displayed significant crack growth and crushing prior to failure.

5. ANALYSIS OF BENT CAP PERFORMANCES

This chapter provides an analysis of the results from RCS-16-12 and PSS-16-12. Section 5.1 discusses the performance of both specimens with respect to the chosen design objectives. Section 5.2 discusses the comparison to expected yield and nominal moment strengths. Section 5.3 discusses the results for constructability and performance in light of the previous work discussed in the literature review. Section 5.4 compares the results from testing between RCS-16-12 and PSS-16-12. Section 5.5 provides a discussion on the hierarchy of failure mechanisms for each specimen.

5.1. Discussion of Design Objectives

Table 5.1 provides a summary of the design objectives and the results seen during testing for both specimens. Check marks show acceptable performance and "X" marks show the unsuccessful performance in achieving the desired design objectives.

Table 5.1. Evaluation of Design Objectives

Design Objectives	RCS-16-12	PSS-16-12
Zero Tension under Dead Load	X	✓
Serviceability Stress Limit of 36-ksi	X	N/A
Zero Cracks for SLS Demands	X	X
No Cracks at ULS Demands	X	X
Low Cracks at ULS Demands	X	✓
Ductile Behavior	✓	✓

One of the strain gages installed in the negative moment region of RCS-16-12 gave a reading corresponding to a dead load tensile stress of 27.8-ksi, indicating tension under

dead loads for RCS-16-12 as expected. At dead load demands, zero tension was only expected only in PSS-16-12.

The expected service stress level for RCS-16-12 in the tension reinforcement was calculated from the steel materials testing and the expected yield moment using the following equation based on the proportional behavior of cracked reinforced concrete sections:

$$f_s = f_y\left(\frac{M_{SLS}}{M_y}\right) \tag{5-1}$$

where f_s = tensile stress at service, f_y = measured yield stress of #8 bars (66-ksi), M_{SLS} = moment at SLS demands (649 k-ft) and M_y = calculated yield moment (1435 k-ft). The expected service stress was calculated to be 30-ksi which is below the 36-ksi serviceability limit state based on the 2015 TxDOT Bridge Design Manual. The strain gage installed on a longitudinal reinforcement bar in the negative moment region of RCS-16-12 showed a tensile stress of 37.7-ksi during SLS demands, exceeding the serviceability stress limit.

Cracking at SLS demands was expected only in RCS-16-12. Observations of RCS-16-12 at SLS demands confirmed this expectation with cracks in both the positive and negative moment regions. PSS-16-12 showed a small hairline crack at SLS demands in the negative moment regions along the centerline of the column. Therefore, PSS-16-12 did not meet the zero cracks at SLS demands. The observed cracking moment (605 k-ft) was 54% of the expected (1125 k-ft).

As anticipated, RCS-16-12 showed a high quantity of crack widths that exceeded the AASHTO Class 1 exposure limit (0.017-in) during ULS demands. Although

PSS-16-12 showed only small hairlines cracks during ULS demands, cracking at this demand was not anticipated since the expected cracking moments for the positive and negative moment regions were calculated to be higher than the ULS demands. Neither specimen met the no cracks under ULS demands design objective. PSS-16-12 did achieve low cracking during ULS demands and performed adequately since it developed only minimal hairline cracks in both the negative and positive moment regions.

Pattern F caused RCS-16-12 to developed a larger flexure-shear failure along a gradual angle across the span while PSS-16-12 developed a steeper flexure-shear failure near the overhang. Although failures developed at different locations and angles, both RCS-16-12 and PSS-16-12 showed desirable ductile behaviors with the development of large cracks and signs of crushing of the compression zones prior to failure.

5.2. Discussion on Comparison to Expected Strengths

Actual yield and nominal moment strengths were examined to determine the performance of both specimens compared to the expected strengths. The performance of the corrugated steel pipe is also covered to determine the performance of the pocket connection in resisting prestressing forces and acting as equivalent shear reinforcing in the joint region.

Results from testing showed that the actual yield strength of RCS-12-16 exceeded the predicted yield moment of 1010 k-ft. Strain gage data collect on a longitudinal reinforcement in the negative moment region for RCS-16-12 showed yield initiated near the applied 140% ULS demands corresponding to a moment of 1204 k-ft. The actual yield strength for PSS-16-12 also exceeded the expected yield strength. The first signs of strands yielding in the positive region of PSS-16-12 were during the applied maximum positive

moment demands (Pattern B) with the appearance of large cracks and the remaining open cracks after loads were decreased to dead load demands in the span. The first signs of yield in the strands in the negative moment region were during the applied maximum negative moment demands (Pattern E) showing large cracks widths and also remaining crack widths following removal of loads. Overall, RCS-16-12 developed more widespread cracks through the negative and positive moment regions with a higher quantity of large cracks in comparison to PSS-16-12, which displayed localized damage near the points of higher moment demands.

The nominal moment strengths for both specimens were also above the expected values. The first signs of crushing (ε_{cu} =0.003) in the compression zone of RCS-16-12 in the negative moment region appeared during Pattern E and crushing in the positive moment region did not appear until Pattern F. The first signs of crushing in PSS-16-12 were only observed in the positive moment region close to Pattern F, and no signs of crushing were observed in the negative moment region.

The pocket connection performance during testing was also considered successful for both specimens. No cracks developed along the edges of the void (thin wall sections in the bent cap) during the transfer of prestressing forces or any time before testing. The chosen 12-gage pipe showed an acceptable uniform distribution of prestressing forces preventing the development of concentrated stresses above the cracking moment in the 10.5-in walls in the bent cap at the sides of the void. At maximum moments in the connection region during Pattern E, no signs of yield were recorded in the strain gages

installed on the corrugated pipe and dowel bars and no cracks developed in the confined concrete.

5.3. Discussion of Results in Light of Previous Work

This section discusses the constructability and performance of RCS-16-12 and PSS-16-12 in consideration of the previous work studied in the literature review. The discussion of constructability covers end region detailing, prestressing construction techniques, corrugated pipe installation, and bedding layer construction. The discussion of performance covers end region cracking at release and at the time of delivery to the laboratory, pretensioned construction temperatures, and ambient conditions, crack pattern observations in the bent cap and pocket connection performance during testing.

5.3.1. *Constructability*

The tie down of the corrugated pipe was an important constructability issue in comparing the performance of the pocket connection to previous work on connections. While casting RCS-16-12, the corrugated pipe shifted due to high concrete discharge rates and improper fastening at the top and bottom. This highlights the necessity for proper anchoring and careful casting practices to prevent any shifts in the corrugated pipe.

The large density of reinforcement at the end region of PSS-16-12 to resist spalling and bursting stresses did not affect constructability as emphasized by Avendaño et al. (2013). Flame cutting techniques were used to release the strands in PSS-16-12 with top strands cut initially followed by the release of the bottom stands. The release technique and pattern were similar to fabrication practices used by Ross et al. (2014) during the

construction of pretensioned Florida girders and provided an acceptable means for strand release.

The use of a precast 21-in diameter corrugated pipe connection increased the misalignment construction tolerances in the dowel bars and columns during the placement of the bent cap onto the column. The use of the dowel bars to connect the column and the bent cap also increased the misalignment tolerances in the 21-in diameter corrugated pipe compared to the extension of column longitudinal bars in the pocket connection constructed by Restrepo et al. (2011). The increased tolerances and use of normal weight concrete to complete the connection eliminated many of the constructability issues reported by Matsumoto et al. (2001) during the implementation of grouted vertical corrugated ducts in the connection between the precast bent cap and cast-in-place column.

When forming the bedding layer, the plastic shims were easily installed and, in contrast to observations by Restrepo et al. (2001), did not shift during the installation of the bent cap onto the column. Smoothing of the concrete top surface concrete (shortly after casting or with a concrete grinder) where the shims would be placed was sufficient to provide an even and stable surface for the shims without the need of glue. During casting of the bedding layer, smaller size aggregates and placement of shims away from the outside surface helped ensure concrete dispersion throughout the entire bedding layer and behind the shims as recommended by Restrepo et al. (2001). Although proper dispersion behind the shims required more vibration efforts, it was easily achieved. Using vents in the bedding layer formwork, as recommended in the grouted vertical duct connections by Matsumoto et al. (2001), did not yield positives results with the use of normal weight

concrete due to higher viscosity. Voids were prevented with the additional consolidation of concrete at the bedding layer and small voids in the formwork of about 1/8-in to release entrapped air. To increase the concrete bond between the column and bedding layer all surfaces in contact with the concrete were prewetted to saturated surface-dry conditions as recommended by TxDOT. The normal weight concrete used to cast the pocket connection and bedding layer eliminated the need for a separate grouting process, strict grouting specifications, and issues in segregation of fine aggregates during casting.

5.3.2. *Performance*

Spalling and bursting stress cracks were not seen in PSS-16-12 during the transfer of prestress forces during the release of strands. This observation is potentially due to the positive implementation of recommendations for end region detailing by O'Callaghan and Bayrak (2008), although the low amount of total prestressing may have been a contributing factor. The concrete release strengths in the two batches of PSS-16-12 were 4.13-ksi and 4.06-ksi (TxDOT minimum of 4-ksi). These release strengths were lower than the minimum release strengths used by O'Callaghan and Bayrak (2008), Avendaño et al. (2013), Ross et al. (2014) of 6.5-ksi. The thermocouples installed at the center of the bent cap recorded maximum curing temperatures of 160°F (10°F below the TxDOT allowable curing temperatures of 170°F) and the maximum ambient temperatures were 102°F. Both maximum temperatures were higher than the those observed during the fabrication of U-beam girders by Avendaño et al. (2013) which recorded 155°F maximum curing and 88°F maximum ambient temperatures. The lower concrete release strength and higher

temperatures compared to previous tests showed no impact on cracking at the transfer of prestress forces.

The use of a concentric strand layout showed bursting stress cracks propagating horizontally along the sides of PSS-16-12 while eccentric strand layouts in tests by O'Callaghan and Bayrak (2008), Avendaño et al. (2013), Ross et al. (2014) showed both horizontal and vertical inclined cracks. After delivery of PSS-16-12 to the research laboratory 66 days after strand release, cracks developed within the transfer length. These cracks extended a maximum of 28-in into the bent cap. The appearance cracks within the transfer length days after strand release follows observations noted by Ross et al. (2014) prior to load testing of pretensioned Florida I-beam girders. The cracks in the end region of PSS-16-12 were limited to hairlines cracks and much smaller than the damage observed in the pretensioned Florida I-Beam girders. The additional end region reinforcement at the square showed benefits in PSS-16-12 by preventing the appearance of cracks at the square end face. This aligned with the results from the additional end region reinforcement installed in the end blocks of U-beam box girders by Avendaño et al. (2013).

The use of a test setup capable of generating demands representative of multi-column bent caps provided better insight to potential damage in current TxDOT designs than do previous studies. Each specimen was capable of investigating three different span ratios while previous studies that reached failure demands were limited to one span ratio in the negative moment region. The span ratios for both RCS-16-12 and PSS-16-12 were 0.14 in the overhang, 1.57 in the span, and 0.86 at the square end. Each shear span ratio developed different crack patterns. RCS-16-12 first exhibited cracks at

the top of the bent cap in the negative moment region at 74% of SLS demands in a similar fashion to the cantilever bent caps tested by Bracci et al. (2001) which showed general initial cracking at approximately 63% of service loads. PSS-16-12 showed an increase in performance compared to the other tests by not cracking until approximately SLS demands. During the application of bridge demand loads, flexure cracks began in the negative moment of both specimens at the joint region and propagated vertically. These initial vertical flexure cracks were similar to the flexure cracks seen in tests by Bracci et al. (2001) and Matsumoto et al. (2001). Additional flexure cracks and new flexure-shear cracks developed in both specimens during Pattern E and showed a shift in the cracks as they propagated towards the inside face of the column. These crack patterns at higher loads deviated from results seen by Bracci et al. (2001) (a/D = 1.08) and phase 2 testing by Matsumoto et al. (2001) (a/D = 0.87). These previous tests showed the flexure cracks continuously propagating vertically while the shear-flexure cracks propagated to the nearest side face of the support in a generally symmetric pattern about the center of the column. The convergence of cracks at the inside face of the column for RCS-16-12 and PSS-16-12 agreed with previously recognized behavior highlighted in tests performed by Ferguson (1964), who suggested this behavior was due to the higher strain profiles at the inside face of the column as a result of uneven distribution of forces along the top surface of the column. Cracks in the positive moment region for both specimens were more symmetric and propagated from each side of the bearing pad similar to the behavior observed in tests by Bracci et al. (2001) and Matsumoto et al. (2001). Failure in RCS-16-12 took place along the flexure-shear cracks in the span at an approximate angle

of 40°. PSS-16-12 develop a failure along the flexure-shear cracks near the square end at an angle of 55°. Failure planes in both RCS-16-12 and PSS-16-12 developed in the span as opposed to failures in the overhangs observed by Fonseca et al. (1963) and Bracci et al. (2001). Damage to the connection region and mid-span was much more contained in PSS-16-12 compared to the previous testing performed on reinforced concrete bent caps. The prestressing effects of PSS-16-12 followed the findings in the retrofitted bent cap column assemblies tested by Mander et al. (1996) showing enhanced elasticity in the cap beam and strengthening of both the bent cap and joint.

Cracks at the top of the bent cap near the pocket concrete were contained to the outside circumference of the corrugated pipe during all load combinations and showed no signs of yielding of the corrugated pipe for both RCS-16-12 and PSS-16-12. In this regard, the pocket connection matched the performance of the corrugated vertical ducts by Matsumoto et al. (2001). No signs of pull out were seen in the dowels bars during any of the applied vertical or joint demands reemphasizing the findings the conclusions by Matsumoto et al. (2001) on typical bent cap sizes having adequate embedment and anchorage depths for dowel bars up to #11. The high-density plastic shims showed no signs of creating concentrations of forces in the bedding layer and allowed proper distribution of the loads between the column and bent cap as seen in the pocket connection tests by Restrepo et al. (2011). The bedding layer concrete did not develop any cracks during the applied bridge demands, showing that a bedding layer did not create a weak link between the column and the bent cap as also observed in tests conducted by both Matsumoto et al. (2001) and Restrepo et al. (2011). Lateral loads imposed during joint

opening and joint closing showed the most significant damage to the joint in both RCS-16-12 and PSS-16-12 with cracks only developing in the bedding layer and column. These observations were different from the connection tests by Restrepo et al. (2011) which showed cracking also developing in the connection region of the bent cap during the application of reverse cyclic lateral loads.

Excessive crack widths at the mid-depth sides were not observed in either RCS-16-12 or PSS-16-12. The greatest crack widths were at the top (negative moment region) and bottom (positive moment region) of the bent caps. The layout with evenly distributed longitudinal reinforcement/strands along the sides coincided with recommendations by Frantz and Breen (1978) to control side cracking in inverted T-bent caps. Thus, the longitudinal reinforcement served a dual purpose of acting as the flexure reinforcement and also providing effective side crack control without the need for additional skin reinforcement.

5.4. Discussion on Comparison of RCS-16-12 and PSS-16-12.

Behaviors observed during testing of the reinforced and prestressed bent caps are discussed to analyze the difference in performance between the two specimens. Table 5.2 highlights key aspects that were monitored during testing of RCS-16-12 and PSS-16-12. Check marks show which specimen performed the best for each aspect and "=" show aspects that performed equally for both specimens.

Table 5.2. Comparison of Key Performance Aspects between RCS-16-12 and PSS-16-12

Key Performance Aspects	RCS-16-12	PSS-16-12
Highest Cracking Moment		✓
Highest Creep Resistance		✓
Highest Crack Closure Ability		✓
Lowest Maximum Crack Widths	=	=
Lowest Average Crack Widths		✓
Localized Damage		✓

PSS-16-12 showed higher cracking moments (near SLS demands) compared to RCS-16-12 (at approximately 74% of SLS demands). The actual cracking moment of PSS-16-12 was 605 k-ft in the negative moment region and 784 k-ft in the positive moment region while the cracking moment in the RCS-16-12 was 520 k-ft in the negative moment region and 523 k-ft in the positive moment region. During the study of creep at ULS demands, PSS-16-12 demonstrated minimal crack extension with no crack widening as opposed to the noticeable crack extensions and widening observed in RCS-16-12. Throughout the multiple unloads in both specimens, PSS-16-12 provided a significantly higher ability than RCS-16-12 to close and reduce crack widths after removal of loads, as shown in the Figure 4.18, Figure 4.19, and Figure 4.20.

During Pattern A and Pattern B, PSS-16-12 consistently showed the lowest maximum cracks widths in comparison to RCS-16-12. Figure 5.1.a provides the maximum crack width envelopes for both specimens plotted against the normalized nominal moments in the positive and negative moment regions and also displays the limits for the AASHTO LRFD Class 1 (0.017-in) and Class 2 (0.013-in) exposure limits. The green

region represents crack widths lower than the Class 2 exposure limit, the yellow region represents cracks widths between the Class 1 and Class 2 exposure limits, and the red region represents crack widths greater than the Class 1 exposure limit. PSS-16-12 shows most cracks remain within the Class 2 exposure limit at demands below the expected nominal strength capacity while RCS-16-12 had widths greater than the Class 1 exposure limit before reaching its expected nominal moment strength. The widest positive and negative moment crack widths seen in the figure correspond to the maximum negative and positive moment demands (Pattern B and Pattern E) for both specimens. Figure 5.2.a provides a logarithmic scale of the maximum crack width envelopes.

It is important to note that although equal maximum crack widths of 0.198-in were seen in both specimens, this crack width only occurred at one of the cracks in the more centralized damage area of PSS-16-12. RCS-16-12 developed a higher quantity of cracks with this same maximum width and several others nearly as large. Consequently, PSS-16-12 displayed more localized damage areas concentrating near the maximum moment locations while RCS-16-12 developed very widespread, higher quantity and larger crack widths average widths throughout both the negative and positive moment regions. The visual representation of this behavior is shown in the figures of Section 4.7. Figure 5.1.b provides a summary of the average crack width envelopes for both RCS-16-12 and PSS-16-12. Figure 5.2.b provides a logarithmic scale of these average crack width envelopes.

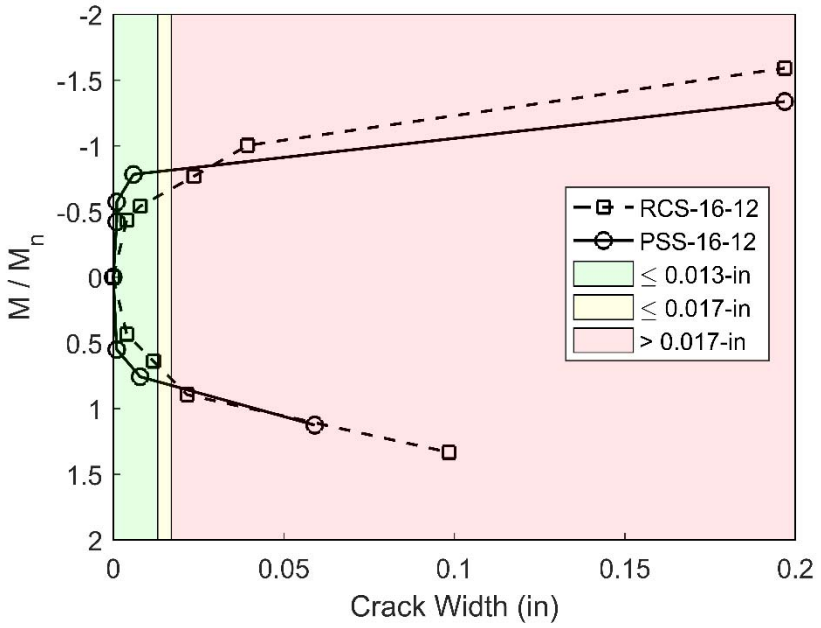

(a) Maximum Crack Widths

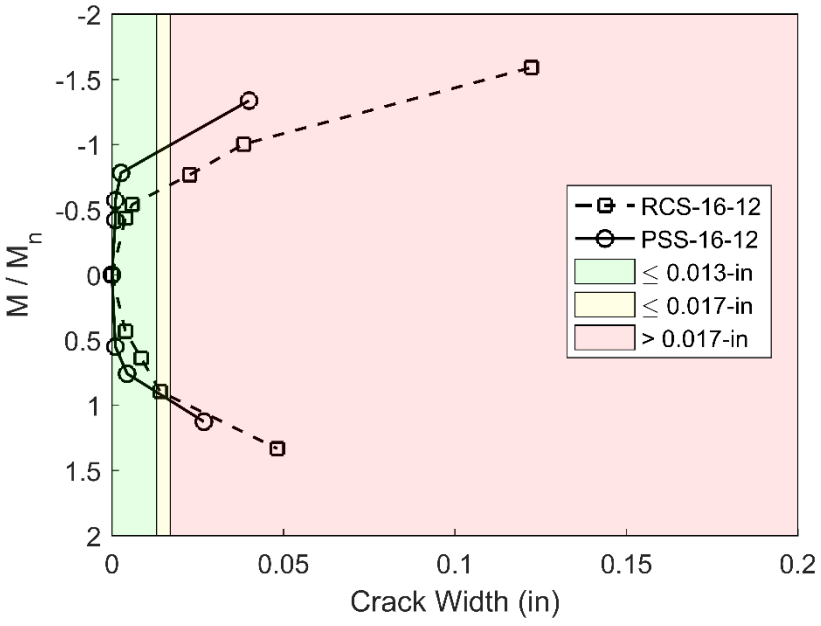

(b) Average Crack Widths

Figure 5.1. Crack Width Envelopes – RCS-16-12 and PSS-16-12

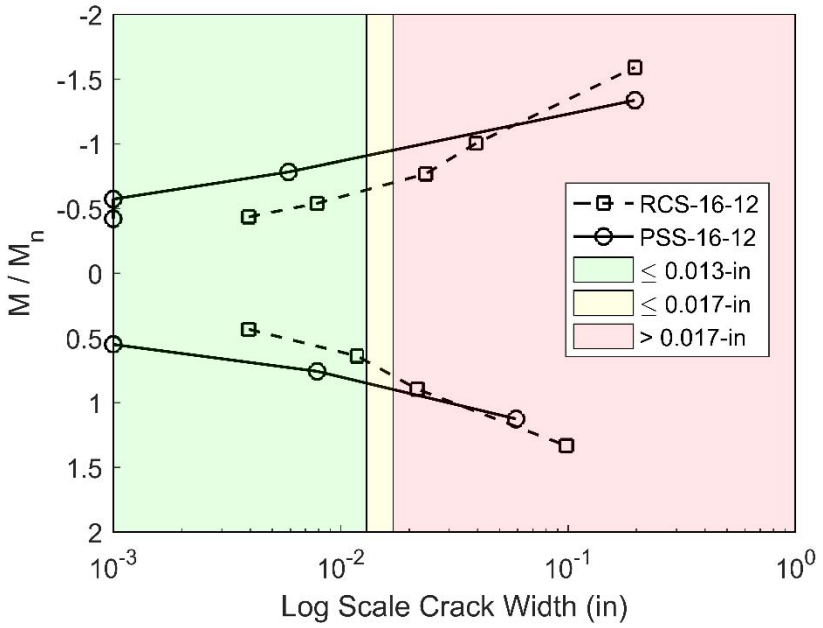

(a) Maximum Crack Widths

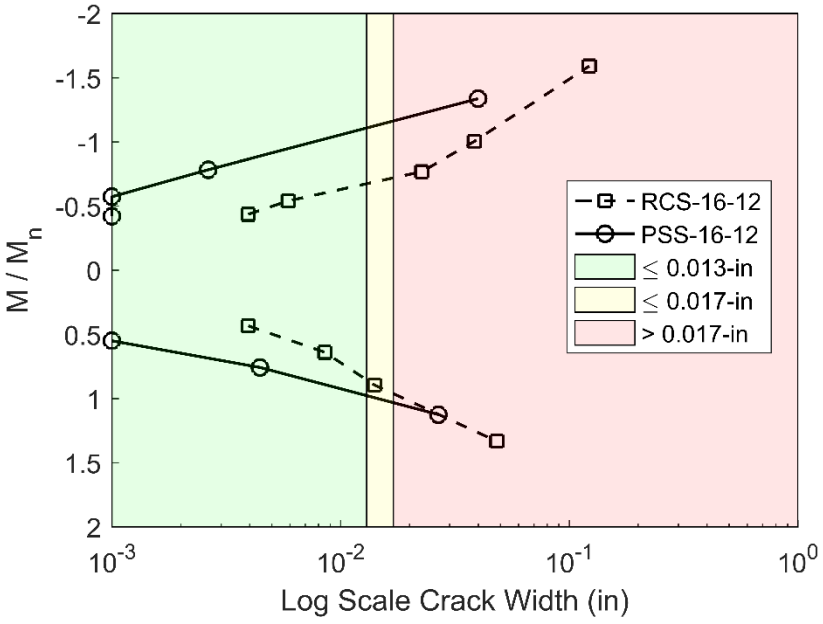

(b) Average Crack Widths

Figure 5.2. Crack Width Envelopes Plotted to a Logscale – RCS-16-12 and PSS-16-12

5.5. Discussion on the Hierarchy of Failure Mechanisms

This section discusses the hierarchy of failure mechanisms based on as-built capacities of members for each of the experimental specimens. As shear failures are brittle, they are the most undesirable failure mode. Conversely, flexure, when properly detailed, is a preferred mode of failure due to its ductile behavior.

The relative strength of members also affects the failure mode. For example, if a bent cap is stronger than the column, this is said to be a strong–beam/weak–column system. This is a preferred failure mode for bridge piers. Also, a column stronger than the joint, known as strong–column/weak–joint, is also preferred to prevent joint failure and a plastic hinge from developing at the bent cap.

5.5.1. *Shear*

The first step is to check for a ductile behavior in the bent cap. Ductile behavior are characterized by large deformations with multiple tensile cracks and crushing in the compression zones that appear in members prior to failure, as opposed to abrupt/brittle shear failures. Such ductile behavior takes place when the shear capacity is higher than the flexure capacity. Ensuring ductile behavior in the bent cap can be achieved by checking the shear overstrength factors using the following equation for both RCS-16-12 and PSS-16-12:

$$\Omega_o^{shear} = \frac{\phi V_n}{M_n / a} \geq 1 \qquad (5\text{-}2)$$

where ϕ_o^{shear} = shear overstrength factor, ϕ = 0.9 for shear, V_n = nominal shear capacity, M_n = nominal shear capacity and a = the shear span length.

5.5.2. *Flexure*

The preferred failure hierarchy for a precast bent cap-to-column system is to provide the following order of flexure capacities based on joint design such that:

$$M_n^{joint} < M_n^{column} < \phi M_n^{beam} \tag{5-3}$$

where ϕ = 1.0 for flexure, and M_n = to the nominal capacities for the beam, column and joint.

This concept requires a plastic hinge failure mechanism occurring at the top of column adjacent to the joint. This joint design assumes a strong column-weak joint and a stronger bent cap to prevent a plastic hinge forming at the bent cap during the presence of strong vertical and lateral loads. The following flexure overstrength factors were calculated using the following equations:

$$\Omega_o^{beam} = \frac{\phi M_n^{beam}}{M_n^{column}} \geq 1 \tag{5-4}$$

$$\Omega_o^{column} = \frac{\phi M_n^{column}}{M_n^{joint}} \geq 1 \tag{5-5}$$

in which M_n^{column} = flexural capacity based on the perimeter rebars in the column; and M_n^{joint} = flexural capacity based on the dowel bars that pass through the central region (just above the head of the column) through the bedding layer and anchored within the cap beam pocket region.

The nominal moment capacities of the bent caps (beam) were calculated in Section 3.8.1. The moment capacity of the column was determined using the P-M (axial load versus moment) interaction diagrams for each specimen. The moment capacity of the joint is determined in a similar manner to the column capacity using an approach used by Barooah (2016) following the approach set forth in Dutta and Mander (2001). Figure 5.3 shows the section, strain, stress and internal forces acting in the joint using this method.

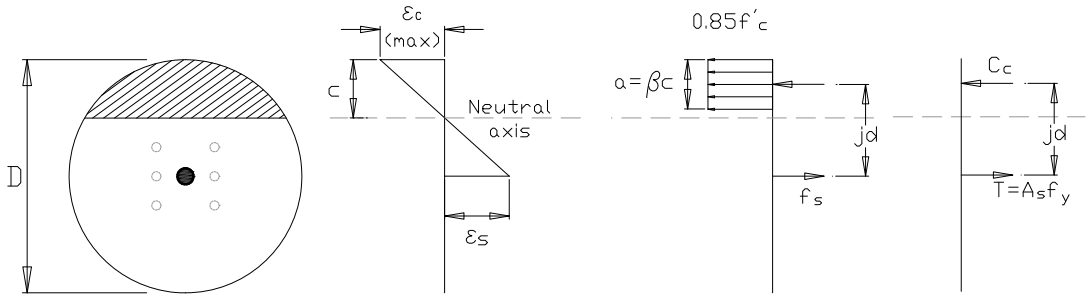

(a) Column Section *(b) Strain Distribution* *(c) Stresses* *(d) Internal Forces*

Figure 5.3. Joint Moment Capacity.

In the approach by Dutta and Mander (2001), the concrete compression force in a circular configuration is approximated by an eccentric concrete stress block. The tensile force provided by the steel dowel bars are lumped at the column centroid and as shown by the concentric black dot in Figure 5.3.a. The depth of the concrete compression stress block may be formed from (see Figure 5.3c):

$$\frac{C_c}{f'_c} = 1.32\alpha(\beta\frac{c}{D})^{1.38} \tag{5-6}$$

where C_c= concrete compression force considering core dimensions of joint in which:

$$C_c = N + T = \rho f_y A_g \tag{5-7}$$

in which N = normalized axial force from dead loads, ρ = joint reinforcement ratio, f_y = steel tensile stress (ksi) and A_g = gross cross-section area of column (in^2), D = diameter of the column; f'_c = unconfined compressive strength of concrete.

The loads in the joint are assumed in a conservative manner to be the result of dead loads only using the minimum load factors corresponding to the strength limit state load combinations, at which the joint demand is the highest. The following equation was used by Barooah (2016) to calculate the moment in the joint and construct the P-M interaction diagrams to represent the moment capacity of the joints for each specimen shown in Figure 5.4.a and Figure 5.4b:

$$\frac{\phi M_n^{joint}}{f'_c A_g D} = 1.32 \frac{\alpha}{2} \phi \left(\frac{a}{D}\right)^{1.38} \left(1 - 1.2 \frac{a}{D}\right) \tag{5-8}$$

where α = 0.85 for the unconfined concrete within the bedding layer.

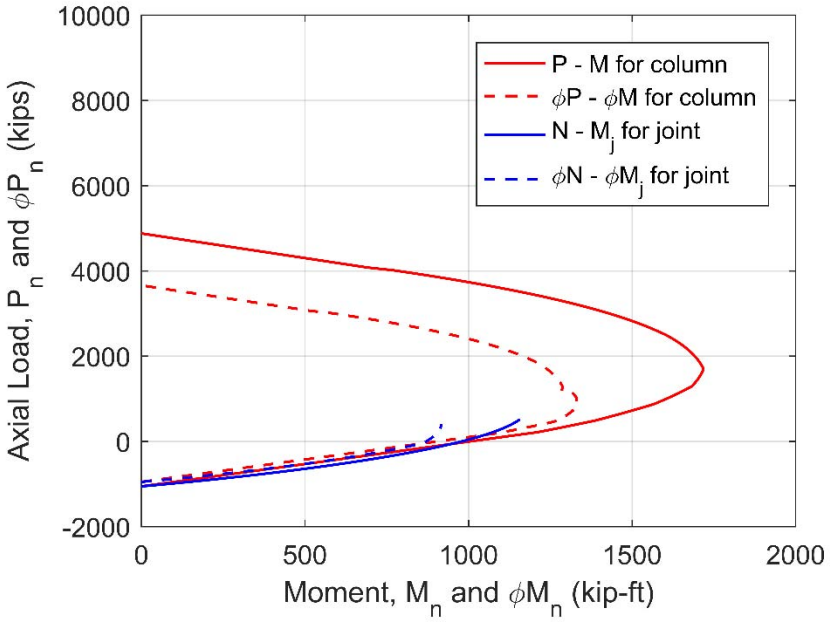

(a) RCS-16-12

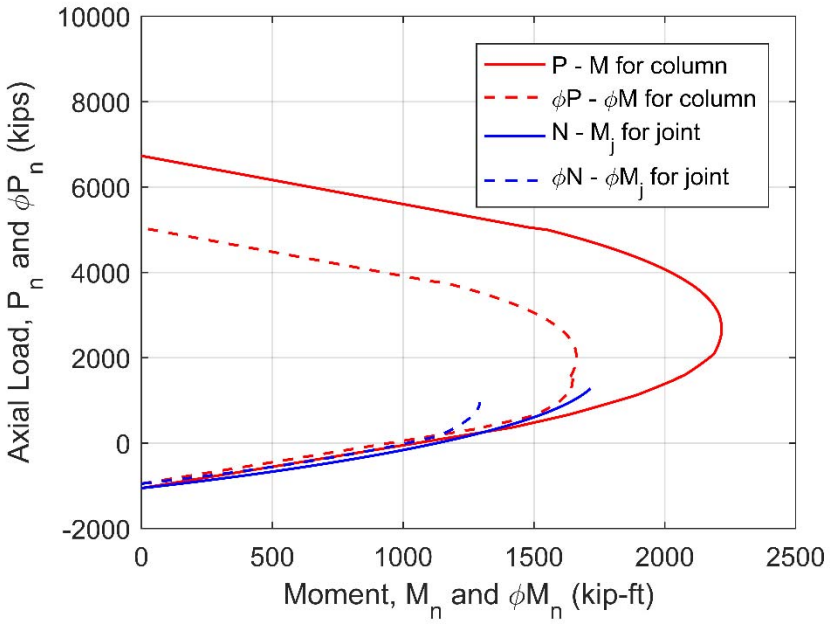

(b) PSS-16-12

Figure 5.4. P-M Interaction Diagrams for the Column and the Joint Within the Bedding Layer Adjacent to the Column.

The results for the failure hierarchy mechanisms are presented in Table 5.3. The overstrength factor for shear (Ω_o^{shear}) in PSS-16-12 was greater than RCS-16-12 which shows the benefits seen in prestressed concrete in increasing the shear capacity of members. Figure 5.5 provides a visual representation of the flexure hierarchy values for both specimens. In this figure, the moment capacity of the joint is shown in green and column capacity is shown in blue and the respective bent cap moment capacity for each specimen is represented by the dashed red line. PSS-16-12 also displayed a higher beam overstrength factor (Ω_o^{beam}) for the concept of strong beam-weak column and this highlights the benefits of the enhanced strength of pretensioned bent caps to ensure a plastic hinge failure mechanism does not occur in the bent cap. The strong column-weak joint concept had a higher column overstrength factor (Ω_o^{colum}) for RCS-16-12 in comparison to PSS-16-12. This is due to the higher concrete compressive strength used in the column of PSS-16-12 (6.66-ksi) compared to the column of RCS-16-12 (4.49-ksi). The higher concrete strength has a large influence on the moment capacity of the joint and therefore could potentially prevent the desired plastic hinge mechanism at the joint and cause a failure within in the column.

Table 5.3. Summary of Failure Hierarchy

Specimen	Overstrength Factors		
	Ω_o^{shear}	Ω_o^{beam}	Ω_o^{column}
RCS-16-12	1.58	0.99	1.12
PSS-16-12	1.75	1.12	1.00

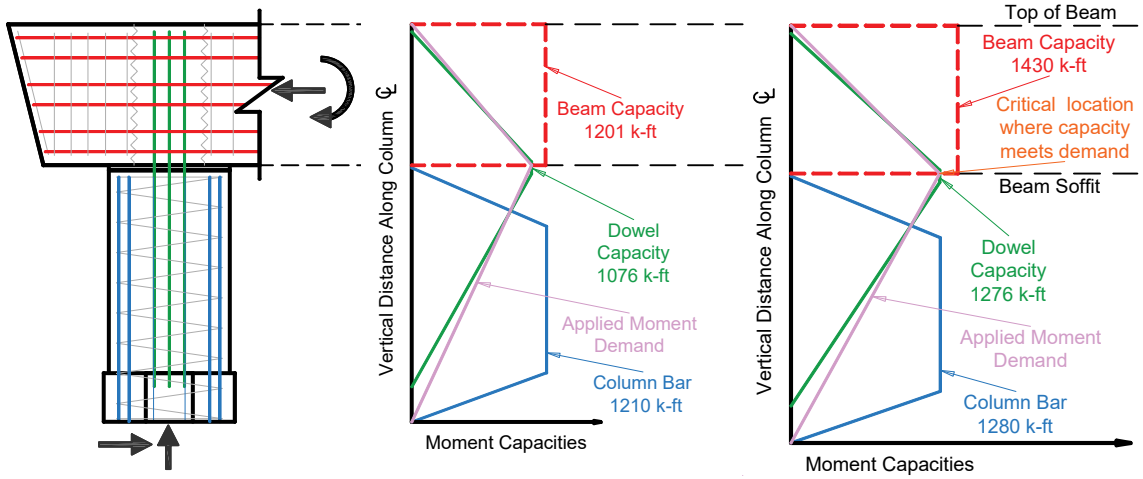

(a) Schematic *(b) RCS-16-12* *(c) PSS-16-12*

Figure 5.5. Beam and Column Flexure Strength Capacities Showing the Critical Location at the Beam-to-Column Joint Interface.

5.6. Key Findings from the Bent Cap Performances

The key observations from the analysis of bent cap performances are as follows:

- The pretensioned bent cap was the only specimen to show evidence of zero tension under dead load demands.
- The reinforced concrete and pretensioned specimens did not attain the design objective of zero cracking under SLS demands.

- The pretensioned specimens was the only specimen to achieve minimal damage at ULS demands.
- Both the reinforced and pretensioned specimens exceed the expected yield and nominal moment strengths during testing and displayed ductile behavior prior to failure.
- The dense end region detailing did not affect the constructability of the pretensioned bent cap and was effective in preventing spalling and bursting stress cracks during the release of strands.
- The secure tie down of the corrugated pipe was an important constructability issue to ensure the proper location of the pocket connection.
- The use of the 21-in diameter corrugated pipe provided a high misalignment tolerance of 3-in and performed successfully during testing with no signs of cracks developing in the confined concrete of the pocket connection and no signs of yielding in the strain gages installed on the corrugated pipe.
- The use of a bedding layer and plastic shims did not affect the performance of the connection during testing.
- No signs of pull out of the dowel bars demonstrated the depth of the specimens was sufficient to develop the necessary embedment depth for #11 bars.
- The lack of excessive side cracks in the both specimens demonstrated the side longitudinal reinforcement layout prevented the need for additional skin reinforcement.

- The use of a test setup that generated demands representative of multi-column bent caps provided better insight to potential damage in current TxDOT compared to previous studies.
- In comparison to the reinforced concrete specimen, the pretensioned specimen delayed initial cracking, provided higher creep resistance and the ability to close cracks after the removal of loads, and also lowered the average crack widths and localized the areas of damage.
- The pretensioned specimen provided a higher shear overstrength factor compared to the reinforced concrete specimen ensuring a ductile behavior characterized by large deformations and crushing in the compression zones prior to failure.
- The pretensioned specimen provided a higher beam overstrength factor than the reinforced concrete specimen ensuring a plastic hinge failure mechanism does not occur in the bent cap.

6. SUMMARY, CONCLUSIONS, AND RECOMMENDATIONS

6.1. Summary

The Texas Department of Transportation is seeking to improve the strength and serviceability of precast substructures by implementing the use of prestressed concrete bent caps in standard precast bent cap systems. The use of precast, pretensioned bent caps in the State of Texas will continue to reap the benefits of rapid construction, reduction of traffic disruption, increased worker safety and increased controlled conditions within the precast plants.

In this TxDOT sponsored research project, Texas A&M Transportation Institute personnel conducted an experimental investigation to study the behavior of precast reinforced and pretensioned concrete bent caps during the application of realistic loads and failure demands. The research presented in this thesis focused on a performance comparison between reinforced and pretensioned specimens under realistic loading conditions, and also investigated an alternative connection and end region detailing to resist prestressing effects during the release of strands.

The experimental testing was conducted at the Texas A&M University High Bay Structural and Materials Testing Laboratory and incorporated a test setup consisting of subassemblies representative of a TxDOT prototype bridge. The design load combinations and stress limits were based on the American Association of State Highway and Transportation Officials (AASHTO) Load and Resistance Factor Design (LRFD) Bridge Design Specifications and TxDOT Bridge Design Standards.

The objective of the experimental testing was to prove the enhanced performance provided by precast, pretensioned bent caps by validating the following design considerations:

- Achieve zero tension under dead load.
- Remain within allowable tensile and compressive service stress limits.
- No cracking under service loads (SLS).
- Minimal cracking under ultimate loads (ULS).
- Provide sufficient reinforcement to ensure a ductile failure.

An alternative connection that does not require the use of grout was implemented on both specimens at the request of TxDOT engineers. The design of the end region detailing to resist bursting stresses at the time of prestress transfer took into consideration the current AASHTO LRFD code provisions, previous research, and recommendations by the precaster.

Material property tests were performed to calculate the expected strengths of the specimens and predict the behavior during testing. Multiple load patterns were applied to the specimens to study their behavior during bridge demands and also maximum achievable moments, joint, and failure demands. Visual observations of the damage progression were presented in detail for each load pattern.

Results from testing were analyzed for each specimen to evaluate the chosen design considerations, examine performance and constructability of the specimens in light of previous literature, compare the results between the reinforced and pretensioned specimens, and discuss the hierarchy of failure mechanisms. Conclusions were made

based on the constructability and performance of the bent caps, pocket connection and end region detailing followed by recommendations for field implementation and future research.

6.2. Conclusions

This section presents the key conclusions for the bent caps, pocket connection, and end region detailing that can be drawn from the experimental testing results and analysis of RCS-16-12 and PSS-16-12.

6.2.1. *Bent Caps*

The following conclusions are presented for both the reinforced and pretensioned specimens:

1. The use of an experimental test setup capable of generating demands in both the positive and negative moment along with realistic shear-moment ratios representative of multi-column bent caps provided insight to potential damage in current TxDOT designs.
2. The prestressing effects, along with contributions from higher strength concrete, provided a larger cracking moment capacity than the reinforced concrete specimen.
3. The ability for cracks to close under the removal of service load demands in the pretensioned specimen validated the design objective of achieving zero tension under dead loads. The pretensioned specimen also displayed the ability to significantly reduce crack widths after the removal of loads greater than the expected yield and nominal moment strengths.

4. The reinforced concrete specimen did not allow the closure of cracks after the removal of loads and showed a low ability to reduce crack widths after the removal of loads greater than the expected yield and nominal strengths.
5. The effects from prestressing strengthened both the bent cap and connection region. This was shown as the pretensioned bent cap developed smaller average cracks widths and more localized damage areas than the reinforced concrete specimen.
6. The higher cracking capacity and ability to close cracks after the removal of loads in the pretensioned bent cap will prevent corrosive agents from reaching the reinforcement and provide a longer lifespan to the substructure and consequently the entire bridge system.
7. Ductile behavior was observed in both reinforced and pretensioned specimens, which produced large cracks widths and signs of crushing prior to failure.

6.2.2. *Pocket Connection*

The following conclusions are presented for the pocket connections implemented during both the reinforced and pretensioned specimens:

1. The use of a 21-in diameter 12-gage pipe in a 42-in square cross-section was sufficient to uniformly distributed the prestressing forces from 16 strands and showed no signs of damage at the joint region during the transfer of prestress forces or prior to testing.
2. A 21-in diameter pocket connection was an effective alternative to the vertical corrugated duct connection. The use of the larger pocket filled with normal weight

concrete also increased the constructability of the connection by providing greater construction misalignment tolerances and eliminating the need for a separate grouting process.

3. The use of a bedding layer and high-density plastic shims did not affect the performance of the bent cap. The plastic shims showed no signs of creating hard spots and the use of a bedding layer did not create a weak link between the column and bent cap. No cracks develop in the bedding layer during the applications of loads up to 140% ULS demands.

6.2.3. *End Region Detailing*

The following conclusions are presented for the end region detailing from the results of the pretensioned specimen:

1. The recommendations by O'Callaghan and Bayrak (2008) in providing bursting stress reinforcement from D/4 to the transfer length were effective in controlling cracks during the transfer of prestressing forces at release but did not prevent cracks from forming within the transfer length after extended periods of time after the release of strands.

6.3. Recommendations

Based on the research in this thesis, a number recommendations can be made for the implementation of bent caps in the field and future research in the areas of precast bent caps and connections.

6.3.1. *Recommendations for Field Implementation*

The following recommendations for field implementation are provided based on bent cap design, fabrication, and assembly and connection.

6.3.1.1. Design

The following recommendations are presented for the design of bent caps for future field implementation:

1. Provide side configurations of longitudinal reinforcement to eliminate the need and cost of additional skin reinforcement for both the reinforced and pretensioned bent caps.
2. Use the thickest readily available 21-in diameter corrugated pipe to form a pocket connection that does not require the use of grout. The pipe provides equivalent hoop reinforcement and uniform dispersion of prestressing forces.
3. Provide shrinkage admixture to the bedding layer and pocket concrete to prevent shrinkage cracks and ensure bond with existing concrete and corrugated pipe surfaces.
4. Do not lower the paste content in the connection concrete as this creates constructability issues by decreasing the workability and dispersion of concrete causing voids in the bedding layer.
5. Provide spalling reinforcement up to a fourth of the member depth (D/4) and bursting stress reinforcement from D/4 to the transfer length in pretensioned bent caps.

6.3.1.2. Bent Cap Fabrication

The following recommendations are presented for future bent cap fabrication:

1. Tie down the corrugated pipe at the top and bottom prior to casting the bent cap to prevent floating of the pipe, shifts, and misalignments of the connection.
2. Limit the discharge rate of concrete near the corrugated pipe to prevent any shifts and misalignment in the pocket connection.

6.3.1.3. Assembly and Connection

The following recommendations are presented for the assembly and connection of bent caps to columns:

1. Use high-density polyethylene plastic shims to support the bent caps assembled onto the columns and to create the required thickness of the bedding layer.
2. Use plastic shims to prevent hard spots from developing in the bedding layer and the potential for corrosion from steel shims.
3. Provide a smooth surface for the placement of shims at the top of the column shortly after casting. Limit the smoothed surface to the equivalent area and predetermined location of the shims.
4. Place the shims away from the edge of the outside surface of the bedding layer, and use aggregates at least 50% smaller than the thickness of the bedding to allow dispersion of concrete throughout the bedding layer and behind the shims.
5. Provide a sealed formwork (cardboard or sheet metal) around the column to cast the bedding layer and pre-drill voids in the formwork to allow trapped air pockets to escape while casting the connection.

6. Before casting the bedding layer and pocket concrete, pre-wet the surface in contact with the new concrete to saturated surface dry conditions as recommended by TxDOT in the grouted vertical duct connections.
7. Additional consolidation is required to ensure the concrete is dispersed behind the shims.

6.3.2. *Recommendations for Future Research*

The following recommendations for future research are provided for bent cap design, fabrication, and assembly:

6.3.2.1. Design

The following recommendations are presented for future research in the design of bent caps:

1. Investigate the behavior of longer span bridges with the use of more strands to analyze larger and more realistic bridges demands for pretensioned bent caps.
2. Investigate the effects of increasing the minimum 28-day concrete strength to prevent cracks from forming during SLS demands in the pretensioned bent caps.
3. Explore the use of additional end region reinforcement to prevent crack formation in the transfer length during long periods of time after the release of strands.
4. Further explore the effects from ambient and curing temperatures during the construction of pretensioned bent caps to prevent cracking in the end regions.
5. Investigate the performance of the largest readily available 12-gage pipe in bent caps with larger prestressing forces.

6. Examine the use of voids in the span and overhang of bent caps to lower the weight and improve transportation capabilities of longer members to job sites for both reinforced and pretensioned bent caps.
7. Introduce hoops at the top of the corrugated pipe to control the formation of cracks at the top of the joint for both reinforced and concrete bent caps.
8. Investigate the use of additional strands near the top of the bent cap to delay cracking and reduce cracks widths when in pretensioned bent caps.
9. With testing results showing low shear damage in the overhang of the pretensioned specimen, examine bent caps with longer overhangs and eccentric strand layouts to seek opportunities in eliminating an inside column and the potential for significant economic savings in standard TxDOT bridges.

6.3.2.2. Bent Cap Fabrication

The following recommendations are presented for future research in the fabrications of precast bent caps:

1. Investigate proper tie down methods for materials used to create voids in pretensioned bent caps.
2. Explore the installation of strands or mild steel reinforcement that travel through the top and bottom of the corrugated pipe to provide a better tie down during casting of the bent caps.

6.3.2.3. Assembly and Connection

The following recommendations are presented for future research in the assembly and connection precast bent caps to columns:

1. Explore the use of a dry joint at the connection between the bent cap and the column to further improve constructability and time of construction.
2. Study the effects of a thicker bedding layer to allow the use of standard aggregate sizes typical of the TxDOT Class C concrete to improve constructability and availability of concrete on site.

REFERENCES

AASHTO LRFD Bridge Design Specifications, U.S. Customary Units, 7th edition (2014). Washington, DC: American Association of State Highway and Transportation Officials, 2014; 7th edition.

Avendaño, A., Hovell, C., Moore, A., Dunkman, D., Nakamura, E., Bayrak, O., and Jirsa, J. (2013). "Pretensioned Box Beams: Prestress Transfer and Shear Behavior," Rep. No. FHWA/TX-13/0-5831-3, Center for Transportation Research, Research Project 0-5831, University of Texas, Austin.

Barooah, U. R. (2016). "The Flexural Design of Pretensioned Bent Caps," Master of Science Thesis, Texas Transportation Institute, Texas A&M University, College Station, Texas.

Bracci, J. M., Keating, P.B., and Hueste, M.B.D. (2001). "Cracking in RC Bent Caps," Rep. No. FHWA/TX-01/1851, Texas Transportation Institute, Texas A&M University, College Station.

CAP18 Version 6.2.2. [Computer Software]. Texas Department of Transportation.

Collins, M. P., and Mitchell, D. (1986). "A Rational Approach to Shear Design – The 1984 Canadian Code Provisions," ACI Structural Journal, V. 83(6), pp. 925-933.

Dutta, A., and Mander, J. B. (2001). "Energy Based Methodology for Ductile Design of Concrete Columns," Journal of Structural Engineering, 127(12), 1374.

Ferguson, P. M. (1964). "Design Criteria for Overhanging Ends of Bent Caps – Bond and Shear," Research Report 3-5-63-52. Center for Highway Research, University of Texas, Austin.

Figg, L., Pate, W. D. (2004). “Precast Concrete Segmental Bridges – America ’s Beautiful and Affordable Icons,” Historical-Technical Series, PCI Journal, pp. 26-39.

Frantz, G. C., and Breen, J. E. (1978). “Control of Cracking on the Side faces of Large Reinforced Concrete Beams,” Research Report 198-1F. Center for Highway Research, University of Texas, Austin.

Freeby, Gregg A., P. E. (2015). "Chapter 2: Damage Assessment and Repair Types, “Concrete Repair Manual: Damage Assessment and Repair Types,” Texas Department of Transportation, 4 Apr. 2015. Web. 12 Aug. 2016.

Freeby, G. A., Hyzak, M., Medlock, R., Ozuna, K., Vogel, J., and Wolf, L. (2003). “Design and Construction of Precast Bent Caps at TxDOT,” Paper presented at the Proceedings of the Transportation Research Board Annual Meeting.

Holle, C. E., (2014) “Pretensioned Interior Bent Option – NB FM 973 at Colorado River,” District of Austin, Travis County, Texas, Texas Department of Transportation.

Jones, K., and Vogel, J. (2001). “New Precast Bent Cap System: Saving Texas Time and Money,” TR News, 212, Jan-Feb. 2001.

Mander, J. B., Ligozio, C., and Kim, J. (1996). “Seismic Performance of a Model Reinforced Concrete Bridge Pier Before and After Retrofit,” Technical Report NCEER-96-0009, National Center for Earthquake Engineering Research, University at Buffalo SUNY, Federal Highway Administration, Buffalo, New York.

Mander, J. B., Ligozio, C., and Kim, J. (1996). “Seismic Evaluation of a 30-Year Old Non-Ductile Highway Bridge Pier and Its Retrofit,” Technical Report NCEER-96-0008, National Center for Earthquake Engineering Research, University at Buffalo SUNY, Federal Highway Administration, Buffalo, New York.

Matsumoto, E. E., Waggoner, M. C., Sumen, G., Kreger, M. E., Wood, S. L., and Breen, J. E. (2001). "Development of a Precast Bent Cap System," Report No. FHWA/TX-0-1748-2, Center for Transportation Research, Texas Department of Transportation, The University of Texas at Austin.

O'Callaghan M. R., and Bayrak, O. (2008). "Tensile Stresses in End Regions of Pretensioned I-Beams at Release," Technical Report: IAC-88-5DD1A003-1, The University of Texas at Austin.

Okumus, P., Oliva, M. G., and Becker S.. (2012). "Nonlinear Finite Element Modeling of Cracking at the Ends of Pretensioned Bridge Girders," Engineering Structures 40: 267-275.

Restrepo, J. I., Tobolski, M. J., and Matsumoto, E. E. (2011). "Development of a Precast Bent Cap System for Seismic Regions," NCHRP Report 681, Transportation Research Board, Washington, D.C.

Ross, B.E., Consolazio, G.R., and Hamilton, H.R. (2013). "End Region Detailing of Pretensioned Concrete Bridge Girders," Technical Report: BDK75 977-05, Florida DOT, University of Florida.

Runzell, B., Shield, C., and French, C. (2007). "Shear Capacity of Prestressed Concrete Beams," Rep. No. MN/RC 2007-47, Minnesota Department of Transportation, University of Minnesota.

Texas Department of Transportation (2016). "Precast Concrete Cap Option for Round Columns," Bridge Division, Texas Department of Transportation.

Texas Department of Transportation (Revised 2015). Bridge Division (English) Standards.

APPENDIX A

SPECIMEN CONSTRUCTION DRAWINGS

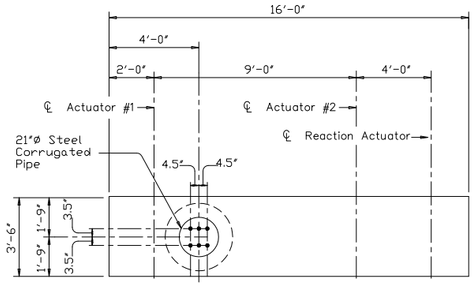

PLAN

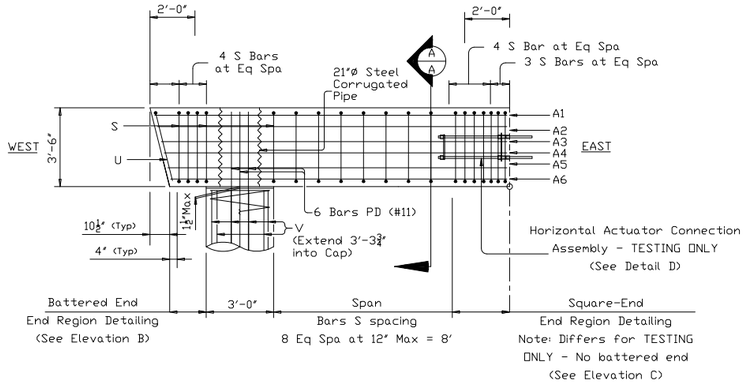

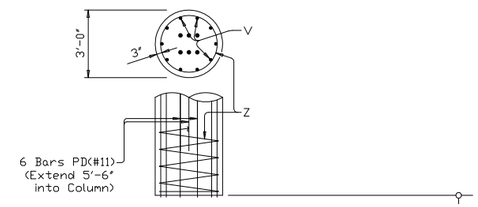

ELEVATION A

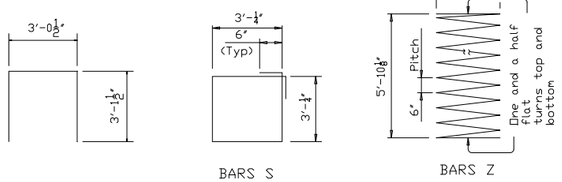

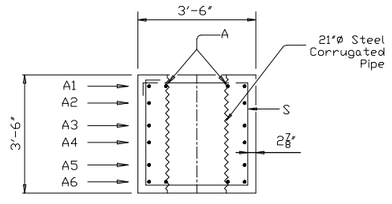

REBAR LAYOUT

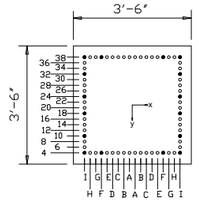

REBAR PATTERN

SECTION A-A

TABLE OF ESTIMATED REBAR QUANTITIES				
Bar	No.	Size	Length	Weight
A1	4	#8	15'-8"	
A2	2	#8	15'-6½"	
A3	2	#8	15-4½"	
A4	2	#8	15-3"	
A5	2	#8	15-1"	
A6	4	#8	14-11⅛"	
PD	6	#11	8'-11½"	
S	20	#5	13'-1"	
U	1	#5	9'-8"	
V	10	#9	6'-3½"	
Z	1	#4	105'-1"	
Reinforcing Steel			Lb	
Class "C" Concrete (Cap)			CY	
Class "C" Concrete (Col)			CY	

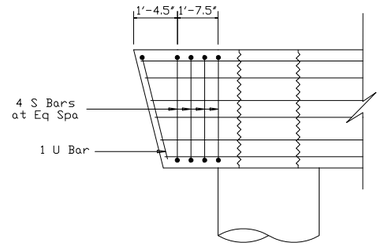

ELEVATION B

BATTERED END - END REGION DETAILING

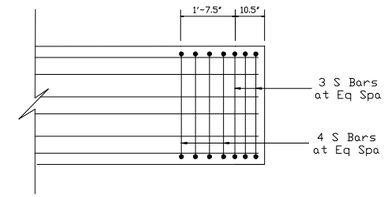

ELEVATION C

DEAD-END END REGION DETAILING

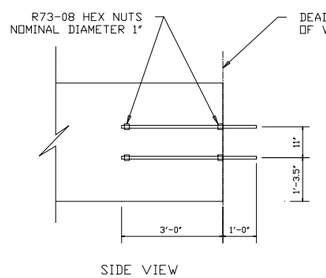

SIDE VIEW

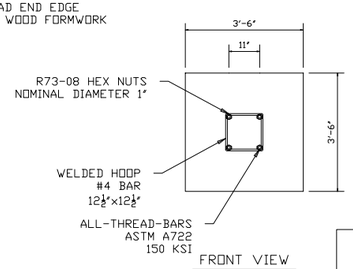

FRONT VIEW

DETAIL D

WOOD FORMWORK HORIZONTAL ACTUATOR CONNECTION ASSEMBLY

DATE: May 29, 2017 - 3:54pm
FILE:

TxDOT 0-6863
Precast Pretensioned
Bent Caps
RCS-16-12

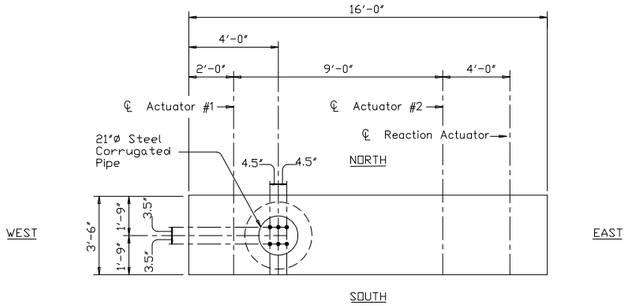

PLAN

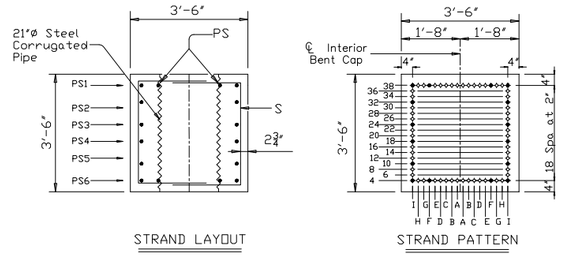

STRAND LAYOUT

STRAND PATTERN

SECTION A-A

TABLE OF ESTIMATED BAR QUANTITIES				
Bar	No.	Size	Length	Weight
PD	6	#11	8'-11¼"	
C	24	#5	5'-6⅛"	
S	18	#5	14'-2"	
B	12	#5	5'-4"	
U	1	#5	9'-3⅛"	
V	10	#9	6'-3¾"	
Z	1	#4	105'-1"	
Reinforcing Steel				Lb
Class "H" Concrete (Cap)				CY
Class "C" Concrete (Col)				CY

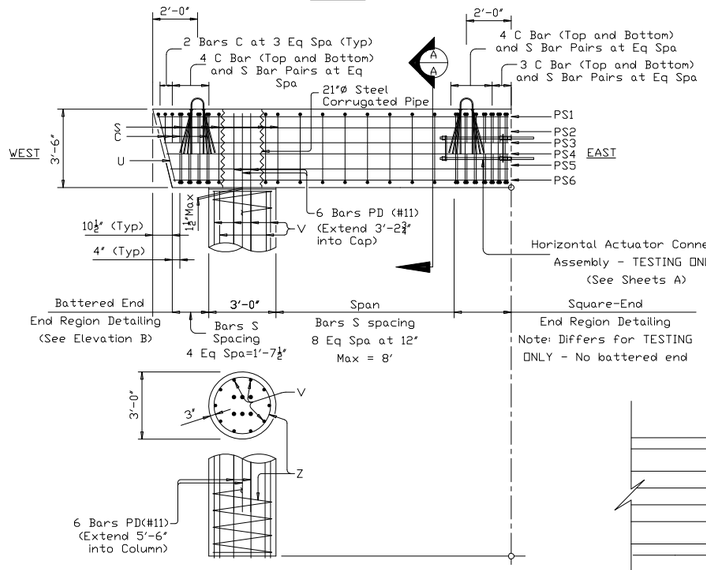

ELEVATION A

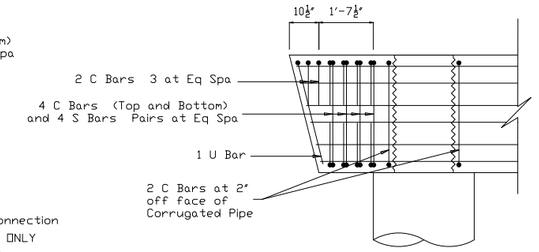

ELEVATION B

BATTERED-END END REGION DETAILING

TABLE OF ESTIMATED PRESTRESSING STRAND QUANTITIES				
Bar	No.	Size	Length	Weight
PS1	4	0.6	15'-8"	
PS2	2	0.6	15'-6"	
PS3	2	0.6	15-4½"	
PS4	2	0.6	15-3"	
PS5	2	0.6	15-1⅛"	
PS6	4	0.6	14-11½"	
PRESTRESSING STRGTH (ksi)				270
CONCRETE RELEASE STRGTH f'ci (ksi)				4.00
MIN. 28-DAY COMP STRGTH f'c (ksi)				5.00
MAX. 28-DAY COMP STRGTH f'c (ksi)				7.00

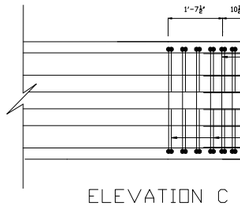

ELEVATION C

SQUARE-END END REGION DETAILING

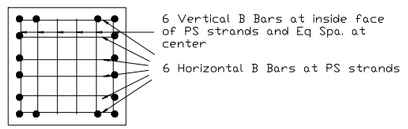

SECTION D-D

SQUARE-END END REGION DETAILING

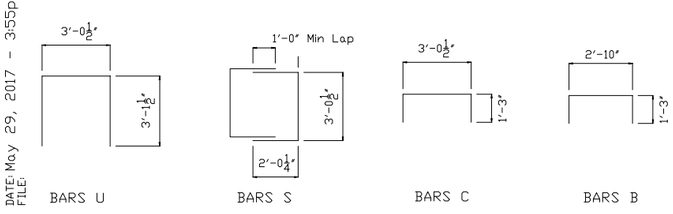

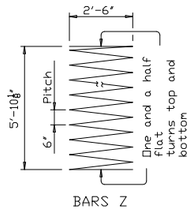

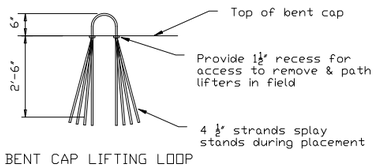

BENT CAP LIFTING LOOP

TxDOT 0-6863
Precast Pretensioned
Bent Caps
PSS-16-12

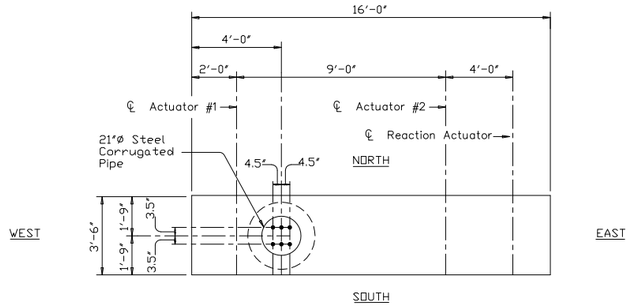

PLAN

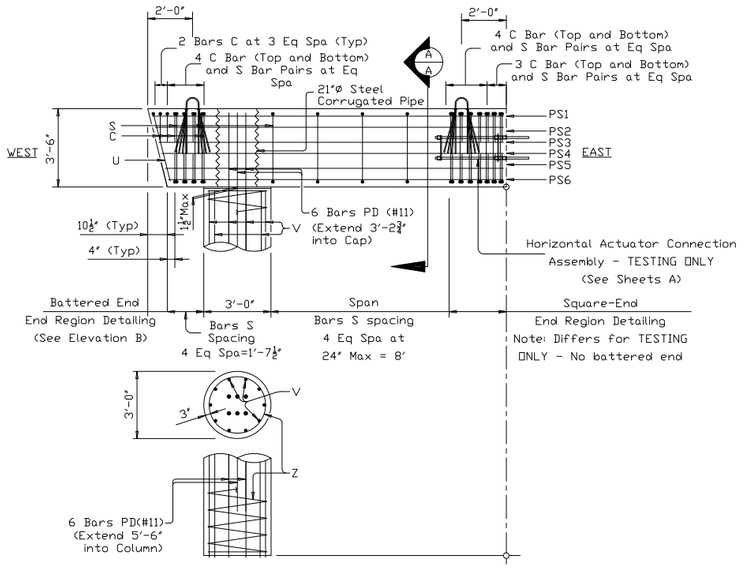

ELEVATION A

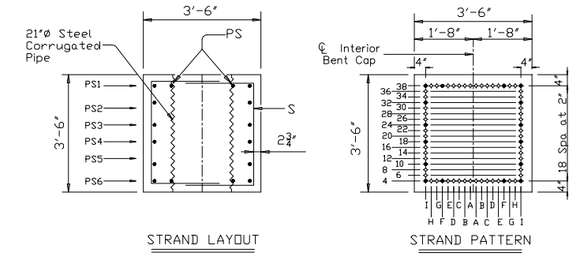

SECTION A-A

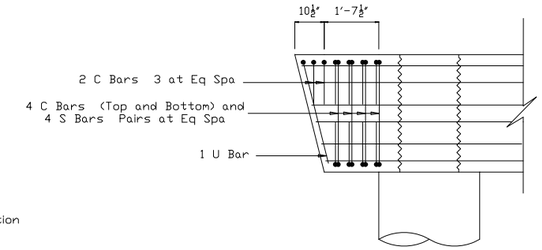

ELEVATION B

BATTERED-END END REGION DETAILING

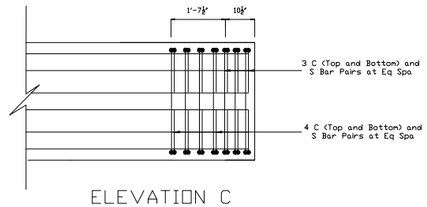

ELEVATION C

SQUARE-END END REGION DETAILING

TABLE OF ESTIMATED BAR QUANTITIES				
Bar	No.	Size	Length	Weight
PD	6	#11	8'-11¼"	
C	24	#5	5'-6⅛"	
S	14	#5	14'-2"	
U	1	#5	9'-3½"	
V	10	#9	6'-3¼"	
Z	1	#4	105'-1"	
Reinforcing Steel			Lb	
Class "H" Concrete (Cap)			CY	
Class "C" Concrete (Col)			CY	

TABLE OF ESTIMATED PRESTRESSING STRAND QUANTITIES				
Bar	No.	Size	Length	Weight
PS1	4	0.6	15'-8"	
PS2	2	0.6	15'-6"	
PS3	2	0.6	15-4½"	
PS4	2	0.6	15-3"	
PS5	2	0.6	15-1½"	
PS6	4	0.6	14-11½"	
PRESTRESSING STRGTH (ksi)				270
CONCRETE RELEASE STRGTH f'ci (ksi)				4.000
MIN. 28-DAY COMP STRGTH f'c (ksi)				5.000
MAX. 28-DAY COMP STRGTH f'c (ksi)				7.000

DATE: May 29, 2017 - 3:55pm
FILE:

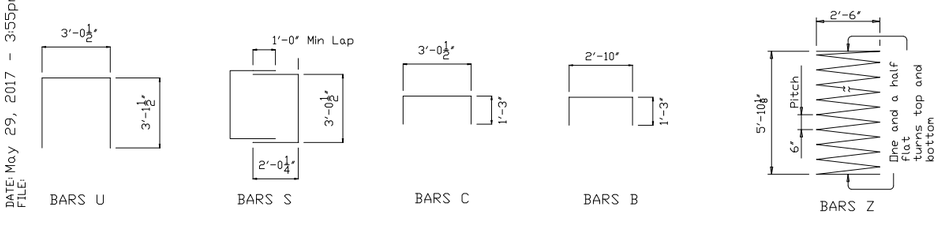

TxDOT 0-6863
Precast Pretensioned
Bent Caps
PSS-16-24

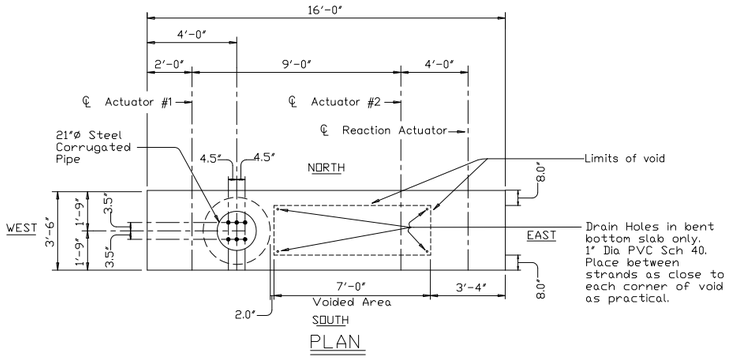

PLAN

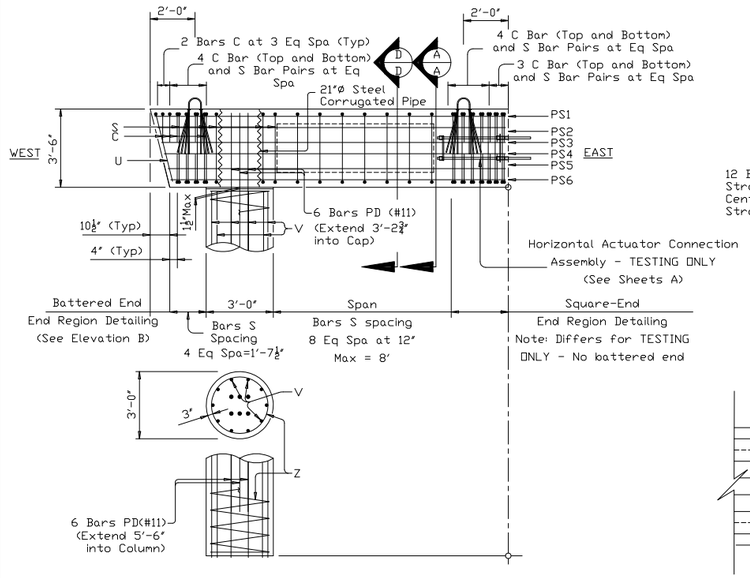

ELEVATION A

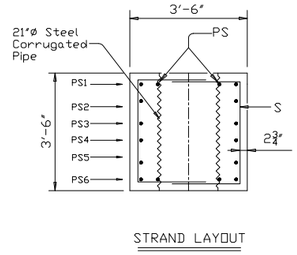

STRAND LAYOUT

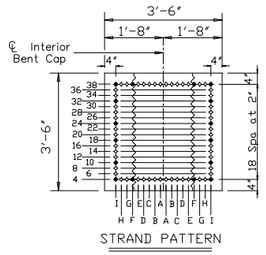

STRAND PATTERN

SECTION A-A

TABLE OF ESTIMATED BAR QUANTITIES				
Bar	No.	Size	Length	Weight
PD	6	#11	8'-11¼"	
C	24	#5	5'-6½"	
S	18	#5	14'-2"	
B	24	#5	5'-4"	
U	1	#5	9'-3½"	
V	10	#9	6'-3¼"	
Z	1	#4	105'-1"	
Reinforcing Steel				Lb
Class "H" Concrete (Cap)				CY
Class "C" Concrete (Col)				CY

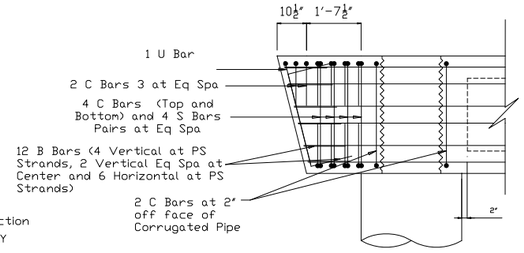

ELEVATION B

BATTERED-END END REGION DETAILING

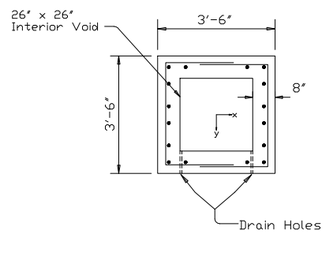

SECTION D-D

VOIDED SECTION DETAILING

TABLE OF ESTIMATED PRESTRESSING STRAND QUANTITIES				
Bar	No.	Size	Length	Weight
PS1	4	0.6	15'-8"	
PS2	2	0.6	15'-6"	
PS3	2	0.6	15-4½"	
PS4	2	0.6	15-3"	
PS5	2	0.6	15-1½"	
PS6	4	0.6	14-11½"	
PRESTRESSING STRGTH (ksi)				270
CONCRETE RELEASE STRGTH f'ci (ksi)				4.00
MIN. 28-DAY COMP STRGTH f'c (ksi)				5.00
MAX. 28-DAY COMP STRGTH f'c (ksi)				7.00

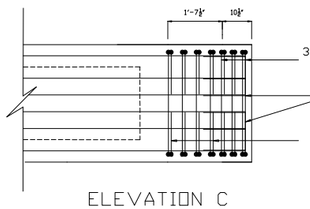

ELEVATION C

SQUARE-END END REGION DETAILING

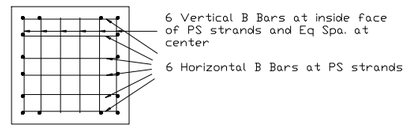

SECTION E-E

SQUARE & BATTERED ENDS END REGION DETAILING

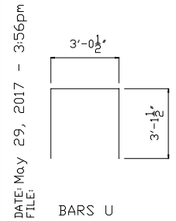

BARS U

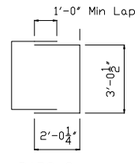

BARS S

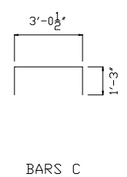

BARS C

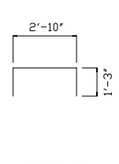

BARS B

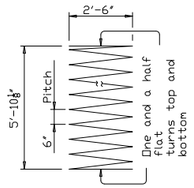

BARS Z

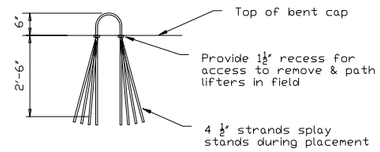

BENT CAP LIFTING LOOP

DATE: May 29, 2017 - 3:56pm
FILE:

TxDOT 0-6863
Precast Pretensioned
Bent Caps
PSV-16-12

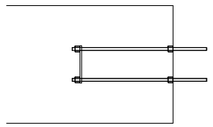

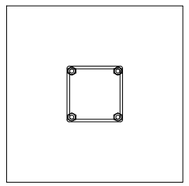

SIDE VIEW

FRONT VIEW

ELEVATION D1

WOOD FORMWORK HORIZONTAL ACTUATOR CONNECTION ASSEMBLY

DATE: May 29, 2017 - 3:56pm
FILE:

TxDOT 0-6863
Precast Pretensioned
Bent Caps
PS Model
Sheet A

APPENDIX B

RCS−16−12 FORMWORK MATERIALS

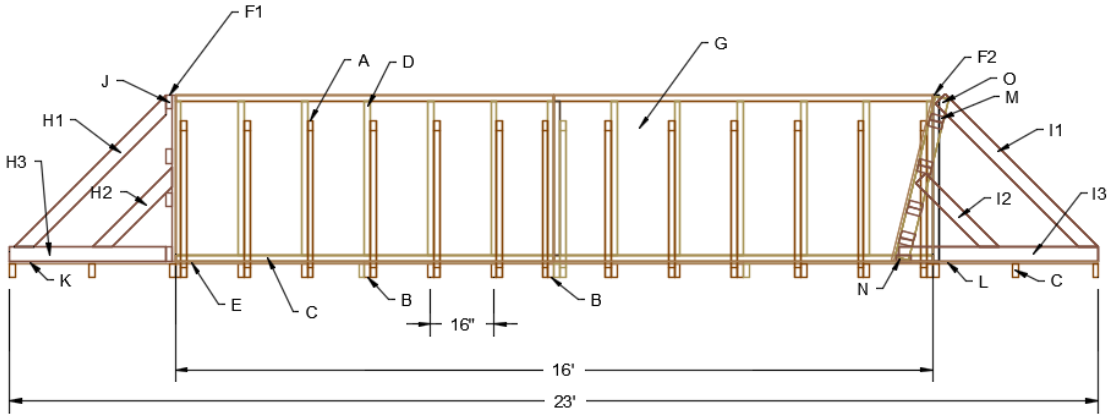

Side View

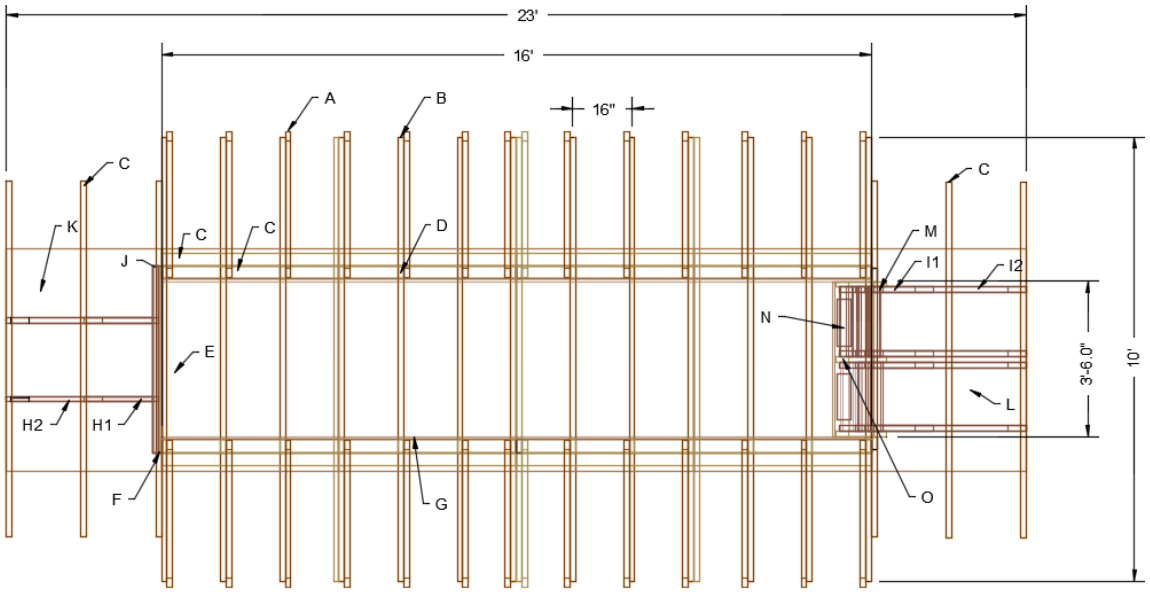

Plan View

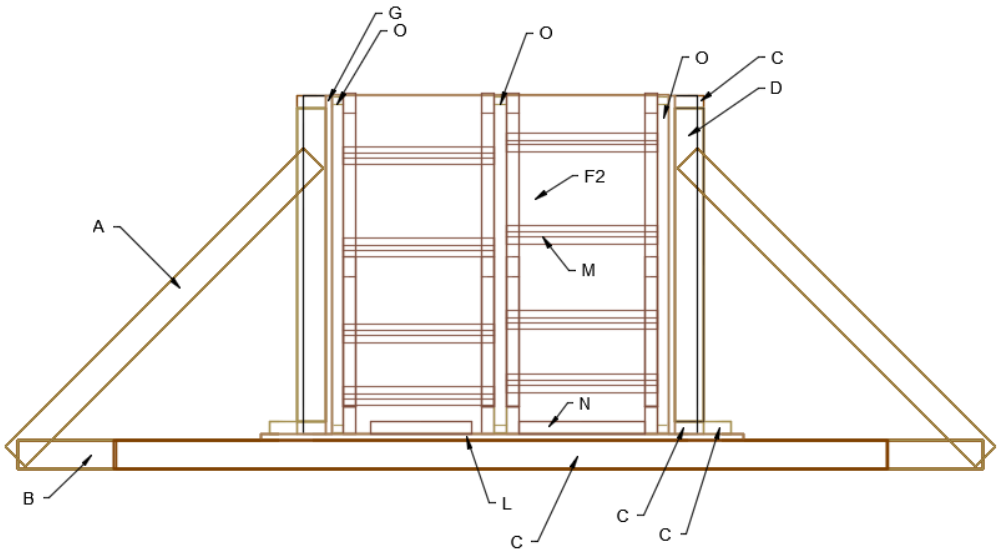

Battered End

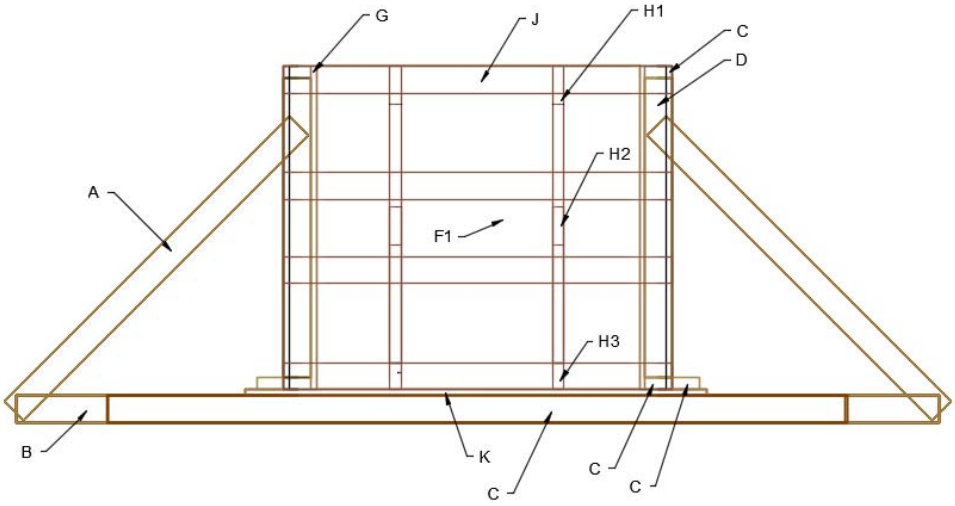

Square End

Table B.1 RCS-16-12 Formwork Lumber Materials

Type	Description	Part	Count	Size
2x4	Longitudinal Diag. Supports	A	28	4'-4.5"
2x4	10' Horiz. Floor Stands	B	16	10'-0"
2x4	8' Longitudinal Rails	C	12	8'-0"
2x4	8' Floor Stands	C	6	8'-0"
2x4	Vert. Frame	D	28	3'-3"
Plywood - 3/4"	Bent Cap Floor	E	4	4'x5'
Plywood - 3/4"	Square End Floor	F1	1	4'-2.5" x 3'-6"
Plywood - 3/4"	Battered End Floor	F2	1	3'-6" x 3'-7.125"
Plywood - 3/4"	Bent Cap Side Wall	G	4	3'-6"x8'
2x4	Top Square End Diag. Brace	H1	2	4'-6.5"
2x4	Bottom Square End Diag. Brace	H2	2	2'-4.5"
2x4	Square End Floor Brace	H3	2	3'-3.75"
2x4	Top Battered End Diag. Brace	I1	4	4'-7"
2x4	Bottom Battered End Diag. Brace	I2	4	2'-2.25"
2x4	Battered End Floor Brace	I3	4	4'-2.75"
2x4	Square End Horiz. Lateral Support	J	1	4'-2.5"
Plywood - 3/4"	Square End Support Floor	K	1	5' x 3'-6"
Plywood - 3/4"	Battered End Support Floor	L	1	5' x 3'-6"
2x4	Battered End Horiz. Wall Braces	M	8	1'-6.75"
2x4	Battered End Bottom Stubs	N	2	1'-3.75"
2x4	Battered End Vert. Angle Braces	O	3	3'-6"

APPENDIX C

THERMOCOUPLE TEMPERATURE DATA

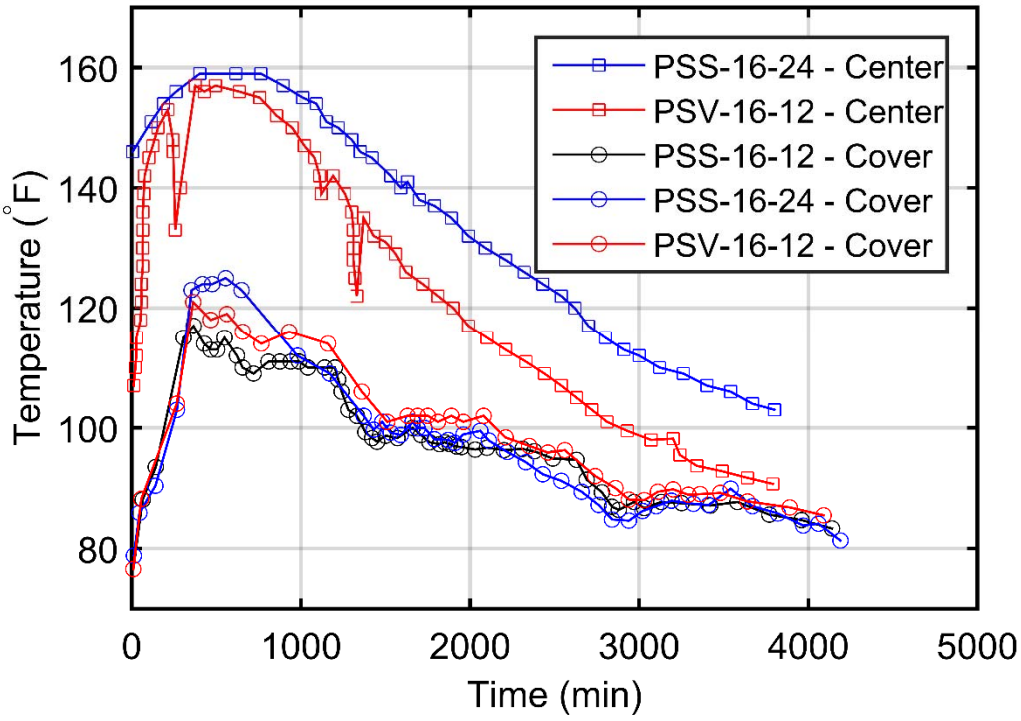
PSS-16-24 - Center
PSV-16-12 - Center
PSS-16-12 - Cover
PSS-16-24 - Cover
PSV-16-12 - Cover
Temperature (°F)
160
140
120
100
80
0
1000
2000
3000
4000
5000
Time (min)

Table C.1 Thermocouple Temperature Data

PSS-16-12 Cover		PSV-16-12 Cover		PSS-16-24 Cover		PSV-16-12 Center		PSS-16-24 Center	
Time (min)	Temp (°F)	Time (min)	Temp (°F)	Time (min)	Temp (°F)	Time (min)	Temp (°F)	Time (min)	Temp (°F)
9	77	9	77	12	79	11	107	5	146
12	80	15	82	15	83	14	107	18	145
16	88	17	86	13	86	17	108	45	146
37	85	24	88	21	86	18	108	84	149
49	87	41	87	29	86	19	109	107	151
64	88	56	88	45	86	21	110	115	151
64	89	76	89	57	88	24	110	127	151
72	89	88	89	69	88	26	111	147	152
84	89	119	91	89	87	26	111	159	153
100	90	208	100	120	89	26	112	166	154
142	94	266	104	140	90	27	112	187	154
227	101	280	109	160	91	28	113	206	154
246	104	293	115	183	94	28	114	214	155
284	110	316	119	225	97	28	114	221	155
290	113	327	120	244	100	28	115	238	156
306	115	363	121	267	103	27	115	262	156
313	115	380	120	297	108	27	116	287	156
321	116	400	120	311	111	25	117	306	157
333	116	420	119	334	115	22	117	325	158
353	117	444	120	340	118	27	118	362	158
365	117	465	118	354	123	53	118	402	159
373	116	480	120	361	125	46	119	422	159
378	116	509	119	373	125	58	120	486	159
394	115	533	119	385	125	60	120	550	159
415	114	549	120	402	125	58	121	583	159
427	114	561	119	418	124	57	121	614	159
435	114	590	119	426	124	57	122	644	159
438	115	602	118	438	125	56	123	675	159
447	114	614	118	446	124	56	123	704	159
451	113	623	117	454	124	55	124	733	159
467	113	655	116	474	124	56	124	762	159
475	114	680	115	482	125	57	125	789	158
483	115	705	114	511	124	60	125	815	158

Table C.1 Continued

PSS-16-12 Cover		PSV-16-12 Cover		PSS-16-24 Cover		PSV-16-12 Center		PSS-16-24 Center	
Time (min)	Temp (°F)	Time (min)	Temp (°F)	Time (min)	Temp (°F)	Time (min)	Temp (°F)	Time (min)	Temp (°F)
495	114	733	114	526	125	62	126	840	158
503	113	753	114	550	126	64	127	866	157
504	113	765	114	554	125	65	127	893	157
508	113	781	114	574	125	66	128	917	157
512	113	801	115	594	126	66	128	940	156
536	114	841	115	615	125	65	129	963	156
543	115	881	116	619	124	65	130	986	155
547	115	929	116	648	123	65	130	1010	155
560	114	962	115	673	121	64	131	1020	154
592	114	1000	115	747	118	65	131	1040	154
604	114	1040	115	833	116	66	132	1060	154
612	113	1110	114	902	114	66	132	1080	154
621	112	1160	114	979	112	66	133	1090	154
621	112	1210	114	1050	110	65	134	1100	153
629	111	1240	111	1070	110	65	134	1110	153
637	111	1260	110	1090	110	65	135	1120	152
646	111	1280	108	1120	109	65	135	1130	152
654	110	1360	106	1170	109	65	136	1150	151
662	110	1390	104	1210	108	66	137	1160	152
675	109	1430	103	1270	106	66	137	1190	152
687	109	1460	102	1300	105	66	138	1200	151
703	109	1490	103	1330	104	68	138	1210	151
719	109	1510	101	1370	102	71	139	1220	150
735	109	1530	102	1390	101	72	139	1230	150
743	109	1560	102	1400	101	72	140	1250	149
759	110	1600	102	1410	101	71	141	1270	149
775	110	1610	102	1420	100	71	141	1290	148
807	111	1630	102	1430	100	76	142	1300	148
835	111	1640	102	1440	100	84	142	1300	147
851	111	1660	104	1440	100	93	143	1310	147
863	111	1670	103	1450	99	99	143	1330	148
871	111	1680	102	1470	100	101	144	1340	147
875	111	1690	102	1480	101	101	145	1350	146

Table C.1 Continued

PSS-16-12 Cover		PSV-16-12 Cover		PSS-16-24 Cover		PSV-16-12 Center		PSS-16-24 Center	
Time (min)	Temp (°F)	Time (min)	Temp (°F)	Time (min)	Temp (°F)	Time (min)	Temp (°F)	Time (min)	Temp (°F)
891	111	1700	102	1490	101	103	145	1360	146
903	111	1710	102	1490	100	105	146	1370	146
919	111	1730	103	1500	99	108	146	1390	145
931	111	1740	102	1510	99	113	147	1410	146
939	111	1750	102	1530	99	124	147	1420	145
947	111	1750	102	1550	99	138	148	1440	145
952	111	1770	102	1560	99	148	148	1460	144
964	111	1780	101	1570	99	152	149	1480	143
976	111	1790	101	1580	99	152	150	1510	144
988	111	1810	101	1590	99	155	150	1530	142
996	111	1840	102	1600	100	163	151	1550	141
1000	111	1860	101	1620	99	177	151	1560	142
1020	111	1870	101	1630	99	194	152	1570	142
1040	111	1880	100	1650	100	210	152	1580	141
1040	110	1890	102	1660	101	213	153	1590	140
1060	110	1910	100	1670	100	232	151	1600	141
1080	110	1920	101	1680	99	230	150	1610	141
1100	110	1930	102	1680	99	235	150	1620	140
1120	110	1950	101	1690	99	240	149	1620	140
1140	110	1960	101	1690	100	243	148	1630	141
1150	110	1980	101	1700	100	243	148	1650	140
1160	110	2000	102	1710	100	244	147	1660	139
1170	110	2030	100	1720	100	244	147	1680	139
1190	110	2050	101	1730	100	244	146	1690	138
1200	110	2080	102	1730	100	245	146	1700	138
1210	109	2100	101	1740	100	245	145	1720	139
1210	109	2150	100	1750	99	245	144	1750	138
1210	109	2180	100	1760	100	244	144	1760	138
1210	108	2210	99	1770	99	245	143	1780	138
1220	108	2210	98	1790	98	257	133	1790	137
1220	108	2240	98	1820	98	272	153	1810	137
1230	108	2270	98	1820	98	282	149	1820	136
1230	107	2320	97	1830	99	286	141	1850	136

Table C.1 Continued

PSS-16-12 Cover		PSV-16-12 Cover		PSS-16-24 Cover		PSV-16-12 Center		PSS-16-24 Center	
Time (min)	Temp (°F)	Time (min)	Temp (°F)	Time (min)	Temp (°F)	Time (min)	Temp (°F)	Time (min)	Temp (°F)
1230	107	2340	97	1850	98	287	140	1870	135
1240	106	2350	97	1870	98	287	140	1890	135
1250	105	2370	97	1880	98	288	139	1910	134
1250	104	2400	96	1890	99	300	153	1930	134
1260	104	2420	96	1900	99	318	157	1950	133
1270	104	2440	96	1900	98	343	157	1970	133
1280	103	2460	96	1910	98	375	157	1990	132
1290	103	2470	95	1920	98	406	157	2010	132
1290	102	2490	96	1920	99	424	158	2030	131
1300	102	2510	96	1930	100	424	157	2050	131
1310	102	2530	96	1940	98	425	156	2070	131
1330	102	2560	96	1960	99	429	156	2090	130
1340	101	2580	96	1980	99	435	155	2120	130
1350	101	2650	96	2000	99	436	155	2140	129
1360	100	2690	94	2020	99	449	157	2160	129
1370	100	2710	93	2040	99	478	158	2190	129
1380	99	2740	92	2060	100	494	157	2210	128
1380	99	2770	92	2070	99	526	157	2230	128
1390	99	2790	91	2090	99	557	157	2250	127
1400	99	2820	90	2090	98	584	157	2270	127
1410	99	2840	89	2100	98	609	157	2300	127
1420	98	2860	90	2110	98	635	156	2320	126
1420	98	2870	89	2130	98	662	156	2340	126
1430	99	2900	89	2160	97	687	156	2360	125
1450	98	2920	89	2180	97	711	155	2380	125
1450	98	2940	89	2190	97	735	155	2410	124
1450	98	2940	88	2220	96	756	155	2430	124
1450	98	2970	90	2240	96	777	154	2450	124
1450	97	2990	89	2260	96	798	154	2470	123
1480	99	3000	88	2280	95	818	153	2490	123
1490	99	3010	90	2310	95	836	153	2520	122
1500	99	3030	88	2330	94	856	152	2540	122
1500	98	3040	88	2350	94	876	152	2550	121

Table C.1 Continued

PSS-16-12 Cover		PSV-16-12 Cover		PSS-16-24 Cover		PSV-16-12 Center		PSS-16-24 Center	
Time (min)	Temp (°F)	Time (min)	Temp (°F)	Time (min)	Temp (°F)	Time (min)	Temp (°F)	Time (min)	Temp (°F)
1510	98	3060	89	2360	94	895	151	2560	121
1510	97	3080	89	2380	93	914	151	2570	120
1530	98	3090	89	2400	93	932	151	2590	120
1570	98	3110	89	2430	92	948	150	2620	120
1600	99	3130	90	2450	92	964	149	2640	119
1610	99	3160	90	2460	91	980	149	2660	119
1630	99	3170	90	2490	91	997	149	2670	118
1630	100	3180	89	2510	92	1010	148	2680	118
1660	100	3200	90	2540	91	1020	147	2700	117
1670	100	3220	90	2560	91	1040	147	2710	117
1670	99	3240	90	2590	91	1050	146	2730	116
1680	99	3270	90	2610	90	1070	146	2760	116
1690	99	3290	89	2640	90	1080	145	2780	116
1710	99	3290	89	2660	89	1080	145	2800	115
1720	100	3300	89	2680	89	1090	144	2830	115
1740	99	3310	88	2700	88	1100	144	2850	114
1750	99	3330	88	2710	88	1110	143	2880	114
1740	98	3340	89	2730	88	1110	143	2900	114
1760	98	3360	89	2760	87	1110	142	2910	113
1770	99	3380	89	2780	87	1110	141	2920	112
1790	97	3390	89	2800	86	1110	141	2920	113
1800	97	3420	88	2820	86	1110	140	2950	113
1810	97	3480	89	2830	85	1120	140	2970	112
1820	97	3480	89	2840	85	1120	139	3000	112
1830	98	3520	90	2860	86	1120	139	3020	111
1830	99	3540	90	2870	85	1130	138	3050	111
1840	99	3580	89	2900	85	1150	138	3070	111
1840	98	3610	89	2910	85	1170	142	3090	110
1850	98	3640	88	2940	85	1190	142	3120	110
1850	97	3700	87	2960	85	1200	141	3150	110
1860	97	3750	87	2970	86	1210	141	3180	110
1870	98	3800	87	2990	86	1230	140	3210	110
1880	98	3870	87	3000	85	1250	139	3230	109

Table C.1 Continued

PSS-16-12 Cover		PSV-16-12 Cover		PSS-16-24 Cover		PSV-16-12 Center		PSS-16-24 Center	
Time (min)	Temp (°F)	Time (min)	Temp (°F)	Time (min)	Temp (°F)	Time (min)	Temp (°F)	Time (min)	Temp (°F)
1880	97	3890	87	3020	86	1260	139	3260	109
1890	97	3930	86	3040	84	1280	138	3290	109
1900	98	3970	86	3050	86	1290	138	3320	108
1910	97	4030	86	3070	87	1300	137	3350	108
1910	96	4060	86	3090	86	1300	137	3370	108
1920	97	4090	86	3100	87	1300	136	3400	107
1920	97	4140	85	3130	87	1300	136	3430	107
1940	98	4150	83	3150	87	1300	135	3450	107
1940	97	4180	83	3160	88	1300	134	3480	106
1950	97	4200	83	3170	87	1310	134	3510	106
1950	97			3190	88	1310	133	3540	106
1960	97			3220	88	1310	133	3560	106
1970	97			3260	88	1310	132	3590	105
1990	97			3270	89	1310	132	3620	105
2000	98			3290	88	1310	131	3640	105
2030	96			3320	87	1310	130	3670	104
2030	97			3330	88	1310	130	3700	104
2060	98			3360	87	1310	129	3720	104
2080	98			3380	88	1310	129	3750	103
2090	97			3390	88	1310	128	3780	103
2100	97			3410	87	1310	128	3800	103
2120	97			3430	88	1310	127	3820	102
2130	96			3450	87	1310	126	3850	102
2150	96			3480	89	1310	126	3880	102
2170	96			3510	89	1310	125		
2200	96			3540	90	1320	125		
2210	96			3560	89	1320	124		
2240	96			3560	89	1320	123		
2270	96			3580	89	1320	121		
2300	96			3620	88	1320	122		
2310	97			3670	87	1330	122		
2340	97			3700	87	1340	121		
2350	97			3730	87	1340	125		

Table C.1 Continued

PSS-16-12 Cover		PSV-16-12 Cover		PSS-16-24 Cover		PSV-16-12 Center		PSS-16-24 Center	
Time (min)	Temp (°F)	Time (min)	Temp (°F)	Time (min)	Temp (°F)	Time (min)	Temp (°F)	Time (min)	Temp (°F)
2370	97			3760	86	1340	127		
2380	96			3790	85	1360	135		
2380	96			3820	86	1370	135		
2400	96			3860	85	1380	134		
2420	96			3910	85	1400	134		
2450	96			3930	84	1410	133		
2470	96			3960	84	1420	133		
2490	95			3970	84	1430	132		
2500	96			3980	83	1430	133		
2530	96			4000	84	1450	132		
2560	95			4030	84	1460	132		
2600	95			4050	84	1480	132		
2630	95			4060	84	1500	131		
2650	94			4070	83	1510	131		
2660	94			4110	83	1520	130		
2670	93			4130	83	1530	130		
2690	92			4160	82	1550	129		
2690	91			4190	81	1560	129		
2700	91			4200	81	1580	128		
2710	90					1590	128		
2730	90					1600	127		
2750	90					1610	127		
2780	89					1620	126		
2790	89					1640	127		
2800	88					1690	125		
2820	88					1690	124		
2820	87					1700	123		
2840	87					1720	124		
2840	87					1750	124		
2850	87					1770	123		
2860	88					1790	123		
2870	87					1810	123		
2880	86					1810	122		

Table C.1 Continued

PSS-16-12 Cover		PSV-16-12 Cover		PSS-16-24 Cover		PSV-16-12 Center		PSS-16-24 Center	
Time (min)	Temp (°F)	Time (min)	Temp (°F)	Time (min)	Temp (°F)	Time (min)	Temp (°F)	Time (min)	Temp (°F)
2890	87					1830	122		
2900	86					1840	121		
2920	87					1860	121		
2940	86					1880	120		
2970	88					1900	120		
2990	87					1920	119		
3010	87					1940	119		
3020	87					1950	118		
3020	87					1970	118		
3030	87					1990	117		
3060	87					2010	117		
3070	87					2030	116		
3100	88					2050	116		
3110	87					2070	116		
3130	88					2100	115		
3150	87					2120	115		
3160	87					2150	114		
3190	88					2170	114		
3230	88					2190	114		
3250	88					2210	113		
3270	88					2240	113		
3310	87					2260	112		
3350	87					2280	112		
3380	87					2310	112		
3420	87					2330	111		
3440	88					2350	111		
3490	88					2380	110		
3520	89					2400	110		
3530	89					2430	110		
3580	88					2440	109		
3610	87					2460	109		
3640	86					2470	108		
3680	86					2490	108		

Table C.1 Continued

PSS-16-12 Cover		PSV-16-12 Cover		PSS-16-24 Cover		PSV-16-12 Center		PSS-16-24 Center	
Time (min)	Temp (°F)	Time (min)	Temp (°F)	Time (min)	Temp (°F)	Time (min)	Temp (°F)	Time (min)	Temp (°F)
3710	86					2520	107		
3770	86					2540	107		
3820	86					2550	106		
3860	86					2570	106		
3900	86					2580	105		
3910	86					2600	105		
3960	85					2630	105		
3990	85					2650	104		
4050	85					2670	104		
4070	85					2690	104		
4110	84					2710	103		
4140	83					2720	103		
4150	81					2740	102		
4190	81					2740	102		
4200	81					2770	102		
						2780	102		
						2810	101		
						2830	101		
						2860	101		
						2880	100		
						2900	100		
						2930	100		
						2950	99		
						2980	99		
						3010	99		
						3040	98		
						3070	98		
						3090	98		
						3110	97		
						3130	98		
						3150	98		
						3200	98		
						3220	98		

Table C.1 Continued

PSS-16-12 Cover		PSV-16-12 Cover		PSS-16-24 Cover		PSV-16-12 Center		PSS-16-24 Center	
Time (min)	Temp (°F)	Time (min)	Temp (°F)	Time (min)	Temp (°F)	Time (min)	Temp (°F)	Time (min)	Temp (°F)
						3230	97		
						3230	97		
						3240	96		
						3240	96		
						3250	95		
						3260	94		
						3280	94		
						3310	94		
						3340	94		
						3370	94		
						3400	93		
						3430	93		
						3460	93		
						3490	93		
						3520	93		
						3550	92		
						3580	92		
						3610	92		
						3640	92		
						3670	92		
						3700	91		
						3730	91		
						3760	91		
						3790	91		
						3820	90		
						3840	90		
						3870	90		

APPENDIX D

INSTRUMENTATION PLANS

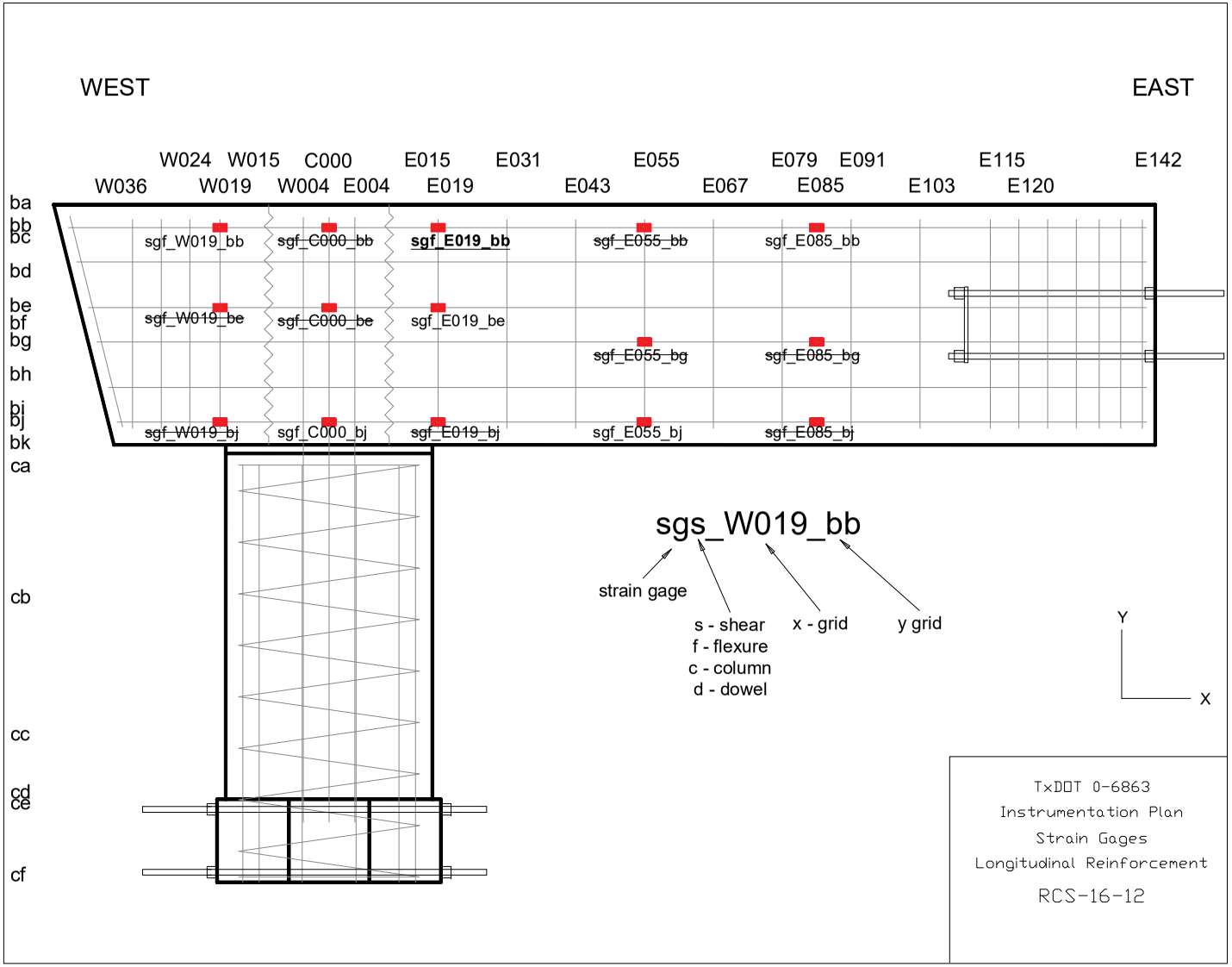
WEST
EAST
W024 W015 C000 E015 E031 E055 E079 E091 E115 E142
W036 W019 W004 E004 E019 E043 E067 E085 E103 E120
ba
bb
bc
bd
be
bf
bg
bh
bj
bj
bk
ca
cb
cc
cd
ce
cf
sgf_W019_bb
sgf_C000_bb
sgf_E019_bb
sgf_E055_bb
sgf_E085_bb
sgf_W019_be
sgf_C000_be
sgf_E019_be
sgf_E055_bg
sgf_E085_bg
sgf_W019_bj
sgf_C000_bj
sgf_E019_bj
sgf_E055_bj
sgf_E085_bj
sgs_W019_bb
strain gage
s - shear
f - flexure
c - column
d - dowel
x - grid
y grid
Y
X
TxDOT 0-6863
Instrumentation Plan
Strain Gages
Longitudinal Reinforcement
RCS-16-12

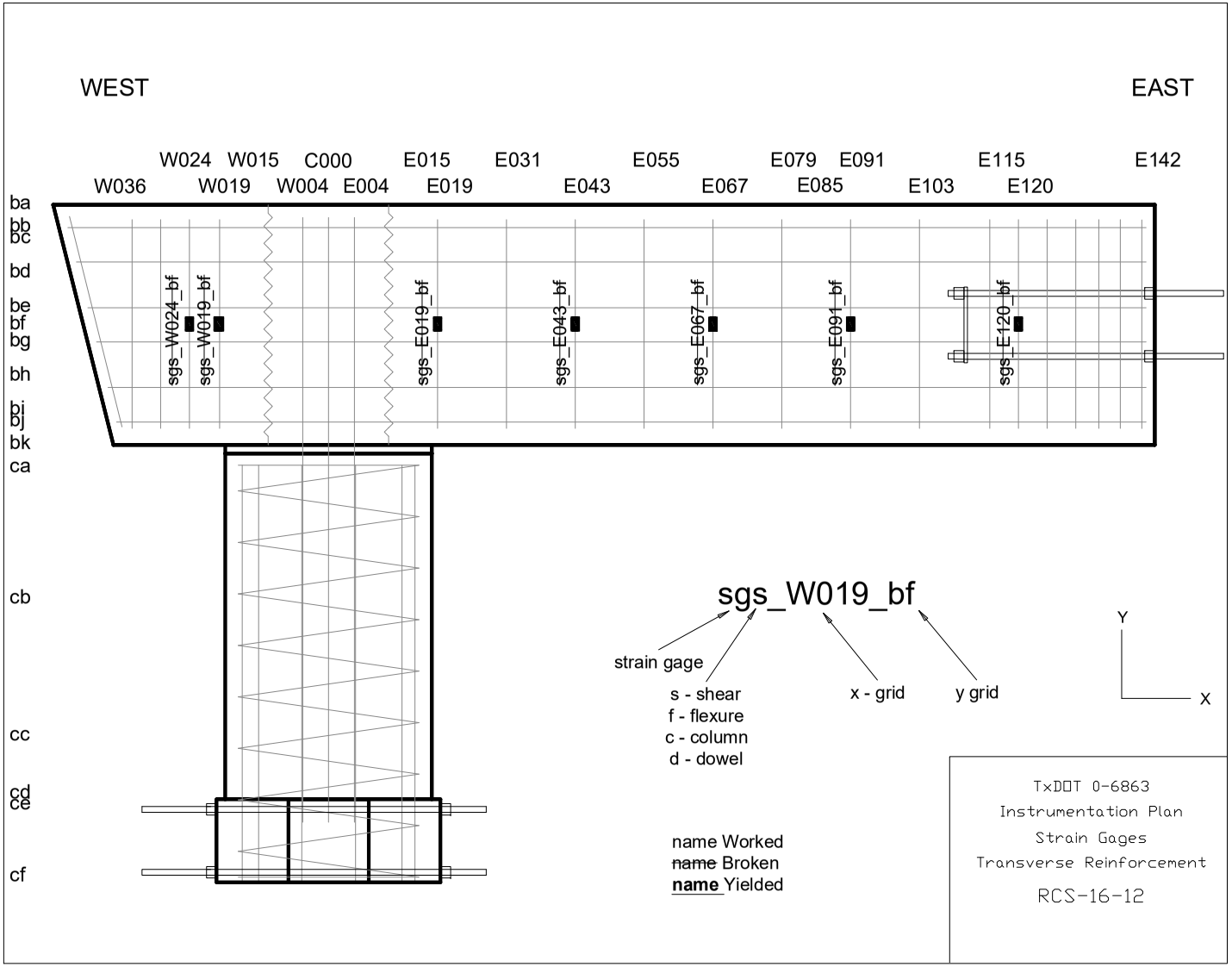
WEST
EAST
W036
W024
W019
W015
W004
C000
E004
E015
E019
E031
E043
E055
E067
E079
E085
E091
E103
E115
E120
E142
ba
bb
bc
bd
be
bf
bg
bh
bj
bj
bk
ca
cb
cc
cd
ce
cf
sgs_W024_bf
sgs_W019_bf
sgs_E019_bf
sgs_E043_bf
sgs_E067_bf
sgs_E091_bf
sgs_E120_bf
sgs_W019_bf
strain gage
s - shear
f - flexure
c - column
d - dowel
x - grid
y grid
Y
X
name Worked
~~name~~ Broken
name Yielded
TxDOT 0-6863
Instrumentation Plan
Strain Gages
Transverse Reinforcement
RCS-16-12

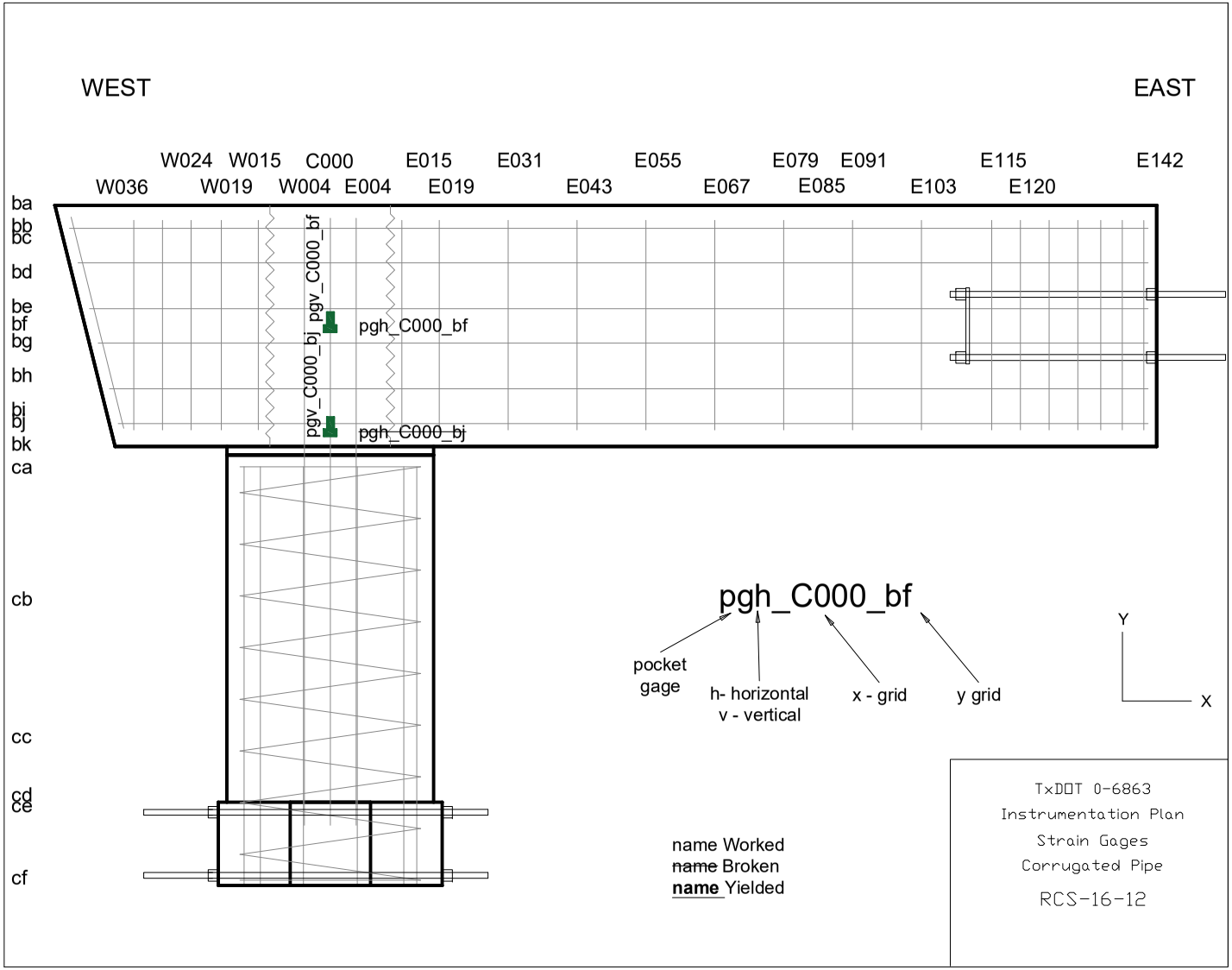
WEST
EAST
W036
W024
W019
W015
W004
C000
E004
E015
E019
E031
E043
E055
E067
E079
E085
E091
E103
E115
E120
E142
ba
bb
bc
bd
be
bf
bg
bh
bi
bj
bk
ca
cb
cc
cd
ce
cf
pgv_C000_bj
pgv_C000_bf
pgh_C000_bf
pgh_C000_bj
pgh_C000_bf
pocket gage
h- horizontal
v - vertical
x - grid
y grid
Y
X
name Worked
~~name~~ Broken
name Yielded
TxDOT 0-6863
Instrumentation Plan
Strain Gages
Corrugated Pipe
RCS-16-12

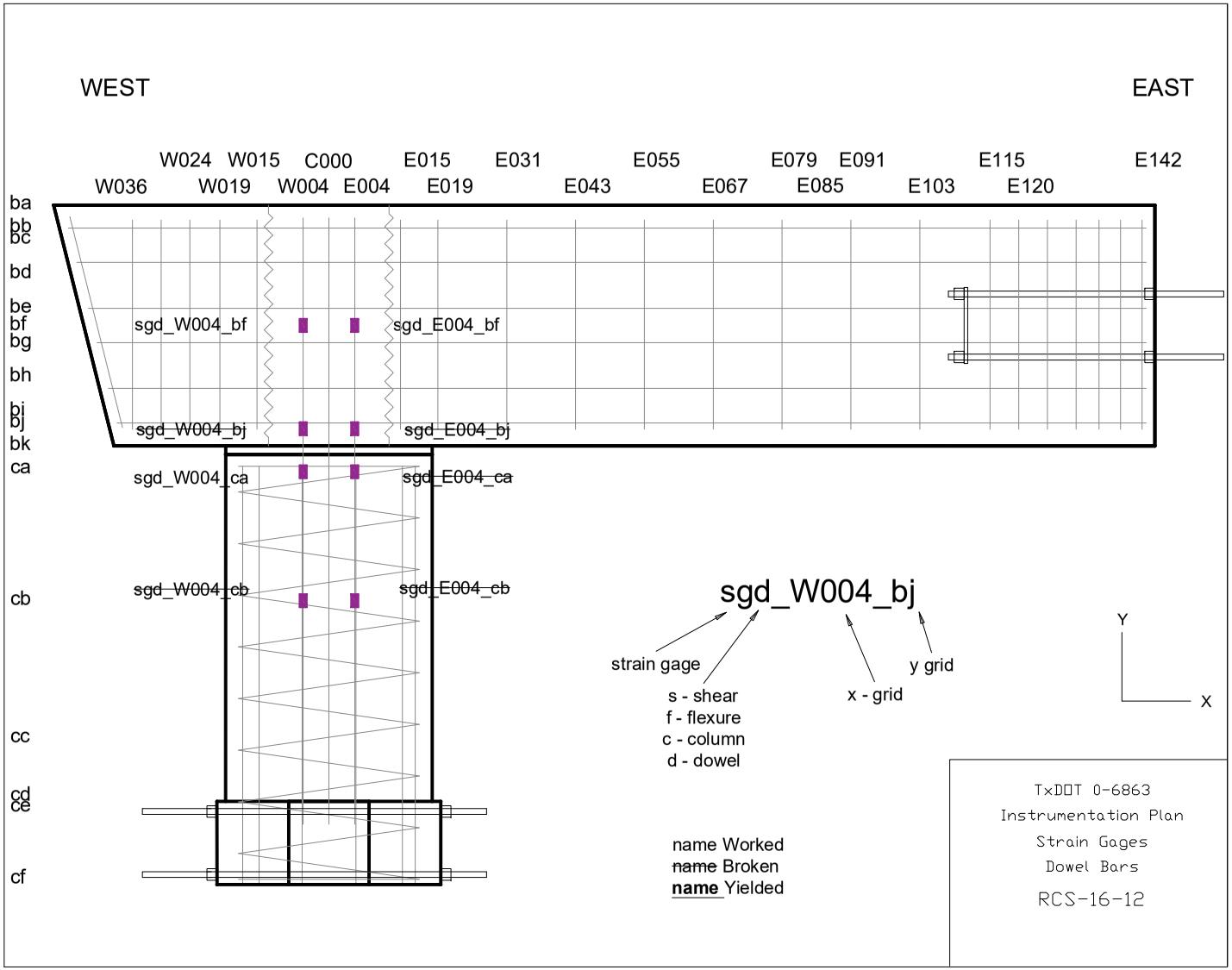
WEST
EAST
W024 W015 C000 E015 E031 E055 E079 E091 E115 E142
W036 W019 W004 E004 E019 E043 E067 E085 E103 E120
ba
bb
bc
bd
be
bf
bg
bh
bj
bj
bk
ca
cb
cc
cd
ce
cf
sgd_W004_bf
sgd_E004_bf
sgd_W004_bj
sgd_E004_bj
sgd_W004_ca
sgd_E004_ca
sgd_W004_cb
sgd_E004_cb
sgd_W004_bj
strain gage
s - shear
f - flexure
c - column
d - dowel
x - grid
y grid
Y
X
name Worked
name Broken
name Yielded
TxDOT 0-6863
Instrumentation Plan
Strain Gages
Dowel Bars
RCS-16-12

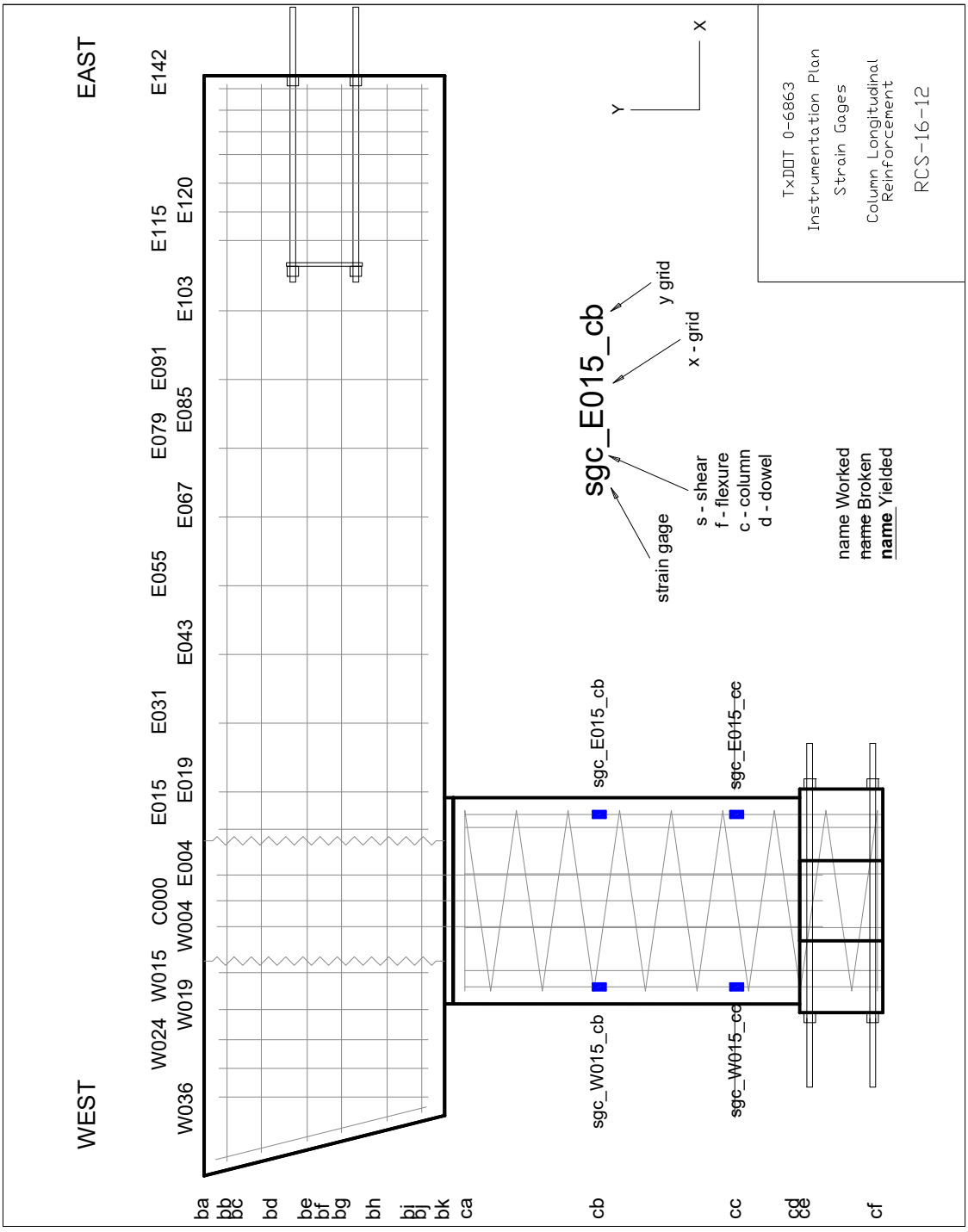
EAST
WEST
W036 W024 W019 W015 C000 W004 E004 E015 E019 E031 E043 E055 E067 E079 E085 E091 E103 E115 E120 E142
ba bb bc bd be bf bg bh bj bk ca cb cc cd ce cf
sgc_W015_cb
sgc_E015_cb
sgc_W015_cc
sgc_E015_cc
sgc_E015_cb
strain gage
y grid
x - grid
s - shear
f - flexure
c - column
d - dowel
name Worked
name Broken
name Yielded
Y
X
TxDOT 0-6863
Instrumentation Plan
Strain Gages
Column Longitudinal Reinforcement
RCS-16-12

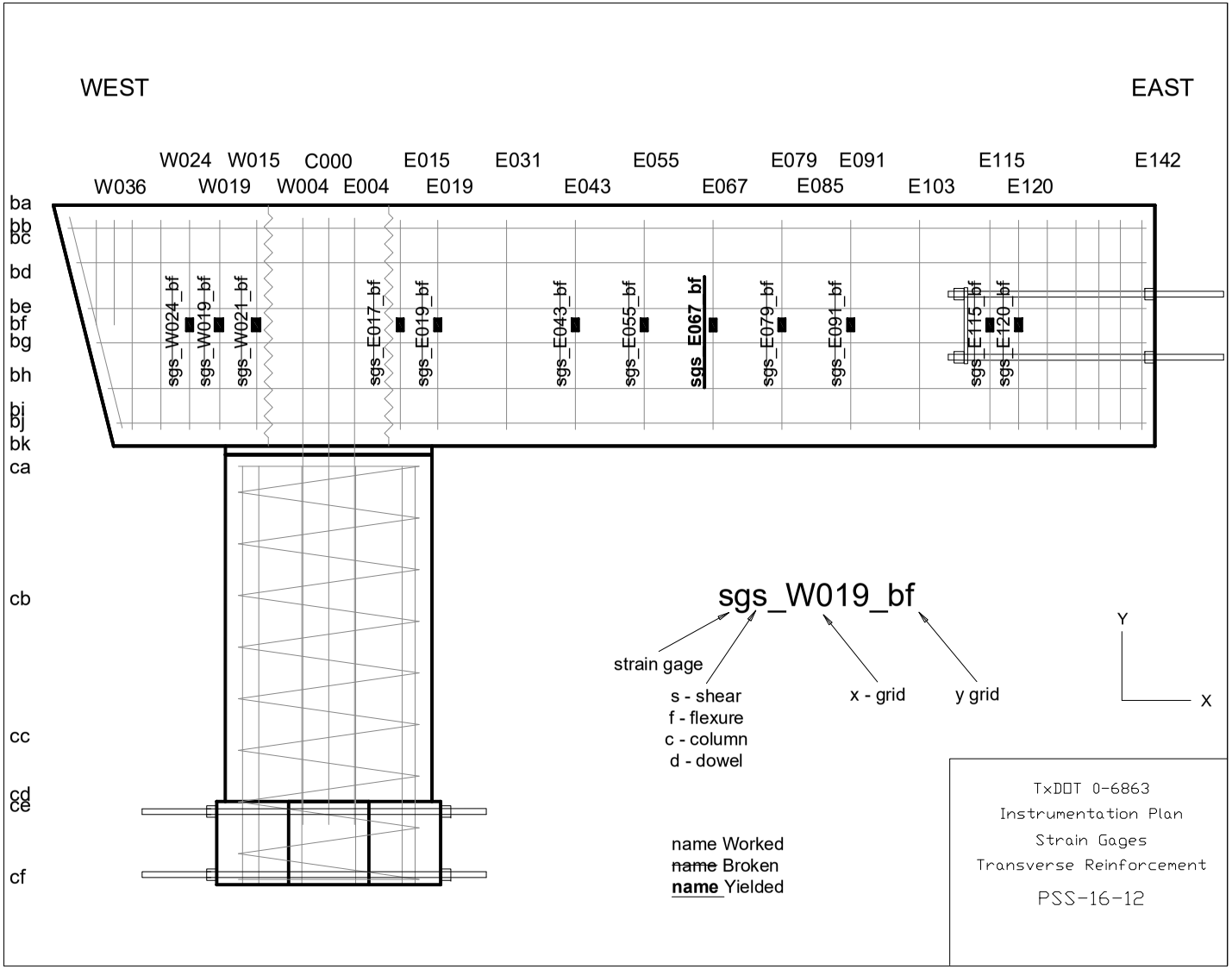
WEST
EAST
W036
W024
W019
W015
W004
C000
E004
E015
E019
E031
E043
E055
E067
E079
E085
E091
E103
E115
E120
E142
ba
bb
bc
bd
be
bf
bg
bh
bi
bj
bk
ca
cb
cc
cd
ce
cf
sgs_W024_bf
sgs_W019_bf
sgs_W021_bf
sgs_E017_bf
sgs_E019_bf
sgs_E043_bf
sgs_E055_bf
sgs_E067_bf
sgs_E079_bf
sgs_E091_bf
sgs_E115_bf
sgs_E120_bf
sgs_W019_bf
strain gage
s - shear
f - flexure
c - column
d - dowel
x - grid
y grid
Y
X
name Worked
~~name~~ Broken
name Yielded
TxDOT 0-6863
Instrumentation Plan
Strain Gages
Transverse Reinforcement
PSS-16-12

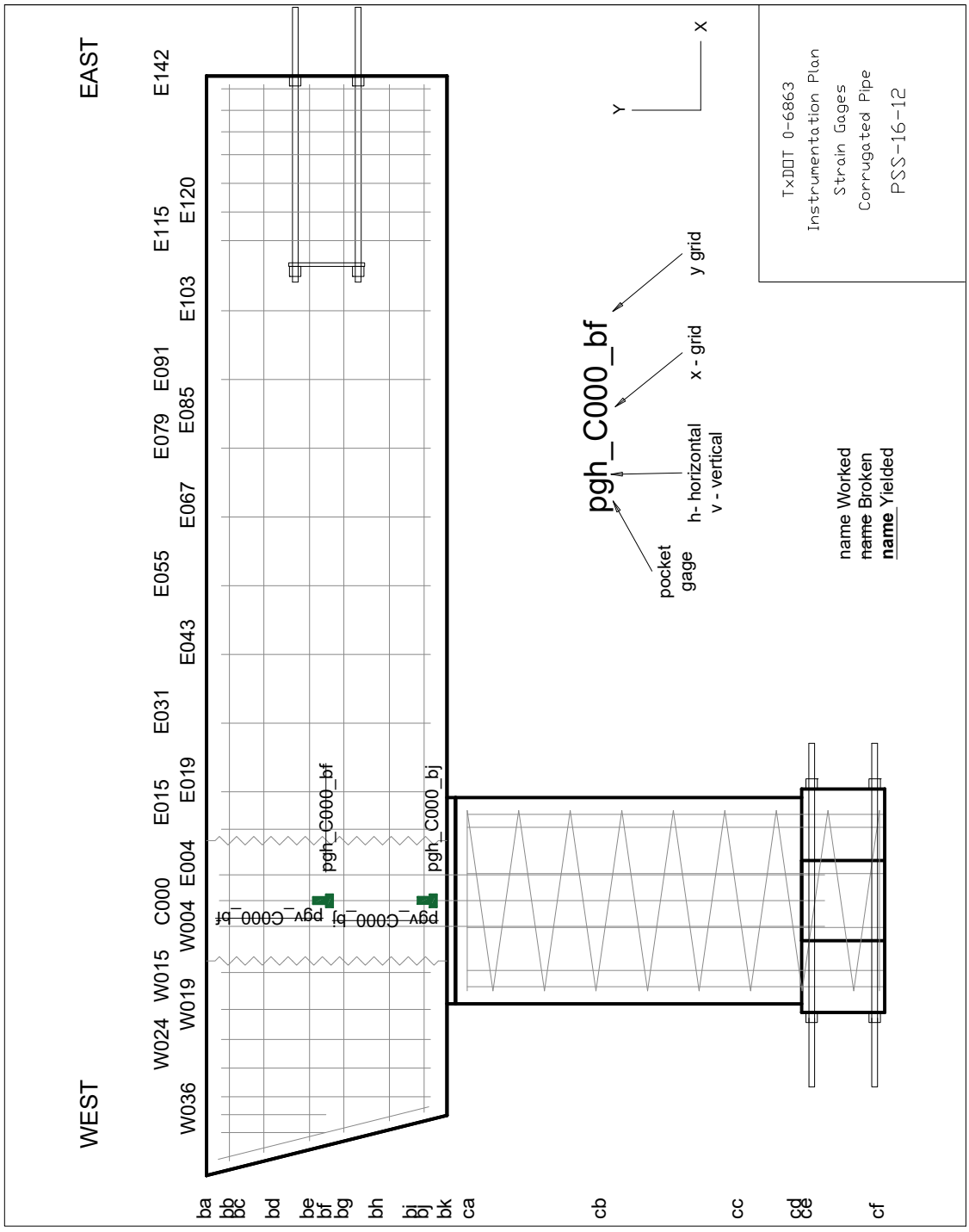
EAST
WEST
E142
E120
E115
E103
E091
E085
E079
E067
E055
E043
E031
E019
E015
E004
C000
W004
W015
W019
W024
W036
pgv_C000_bf
pgv_C000_bj
pgh_C000_bf
pgh_C000_bj
ba
bb
bc
bd
be
bf
bg
bh
bj
bk
ca
cb
cc
cd
ce
cf
Y
X
pgh_C000_bf
y grid
x - grid
h- horizontal
v - vertical
pocket
gage
name Worked
name Broken
name Yielded
TxDOT 0-6863
Instrumentation Plan
Strain Gages
Corrugated Pipe
PSS-16-12

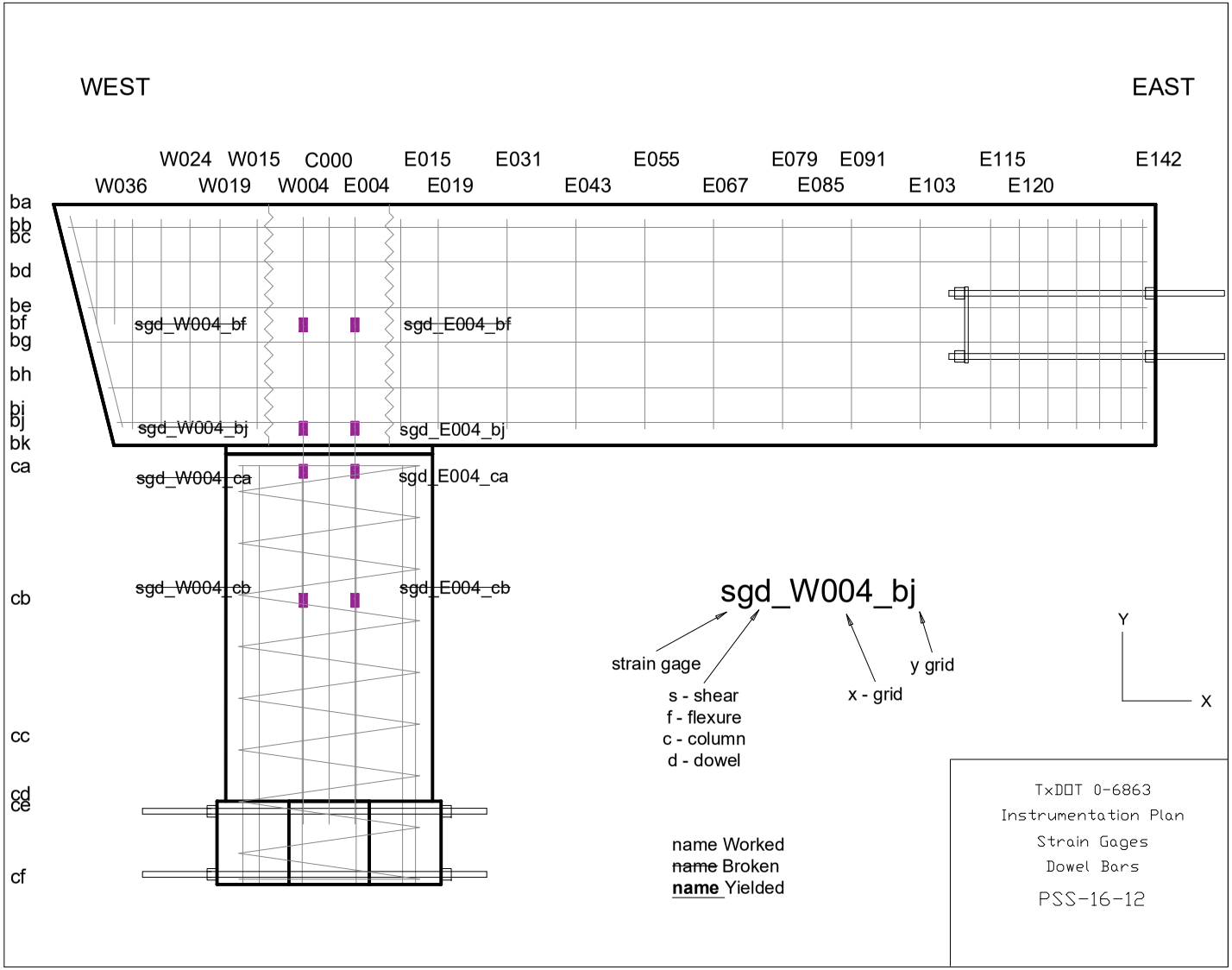
WEST
EAST
W036
W024
W019
W015
W004
C000
E004
E015
E019
E031
E043
E055
E067
E079
E085
E091
E103
E115
E120
E142
ba
bb
bc
bd
be
bf
bg
bh
bi
bj
bk
ca
cb
cc
cd
ce
cf
sgd_W004_bf
sgd_E004_bf
sgd_W004_bj
sgd_E004_bj
sgd_W004_ca
sgd_E004_ca
sgd_W004_cb
sgd_E004_cb
sgd_W004_bj
strain gage
s - shear
f - flexure
c - column
d - dowel
x - grid
y grid
Y
X
name Worked
name Broken
name Yielded
TxDOT 0-6863
Instrumentation Plan
Strain Gages
Dowel Bars
PSS-16-12

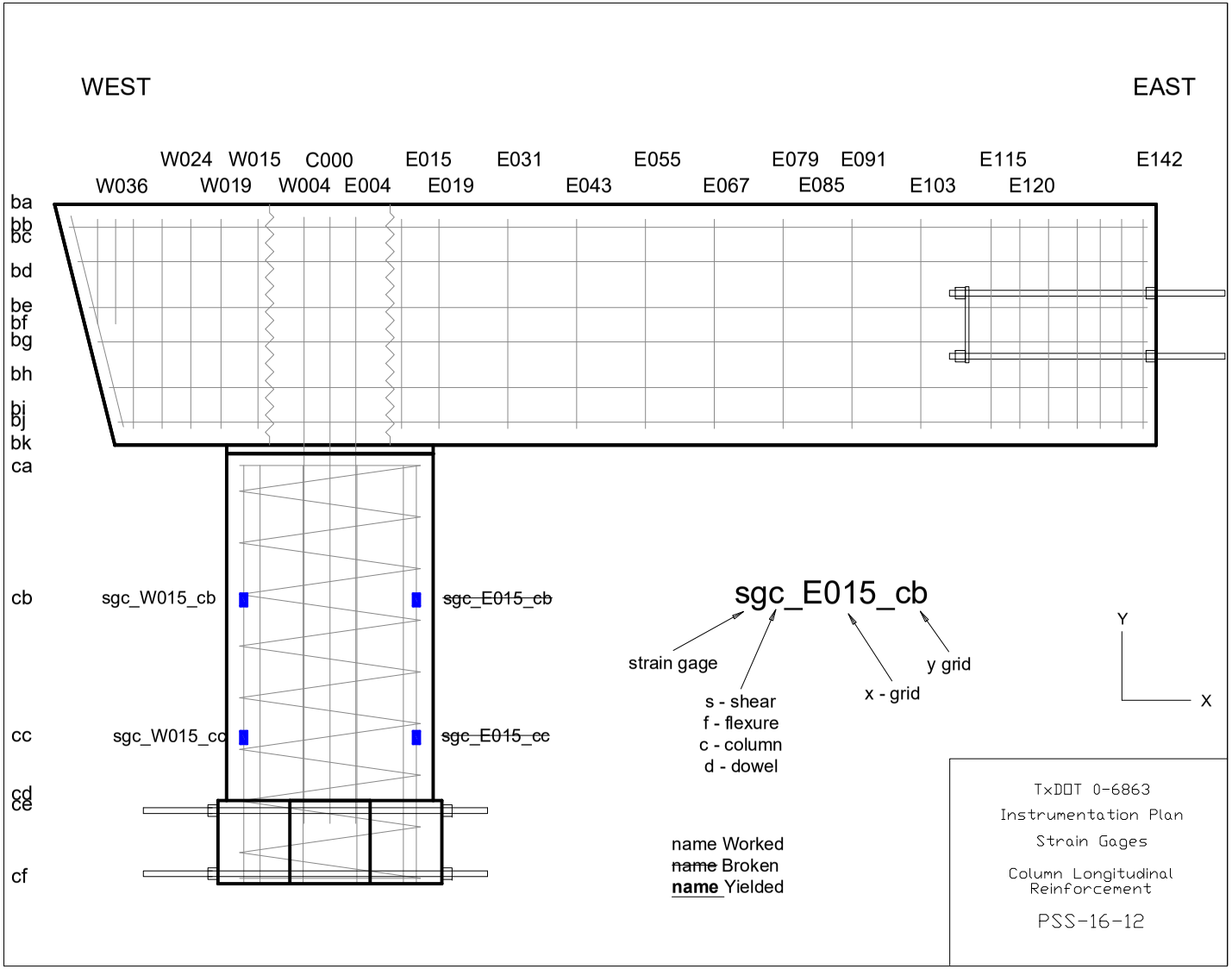
WEST
EAST
W036
W024
W019
W015
W004
C000
E004
E015
E019
E031
E043
E055
E067
E079
E085
E091
E103
E115
E120
E142
ba
bb
bc
bd
be
bf
bg
bh
bj
bj
bk
ca
cb
cc
cd
ce
cf
sgc_W015_cb
sgc_E015_cb
sgc_W015_cc
sgc_E015_cc
sgc_E015_cb
strain gage
s - shear
f - flexure
c - column
d - dowel
x - grid
y grid
Y
X
name Worked
name Broken
name Yielded
TxDOT 0-6863
Instrumentation Plan
Strain Gages
Column Longitudinal Reinforcement
PSS-16-12

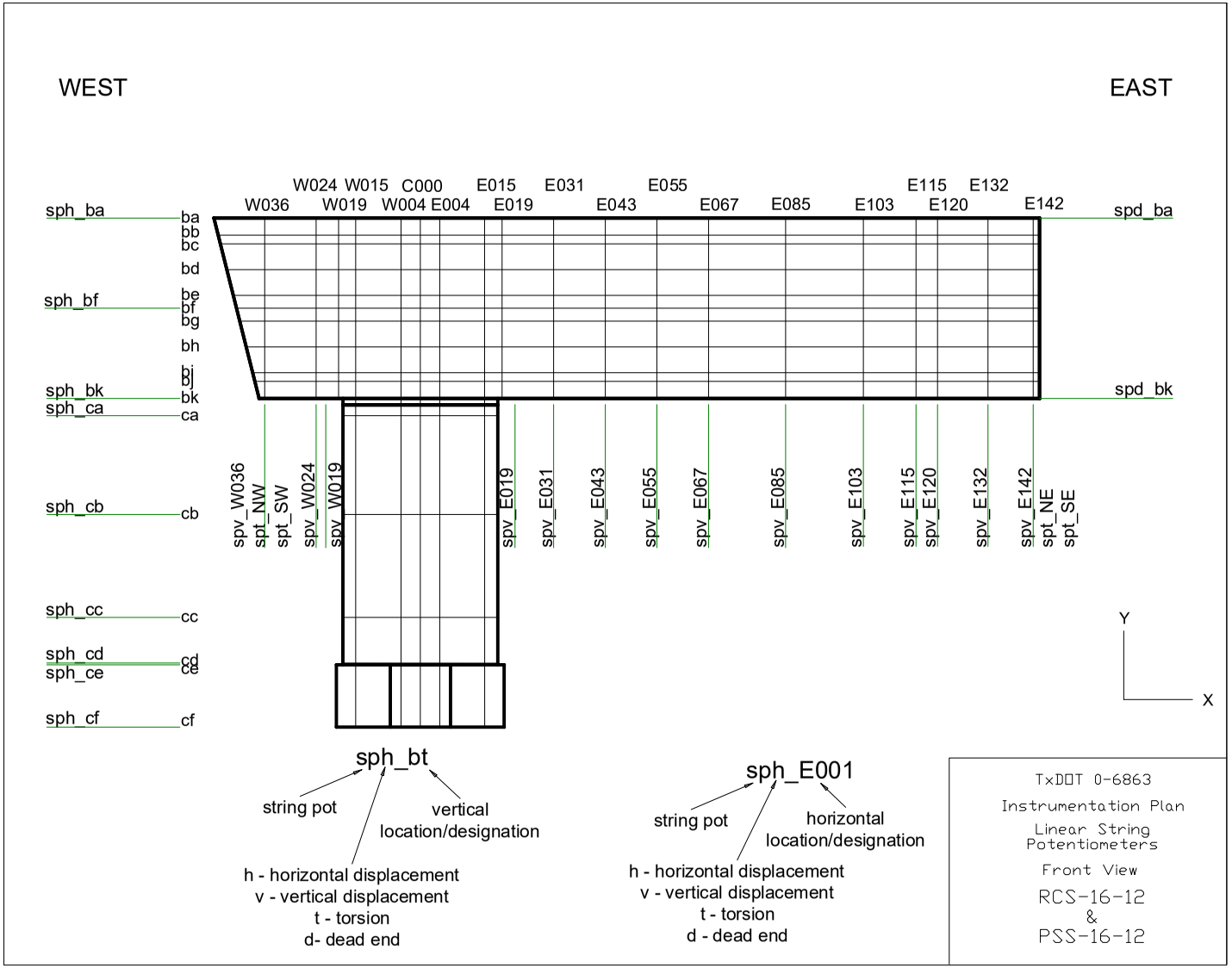
WEST
EAST
W036
W024
W019
W015
W004
C000
E004
E015
E019
E031
E043
E055
E067
E085
E103
E115
E120
E132
E142
sph_ba
sph_bf
sph_bk
sph_ca
sph_cb
sph_cc
sph_cd
sph_ce
sph_cf
ba
bb
bc
bd
be
bf
bg
bh
bi
bj
bk
ca
cb
cc
cd
ce
cf
spd_ba
spd_bk
spv_W036
spt_NW
spt_SW
spv_W024
spv_W019
spv_E019
spv_E031
spv_E043
spv_E055
spv_E067
spv_E085
spv_E103
spv_E115
spv_E120
spv_E132
spv_E142
spt_NE
spt_SE
Y
X
sph_bt
string pot
vertical location/designation
h - horizontal displacement
v - vertical displacement
t - torsion
d- dead end
sph_E001
string pot
horizontal location/designation
h - horizontal displacement
v - vertical displacement
t - torsion
d - dead end
TxDOT 0-6863
Instrumentation Plan
Linear String Potentiometers
Front View
RCS-16-12
&
PSS-16-12

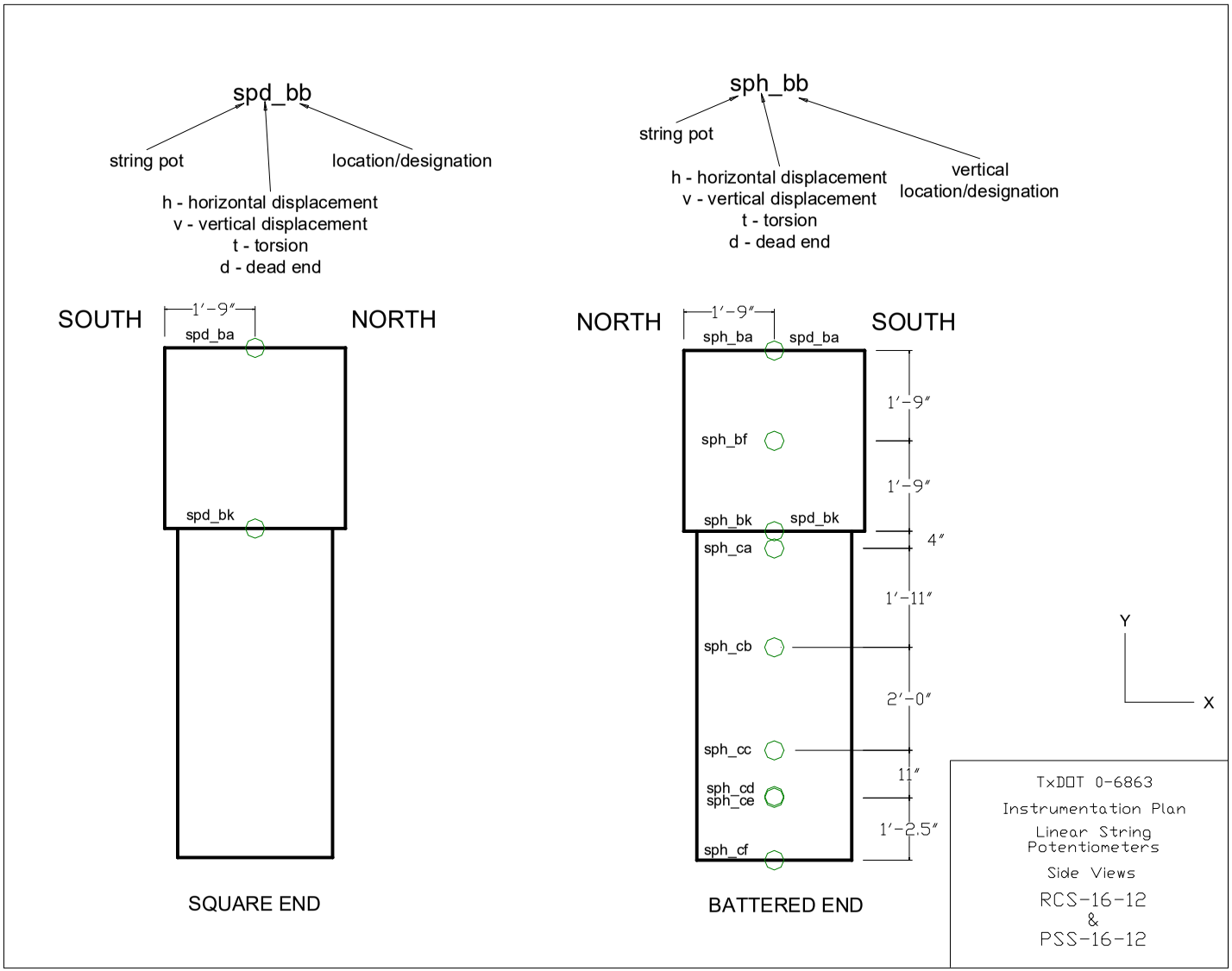
spd_bb
string pot
location/designation
h - horizontal displacement
v - vertical displacement
t - torsion
d - dead end
sph_bb
string pot
h - horizontal displacement
v - vertical displacement
t - torsion
d - dead end
vertical
location/designation
SOUTH
NORTH
1′-9″
spd_ba
spd_bk
SQUARE END
NORTH
SOUTH
1′-9″
sph_ba
spd_ba
sph_bf
sph_bk
spd_bk
sph_ca
sph_cb
sph_cc
sph_cd
sph_ce
sph_cf
1′-9″
1′-9″
4″
1′-11″
2′-0″
11″
1′-2.5″
BATTERED END
Y
X
TxDOT 0-6863
Instrumentation Plan
Linear String
Potentiometers
Side Views
RCS-16-12
&
PSS-16-12

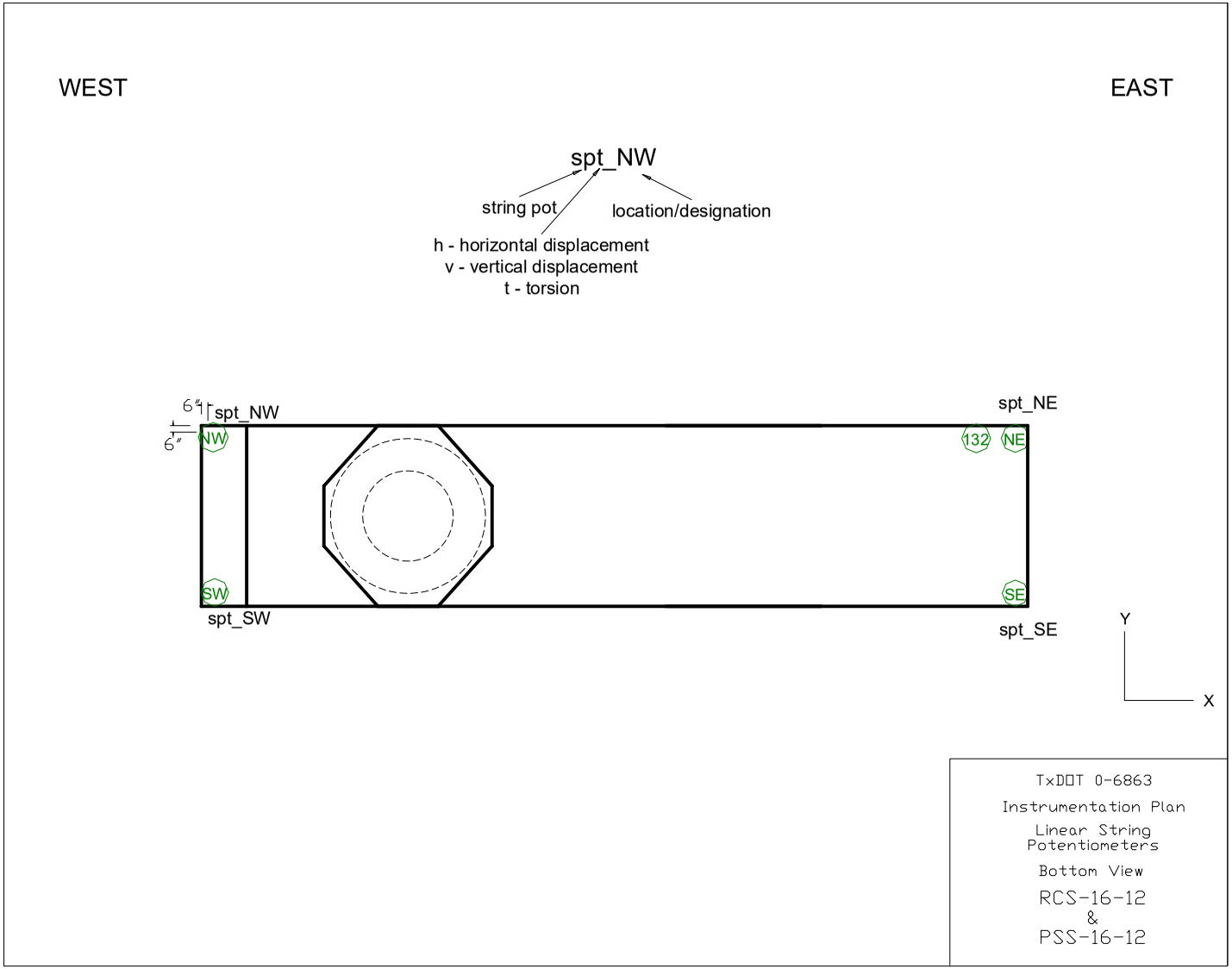
WEST
EAST
spt_NW
string pot
location/designation
h - horizontal displacement
v - vertical displacement
t - torsion
6"
6"
spt_NW
NW
spt_NE
132
NE
SW
SE
spt_SW
spt_SE
Y
X
TxDOT 0-6863
Instrumentation Plan
Linear String Potentiometers
Bottom View
RCS-16-12
&
PSS-16-12

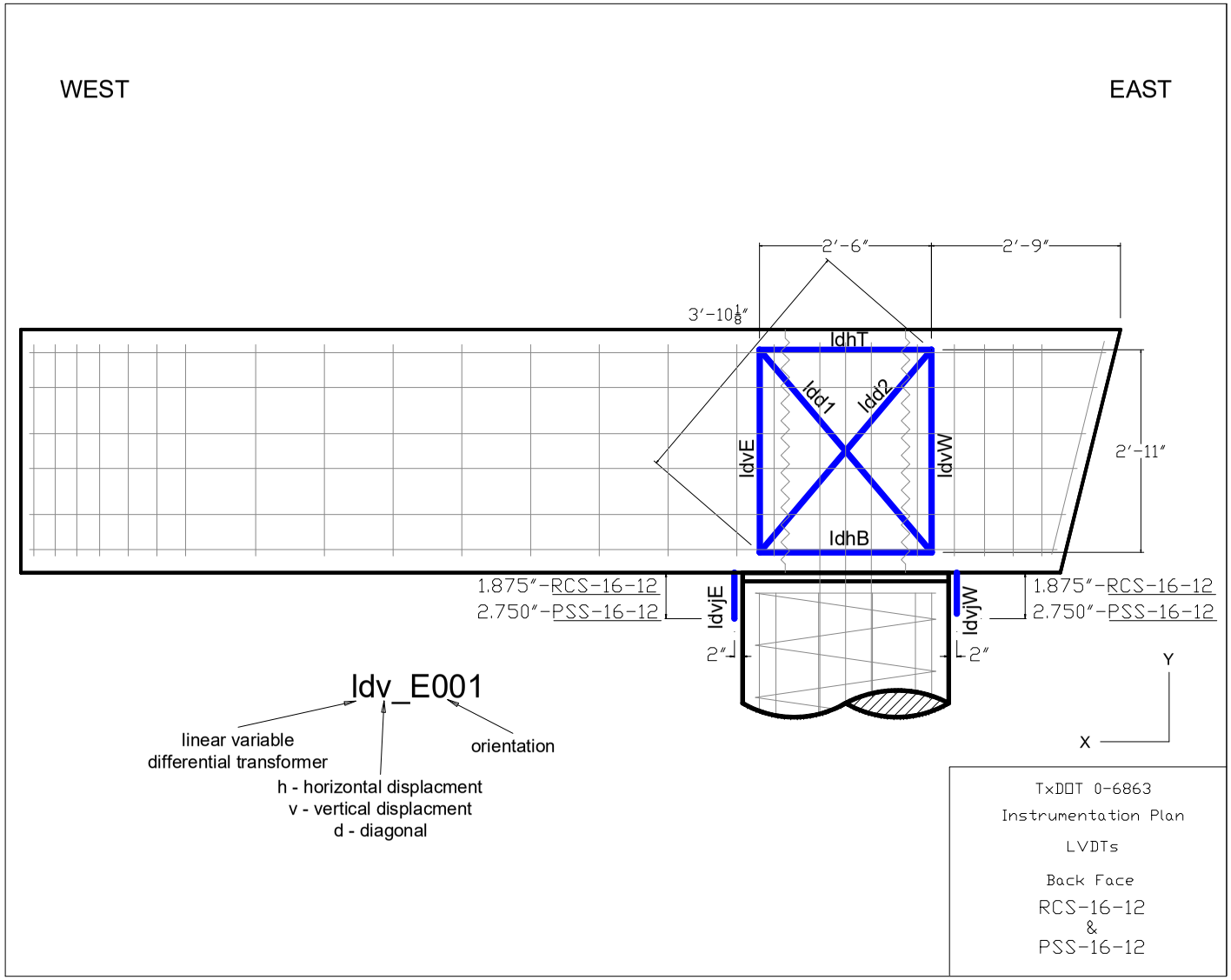
WEST
EAST
2′-6″
2′-9″
3′-10⅛″
ldhT
ldd1
ldd2
ldvE
ldvW
2′-11″
ldhB
1.875″-RCS-16-12
2.750″-PSS-16-12
ldvjE
ldvjW
2″
2″
1.875″-RCS-16-12
2.750″-PSS-16-12
Y
X
ldv_E001
linear variable
differential transformer
orientation
h - horizontal displacment
v - vertical displacment
d - diagonal
TxDOT 0-6863
Instrumentation Plan
LVDTs
Back Face
RCS-16-12
&
PSS-16-12

APPENDIX E

CRACK DATA

Table E.1 RCS-16-12 Front Face Crack Widths

South Face	Load Combinations	Crack Widths and Locations (East and West) from Centerline of Column (in)																			
		Negative Moment Region								Positive Moment Region										Column and Bedding Layer	
		W*0[†]	E19	W20	E9	E32	E44	E56	E70	E90	E80	E68	E64	E57	E105	E116	E38	E24	E122	-	-
Day 1	20	-	-	-	-	-	-	-	-	-	-	-	-	-	-	-	-	-	-	-	-
Day 2	50	-	-	-	-	-	-	-	-	-	-	-	-	-	-	-	-	-	-	-	-
	30	-	-	-	-	-	-	-	-	-	-	-	-	-	-	-	-	-	-	-	-
	50	-	-	-	-	-	-	-	-	-	-	-	-	-	-	-	-	-	-	-	-
	75	-	-	-	-	-	-	-	-	-	-	-	-	-	-	-	-	-	-	-	-
	100	-	-	-	-	-	-	-	-	-	-	-	-	-	-	-	-	-	-	-	-
	125.5	-	-	-	-	-	-	-	-	-	-	-	-	-	-	-	-	-	-	-	-
	Bridge Demands - 160 kips	-	-	-	-	-	-	-	-	-	-	-	-	-	-	-	-	-	-	-	-
	Bridge Demands - 200 kips	0.004	-	-	-	-	-	-	-	-	-	-	-	-	-	-	-	-	-	-	-
	Bridge Demands - 270 kips	0.008	0.004	-	-	-	-	-	-	0.004	-	-	-	-	-	-	-	-	-	-	-
	Bridge Demands - 400 kips	0.016	0.020	-	-	-	-	-	-	0.010	0.008	0.004	-	-	-	-	-	-	-	-	-
	Unloaded Specimen	-	-	-	-	-	-	-	-	-	-	-	-	-	-	-	-	-	-	-	-
Day 3	Bridge Demands - 160 kips	-	-	-	-	-	-	-	-	-	-	-	-	-	-	-	-	-	-	-	-
	Bridge Demands - 270 kips	0.008	0.012	-	-	-	-	-	-	0.004	0.004	0.004	-	-	-	-	-	-	-	-	-
	Bridge Demands - 400 kips (Creep)	0.022	0.024	-	-	-	-	-	-	0.012	0.008	0.006	-	-	-	-	-	-	-	-	-
	Residual 270 k	0.020	-	-	-	-	-	-	-	0.010	-	-	-	-	-	-	-	-	-	-	-
	Residual 160 k	0.010	-	-	-	-	-	-	-	0.006	-	-	-	-	-	-	-	-	-	-	-
	Residual 0 k	0.004	0.004	-	-	-	-	-	-	0.001	0.001	0.001	-	-	-	-	-	-	-	-	-
Day 4	Bridge Demands - 160 kips	0.010	0.010	-	-	-	-	-	-	0.004	0.004	0.004	-	-	-	-	-	-	-	-	-
	Bridge Demands - 270 kips	0.020	0.020	-	-	-	-	-	-	0.006	0.006	0.004	-	-	-	-	-	-	-	-	-
	Bridge Demands - 400 kips	0.022	0.022	-	-	-	-	-	-	0.010	0.008	0.004	-	-	-	-	-	-	-	-	-
	460 kips welds yielded	-	-	-	-	-	-	-	-	-	-	-	-	-	-	-	-	-	-	-	-
	Unload Specimen	-	-	-	-	-	-	-	-	-	-	-	-	-	-	-	-	-	-	-	-
	P1, P2 500 kips	-	-	-	-	-	-	-	-	-	-	-	-	-	-	-	-	-	-	-	-
	P1, P2 550 kips	0.035	0.030	-	-	-	-	-	-	0.018	0.022	0.018	-	-	0.006	-	-	-	-	-	-
	Bridge Demands - 140% Design	0.039	0.037	-	-	-	-	-	-	0.018	0.022	0.018	0.004	0.012	0.016	0.010	-	-	-	-	-
	High Positive (1) - V=360 kips	0.016	0.010	-	-	-	-	-	-	0.037	0.037	0.026	0.006	0.030	0.026	0.014	0.030	0.020	0.006	-	-
	High Positive (2) - V=400 kips	0.006	0.004	-	-	-	-	-	-	0.059	0.059	0.059	0.014	0.030	0.039	0.030	0.035	0.035	0.014	-	-
	Maximum Positive	-	-	-	-	-	-	-	-	0.098	0.079	0.069	0.028	0.035	0.059	0.030	0.035	0.035	0.014	-	-
	Residual Unload	0.004	0.004	-	-	-	-	-	-	0.060	0.058	0.039	0.016	0.012	0.020	0.010	0.008	0.001	0.001	-	-

Table E.1 Continued

South Face	Load Combinations	Crack Widths and Locations (East and West) from Centerline of Column (in)																			
		Negative Moment Region								Positive Moment Region										Column and Bedding Layer	
		W0	E19	W20	E9	E32	E44	E56	E70	E90	E80	E68	E64	E57	E105	E116	E38	E24	E122	-	-
Day 5	P1= 80 kips	-	-	-	-	-	-	-	-	-	-	-	-	-	-	-	-	-	-	-	-
	JO - 50 kips	-	-	-	-	-	-	-	-	-	-	-	-	-	-	-	-	-	-	-	-
	JO-75	-	-	-	-	-	-	-	-	-	-	-	-	-	-	-	-	-	-	-	-
	Unloaded Specimen	-	-	-	-	-	-	-	-	-	-	-	-	-	-	-	-	-	-	-	-
	Joint Opening	-	-	-	-	-	-	-	-	-	-	-	-	-	-	-	-	-	-	0.012	-
	P1= 80 kips	-	-	-	-	-	-	-	-	-	-	-	-	-	-	-	-	-	-	-	-
	HT,HB = 20 kips	-	-	-	-	-	-	-	-	-	-	-	-	-	-	-	-	-	-	-	-
	HT,HB = 48 kips	-	-	-	-	-	-	-	-	-	-	-	-	-	-	-	-	-	-	-	-
	Unloaded Specimen	-	-	-	-	-	-	-	-	-	-	-	-	-	-	-	-	-	-	-	-
Day 6	JC-40	-	-	-	-	-	-	-	-	-	-	-	-	-	-	-	-	-	-	-	0.004
	Joint Closing	-	-	-	-	-	-	-	-	-	-	-	-	-	-	-	-	-	-	-	0.026
	High Negative - P2 - 184k	0.098	0.039	0.001	-	-	0.030	0.010	0.016	-	-	-	-	-	-	-	-	-	-	-	-
	Maximum Negative	0.196	0.157	0.197	0.098	0.118	0.177	0.010	0.024	-	-	-	-	-	-	-	-	-	-	-	-
	Residual Unload	0.018	0.099	0.001	0.079	0.080	0.097	0.002	0.004	-	-	-	-	-	-	-	-	-	-	-	-
Day 7	JO	-	-	-	-	-	-	-	-	-	-	-	-	-	-	-	-	-	-	-	-
	Max Positive	-	-	-	-	-	-	-	-	-	-	-	-	-	-	-	-	-	-	-	-
	~Max P1, P2, HB and HT (tension)	-	-	-	-	-	-	-	-	-	-	-	-	-	-	-	-	-	-	-	-
	Release HB and HT, Unload P1 P2	-	-	-	-	-	-	-	-	-	-	-	-	-	-	-	-	-	-	-	-

** - W/E indicates direction about the centerline of the column*

† - # indicates distance in inches from the centerline of the column

Table E.2 RCS-16-12 Back Face Crack Widths

Back Face	Load Combinations	Crack Widths and Locations (East and West) from Centerline of Column (in)																			
		Negative Moment Region								Positive Moment Region										Column and Bedding Layer	
		W*1[†]	E17	W9	E67	E52	E45	E42	E20	E91	E100	E77	E63	E113	E52	E122	E42	E30	E22	-	-
Day 1	20	-	-	-	-	-	-	-	-	-	-	-	-	-	-	-	-	-	-	-	-
Day 2	50	-	-	-	-	-	-	-	-	-	-	-	-	-	-	-	-	-	-	-	-
	30	-	-	-	-	-	-	-	-	-	-	-	-	-	-	-	-	-	-	-	-
	50	-	-	-	-	-	-	-	-	-	-	-	-	-	-	-	-	-	-	-	-
	75	-	-	-	-	-	-	-	-	-	-	-	-	-	-	-	-	-	-	-	-
	100	-	-	-	-	-	-	-	-	-	-	-	-	-	-	-	-	-	-	-	-
	125.5	-	-	-	-	-	-	-	-	-	-	-	-	-	-	-	-	-	-	-	-
	Bridge Demands - 160 kips	-	-	-	-	-	-	-	-	-	-	-	-	-	-	-	-	-	-	-	-
	Bridge Demands - 200 kips	-	-	-	-	-	-	-	-	-	-	-	-	-	-	-	-	-	-	-	-
	Bridge Demands - 270 kips	-	-	-	-	-	-	-	-	-	-	-	-	-	-	-	-	-	-	-	-
	Bridge Demands - 400 kips	-	-	-	-	-	-	-	-	-	-	-	-	-	-	-	-	-	-	-	-
	Unloaded Specimen	-	-	-	-	-	-	-	-	-	-	-	-	-	-	-	-	-	-	-	-
Day 3	Bridge Demands - 160 kips	-	-	-	-	-	-	-	-	-	-	-	-	-	-	-	-	-	-	-	-
	Bridge Demands - 270 kips	-	-	-	-	-	-	-	-	-	-	-	-	-	-	-	-	-	-	-	-
	Bridge Demands - 400 kips (Creep)	0.020	0.024	-	-	-	-	-	-	0.012	0.004	0.008	0.006	-	-	-	-	-	-	-	-
	Residual 270 k	-	-	-	-	-	-	-	-	-	-	-	-	-	-	-	-	-	-	-	-
	Residual 160 k	-	-	-	-	-	-	-	-	-	-	-	-	-	-	-	-	-	-	-	-
	Residual 0 k	0.001	0.00	-	-	-	-	-	-	0.001	0.001	0.001	0.001	-	-	-	-	-	-	-	-
Day 4	Bridge Demands - 160 kips	-	-	-	-	-	-	-	-	0.004	0.004	0.004	0.004	-	-	-	-	-	-	-	-
	Bridge Demands - 270 kips	0.012	0.014	-	-	-	-	-	-	0.004	0.004	0.004	0.004	-	-	-	-	-	-	-	-
	Bridge Demands - 400 kips	0.018	0.020	-	-	-	-	-	-	0.008	0.004	0.006	0.006	-	-	-	-	-	-	-	-
	460 kips welds yielded	-	-	-	-	-	-	-	-	-	-	-	-	-	-	-	-	-	-	-	-
	Unload Specimen	-	-	-	-	-	-	-	-	-	-	-	-	-	-	-	-	-	-	-	-
	P1, P2 500 kips	-	-	-	-	-	-	-	-	0.014	0.014	0.010	0.016	0.004	-	-	-	-	-	-	-
	P1, P2 550 kips	-	-	-	-	-	-	-	-	0.016	0.014	0.016	0.020	0.006	-	-	-	-	-	-	-
	Bridge Demands - 140% Design	0.030	0.035	0.004	-	-	-	-	-	0.018	0.016	0.018	0.024	0.008	0.016	-	-	-	-	-	-
	High Positive (1) - V=360 kips	-	-	-	-	-	-	-	-	0.030	0.024	0.031	0.031	0.020	0.024	-	0.024	0.004	-	-	-
	High Positive (2) - V=400 kips	-	-	-	-	-	-	-	-	0.079	0.030	0.059	0.098	0.028	0.039	0.006	0.030	0.018	0.028	-	-
	Maximum Positive	-	-	-	-	-	-	-	-	0.098	0.049	0.098	0.128	0.039	0.079	0.006	0.035	0.018	0.030	-	-
	Residual Unload	0.004	0.004	0.004	-	-	-	-	-	0.059	0.018	0.039	0.035	0.004	0.022	0.001	0.004	0.001	0.004	-	-

Table E.2 Continued

Back Face	Load Combinations	Crack Widths and Locations (East and West) from Centerline of Column (in)																			
		Negative Moment Region								Positive Moment Region										Column and Bedding Layer	
		W*1†	E17	W9	E67	E52	E45	E42	E20	E91	E100	E77	E63	E113	E52	E122	E42	E30	E22	-	-
Day 5	P1= 80 kips	-	-	-	-	-	-	-	-	-	-	-	-	-	-	-	-	-	-	-	-
	JO - 50 kips	-	-	-	-	-	-	-	-	-	-	-	-	-	-	-	-	-	-	-	-
	JO-75	-	-	-	-	-	-	-	-	-	-	-	-	-	-	-	-	-	-	-	-
	Unloaded Specimen	-	-	-	-	-	-	-	-	-	-	-	-	-	-	-	-	-	-	-	-
	Joint Opening	-	-	-	-	-	-	-	-	-	-	-	-	-	-	-	-	-	-	-	-
	P1= 80 kips	-	-	-	-	-	-	-	-	-	-	-	-	-	-	-	-	-	-	-	-
	HT,HB = 20 kips	-	-	-	-	-	-	-	-	-	-	-	-	-	-	-	-	-	-	-	-
	HT,HB = 48 kips	-	-	-	-	-	-	-	-	-	-	-	-	-	-	-	-	-	-	-	-
	Unloaded Specimen	-	-	-	-	-	-	-	-	-	-	-	-	-	-	-	-	-	-	-	-
Day 6	JC-40	-	-	-	-	-	-	-	-	-	-	-	-	-	-	-	-	-	-	-	-
	Joint Closing	-	-	-	-	-	-	-	-	-	-	-	-	-	-	-	-	-	-	-	-
	High Negative - P2 - 184k	0.031	0.039	-	0.016	0.004	0.018	-	-	-	-	-	-	-	-	-	-	-	-	-	-
	Maximum Negative	0.118	0.236	0.098	0.024	0.001	0.039	0.177	0.098	-	-	-	-	-	-	-	-	-	-	-	-
	Residual Unload	0.079	0.138	0.059	0.001	0.001	0.001	0.118	0.059	-	-	-	-	-	-	-	-	-	-	-	-
Day 7	JO	-	-	-	-	-	-	-	-	-	-	-	-	-	-	-	-	-	-	-	-
	Max Positive	-	-	-	-	-	-	-	-	-	-	-	-	-	-	-	-	-	-	-	-
	~Max P1, P2, HB and HT (tension)	-	-	-	-	-	-	-	-	-	-	-	-	-	-	-	-	-	-	-	-
	Release HB and HT, Unload P1 P2	-	-	-	-	-	-	-	-	-	-	-	-	-	-	-	-	-	-	-	-

* - *W/E indicates direction about the centerline of the column*

† - *# indicates distance in inches from the centerline of the column*

Table E.3 PSS-16-12 Front Face Crack Widths

Front Face	Load Combinations	Crack Widths and Locations (East and West) from Centerline of Column (in)																
		Negative Moment Region							Positive Moment Region					Column and Bedding Layer				
		E*2[†]	W12	E19	W21	E29	E40	W6	E84	E97	E63	E74	E86	-	-	-	-	-
Day1	Bridge Demands - 160 kips	-	-	-	-	-	-	-	-	-	-	-	-	-	-	-	-	-
	Bridge Demands - 270 kips	0.001	-	-	-	-	-	-	-	-	-	-	-	-	-	-	-	-
	Residual (160 kips)	0.000	-	-	-	-	-	-	-	-	-	-	-	-	-	-	-	-
	Bridge Demands - 400 kips	0.001	-	-	-	-	-	-	0.001	-	-	-	-	-	-	-	-	-
	Creep – 400k – 1-hr	0.001	-	-	-	-	-	-	0.001	-	-	-	-	-	-	-	-	-
	Bridge Demands - 140% Design	0.006	0.001	0.001	-	-	-	-	0.008	0.001	-	-	-	-	-	-	-	-
	Maximum Positive	-	-	-	-	-	-	-	0.059	0.004	0.035	0.004	0.031	-	-	-	-	-
	Residual (160 kips)	0.000	0.000	0.000	-	-	-	-	0.006	0.000	0.000	0.000	0.004	-	-	-	-	-
	Residual Unload	0.000	0.000	0.000	-	-	-	-	0.004	0.000	0.000	0.000	0.004	-	-	-	-	-
	Joint Opening	0.000	0.000	0.000	-	-	-	-	0.004	0.000	0.000	0.000	0.004	0.004	0.004	-	-	-
	Joint Closing	0.000	0.000	0.000	-	-	-	-	0.004	0.000	0.000	0.000	0.004	0.004	0.004	0.001	0.001	0.001
	Maximum Negative	0.197	0.001	0.001	0.001	0.020	0.001	0.059	-	-	-	-	-	-	-	0.001	0.001	0.001
	Residual Unload	0.026	0.000	0.000	0.000	0.000	0.000	0.004	0.001	0.000	0.000	0.000	0.004	0.004	0.004	0.001	0.001	0.001
Day 2	Bridge Demands - 160 kips	0.026	0.000	0.000	0.000	0.000	0.000	0.000	0.001	-	-	-	0.004	-	-	-	-	-
	Bridge Demands - 270 kips	0.026	0.000	0.000	0.000	0.000	0.000	0.000	0.001	-	-	-	0.004	-	-	-	-	-
	Bridge Demands - 400 kips	0.039	0.000	0.000	0.000	0.000	0.000	0.000	0.004	-	-	-	0.004	-	-	-	-	-
	Bridge Demands - 140% Design	0.059	-	-	-	-	-	-	0.026	-	-	-	0.014	-	-	-	-	-
	Residual (270 kips)	0.037	-	-	-	-	-	-	-	-	-	-	-	-	-	-	-	-
	Residual (160 kips)	0.026	-	-	-	-	-	-	-	-	-	-	-	-	-	-	-	-
	Failure	-		-	-	-	-	-	-	-	-	-	-	-	-	-	-	-

* - *W/E indicates direction about the centerline of the column*
[†] - *# indicates distance in inches from the centerline of the column*

Table E.4 PSS-16-12 Back Face Crack Widths

Back Face	Load Combinations	Crack Widths and Locations (East and West) from Centerline of Column (in)																		
		Negative Moment Region						Positive Moment Region						Column and Bedding Layer						
		W*7†	E13	E24	E32	E1	W10	E70	E92	E77	E97	E84	E60	-	-	-	-	-	-	-
Day1	Bridge Demands - 160 kips	-	-	-	-	-	-	-	-	-	-	-	-	-	-	-	-	-	-	-
	Bridge Demands - 270 kips	0.001	-	-	-	-	-	-	-	-	-	-	-	-	-	-	-	-	-	-
	Residual (160 kips)	0.000	-	-	-	-	-	-	-	-	-	-	-	-	-	-	-	-	-	-
	Bridge Demands - 400 kips	0.001	-	-	-	-	-	0.001	-	-	-	-	-	-	-	-	-	-	-	-
	Creep – 400k – 1-hr	0.001	-	-	-	-	-	0.001	0.001	-	-	-	-	-	-	-	-	-	-	-
	Bridge Demands - 140% Design	0.004	0.001	-	-	-	-	0.001	0.001	0.008	-	-	-	-	-	-	-	-	-	-
	Maximum Positive	0.000	0.000	-	-	-	-	0.001	0.001	0.098	0.001	0.001	0.033	-	-	-	-	-	-	-
	Residual (160 kips)	0.000	0.000	-	-	-	-	0.000	0.000	0.014	0.000	0.000	0.004	-	-	-	-	-	-	-
	Residual Unload	0.000	0.000	-	-	-	-	0.000	0.000	0.004	0.000	0.000	0.004	-	-	-	-	-	-	-
	Joint Opening	0.000	0.000	-	-	-	-	0.000	0.000	0.004	0.000	0.000	0.004	0.004	0.001	0.001	0.001	-	-	-
	Joint Closing	0.000	0.000	-	-	-	-	0.000	0.000	0.004	0.000	0.000	0.004	0.004	0.001	0.001	0.001	0.001	0.001	0.001
	Maximum Negative	0.118	0.001	0.020	0.001	0.020	0.001	0.000	0.000	0.004	0.000	0.000	0.004	-	0.001	0.001	0.001	0.001	0.001	0.001
	Residual Unload	0.016	0.000	0.000	0.000	0.000	0.000	0.000	0.000	0.004	0.000	0.000	0.004	-	0.001	0.001	0.001	0.001	0.001	0.001
Day 2	Bridge Demands - 160 kips	-	-	-	-	-	-	-	-	-	-	-	-	-	-	-	-	-	-	-
	Bridge Demands - 270 kips	-	-	-	-	-	-	-	-	-	-	-	-	-	-	-	-	-	-	-
	Bridge Demands - 400 kips	-	-	-	-	-	-	-	-	-	-	-	-	-	-	-	-	-	-	-
	Bridge Demands - 140% Design	-	-	-	-	-	-	-	-	-	-	-	-	-	-	-	-	-	-	-
	Residual (270 kips)	-	-	-	-	-	-	-	-	-	-	-	-	-	-	-	-	-	-	-
	Residual (160 kips)	-	-	-	-	-	-	-	-	-	-	-	-	-	-	-	-	-	-	-
	Failure	-	-	-	-	-	-	-	-	-	-	-	-	-	-	-	-	-	-	-

** - W/E indicates direction about the centerline of the column*

† - # indicates distance in inches from the centerline of the column

APPENDIX F

BACK FACE CRACK MAPS

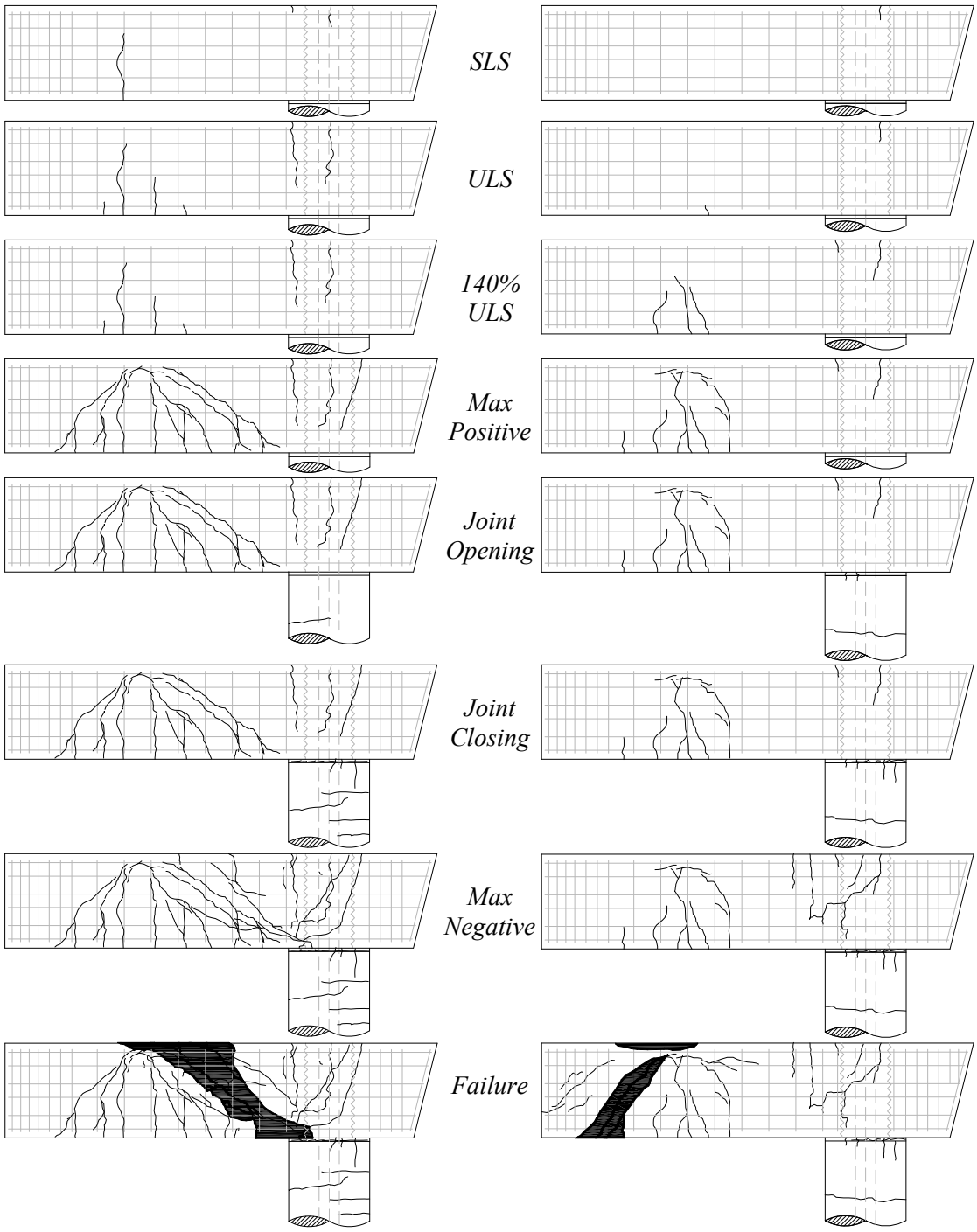

RCS-16-12 *PSS-16-12*

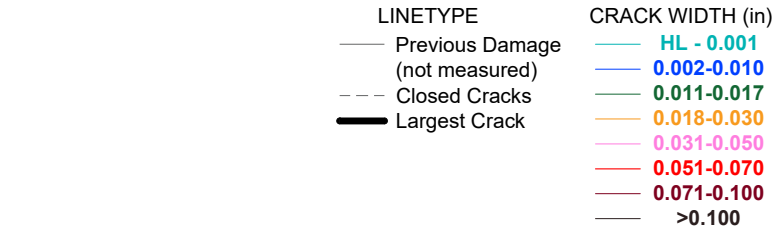

Legend

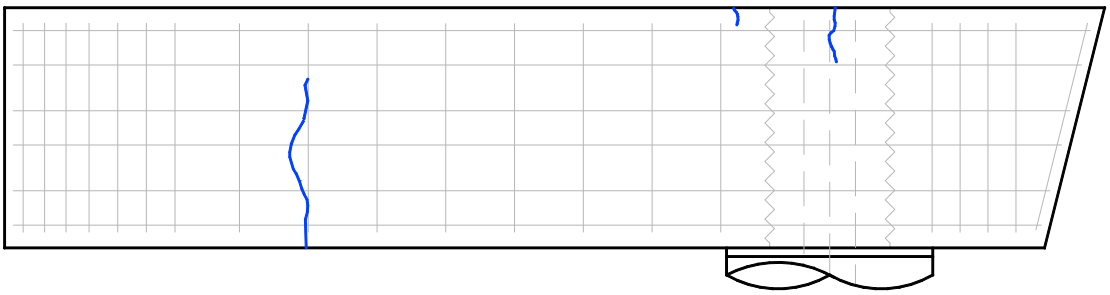

RCS-16-12 – SLS

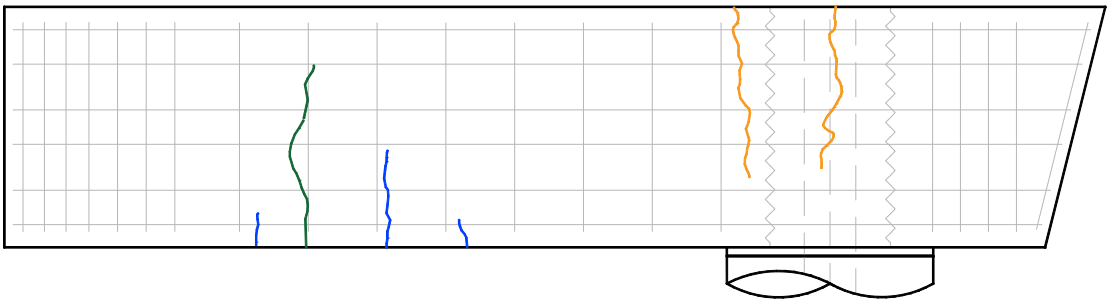

RCS-16-12 – ULS

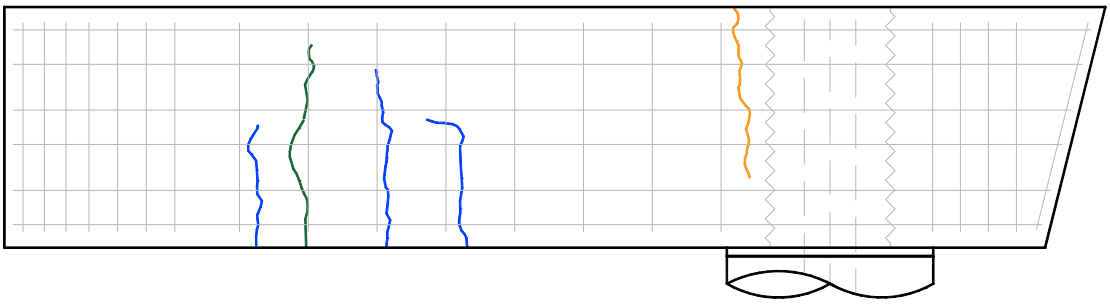

RCS-16-12 – CREEP

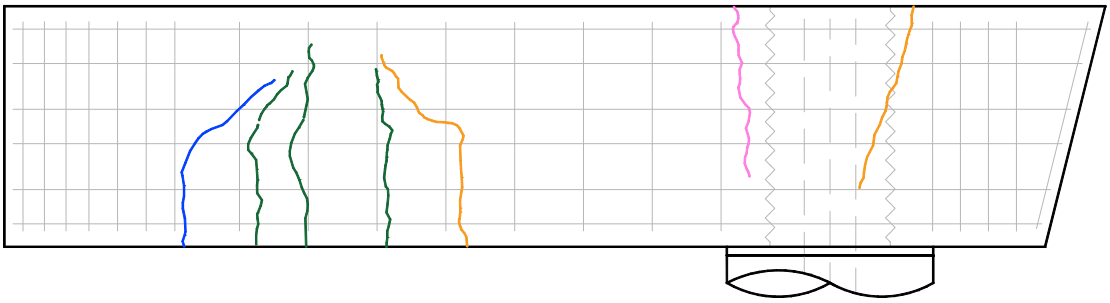

RCS-16-122 – 140% ULS

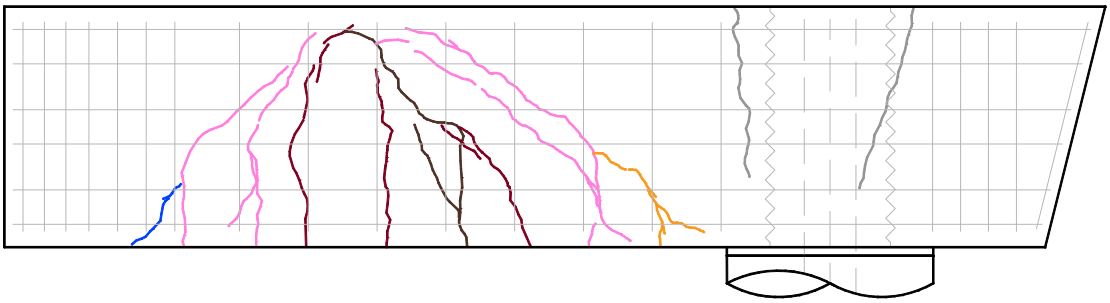

RCS-16-12 – Pattern B

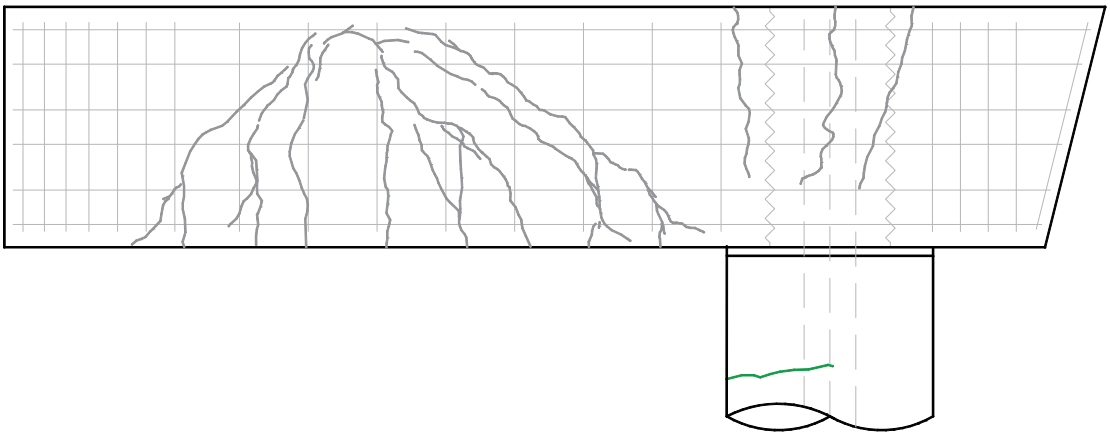

RCS-16-12 – Pattern C

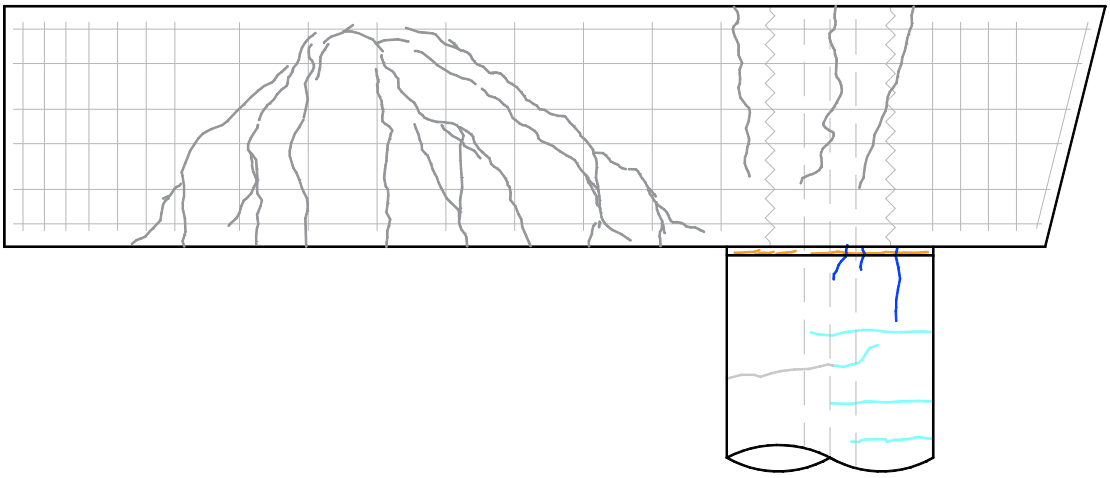

RCS-16-12 – Pattern D

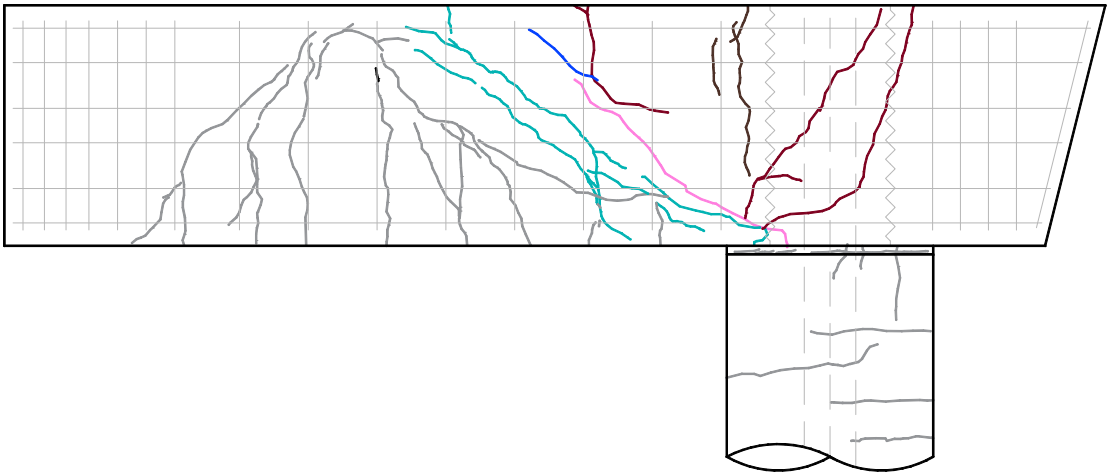

RCS-16-12 – Pattern E

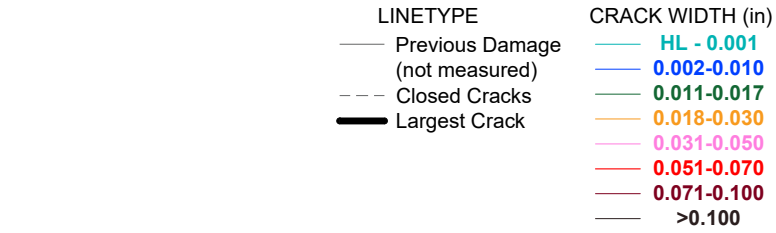

Legend

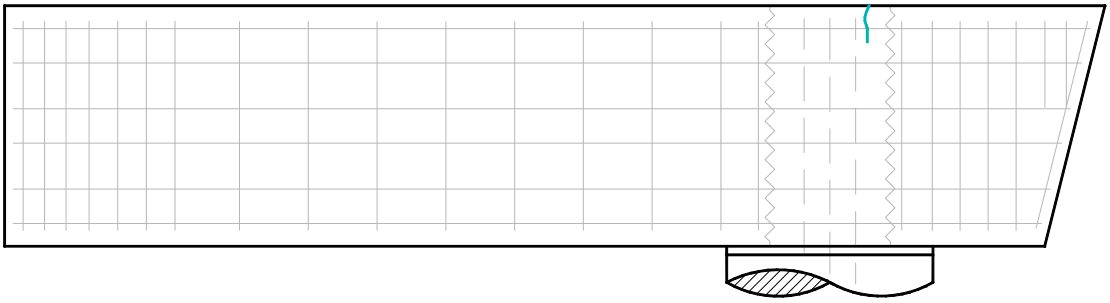

PSS-16-12 – SLS

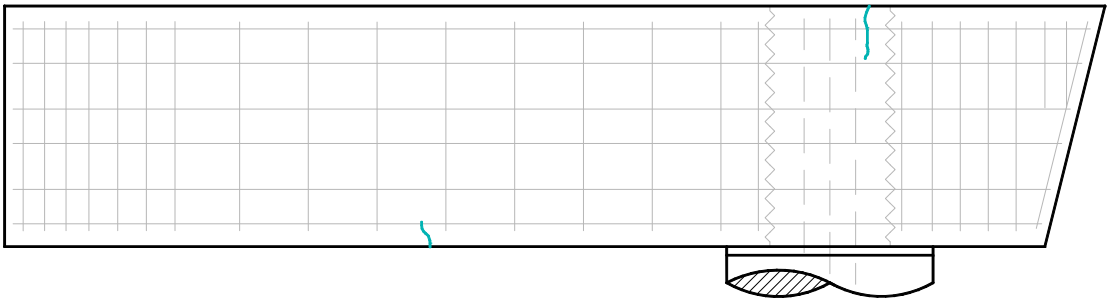

PSS-16-12 – ULS

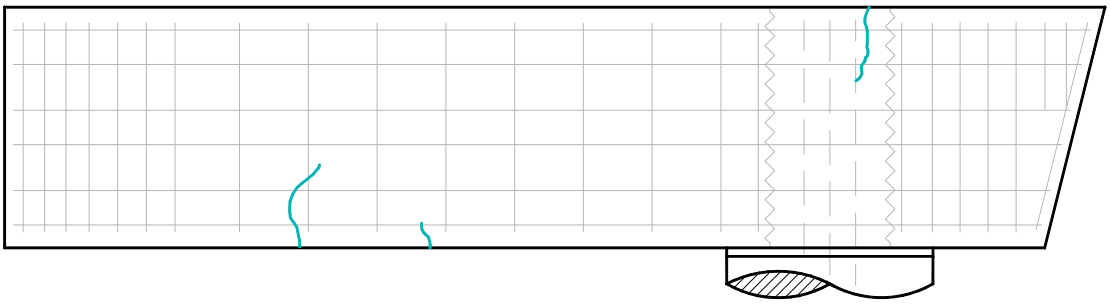

PSS-16-12 – CREEP

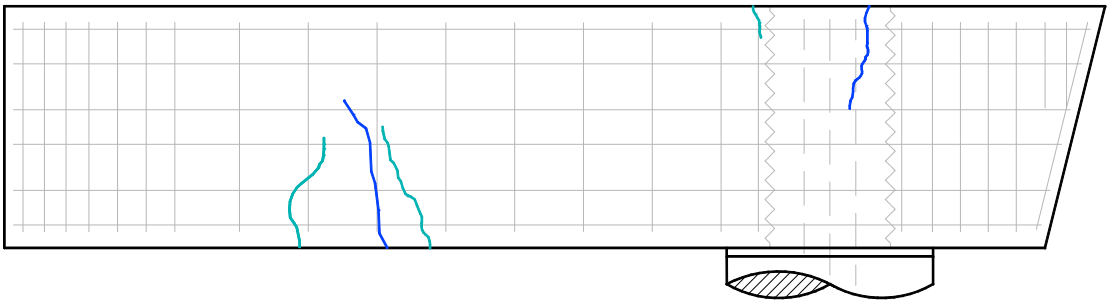

PSS-16-12 – 140% ULS

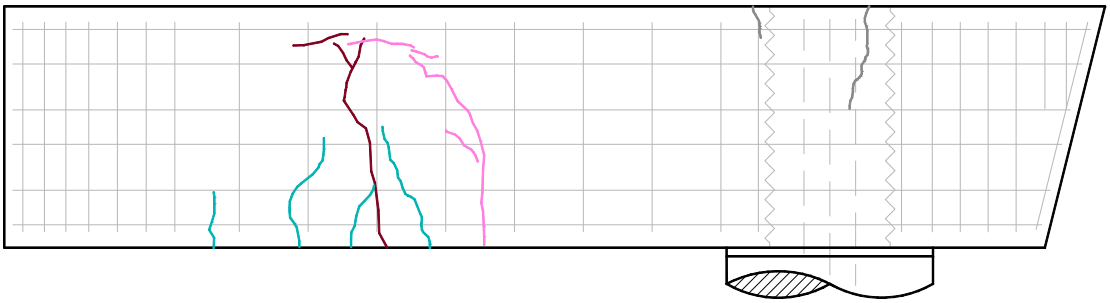

PSS-16-12 – Pattern B

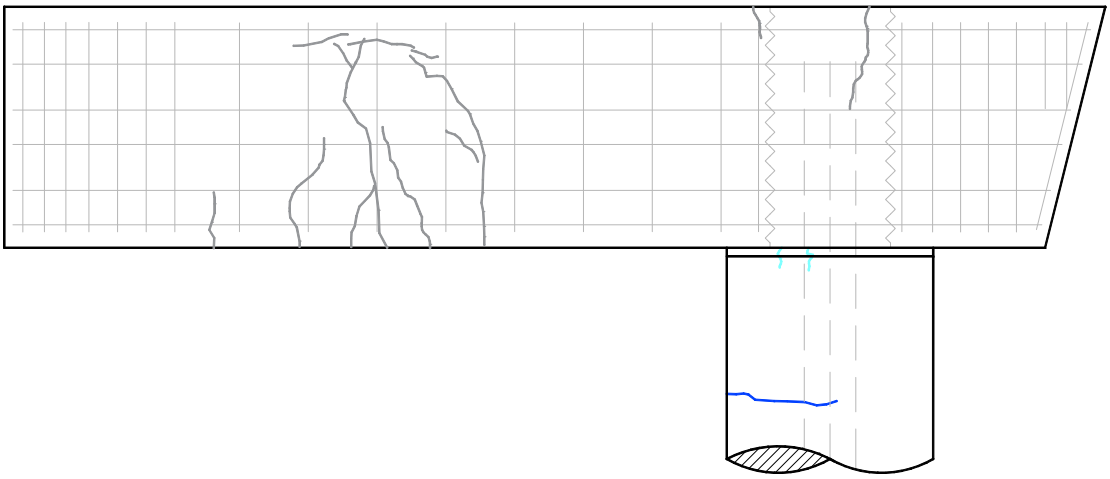

PSS-16-12 – Pattern C

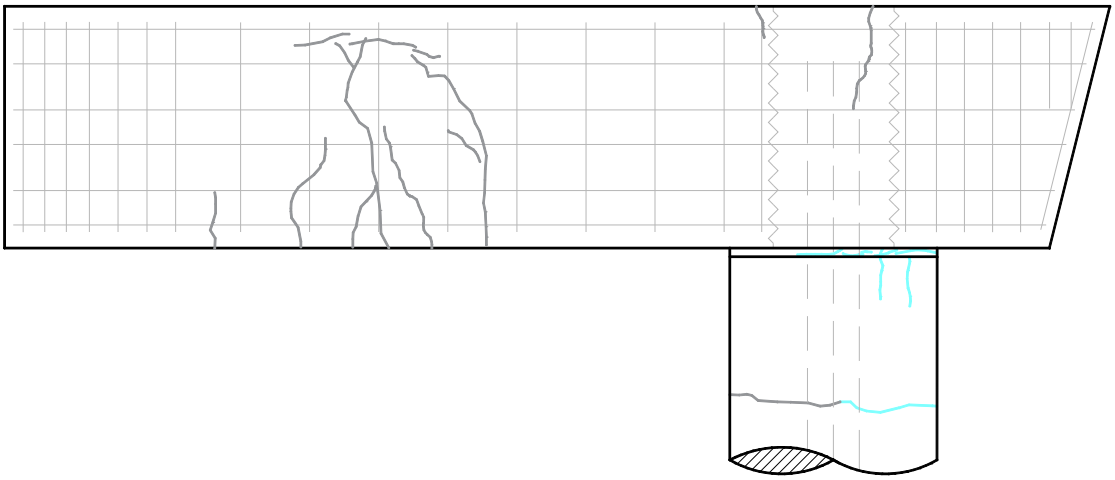

PSS-16-12 – Pattern D

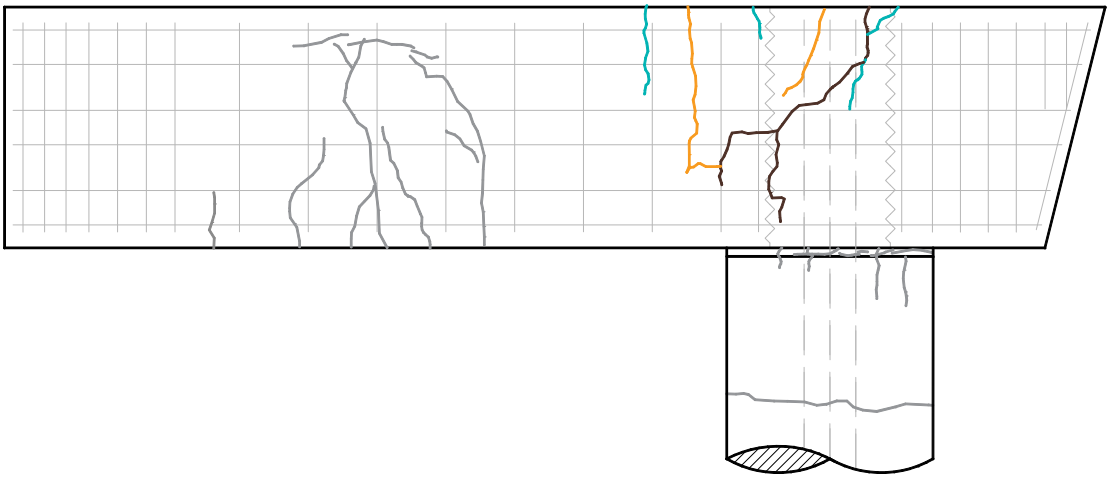

PSS-16-12 – Pattern E

APPENDIX G

FRONT FACE CRACK MAPS

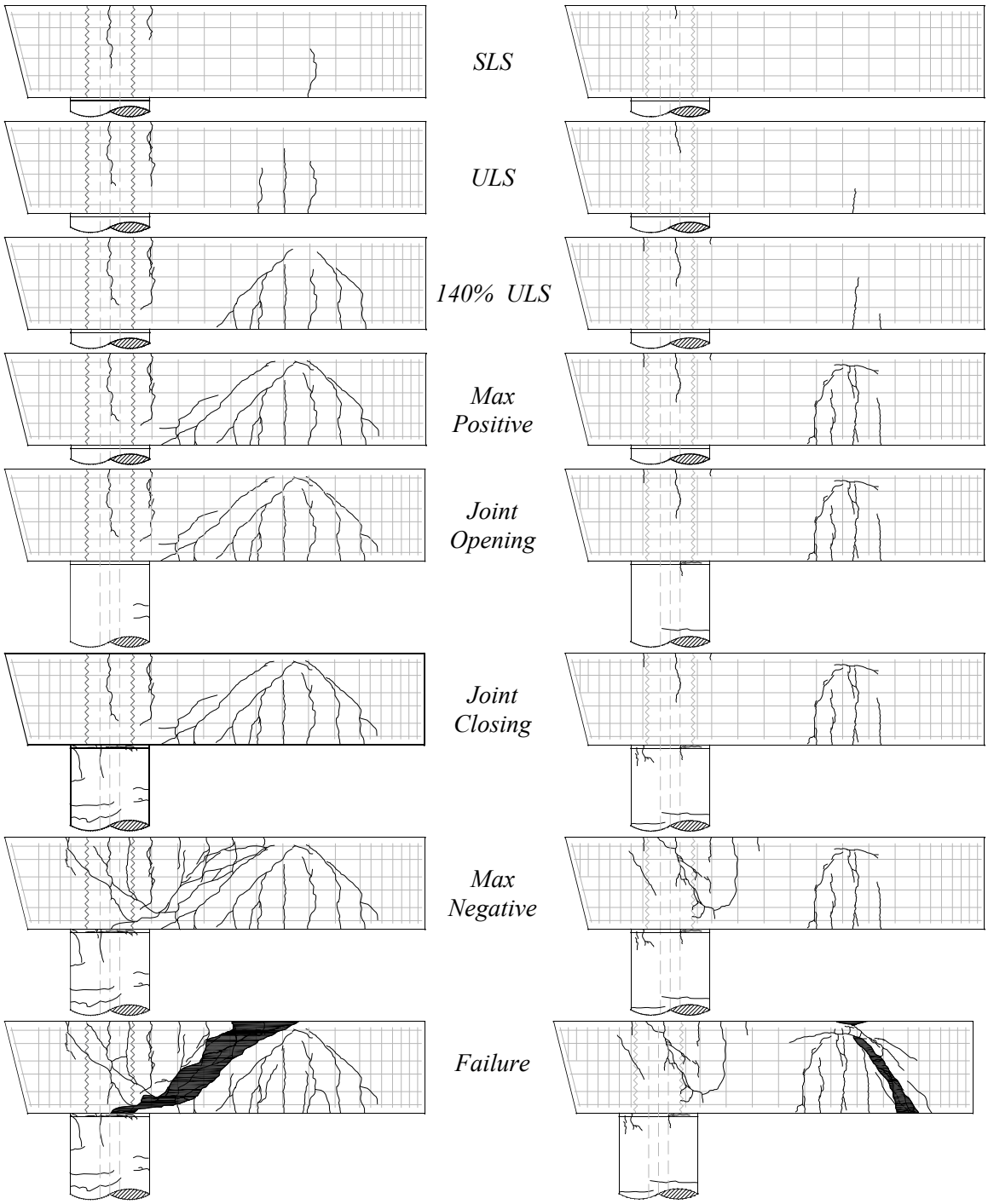
SLS
ULS
140% ULS
Max Positive
Joint Opening
Joint Closing
Max Negative
Failure

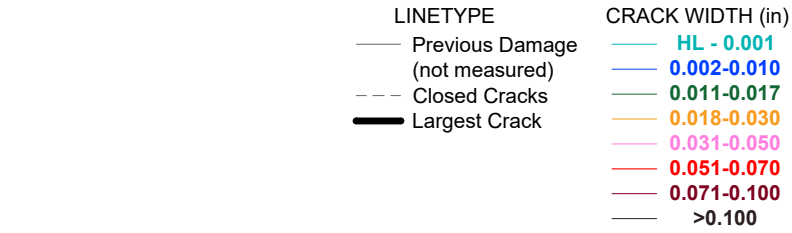

Legend

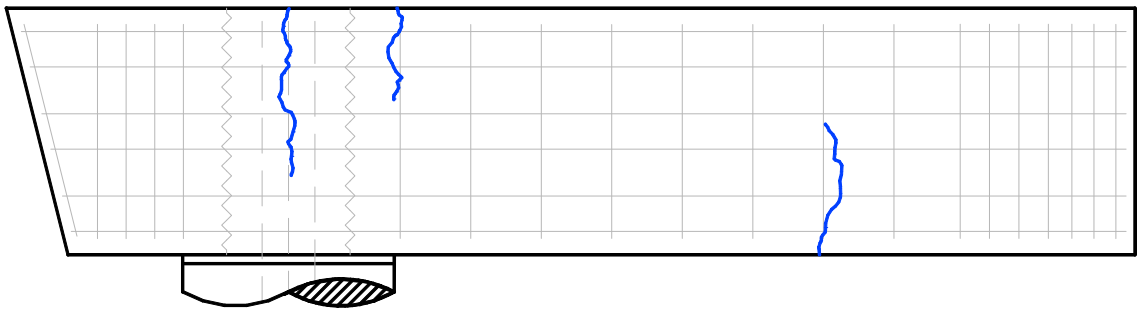

RCS-16-12 – SLS

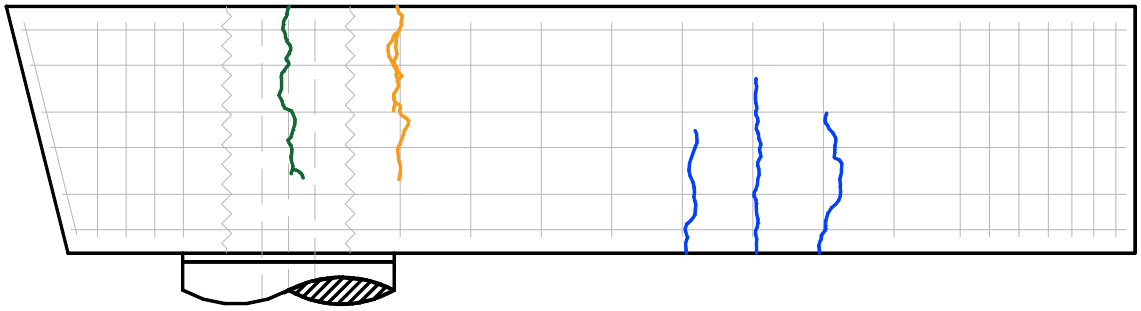

RCS-16-12 – ULS

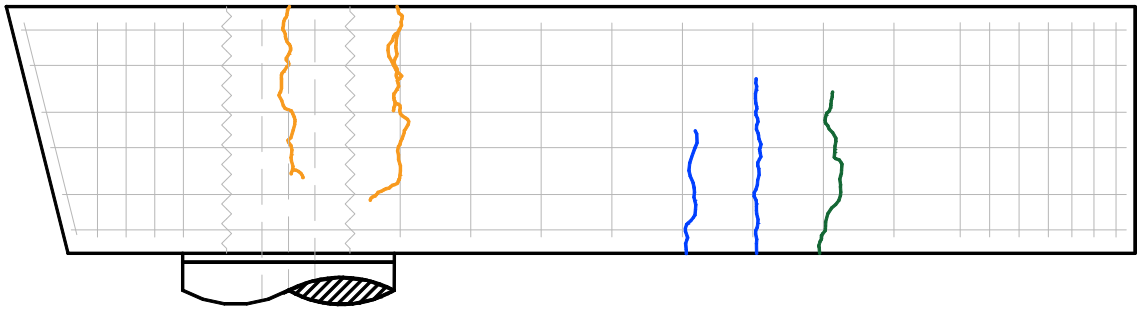

RCS-16-12 – CREEP

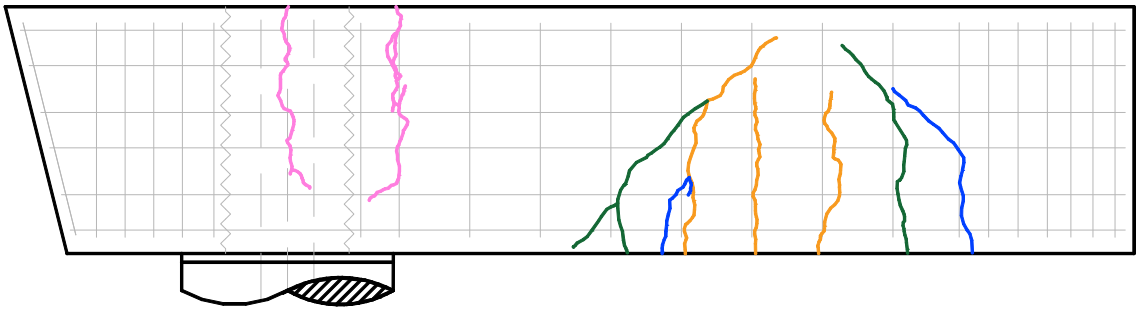

RCS-16-122 – 140% ULS

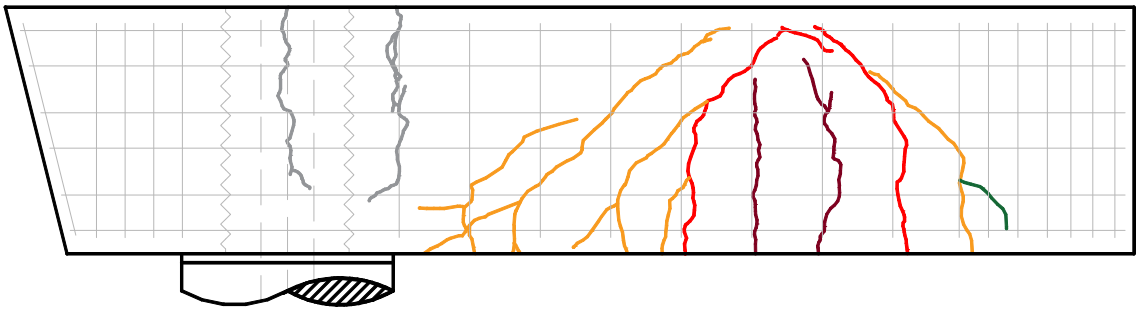

RCS-16-12 – Pattern B

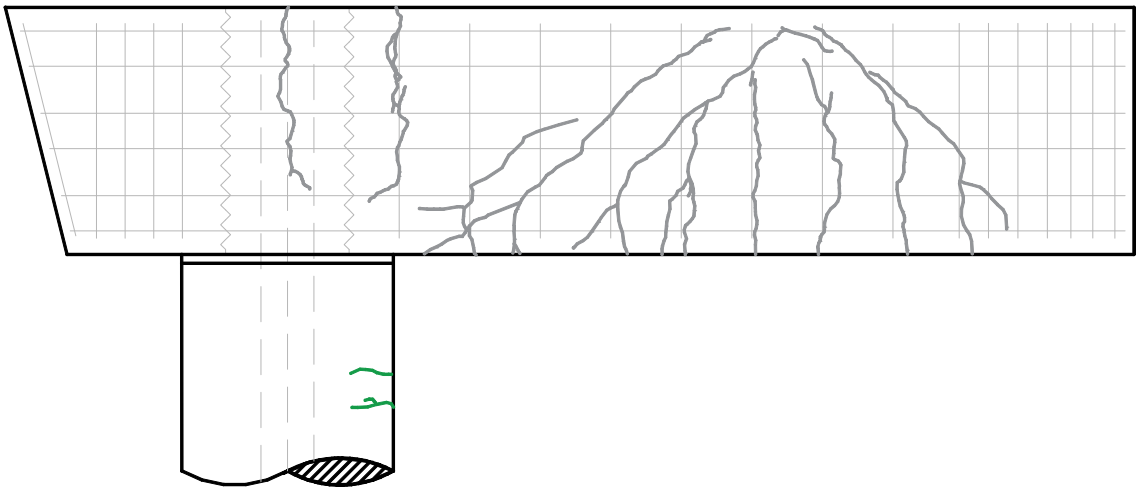

RCS-16-12 – Pattern C

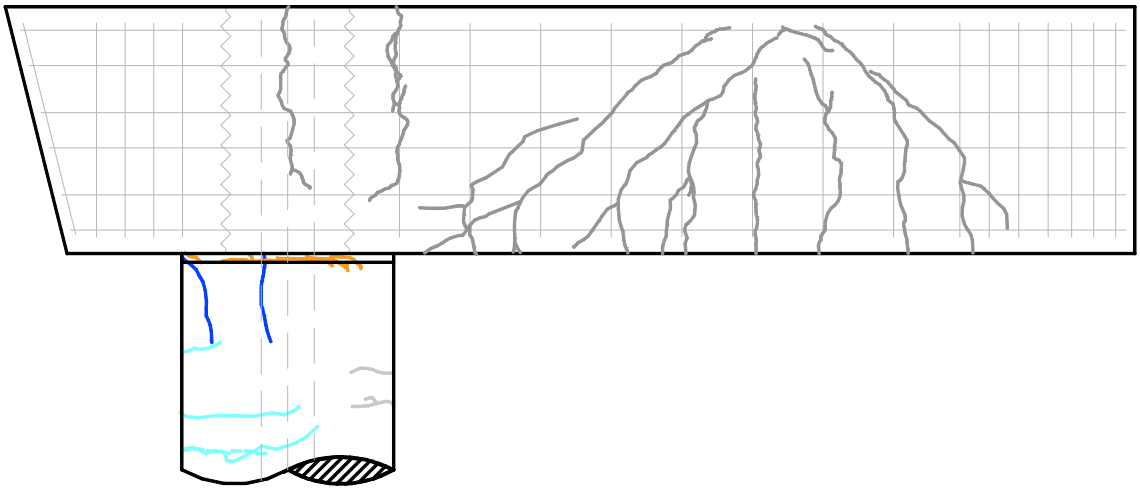

RCS-16-12 – Pattern D

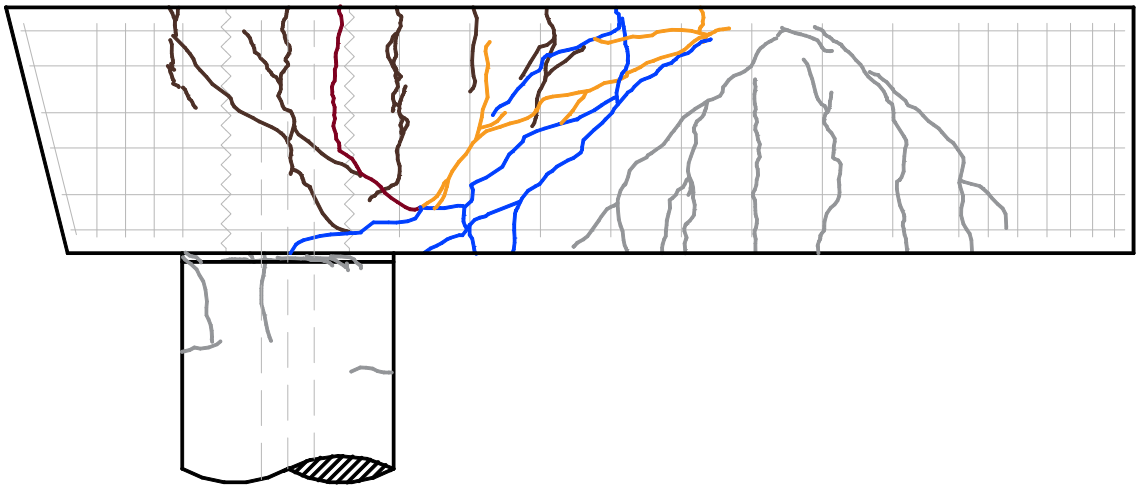

RCS-16-12 – Pattern E

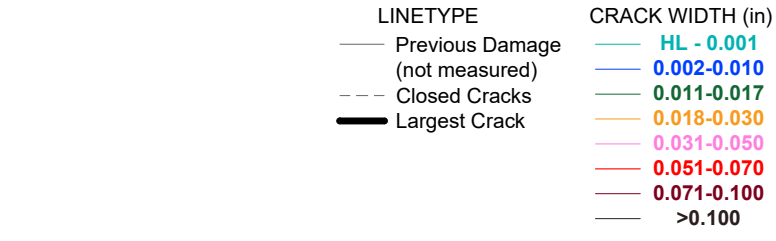

Legend

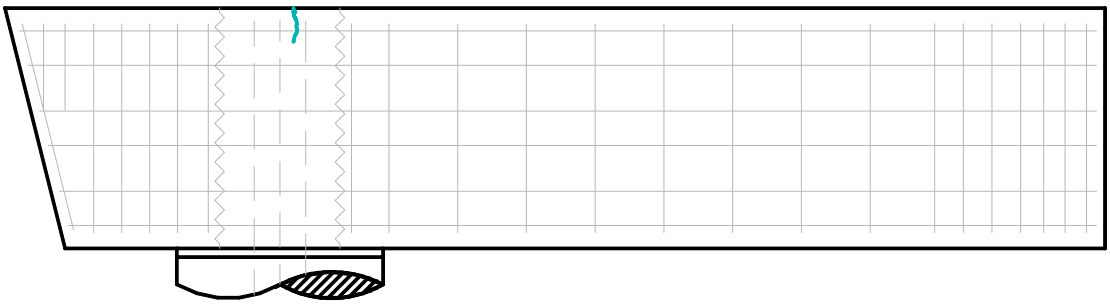

PSS-16-12 – SLS

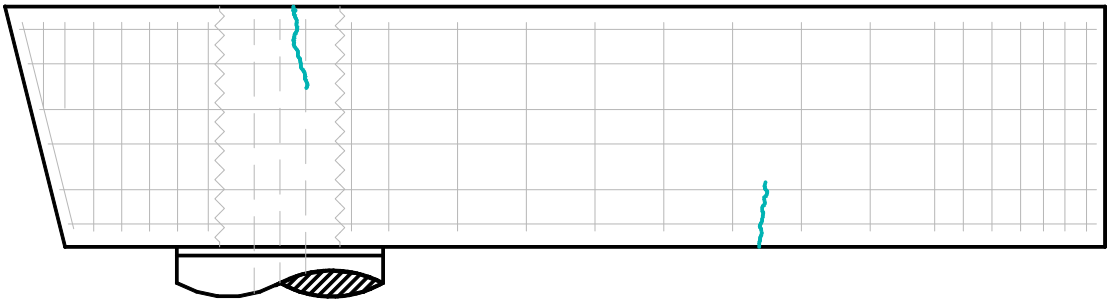

PSS-16-12 – ULS

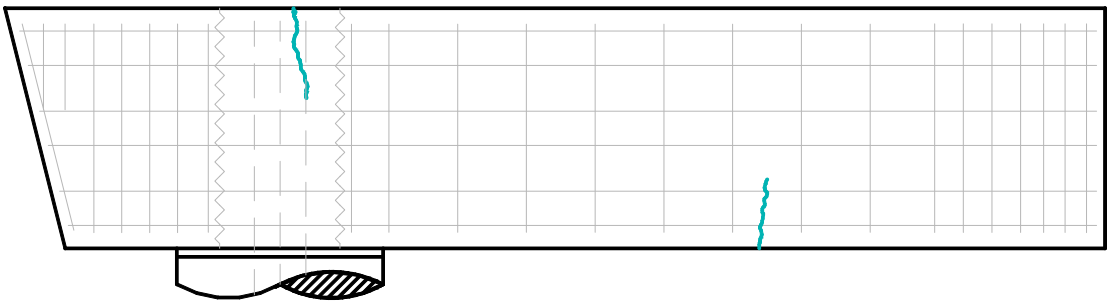

PSS-16-12 – CREEP

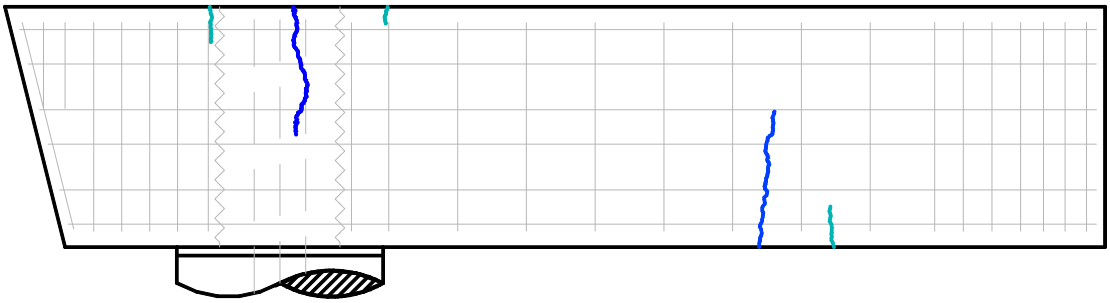

PSS-16-12 – 140% ULS

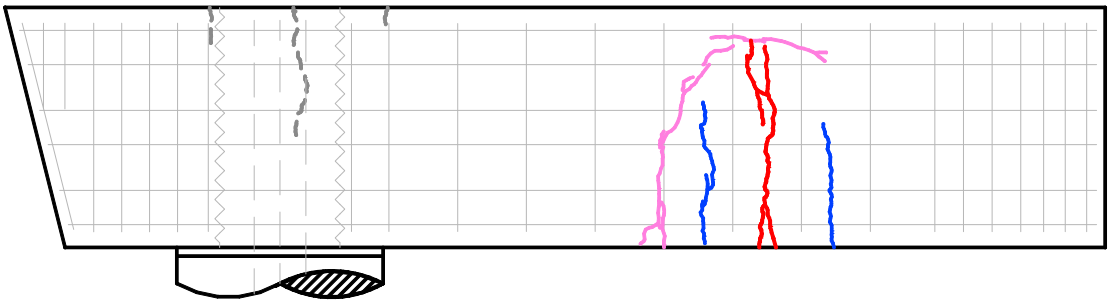

PSS-16-12 – Pattern B

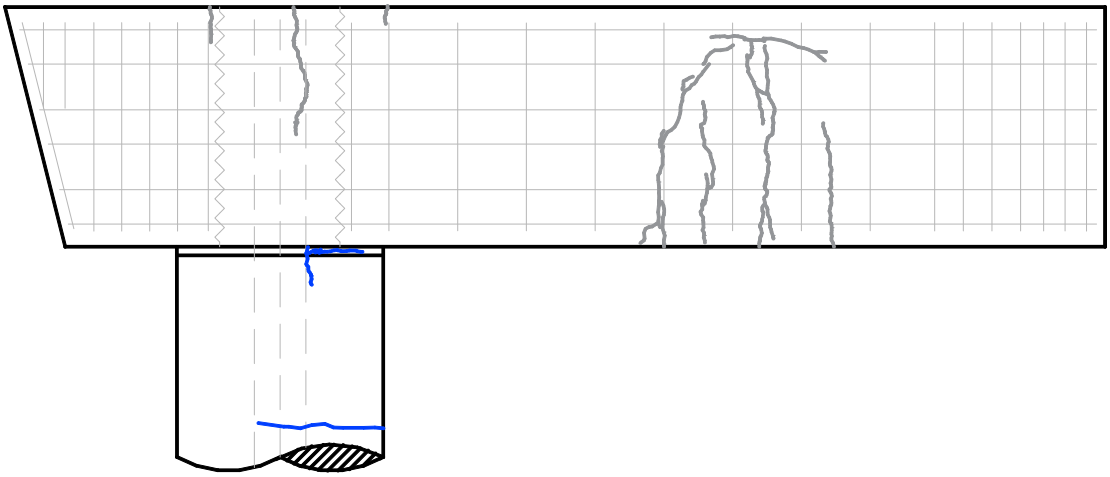

PSS-16-12 – Pattern C

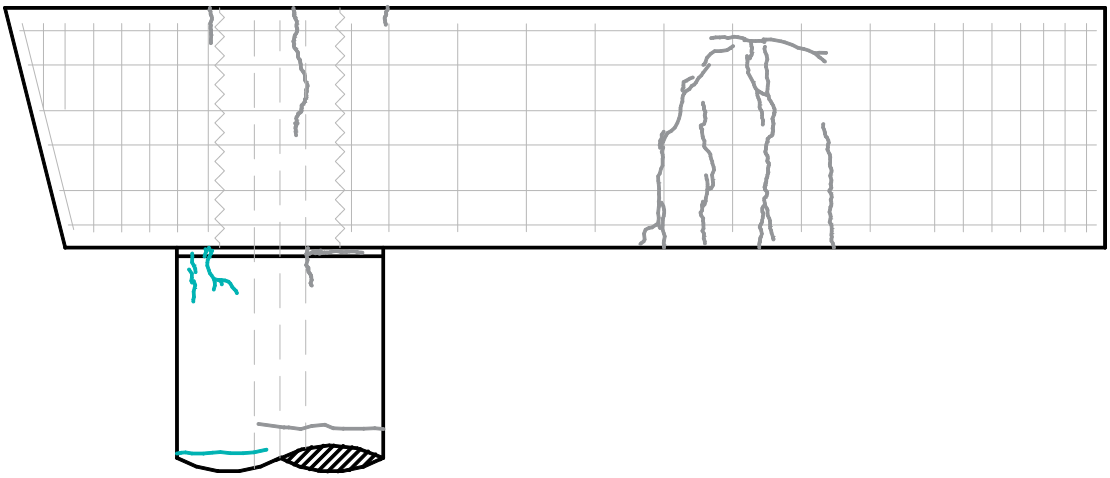

PSS-16-12 – Pattern D

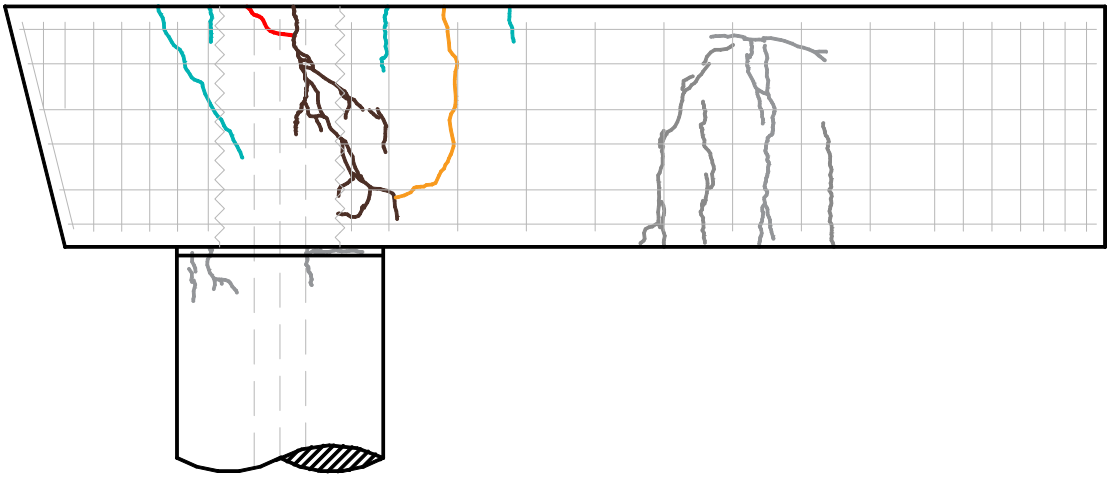

PSS-16-12 – Pattern E